Analysis and Development of Algorithms for Identification and Classification of Dynamic Drillstring Dysfunctions

THESIS

Author: Heinrich Mayer

Submitted to the
Department Mineral Resources and Petroleum Engineering
Chair of Drilling Engineering
University of Leoben, Austria

September 2007

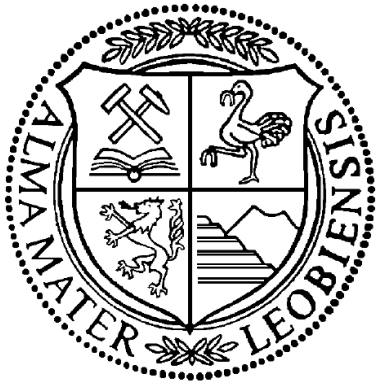

Advisers

Dr.-Ing. Hanno Reckmann
Baker Hughes INTEQ

Univ.-Prof. Dipl.-Ing. Dr.mont. Gerhard Thonhauser
University of Leoben

I declare in lieu of oath that I did this work by myself using only literature cited at the end of this volume.

Heinrich Mayer
Leoben, September 2007

Acknowledgement

I would like to express my many thanks to **Dr.-Ing. Hanno Reckmann** for his great advice and support over the course of this thesis project. His intellectual inputs, the fruitful discussions, and last but not least the freedom he offered me in approaching the tasks are remarkable and prepared the ground for the successful completion of this work.

Special thanks to **Univ.-Prof. Dipl.-Ing. Dr.mont. Gerhard Thonhauser** who provided professional consultation and general advice for writing this thesis. Numerous counsels and unconcealed and helpful feedback enhanced the quality of this work.

I especially want to thank **Dipl.-Ing. Claus Grafelmann** who generously offered me so many opportunities at Baker Hughes INTEQ. An internship and this thesis represent just two of them. His support and commitment were outstanding – thank you very much!

Further, I would like to thank **John D. Macpherson, B.Sc.,** for providing me with information about CoPilot®, showing me new points of view, and answering all my lots of questions.

Great thanks go to **Dipl.-Ing. Christian Herbig** and **Dipl.-Ing. Frank Schuberth** who were always willing to listen to my problems. Their frank and friendly nature, skills, and experience were very helpful countless times.

Moreover, I would like to show my appreciation to all the great minds at the **Dynamics and Telemetry Group** of Baker Hughes INTEQ Celle, **Baker Hughes INTEQ**, and **Baker Hughes Incorporated**, who provided me with their help many times.

Also many thanks to the (former) **Department of Petroleum Engineering** for all the knowledge, guidance, and skills they have given to me. I especially would like to express my deepest gratitude to **Irene Jauck** who helped me, right there in Leoben or at whatever (international) location I was, time and again to tackle bureaucratic barriers, administrative pitfalls, and all the other minor and major problems came along during my studies. Without her great and all the time friendly support the course of studies would have been more like running the gauntlet.

Last but not least, a very special thanks to my **parents** for all the years of unreserved support and all the opportunities they have made available to me. Without them this work would not have been possible.

Abstract

Petroleum exploration is a challenging task. To get access to (potential) hydrocarbon accumulations deeply buried in the ground wells are drilled up to several kilometers in length. In the course of drilling a well, drillstrings can experience a number of detrimental dynamic phenomena. Their causations are primarily related to: the strings geometry, borehole diameter, physical properties of steel, and the instantaneous drilling parameters. Almost always is the occurrence of such phenomena in accord with increased tool wear, elevated fatigue, and/or reduced tool's service quality.

The chance to detect such phenomena at the surface is very limited. The enormous lengths drillstrings usually achieve cause their spring like mechanical characteristic. As a result, bottomhole dynamic effects are considerably attenuated while transmitted to the top end or even do not affect it at all. Latest drilling technology enables downhole detection of dynamic dysfunctions and real-time indication at the rig floor.

Baker Hughes INTEQ has developed a corresponding system – CoPilot®. Sensors placed close to the bit provide the necessary data. The available rate for data transmission from downhole to surface is by far too low to transmit in real-time the whole quantity of sampled data. Therefore, relevant data interpretation must be performed already downhole. Stable diagnostics algorithms are executed for this purpose.

The currently used algorithm to diagnose stick-slip has shown some deficits at its diagnostics ability under certain conditions. This work examines the whole course of automated downhole stick-slip detection – from data sources (sensors) to diagnostic words (output). The diagnostics algorithm itself, as an elementary part of the entire stick-slip monitoring sequence, is extensively analyzed. The following faults are discovered: a RPM oscillation frequency influence, FSR fringe effects, identical diagnostic results at constant RPM oscillation amplitude to average RPM ratios, and an overestimation at very low average RPM levels.

The development of a new approach for stick-slip identification and severity classification finally concludes the work. The new algorithm is a changeover from a statistical RPM trend analysis to a time-based, single event focused severity interpretation. This new approach enables the utilization of other data channels and therefore allows also the detection of stick-slip causation as well as the differentiation of backward rotation types. Furthermore, a mud motor does no longer limit the diagnostic ability of the tool. In the context of developing a new algorithm also the tool 's potential for tool life monitoring is discussed.

Additional topics covered by the text are the development of a magnetometer readings and RPM data simulator and a software-based tangential acceleration data correction. The latter is the consequence of a discovered wrong accelerometer placement.

Table of Contents

List of Figures

List of Tables

1 Introduction – The Drillstring

Hydrocarbons are usually trapped in the ground separated quite a distance from surface by layers of numerous types of rocks. Moreover, it is sometimes not feasible to take the short (vertical) way to reach such accumulations as surface areas right above the reservoir might be limited in access, their access is prohibited, or simply not possible at all. Examples for such restrictions are residential areas, wildlife sanctuaries, lakes, or mountains to name just a few. Also economic aspects can favor a horizontally shifted rig location. Especially offshore does it normally not pay to position a drilling rig right above the target as mobilization and demobilization of the offshore structure per individual well would be too costly. Hence, not only the vertical depth but also the horizontal departure to the oil and gas potential formations bears challenges – beside the solid rock that is always in between.

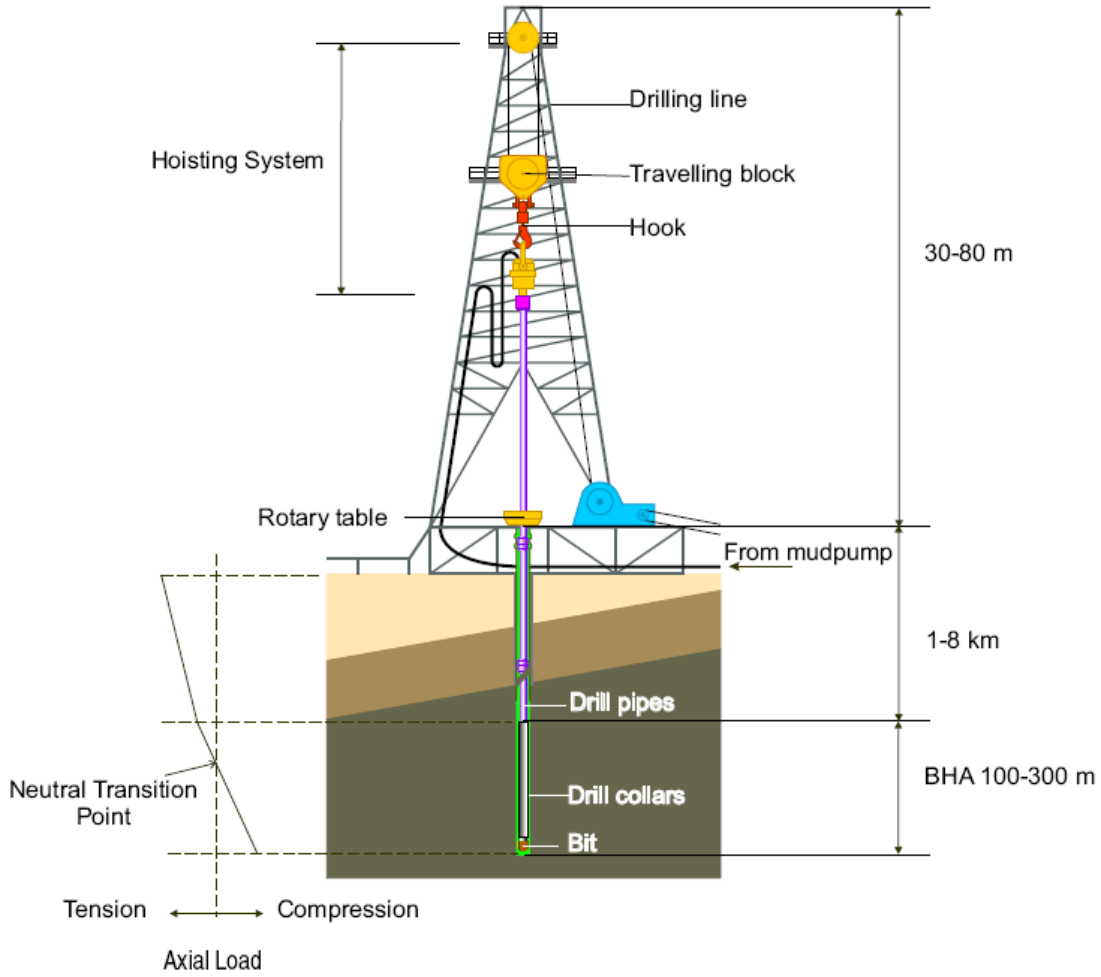

Figure 1 – Drilling rig.[1]

To get access to oil and gas reservoirs, holes of hundreds to several thousands of meters length need to be drilled. These holes are not just straight but their trajectory can be customized to virtually reach every point in a 3D subsurface space that is

located within the rig's reach. There are a few methods to drill wells but all utilize a steel tube – the drillstring. A drillstring is composed of a large number of pipes, different in outer diameter (OD), inner diameter (ID), and length. One method – coiled tubing drilling (CTD) – utilizes a drillstring that almost totally consists of just one single tube (coiled tubing), spooled on a giant reel (coil) and long enough to drill a several kilometers long well without that any connection needs to be made. Another method uses large diameter pipes (casing) for building up the drillstring and after the job is done (most of) the string stays where it is – in the hole – and is cemented there. This method is known as casing while drilling (CWD). Both mentioned methods employ very specialized types of drillstrings and do not represent the standard.

A normal drillstring, described from the bottom up in a vertical well, consists first of all of the bit as its foremost component (of course as at other drillstring types as well). Above the bit a moderate number of drill collars (DC) are screwed on. DCs are very thick walled and thus heavy pipes incorporated to put weight on the bit and keep the rest of the drillstring in tension. DCs are usually followed by several heavy-weight drill pipes (HWDP) those tensile strength and weight is between them of DCs and drill pipes (DP). DPs are the uppermost type of pipe that a standard drillstring is made of. The by far longest section of a drillstring consists of this tubular type.

To drill a hole basically two things are necessary: first, rock must be destroyed, and second, the generated rock fragments (cuttings) must be carried out of the hole.

The destruction of rock is the result of the following two, simultaneous performed processes: the bit is pressed into the rock and a rotary motion is applied to it. The teeth or cutters of the bit eventually crush, shear, or grind the formation and reduce it therewith to small pieces.

Both the necessary force and torque are provided by the drillstring. The force is usually described by a corresponding mass exposed to earth's gravitational field and is referred to as weight on bit (WOB). WOB is generated by adding DC to the bottom end of the drillstring as already mentioned above. Only in very rare cases (e.g. slanted drilling) WOB is supported by an additional, downhole pointing force exerted by the drilling rig that pushes the drillstring into the hole to overcome high friction loses.

The bit can be driven either at the surface or downhole. In case it is surface driven (rotary mode), the whole drillstring is rotated either by a top-drive system (modern option) or via a Kelly (additional pipe screwed to the top end of the drillstring with a squared or hexagonal cross-section to transfer torque) and a rotary table (old method).

The downhole drive option is a positive displacement motor (PDM; a.k.a.: mud motor, downhole motor). PDMs are used for directional drilling where just the bit is driven by the motor and the string is kept stationary (oriented/sliding/directional mode) or as revolutions booster where the drillstring is rotated at relative low RPM and the PDM provides the additional rotary speed to reach an appropriate rate of penetration (ROP).

After assembling a drillstring, putting weight on bit, turning it, and consequently destroying rock, eventually the generated cuttings must be brought out of the wellbore. Do-it-yourselfers, who are familiarized with a power drill, know that the purpose of the spiral grooves in the drill is cuttings transport and therefore might would expect to find a similar system at a drillstring as well. Actually, this is not the case.

In oilwell drilling the drilled holes are too long to transport the generated cuttings volume to surface by mechanical action. The by such a mechanical system caused tremendous high friction would hinder any drillstring rotation after a very short distance drilled. In fact, there are also almost no spiral grooves on the surface of a drillstring. Moreover, a drillstring is hollow (a tube) which is in contrast to a solid spiral grooved drill.

The inner bore of the drillstring has a special purpose. Through this bore, which reaches from surface to bottom, drilling fluid (mud) is pumped. Due to the fact that the bit is always larger in diameter than the drillstring also an adequate flow path between the string and the formation exists – the annulus. The entire flow path of the mud is: the mud is pumped down through the bore, pressed through small holes in the bit (nozzles), turns round and flows in the annulus back to surface.

Drilling fluids bear a variety of functions. In this context the drilling fluid transports the cuttings out of the hole which are picked up right after the drilling fluid had left the bit. That means, the energy for cutting transport is not withdrawn from the drillstring but provided by the drilling fluid.

Drilling fluids have different functions and properties. Cutting transport is only one (important) function. Others are:

- hydrostatic pressure/specific gravity (SG) (to avoid uncontrolled inflow into the wellbore (kick)),
- lubrication (friction reduction leads to longer drillable distances and less wear)
- cooling (ensures better operating temperatures),
- sealing (mud plugs porous formations thus avoiding contamination and fluid loss),
- borehole stability (the integrity of the borehole is supported),
- energy transmission (to drive PDM, downhole power generation),
- corrosion (a certain (alkaline) pH-level and additives can reduce corrosion),
- rheological properties (viscosity and yield point are important for cutting transport),
- reactivity (how the drilling fluid reacts with formations and formation fluids),
- damping (drillstring motions are slightly damped by liquid drilling fluids which especially needs to be considered while pulling out of (POOH) or running in hole (RIH)),
- environmental constraints (some drilling fluids/additives are environmental sensitive),
- large cost factor.

The paragraphs above describe the basics concerning the drillstring and the drilling process. This work is about dynamic effects that might occur when a drillstring is rotated. In this respect the bottom-hole-assembly (BHA) is of sole interest as it contains expensive and sensitive tools for directional control (MWD, measurements while drilling) and formation evaluation (LWD, logging while drilling). The term BHA refers to the lowest part of the drillstring which includes all collars no matter of their dimensions or purposes except DPs. PDM, MWD, and LWD tools are usually incorporated in a BHA right after the bit.

Why is the BHA of that interest? First of all, the bit is a part of it and the physical and dynamic conditions of the bit are highly important as it is the sole piece that is responsible for making hole. Second but not less important, all MWD and LWD tools are parts of the BHA. These tools are equipped with highly sensitive sensors and latest electronics and thus, even if well protected, not that resistant against vibrations.

Even massive steel, which all the collars are made of, will not forever withstand the most severe dynamic conditions a BHA can be exposed to downhole. Just imagine a 40 tones trailer truck stabilized only at two points and rotated with 300 revolutions per minute. How long to you think the trailer truck can withstand such stresses? A couple of seconds, perhaps a minute, or maybe more? A BHA has to survive at such conditions for several days till a week or even two.

Many efforts have been made to investigate dynamic downhole conditions and to extend the reliability of downhole tools. Some of the discovered drilling dynamic dysfunctions will be discussed in this text. A tool designed to detect them will be explained as well. With respect to one dynamic dysfunction – stick-slip – the current detection problems of the tool will be analyzed and a possible solution will be presented at the end of this work.

2 Drilling Dynamic Dysfunctions

At oilwell drilling the generated hole is significantly larger in diameter than most drillstring components. The circular space between the drillstring and the borehole wall is called annulus. Only the drill bit, which destroys the rock and is defining the borehole diameter by that, is actually of identical gauge as the borehole.

Along the BHA a limited number of stabilizers are distributed to centralize sections important for directional control or logging. A stabilizer is a short sub equipped with at least four either spiral shaped or straight and axial aligned blades. The blades are equally spaced all around the sub's circumference. Their identical stand-off centralizes the sub by equally bridging the annulus.

Usually, these subs are "*slightly undergaged to allow efficient weight transfer to the bit and to minimize weight-stacking on the stabilizers*"[2]. Except at the positions of these two types of drillstring components, nothing else is restricting some lateral motion of the string than eventually the borehole wall itself. That means, a drill string at oilwell drilling has always a certain degree of freedom for **lateral motion**.

Also a drillstring's axial motion is not only restricted to one way – downwards. While a normal drilling operation just about 15 [%] of the total drillstring weight is resting on the bit and used for making hole. The by far larger fraction is carried by the derrick. A long, slender, but heavy drillstring is not able to support its own weight anymore and would therefore buckle if not most of it is taken away. The low axial stiffness of a drillstring and the thereof resulting operational limitations allow also undesirable **axial motion** in up-hole direction (vibration) whenever the destructive force of the bit starts to equalize with the compressive strength of parts of the formation to drill.

Furthermore, a drillstring is made of steel (in rare cases aluminum, titanium, or carbon fiber composites are used as well). Steel is elastic up to a certain load applied (elastic limit). That means, below the elastic limit it recovers its original shape after the complete release of the load and no measurable permanent strain remains.[3] During normal drilling operations the elastic limit of steel is not exceeded. However, the elasticity of steel with respect to the shape and scale of a drillstring results in a low torsional stiffness of the string. Due to that flexibility there also exists a remarkable degree of freedom in **rotational motion** – forth and backwards.

Defined limits like the borehole wall at lateral motion do not exist as it is a linear reaction to the applied load (except the elastic limit or ultimately the tensile strength). To get an impression of the dimension of the effect of this steel property the following example is given: in rotary drilling the drillstring is driven from surface. When the string is started to be rotated, the top end has been turned several times before the bottom end (bit) even starts to move at all. This "delay" is the sole effect of the elasticity of steel. The phenomenon can be observed quite well while directional drilling with a PDM together with a MWD.

All these degrees of freedom in motion allow the development of specific drilling dynamic dysfunctions when the drillstring follows its intention and is rotated, see Figure 2. In the subsequent subchapters three of them will be discussed in more detail. Stick-slip is the one that is primarily focused on throughout this work.

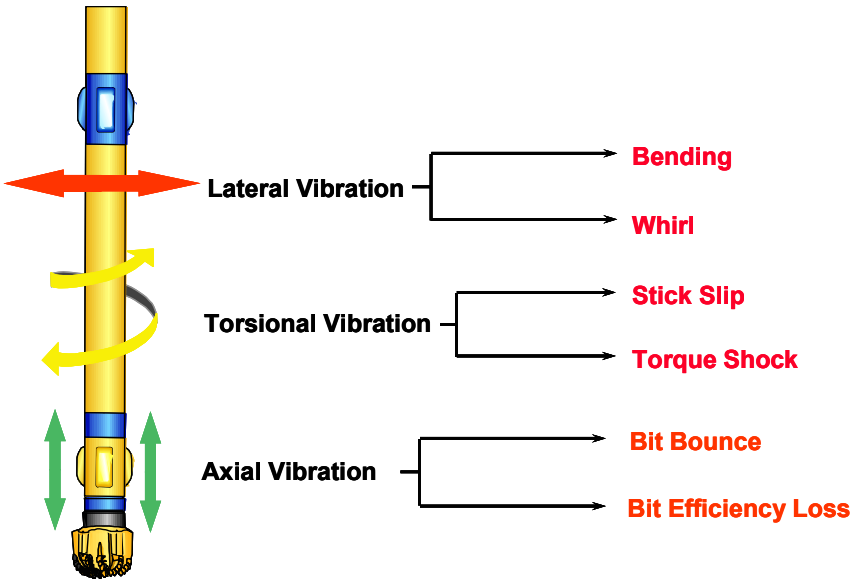

Figure 2 – The three main modes of vibration a BHA can be subject to.[4]

2.1 Stick-Slip

Stick-slip is a phenomenon whose occurrence is enabled by the low torsional stiffness of drillstrings. At the surface a drillstring is driven with a constant rotary speed. "*However, the rotary speed at the opposite end of the drillstring, at the bit, oscillates around the surface RPM*"[5]. The RPM oscillations can reach severity levels where the bit comes to a complete stop for a short moment (stick). Due to the continuing surface drive, after the short stick period the bit is forced to catch up the developed downhole to surface revolutions difference. The consequence is a phase of rotational acceleration up to peak velocities of two or three times the surface RPM. As the drillstring is slipping its rotational restriction, this phase is named slip. Sequences of stick and slip phases are known as stick-slip, see Figure 3.

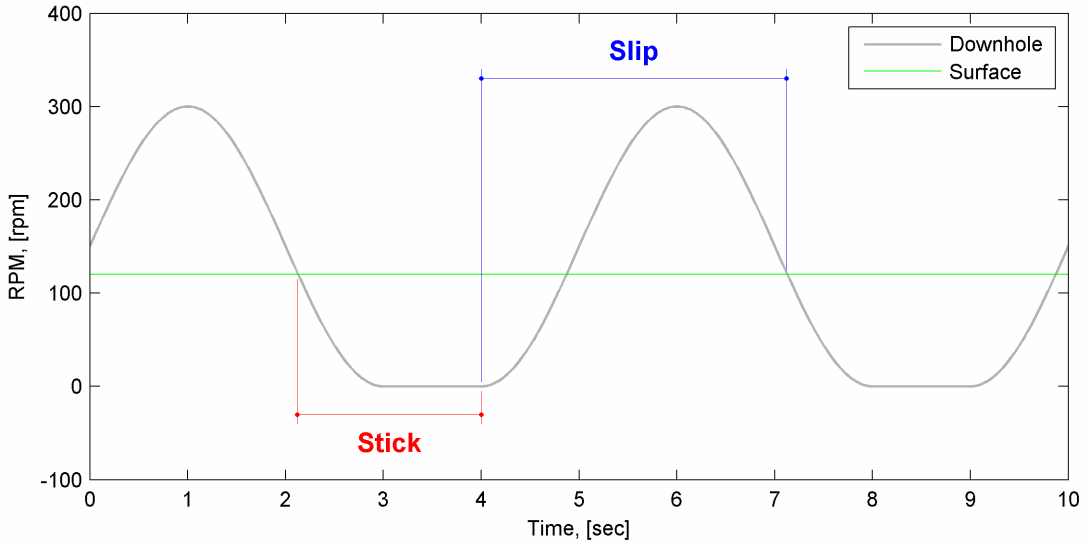

Figure 3 – Stick-slip.

Emergence, development, and severity of RPM oscillations and eventually stick-slip is influenced by the following parameters:

- drillstring length and diameter,
- rock/bit interaction,
- friction between drillstring and borehole wall,
- properties of the surface drive system[5],
- high WOB and low RPM.

The drillstring dimensions define the string's torsional stiffness and therewith the susceptibility to stick-slip and the stick-slip oscillation frequency. A short, large in diameter drillstring is less prone to stick-slip. However, in case of stick-slip it oscillates at higher frequencies than a long slender string would do. "*The measured frequency f_0 of torsional and stick-slip oscillations is found to be close to the estimated first natural frequency of the drill string assembly in torsion*"[6].

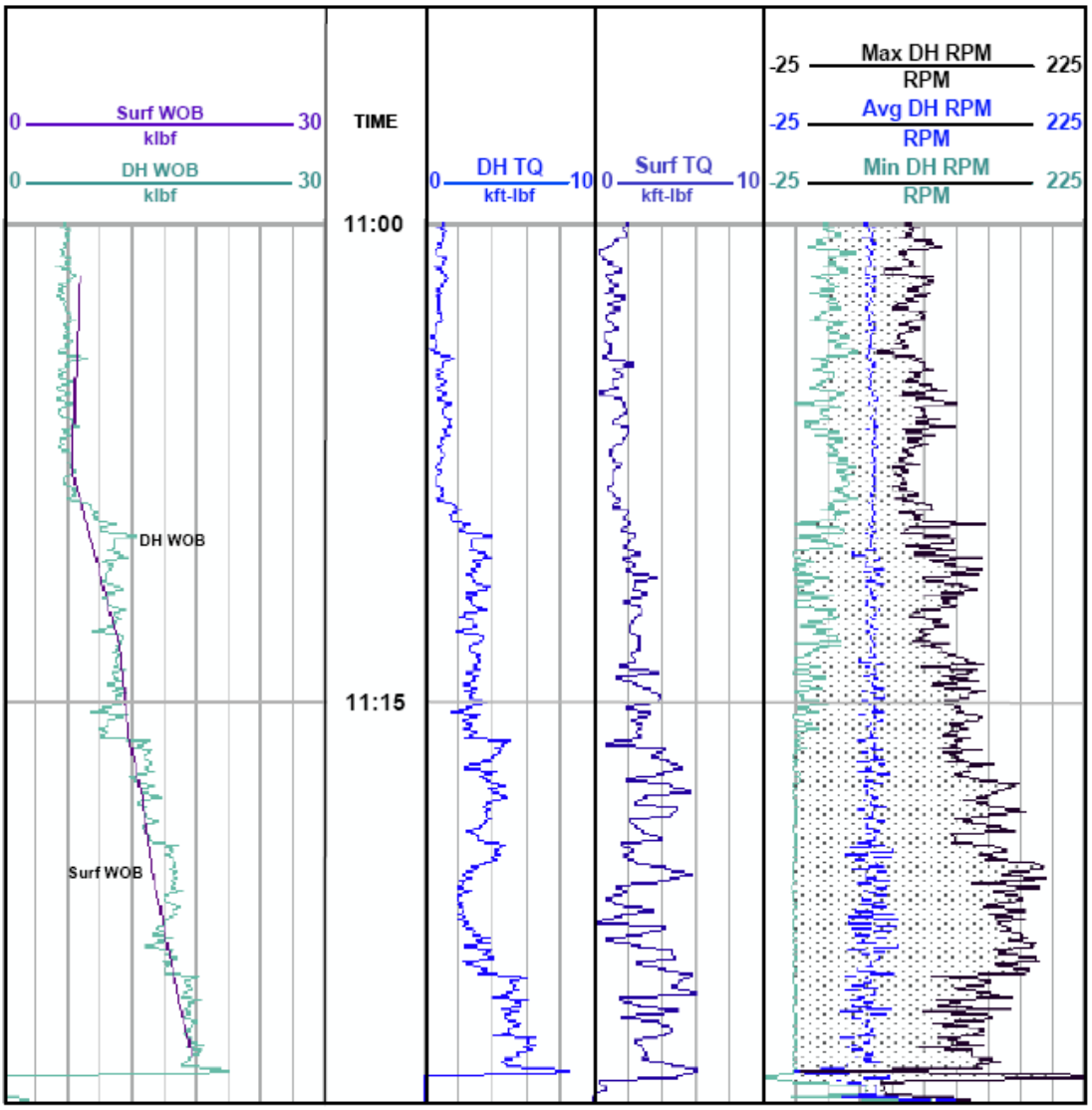

Figure 4 – Time-based log showing stick-slip.[5]

A torsion spring with a linear characteristic is a good drillstring model (Figure 5). To induce torsional oscillations at a rotating torsion spring a resistance against rotation – friction – must be applied/present. Regarding the real counterpart, primarily two areas with high friction can be figured out: at the bottom of the string and at the contact area between drillstring and wellbore along the whole trajectory. The latter does always matter whenever the drillstring is rotated. Friction at the contact area between the bit and the formation only occurs if the bit is on bottom and rotated. Besides these two of course there exist further resistances against rotation like doglegs, cutting beds, or an optional reamer.

None of these fiction forces is constant in size. Contact areas are permanently changing, formation properties vary, cutting beds accumulate and are stirred up again, WOB transfer is unsteady, and eventually the ongoing transition between adhesion and dynamic friction during stick-slip influences friction magnitude – to name just a couple of friction loses/parameters. The interaction of the rotating string/spring and the fluctuating friction forces finally results in torsional oscillations or stick-slip in

extreme. Severe stick-slip vibrations can even lead to a short period of backward spinning of the bit.

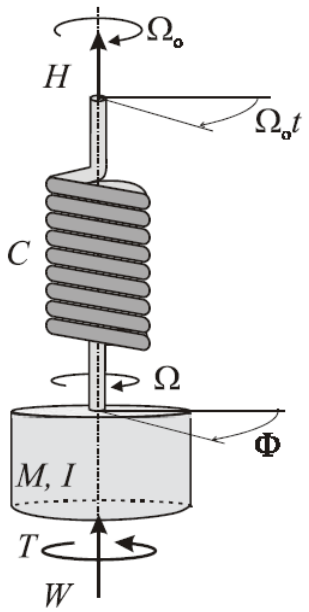

Figure 5 – Simplified model of a drilling system.[6]

Detrimental effects of stick-slip are:

- PDC cutter damage by reverse bit rotation,
- increased fatigue,
- overtorquing of pipe connections,
- damage to the surface drive system,
- low ROP.[5]

Remedial actions for stick-slip situations affect its causation – friction. Either WOB is reduced to lower friction at the bit (Figure 6) which is usually performed in conjunction with a RPM elevation to ensure a similar ROP or the drillstring friction is reduced by changing the mud properties (e.g. add-on of lubricants or change to oil-based mud (OBM)). Unfortunately, high rotational speeds can cause the development of other abnormal dynamic drilling dysfunctions like whirl.

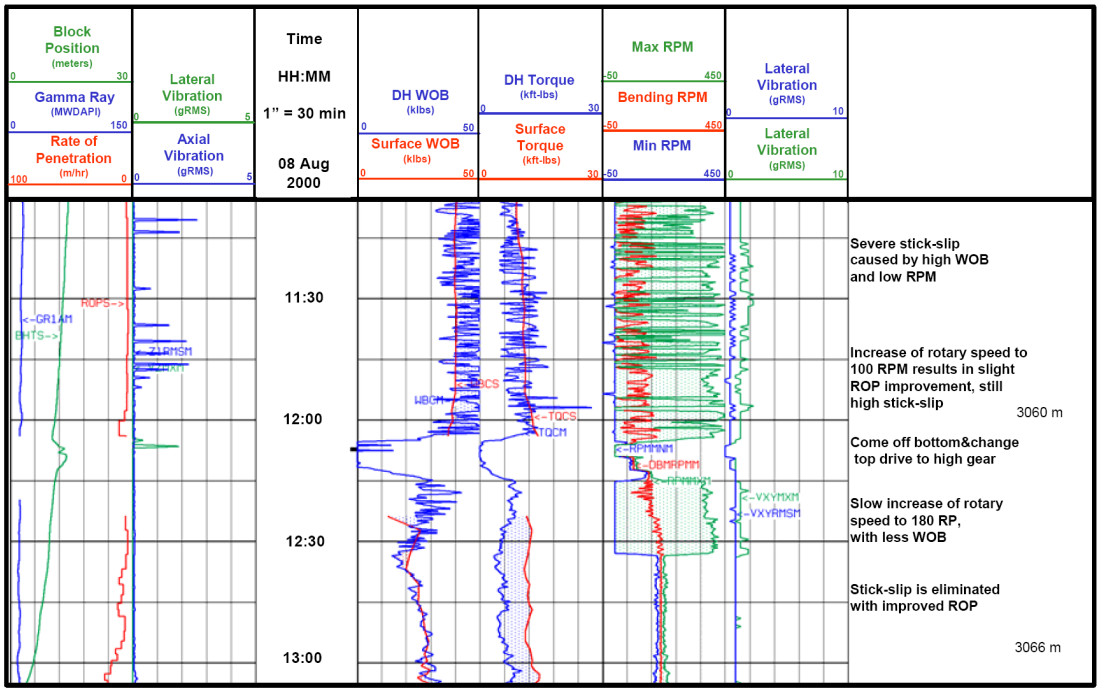

Figure 6 – Successful stick-slip elimination.[8]

2.2 Whirl

"*Drillstring whirl is defined as the off-center rotation of the components in the BHA. Any imbalanced mass in the drill string, buckling, or natural contacts between well bore and BHA will cause the axis of the drill string to rotate off the axis of the hole, creating BHA whirl. Many types of drill string whirl are recognized, from forward synchronous whirl, which causes eccentric component wear, to backward whirl, which causes cyclic stress reversals leading to cumulative fatigue and failure.*"[8]

"***Forward whirl*** *occurs as a bent drill collar rotates clockwise and comes into contact with the borehole wall. This contact can be periodic or continuous. The whirl is "synchronous" when the same side of the collar is in constant contact with the side of the borehole, meaning that the whirl rate of the collar and rotation rate of the collar are the same. This type of whirl will cause wear in one location on the collar. Though not too detrimental on collar, synchronous forward whirl can be catastrophic on MWD tools.*"[8]

"***Full Backward whirl*** *occurs when the drill collar rolls, without slipping, against the borehole wall in a direction opposite to the drillstring rotation. When this happens, the center of the collar is moving around the borehole faster than the rotary speed. This whirling motion usually does not cause much O.D. surface damage, but backward whirl does increase bending cycles, which result in connection fatigue failure.*"[8] "*Often, Backward Whirl has been seen to be self-sustaining; i.e., active intervention is often needed to change conditions in order to correct the improper motion.*"[8]

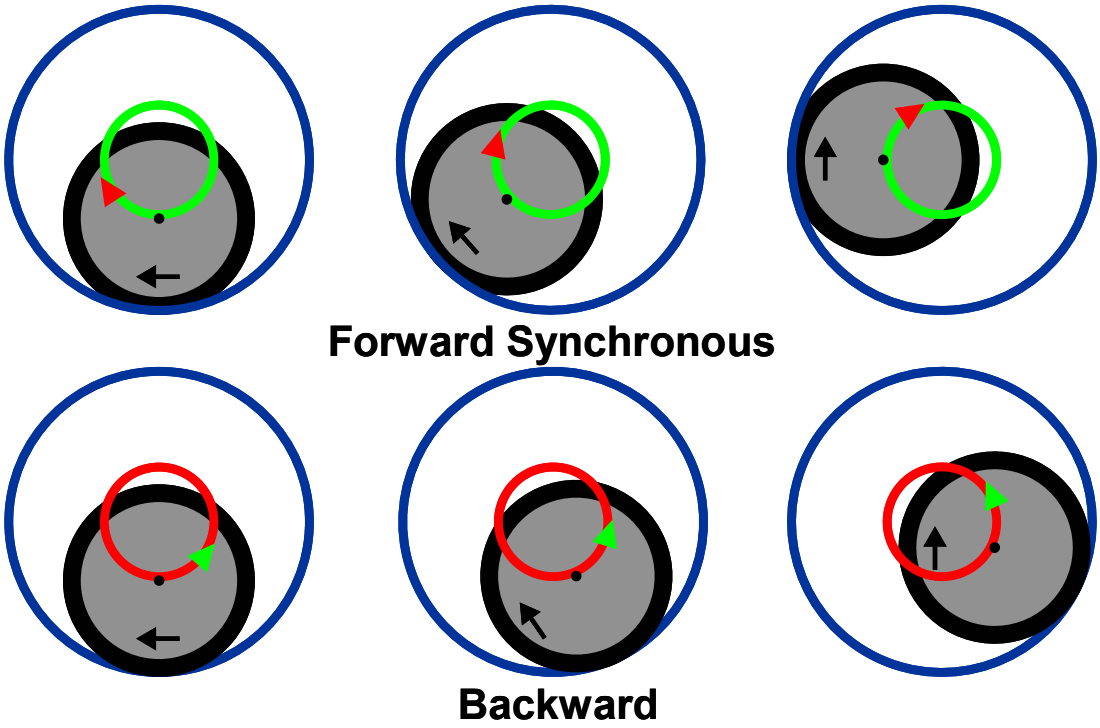

Figure 7 – Synchronous forward whirl (top) and full backward whirl (bottom).[4]

2.3 Bit Bounce

Up to a certain extend, axial vibrations are always present during the normal drilling process. Their major source is the interaction between the bit and the formation to drill. Extraordinary severe axial vibrations can cause the bit to lose contact with the hole bottom. This extreme form of axial vibration is called bit bounce (Figure 8).

"*Bit Bounce occurs predominately when using tricone bits in harder drilling formations, especially when running very low WOB. The tricone bit will bounce over the tricone pattern created in the rock at the drilling face at a frequency of three times the RPM. Bit Bounce may also occur is when using a tricone bit and stick-slip is already occurring. It has been seen to also occur with PDC bits with low WOB when running a mud-motor.*"[8]

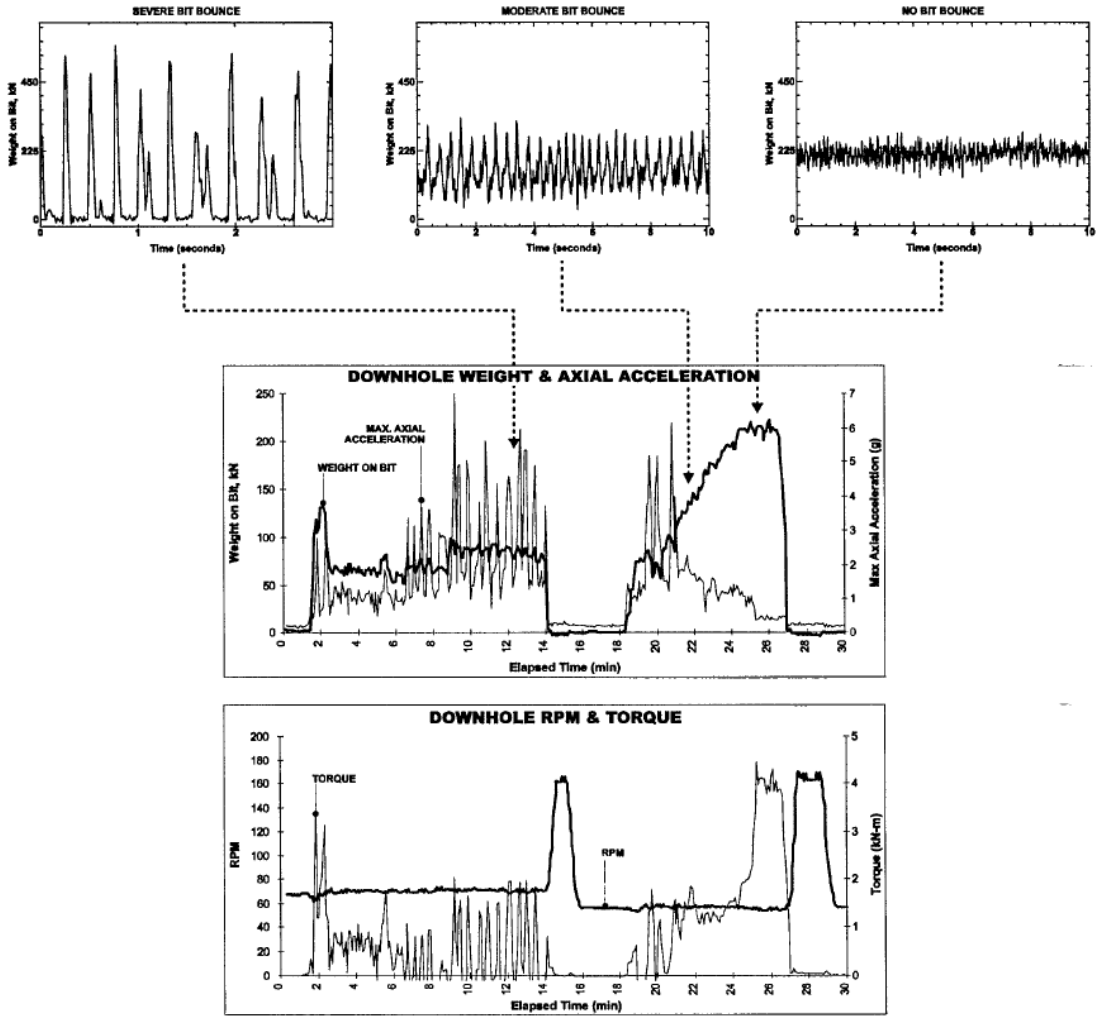

Figure 8 – Bit bounce and how it is suppressed by increasing WOB.[14]

2.4 Conclusions

The last three subchapters have demonstrated that a rotating drillstring is a very complex dynamic system. Many drilling parameter influence the dynamic behavior of a BHA. Just adjustments of WOB and RPM can have multiple effects which are unfortunately not always advantageous to the drilling process. For example, if attempts are made to get rid of stick-slip by reducing WOB and simultaneously increasing RPM, perhaps the stick-slip problem is solved but other drilling dynamic dysfunctions, like bit bounce due to low WOB or whirl because of a too high RPM level, might be induced. To enable a fully controlled dynamic observation, diagnostics, and remedial action cycle of drilling operations, Baker Hughes INTEQ has developed a real-time drilling optimization service – CoPilot®.

3 CoPilot®

In its simplest sense CoPilot® is a near-bit sensor sub. A collar equipped with a number of sensors intended to sample mechanical and dynamic data downhole. CoPilot®'s actual strength and potential is not primarily its sensor fleet but its ability to record, process and transmit (via mud-pulse telemetry of the MWD) sensor data and diagnostic words in real-time. This chapter provides a detailed description of CoPilot® and its corresponding service by presenting selected chapters of the CoPilot® Operations Manual. Notes and comments are made by the author where it appeared helpful for a better general understanding.

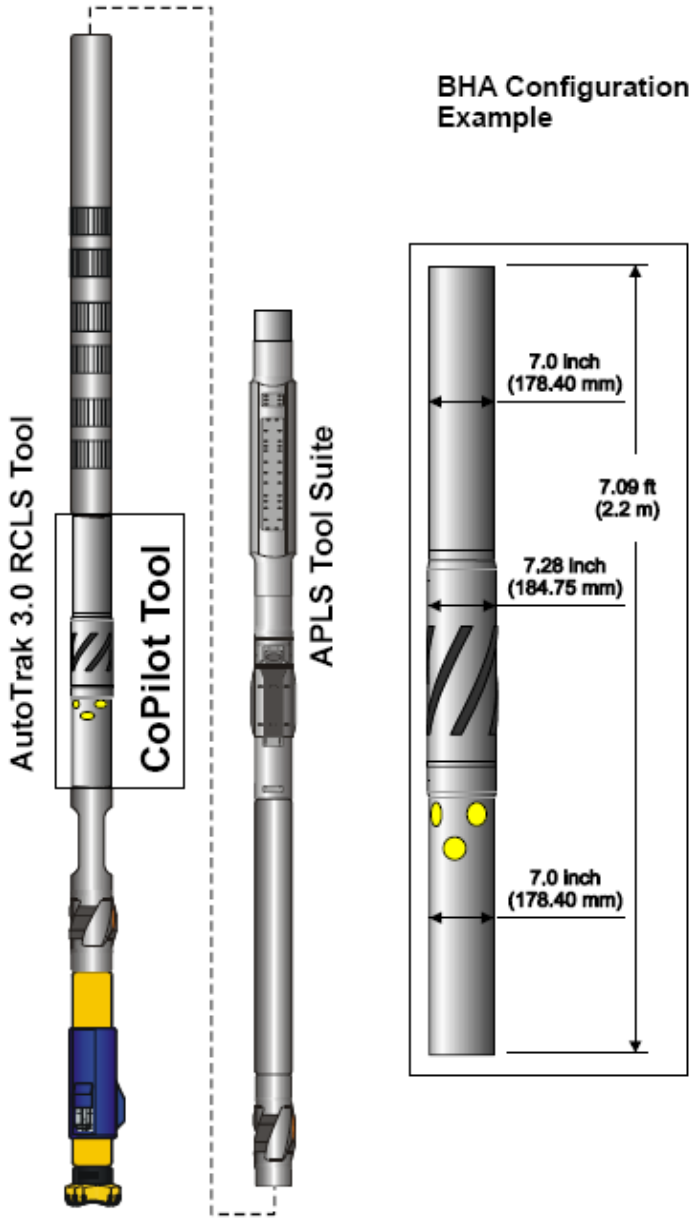

Figure 9 – BHA configuration example with a 6 ¾" CoPilot®.[31]

3.1 Service Overview

"*The CoPilot service is usually run in order to help understand and prevent any vibration that might occur while drilling, as well as to deliver maximum performance while operating within a safe dynamic drilling parameter window to maintain the reliability of the drill bit and BHA. Downhole WOB, Torque and Bending Moment are monitored to optimize the drilling process, provide understanding of drillstring torque and drag, improve bit and mud motor performance, and maximize borehole quality. In addition, if alternative pressure services (PressTeq) are not being used, real-time Equivalent Circulating Density (ECD) is monitored using the CoPilot tool's annular pressure sensor in order to provide optimum hole cleaning.*"[8]

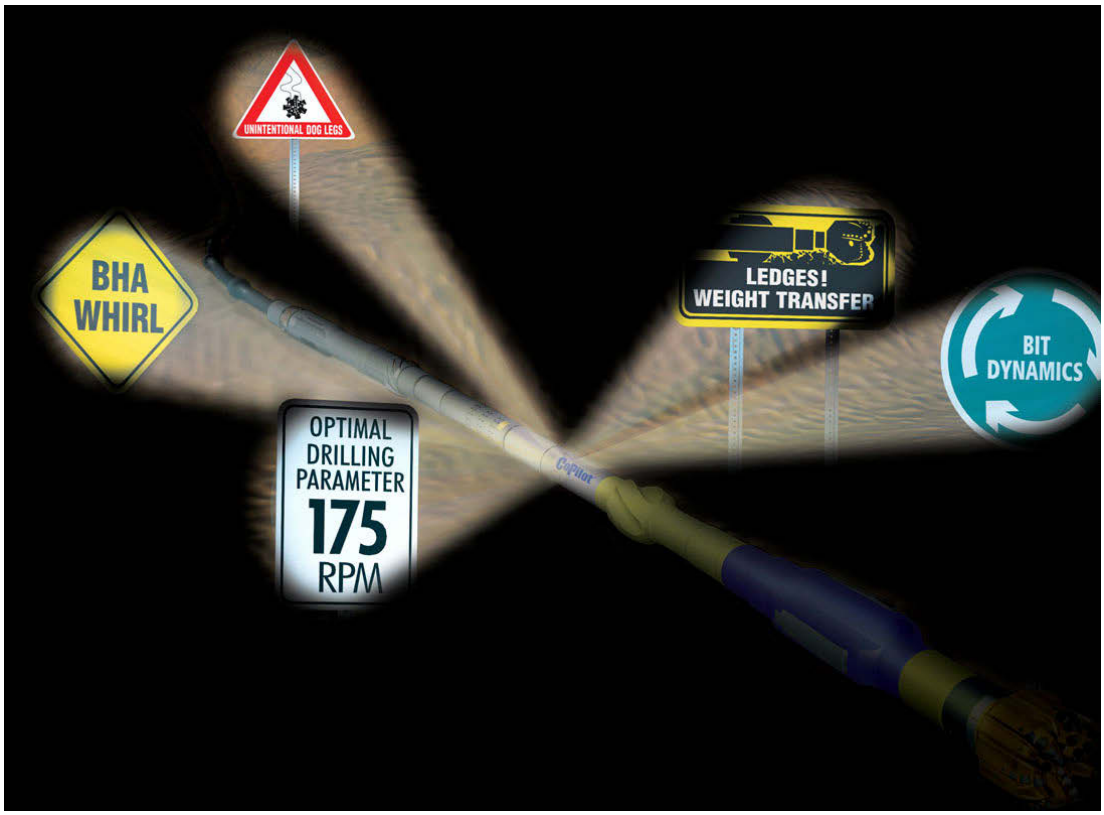

Figure 10 – CoPilot® service.[13]

"*The data resulting from measurements made in the CoPilot tool are used to provide information on the downhole mechanical environment affecting the BHA, and also to generate diagnostic values indicating the severity of specific vibration related events. Values for several different drilling dysfunction diagnostics are transmitted to the surface via mud pulse telemetry, and are color-coded for display in the logging unit and on the drill floor. The drill floor display allows the driller to have immediate feedback to the downhole dynamics response when changes are applied to the drilling parameters such as WOB, RPM, and flow rate*"[8], see Figure 11.

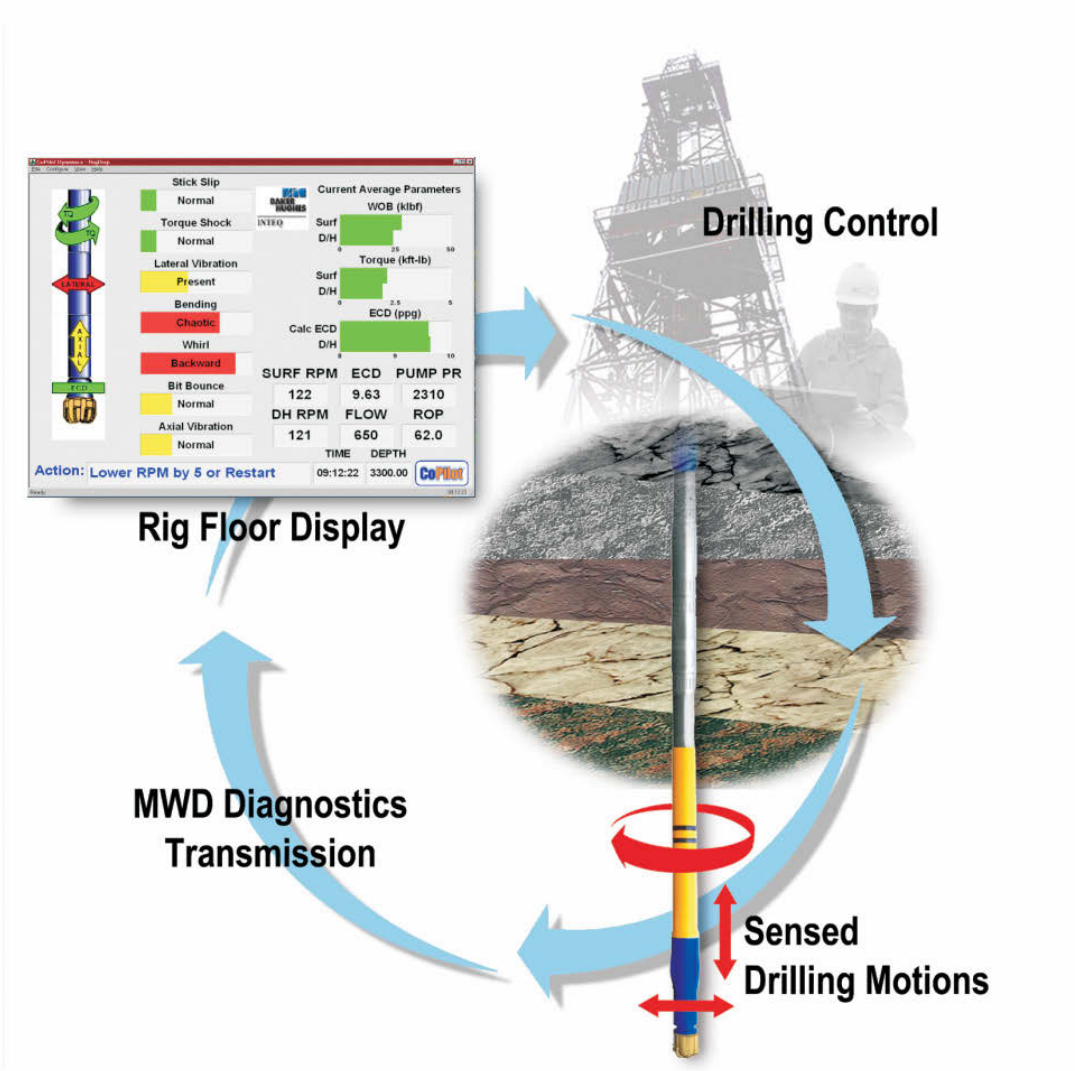

Figure 11 – Real-time optimization loop of CoPilot® service.[13]

The driller's access to information about what is actually going on downhole is very limited without systems like CoPilot®. Based on his experience and feel for the drilling system he is interpreting e.g. surface torque, hook load or pump pressure changes, all measured up to kilometers away from the BHA, to get some indications about the effects of made adjustments. To optimize the drilling process and to avoid periods of undetected dynamic dysfunctions, CoPilot® service provides a real-time optimization loop making use of real-time downhole data (loop description from [13] and [14]):

- *"The driller adjusts drilling parameters such as WOB, RPM and flow rate at the surface.*
- *The drillstring and the bit respond to these adjustments.*
- *The downhole tool continuously acquires data on multiple channels at a high rate.*
- *Robust downhole algorithms search for patterns of dynamic dysfunctions in the data stream and diagnose their severity.*

- *Diagnostic words (severity levels on a scale of 0 to 7) are transmitted via MWD mud pulse telemetry to the surface.*
- *The diagnostics are presented along with other downhole and surface data directly to the driller on a rig floor display.*
- *The driller observes the response to his current drilling parameter adjustments and makes changes as required."*

The CoPilot® service is not designed for just a single drilling application but can be productive while almost every drilling operation. However, most beneficial is its deployment at advanced operations like multilateral wells, extended reach drilling, offshore, or when critical formations are expected.

CoPilot® service benefits summed up(from [30]):

- *"Immediate detection and resolution of*
  - *dynamic related problems*
  - *weight transfer problems*
  - *drilling hydraulic problems*
- *Enhanced ROP and optimized drilling process*
- *Local dogleg-severity monitoring and control*
- *Improved borehole quality*
- *Improved downhole motor efficiency and extended motor life*
- *Longer bit life*
- *Increased MWD and drilling system reliability*
- *Comprehensive data set for post-job analysis and BHA optimization"*

3.2 Mechanical Design

Figure 12 – 3D graphics of CoPilot®.[8]

CoPilot® consists of three main parts: Electronic Sub, Sleeve and Top Sub (see Figure 12). "*The Electronic Sub takes the loads and incorporates the sensors as well as the electronics. The electronic boards are mounted in slots that are covered by the Sleeve. The Sleeve is pressfitted by the Top Sub, which is mounted onto the Electronic Sub. CoPilot is available in four tool sizes: 4 ¾", 6 ¾", 8 ¼", 9 ½".*"[8] Its corresponding tool lengths, listed in identical order as the sizes, are: 2.72 [m], 2.16 [m], 2.48 [m], 2.29 [m]. The smallest tool is at the same time the longest one as its internal design needed to be modified in contrast to larger tool sizes. Its electronic boards are mounted in a different manner due to the lack in radial space.

3.3 Coordinate System

"*A standard positive clockwise x/y/z coordinate system is used for the tool, where the z coordinate is aligned with the drillstring and pointing up-hole, and x and y are accordingly pointing in a radial direction.*"[8]

"*However, in the CoPilot tool, the coordinate system of the oriented measurements of magnetometers, accelerometers and bending are not aligned, i.e. the x and y coordinates do not point to the same direction. Because of a 45° misalignment between the bending and the acceleration measurements, there are two directions for x and y marked on the tool for calibration purposes. The bending measurement is the tool reference coordinate system, while the accelerometer axis misalignment is corrected during the calibration of the tool by a software based coordinate transfer. The tool will show a positive x or y bending value if the tool is bent in the x or y direction, and a positive x, y or z acceleration value if it is accelerated towards the x, y or z direction.*"[8]

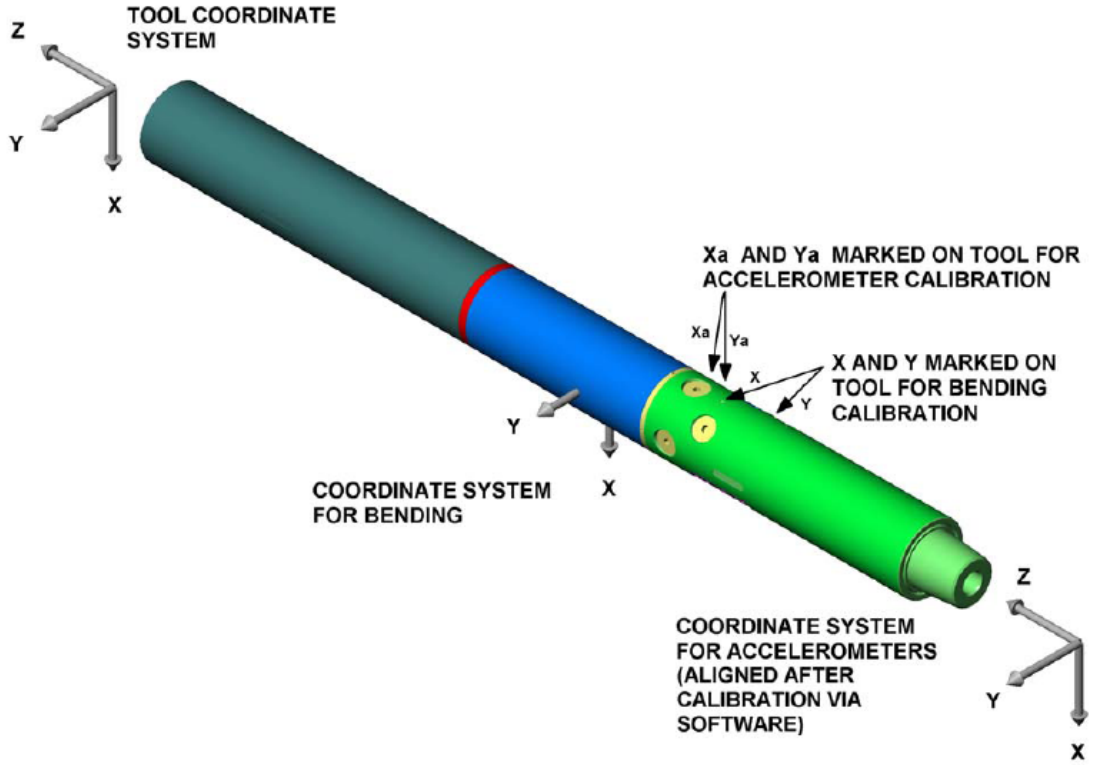

Figure 13 – CoPilot®'s coordinate systems.[8]

3.4 Transducers

"*The tool is equipped with four full strain gauge bridges to measure: 1) bending in the x and y directions and 2) weight and torque. Pressure transducers mounted in a hatch cover measure both the bore pressure and the annulus pressure. Two three-axial accelerometer packages are mounted onto the sub. They sense axial, lateral-x,*

and lateral-y acceleration. The y accelerometers are also summed in a different manner in order to produce tangential acceleration. Additionally, x and y magnetometers are used to monitor the downhole rotational speed. The magnetometers are mounted onto the electronic boards. A thermocouple, which provides internal temperature data, and a Resistive Temperature Device (RTD) in the pressure hatch cover for external temperature, completes the sensor set."[8]

"*The sensors for the strain gauge bridges are contained in several Strain Gauge Transducer modules which are mounted into six cylindrical pockets. The four pockets towards the up-hole end of the tool carry the weight and the bending transducers. These pockets are orthogonal around the circumference of the tool. The torque transducers are mounted into the two pockets closer to the bit.*"[8]

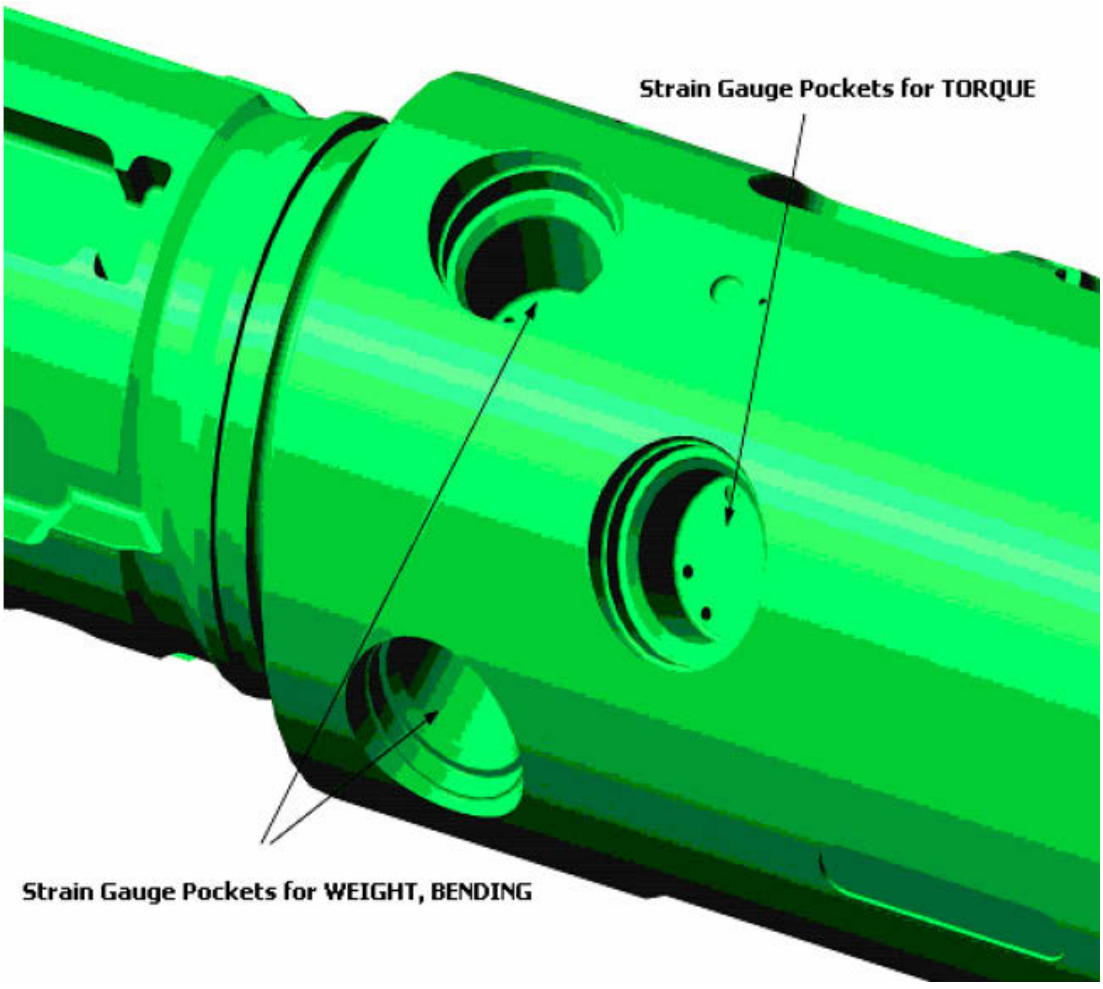

Figure 14 – Strain gauge transducers.[8]

3.5 Data Acquisition

"*In total, there are fourteen sensor channels in the tool. All fourteen data channels are simultaneously sampled at 1000 Hz. A real-time clock is employed to time-stamp the signal and to ensure a chronological data stream.*"[8]

Channel	Description	Unit
1	Lateral (x-axis) magnetometer	*[-]*
2	Lateral (y-axis) magnetometer	*[-]*
3	Lateral (x-axis) accelerometer	*[g]*
4	Lateral (y-axis) accelerometer	*[g]*
5	Axial (z-axis) accelerometer	*[g]*
6	Tangential acceleration	*[g]*
7	Lateral (x-axis) bending moment	*[Nm]*
8	Weight (WOB)	*[N]*
9	External hydraulic pressure	*[kPa]*
10	Lateral (y-axis) bending moment	*[Nm]*
11	Torque	*[Nm]*
12	Internal hydraulic pressure	*[kPa]*
13	Internal temperature (on magnetometer PCB)	*[°C]*
14	External temperature (RTD in pressure hatch cover)	*[°C]*

Table 1 – Data channels (modified after [8]).

3.6 Data Processing

"*The processing power in the Digital Signal Processor (DSP) permits a continuous evaluation of the acquired data stream using a 5-second loop. The DSP processes a 5-second long data stream segment while the next segment is being acquired and buffered. Within each 5-second segment, 70,000 raw data values (14 channels x 1,000 Hz x 5 seconds) are converted into static and diagnostic information. The static information is comprised of the average values of the various sensor channels, the average downhole RPM, the statistical moments for most of the channels and the minimum and maximum values of selected channels. Prior to any dynamics processing, the data are corrected for temperature effects and then scaled and offset-compensated.*"[8] In total, 47 static items are calculated.[15]

"*Ten diagnostic flags indicate the severity of various dynamic phenomena. The processing starts with an analog low-pass filter providing a usable bandwidth from 0-70 Hz. The data stream is filtered and decimated down through different stages as required by the various algorithms. The magnetometer signals are processed to determine the instantaneous and the average rotational speed. A similar algorithm is applied to the bending channels. The combined results provide the input for the whirl diagnostic. The frequency content of the WOB channel is split into two different frequency bands. The information in the high frequency band is used for determination of the cutting efficiency diagnostic of the bit. At this time, the so-called SNAP diagnostic is undergoing reevaluation and is not currently being used in the field.*"[8]

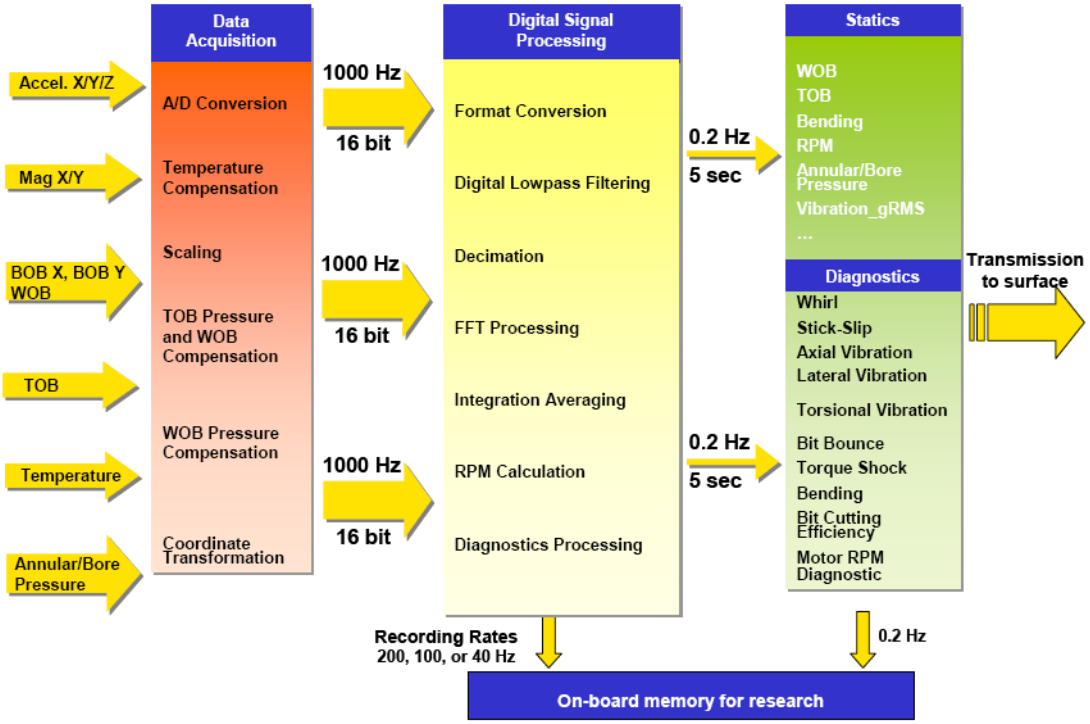

Figure 15 – Data acquisition and processing block diagram.[8]

Data handing in CoPilot® is based on S.I. units. All data downstream the Format Conversion stage is already scaled and converted to S.I. units i.e. data streams of sample rates 200, 100, 40, and 0.2 [Hz] bear physical units according to S.I..

3.7 Diagnostics

Today at oilwell drilling the bottleneck in real-time data transmission from downhole to surface is the used telemetry system. Industry's standard of data transmission is mud-pulse telemetry. Data is sent to surface via a sequences of pressure waves traveling up the inner bore of the drillstring. Downhole, the pressure wave is generated by an adjustable orifice (pulser) located in the bore. At the surface a pressure transducer monitors inflow pressure and hence receives the coded downhole data (pressure waves) which are finally translated back by software.

Standard systems achieve transfer rates in the range of 8 to 12 bits per second. For example, just one of CoPilot®'s sensors produces 16,000 bits of raw data every second (1000 [Hz] x 16 [bit]). Taking a transfer rate of 10 [bit/sec], then it would last nearly 27 minutes till that one second of data, sampled by just one single sensor, will be received at the surface. You would not call that real-time downhole monitoring anymore. For this reason, data is automatically analyzed downhole and just the results (diagnostics) are transmitted. The diagnostics output rate is 0.2 [Hz] in 3-bit words which is an immense reduction in data quantity to transfer.

"*The data output from the DSP are used to calculate diagnostic information. There are ten diagnostics, five of which*"[8]…"*are currently relied on for real-time optimization:*"[8]

#	Diagnostics
1	Bit Bounce
2	Stick-Slip
3	Whirl
4	Axial Vibration
5	Lateral Vibration
6	Torque Shock*
7	Torsional Vibration*
8	Bending*
9	Bit Cutting Efficiency*
10	Motor RPM Diagnostic*

Table 2 – CoPilot®'s diagnostics (*: currently not used for real-time optimization).

"*Various statistical calculations are used to determine these diagnostics values. The outputs are compared against eight (0 through 7) user defined threshold levels. The levels are color-coded when output to remote displays.*"[8]

Diagnostics	Source
Bit Bounce	• WOB strain gauges • pressure transducers • temperature sensor
Stick-Slip	• x and y axis magnetometers
Whirl	• x and y axis magnetometers • bending strain gauges • temperature sensor
Axial Vibration	• z-axis accelerometers
Lateral Vibration	• x and y axis accelerometers
Torque Shock	• torque strain gauge transducers • temperature sensor
Torsional Vibration	• y-axis accelerometers
Bending	• bending strain gauges • temperature sensor
Bit Cutting Efficiency	• WOB strain gauges • temperature sensor
Motor RPM Diagnostic	• x, y, or both bending strain gauges or accelerometers, defined by user

Table 3 – Sensors ultimately affecting specific diagnostics.[8]

3.8 Data Recording

"*In total, 32 MBytes of memory space is provided in the tool for storage of the five-second processed data and high-speed sensor raw data. The output of the DSP (statics and diagnostics as described above) is recorded every 5 seconds after the tool is powered up. These recorded processed data are used to create the logs, which show the related drilling process data in context.*"[8]

"*A circular data buffer and an "RPM trigger" in the downhole tool allow controlled recording of high speed raw sensor data from the surface in a post-event mode. The data channels to be recorded, as well as the recording rate, can be selected during tool configuration prior to a tool run. The data rates available are 40, 100, and 200 Hz. Depending on the selected configuration, the downhole system continuously buffers raw sensor data for the last 5 to 20 minutes. Increasing the surface RPM above a preset RPM threshold for a preset time triggers the transfer of the data from the circular buffer to the on-board research flash memory. This capability allows the selective recording of events of interest. Several events can be stored until memory is full.*"[8]

3.9 Data Transmission

For data transmission only diagnostic words and processed five second data (FSD, static items) are made available. Research memory data (RMD, high-speed data) is not pulsed to surface. The output sample rate (OSR) for transmission is adjustable at integer multiples of the frame sample rate (FSR, 0.2 [Hz]).

4 Introduction to Sensor Mechanics

Humans feel, smell, hear, see, and taste their environment. In the course of evolution five senses have been developed to capture all necessary information to survive in men's environment. Since childhood, years of experience trusting our senses has increasingly confirmed the picture of the macrocosm we have perceived. Subjectively, we are getting the impression the world looks like as we perceive it.

Obvious signs that our senses provide us with limited or even wrong information are rare or in case are mostly misinterpreted. For example, when using a modern high-speed elevator in a multistory building to go from ground floor up to top level, a common misperception is a feeling of continuing lifting motion after the elevator had stopped. Or would you ever mind your eye's sample rate when watching a movie? Nowadays we know that our senses are not best in nature. For every human sense a better one can be found at another species. For example, fish recognize smallest pressure changes in water which we cannot feel at all.

By nature our perceptive faculty is restricted. Technology is giving us the opportunity to translate invisible properties into signals we are able to capture. Sensors do not only extend our perception but can also substitute human observations. Wherever it is too dangerous, expensive, or just not possible for man to observe a process in person, the application of a sensor might be an alternative. Almost every human sense can be substituted by sensors today.

Sensors are more close to human perception than might expected. Human perception is subjective and in a very broad sense sensors as well. Different types of sensors measuring an identical property most likely do not show identical output values. Even in case of same type, manufacturer, charge, calibration, and operation history, readings do not necessarily exactly correspond. Sensors do have certain errors which limit their precise and fully reproducible representation of the measurands.

An ideal sensor would react one-to-one solely on its measurand changes. Real sensors can be influenced by other physical properties, manufacture process, operating conditions, material properties, limited reaction range, radiation, wrong mounting, hysteresis, pure calibration, and a number of other factors, which might distort sensor's reaction. For these reasons the measured "picture" needs not necessarily to be a perfect copy of the original object and any observer should be aware of that.

The indention of this chapter is to give the reader an impression of the abilities and limits of sensors with a special focus on sensor types incorporated in CoPilot®. It is seen as very important to understand the sources of data and the risk of offering a distorted picture of the reality if not accurately used or working.

4.1 Magnetoresistive Sensors (Magnetometers)

A magnetoresisitve (MR) sensor is a magnetic field dependent resistor. The physical principle MR sensors are based on is called the anisotropic magnetoresistance effect (AMR). AMR occurs only in ferrous materials. It is a change in electrical conductivity of a thin anisotropic ferrous film when it is exposed to an external magnetic field perpendicular to the current flow (see Figure 16).

The magnitude in resistance change depends on angle and intensity of the applied external magnetic field. The ferrous material shows highest electrical conductivity when the magnetic field is normal to the current flow. The highest resistance value is achieved in case magnetic field and current flow are parallel. In absence of any magnetic field, the resistance reaches roughly the mean value of both the upper and lower extreme.

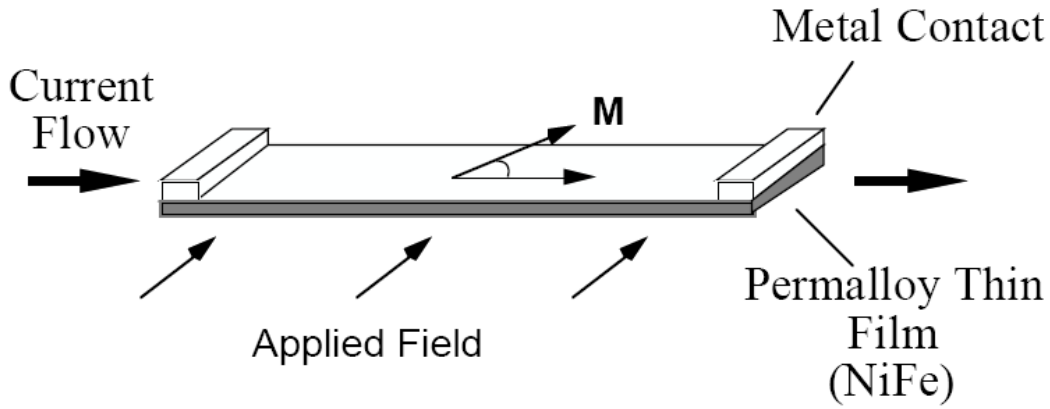

Figure 16 – Principle of operation of MR sensors.[17]

The used ferrous material determines the range of resistance variation. The size of change comes up to several percent of total film resistance. A nickel-iron alloy (Permalloy) is the most common ferrous material MR sensors are made of. A single sensing element consists of a thin Permalloy film deposited on a silicon wafer. Usually the alloy film is completed as a pattern of meanders (see Figure 17) to achieve an as high as possible base resistance of the element. A MR sensor incorporates no moving parts.

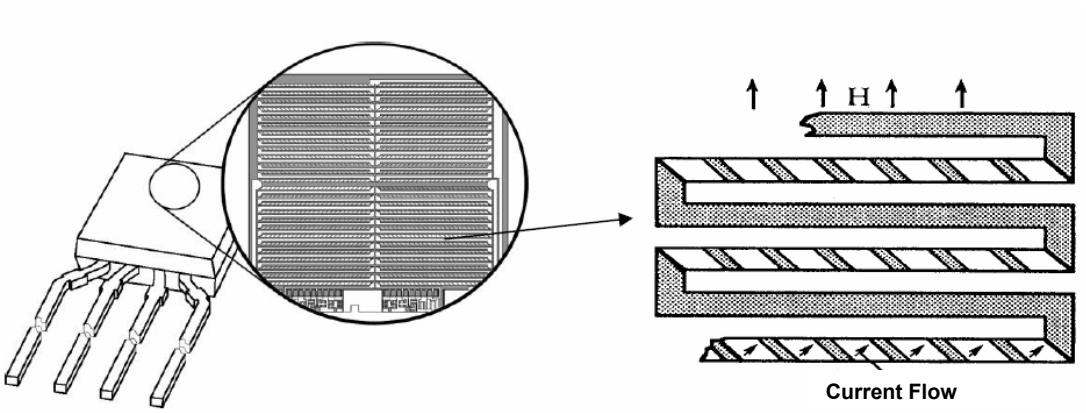

Figure 17 – Typical ferrous material film pattern.[16]

"*During manufacturing, the easy axis (preferred direction of magnetic field) is set to one direction along the length of the film. This allows the maximum change in resistance for an applied field within the permalloy film"*[20], and consequently defines sensor's zero sensing direction but also reduces the hysteresis effect.

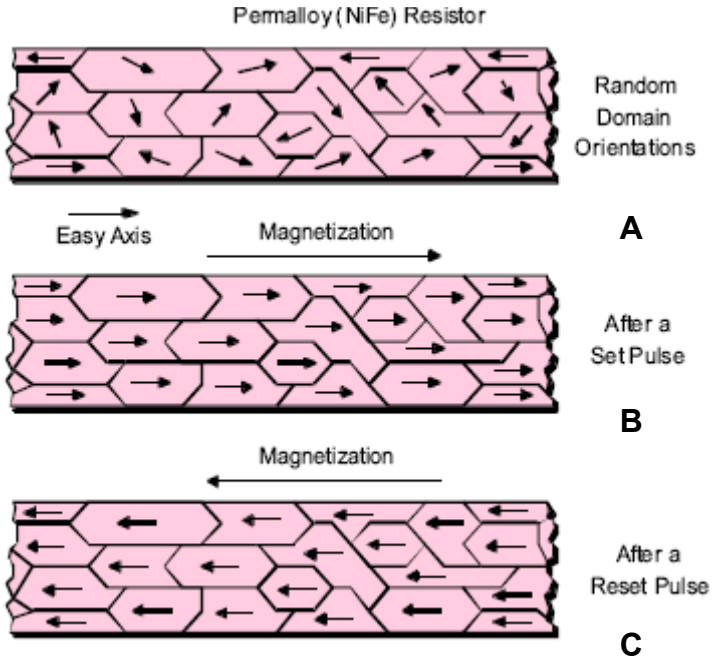

Figure 18 – Set and reset of a MR sensor after been affected by a large, magnetic, disturbing field.[20]

"*When MR sensors exposed to a magnetic disturbing field*" (strong magnetic field of more than 10 gauss) ", *the sensor elements are broken up into randomly oriented magnetic domains that leads to sensitivity degradation.*" See Figure 18A. "*A current pulse (set) with a peak current above minimum current in spec through the Set/Reset strap will generate a strong magnetic field that realigns the magnetic domains in one direction*." Depicted in Figure 18B. "*This will ensure a high sensitivity and repeatable reading. A negative pulse (Reset) will rotate the magnetic domain orientation in the opposite direction*" (Figure 18C) ", *and change the polarity of the sensor outputs. The state of these magnetic domains can retain for years as long as there is no magnetic disturbing field present*."[20]

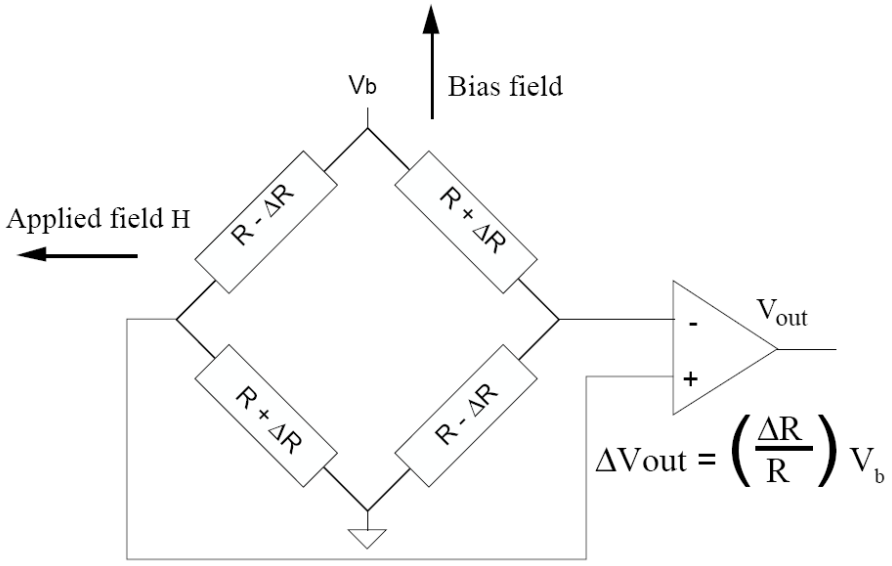

Figure 19 – Magnetoresistive transducer.[17]

A single MR sense element is rarely used. Usual applications make use of four resistive strips interconnected to a simple resistive bridge (Wheatstone bridge). The polarity of the resistors is pairwise diagonally aligned. Figure 19: "*The resistance, R, of all four magnetoresistors is the same. The bridge supply, V_b, causes current to flow through the resistors. A crossed applied field, H, causes the magnetization in two of the oppositely placed resistors to rotate towards the current, resulting in an increase in the resistance, R. In the remaining two oppositely-placed resistors magnetization rotates away from the current resulting in a decrease in the resistance, R. In the linear range the output becomes proportional to applied field $\Delta V = S\ H\ V_b$. The range of the transfer function is inversely proportional to the sensitivity.*"[17]

MR sensors are affordable in price and offer high sensitivity and reliability. As a result a number of applications, especially low field magnetic sensing ones, can be found. For example, sensing of angle, tilt, level, length, distance, RPM, flow, current, but also compassing applications, navigation systems, or traffic detection are typical MR sensor applications.

CoPilot® is equipped with two orthogonally mounted MR sensors to monitor earth's magnetic field for rotational rate and direction measurements. MR sensors are susceptible to influences of nearby ferrous objects and unwanted magnetic field interferences. Both, ferrous objects and magnetic hotspots, are present while drilling a well. Even the flow of conductive mud can induce a magnetic field and adversely affect magnetometer readings. For these reasons, magnetometer readings should be critically investigated for their reasonableness prior any use. However, as MR sensors get not permanently harmed by unwanted magnetic influences, data quality can recover after a set or reset pulse and therefore temporary pure quality data does not a priori preclude a whole MR sensor data set. Some error types of MR sensors (basically also valid for some other types) will be discussed later in this work.

4.2 Accelerometers

CoPilot® is equipped with two triaxial accelerometer modules, each consisting of three individual but constructional identical acceleration sensing elements. Their purpose, position, and structure is covered in detail by one of the following chapters. This subchapter deals with the internal design and operation principle of a single sensing element as actual acceleration data source.

In contrast to the MR sensor type presented above with no moving parts, this type of accelerometer is basically a tiny plate-type capacitor with one flexible mounted plate that is allowed to achieve a certain degree of tilt. The sensed parameter is the capacitance. Capacitance changes due to variations in the gap between both capacitor plates as a result of an applied acceleration force.

"*An capacitive approach allows several benefits when compared to the piezoresistive sensors used in many other accelerometers. In general, gaseous dielectric capacitors are relatively insensitive to temperature. Although spacings change with temperature due to thermal expansion, the low thermal coefficient of expansion of many materials can produce a thermal coefficient of capacitance about two orders of magnitude less than the thermal coefficient of resistivity of doped silicon. Capacitance sensing therefore has the potential to provide a wider temperature range of operation, without compensation, than piezoresistive sensing. As compared with piezoelectric type accelerometers which require a dynamic input of some minimum frequency to generate a response*,"..."*capacitive sensing allows for response to DC accelerations as well as dynamic vibration. This allows the capacitive accelerometer to be used in a wider range of applications*."[21]

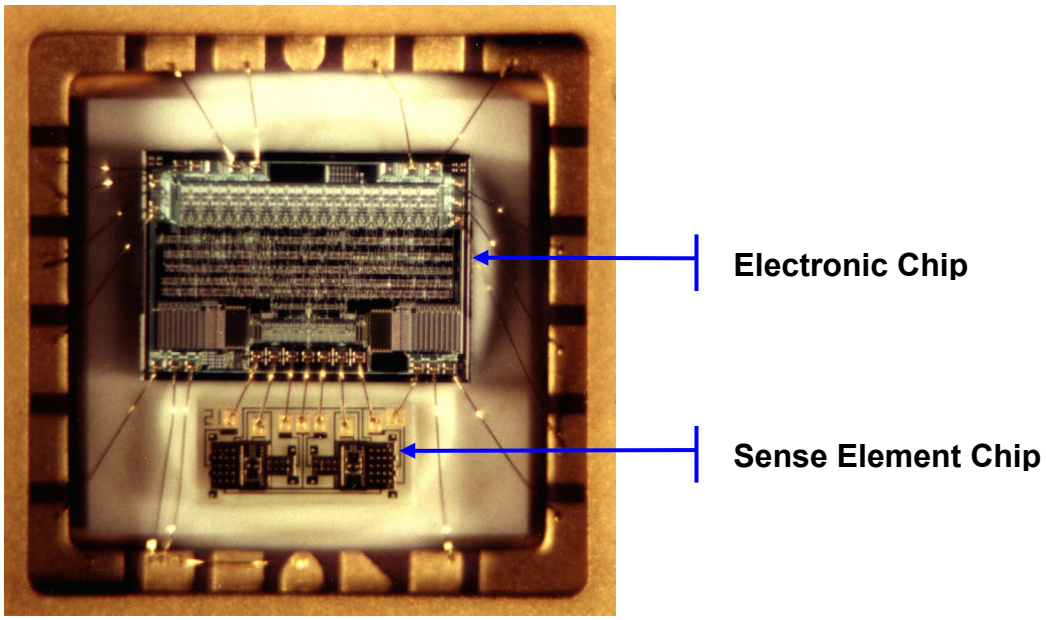

Figure 20 – Close-up of packed accelerometer (modified after [21]).

Figure 21: "*The sense element wing is a flat plate of nickel supported above the substrate surface by two torsion bars attached to a central pedestal. The structure is asymmetrically shaped so that one side is heavier than the other, resulting in a*

center of mass that is offset from the axis of the torsion bars. When an acceleration force produces a moment around the torsion bar axis, the plate or wing is free to rotate, constrained only by the spring constant of the torsion bars."[21]

"*On the substrate surface, beneath the sense element wing, two conductive capacitor plates are symmetrically located on each side of the torsion bar axis. The upper wing and the two lower capacitor plates on the substrate form two air-gap variable capacitors with a common connection. This creates a fully active capacitance bridge. When the wing rotates about the torsion bar axis, the average distance between the wing and one surface plate decreases, increasing the capacitance for that plate, while the distance to the other plate increases, decreasing its capacitance*."[21] A variety of materials can be use for manufacturing this basic design.[21]

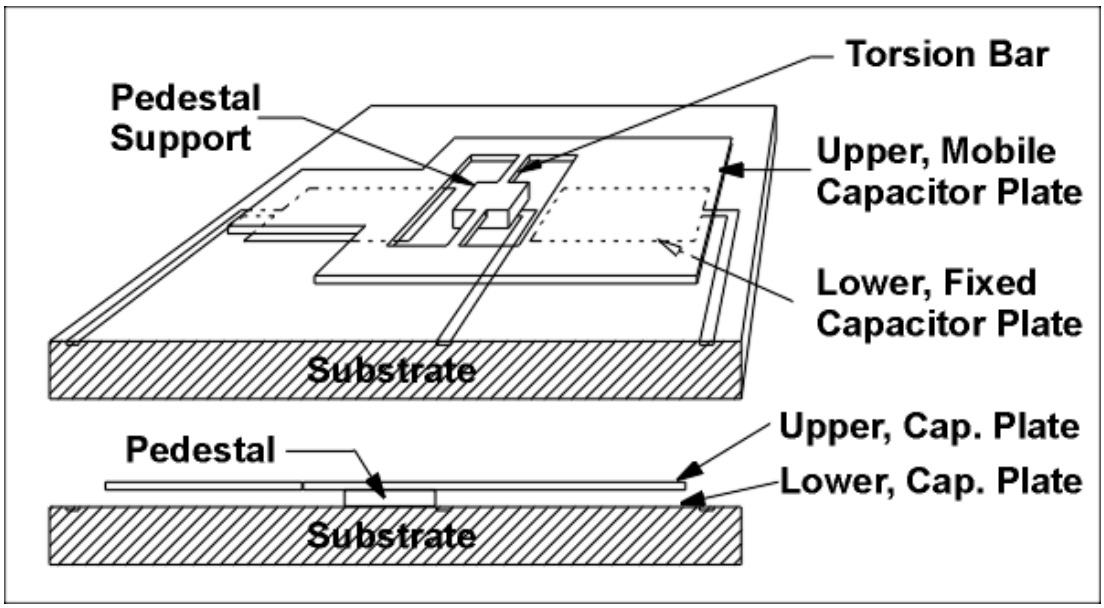

Figure 21 – Basic structure of the sense element.[21]

"*The sense element wings are approximately 1000 microns long by 600 microns wide and 5 to 10 microns thick. The wing to substrate spacing of about 5 microns results in a capacitance from the wing to each lower plate of about 0.15 pF. The sensitivity of the sense elements (the ratio of deflection to acceleration) is determined by the mass of the sense element, the distance from the center of mass to the torsion bar axis, and the torsion bar stiffness. Mechanical stops can be added at the four outside corners of each sense element wing to provide additional protection from overstress of the torsion bars under high shock conditions. Each complete sense element chip contains two wings for a total of four sensing capacitors*."[21]

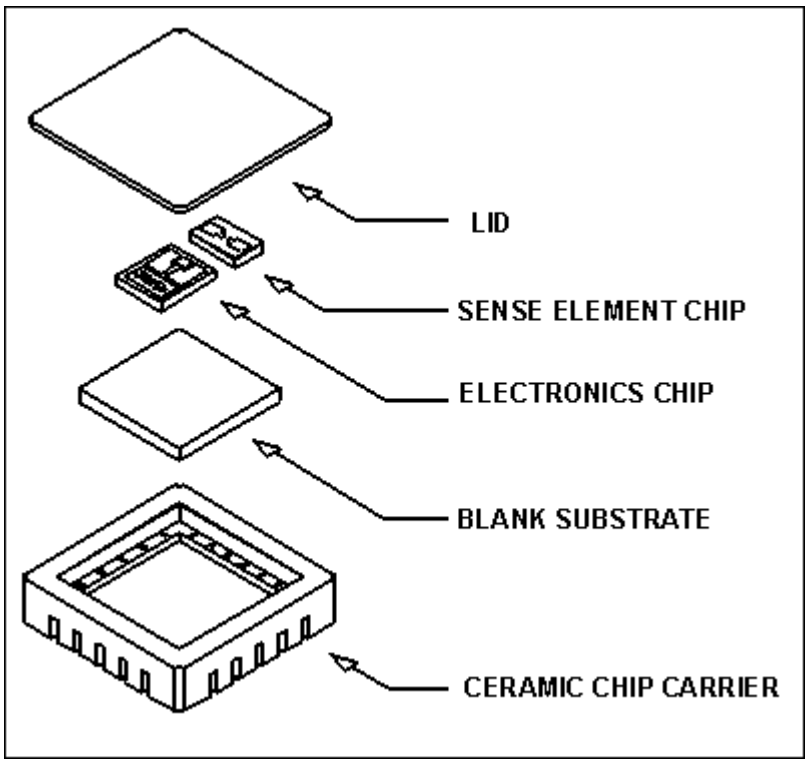

Figure 22 – Accelerometer packaging.[21]

Besides drilling applications where such sensors are used for inclination sensing and vibration monitoring, typical application for this accelerometer type are e.g. air bags, active suspension, adaptive brakes, shipping records, robotics, crash testing, machine control, military applications and many more.

A note concerning the employment of such an accelerometer type in CoPilot®: the actual in CoPilot® incorporated accelerometer model's absolute maximum ratings for operating temperature are -55 to +125 [°C]. Whereas, the operation temperature limit of CoPilot® is specified at +150 [°C]. Thus, in the temperature range from +125 till +150 [°C] CoPilot® is still operating within its specifications limits while its accelerometer modules are already exposed to temperature levels above their specifications. How operations for an extended period of time at or above the absolute maximum ratings would affect sensors reliability cannot be stated. A tool failure analysis with main emphasis on high temperature runs together with laboratory heating test could provide an answer about possible adverse effects.

4.3 Strain Gauges

A strain gauge (S/G) changes its electrical resistance proportionally to the applied strain.[22] The physical principle a S/G makes use of is rather simple. Every electrical conductor (e.g. a wire) has a certain electrical resistance. The size of the resistance depends on type of material, temperature, and shape of the conductor. The important parameter for a S/G is the conductor's shape. An increase in conductor length causes the resistance to increase as well. While on the other hand, with growing cross-

sectional conductor area the electrical resistance is decreasing. Consequently, if a conductor is elongated, i.e. the length is increased while the cross-section decreases, its resistance goes up. This effect can be observed also vice versa as long as the elastic region of the conductor material is not exceeded: the length of the conductor is reduced under compression with an simultaneous cross-sectional gain, which results in a diminished electrical resistance. This simple conductor-shape-resistance relation is used for S/Gs. The ratio of resistance change to strain is called gauge factor (strain factor, k-factor). This factor is a measure for a strain gauge's sensitivity and is material dependent. S/Gs are used for strain ε larger than 10^{-5} [-].[25]

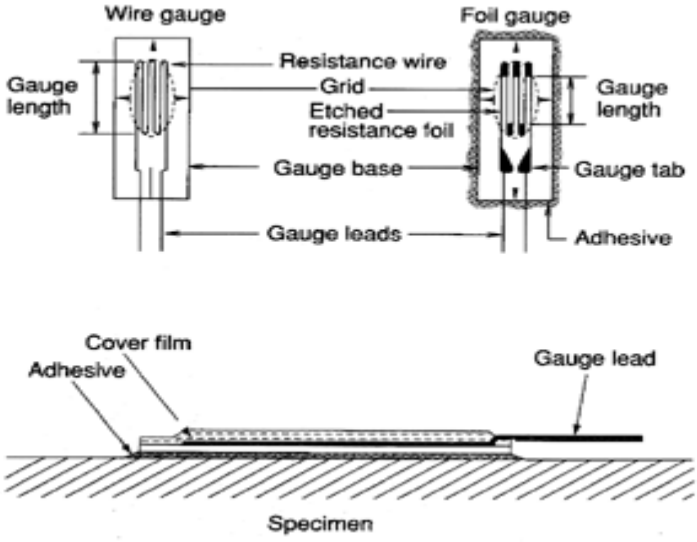

Figure 23 – Strain gauge (two types: wired gauge, foil gauge).[24]

The conductor is predominately made of constantan because of its high thermal stability. Other conductor materials are platinum or alloys of platinum and iridium.

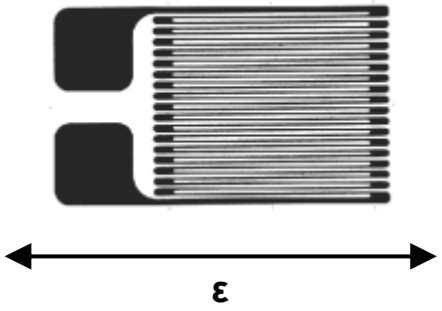

Figure 24 – S/G metallic sensing pattern and direction (modified after [23]).

"*The most common type of strain gauge consists of an insulating flexible backing which supports a metallic foil pattern.*"[18] The conductor pattern is quite similar to that of MR sensors, see Figure 24. Either a wire (old) or a thin foil (new) is deposited in meanders on the flexible backing and protected by a cover film. Sensing direction is parallel to the metallic strips. An elongation or compression normal to them would only insignificantly change the resistance of the whole conductor. Several such grids can be combined on a single gage base to measure strain in multiple directions

(Figure 25). "*The gauge is attached to the object by a suitable adhesive.*"[18] "*As the object is deformed, the foil is deformed, causing its electrical resistance to change.*"[18]

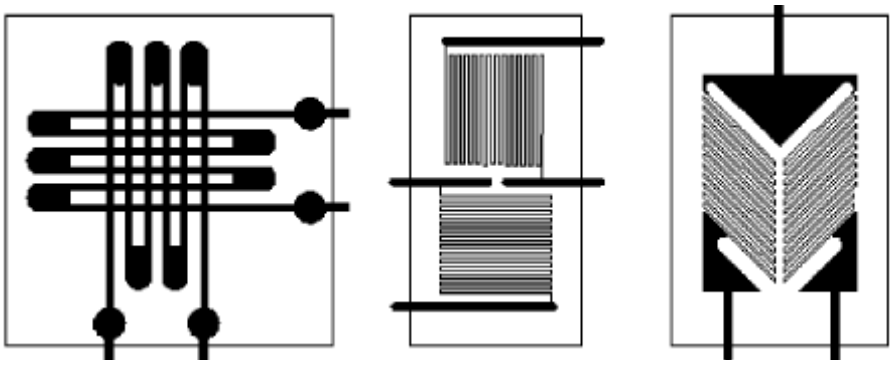

Figure 25 – Three examples of a 2-grid Rosette.[25]

For S/G measurements usually a resistor bridge (Wheatstone bridge) is utilized. Three circuit layouts are applied: with one (quarter-bridge), two (half-bridge), or four S/Gs (full-bridge), see Figure 26. The remaining resistors of each bridge layout are fixed resistors. For the half-bridge circuit layout both S/Gs (R_1 and R_2) need to be mounted on the specimen in a manner that R_1 is under tension while R_2 is compressed. At a full-bridge design R_1 and R_4 must be elongated and R_2 and R_3 compressed at the same time.

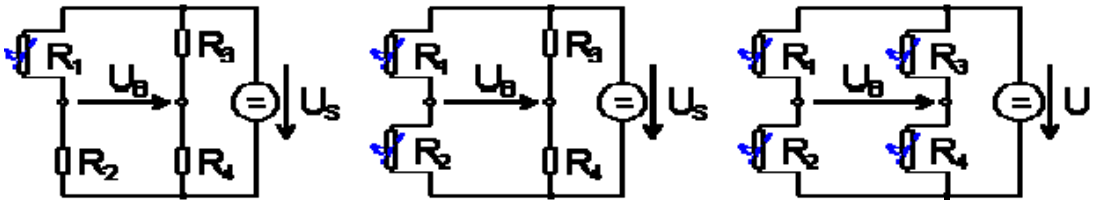

Figure 26 – Bridge layouts with one, two, or four S/G(s) (from left to right).[26]

Temperature influence is very critical when regarding strain measurments with S/Gs. Materials expand (object to be measured and S/G as well) with increasing temperature and unfortunately in a range which S/Gs detect. The specific resistance is also a function of temperature. A glued on S/G is not able to distinguish between strain due to temperature expansion or actual stress related strain. An output signal is produced with actually no mechanical load applied (temperature output). If temperature cannot be controlled, corrective measures are obligatory.

The temperature output of a strain gauge can be controlled e.g. "*through material properties such that the temperature effects are largely compensated*"[22], calculative cancellation of known thermally generated resistance changes based on additionally sensed temperature[27], or employment of "*an identical compensating or "dummy" gage - mounted on an unstrained specimen made from the identical material as the test part, and subjected always to the same temperature as the active gage*"[28] but these three conditions are not easy to be ensured.

In CoPilot® S/Gs are employed for WOB, torque on bit (TOB), and bending moment measurements. All data is compensated for temperature as the tool is exposed to a continuously changing temperature environment while oilwell drilling. Additionally, WOB readings are compensated for internal, external, and hydrostatic pressure as these are responsible for tensile and tangential stresses in the collar of CoPilot®.

"*In standard applications, strain gauges are very often glued directly onto the sub area where the strain is to be measured. Since it would be very time-consuming for the assembling and maintenance of the tool to glue the strain gauges directly onto the sub*"[8], new screw-on-type strain gauge transducers have been designed for CoPilot® application. "*Due to this design, the time needed for assembling a tool is approximately three days shorter than for prototype tools where glue-on-type strain gauges were used. The same applies to the maintenance for each tool where strain gauges need to be replaced*."[8]

4.4 Temperature and Pressure Transducers

CoPilot® is also equipped with temperature and pressure transducers to sense annular and bore conditions. Both are not further discussed in this text for the reason that neither temperature nor pressure data is explicitly used later on. No processing of any kind of that data have been performed for this work which therefore would recommend a detailed data acquisition path analysis. Anyway, temperature and pressure measurements do influence almost every other data channel as most of them are compensated for temperature or pressure effects or even both. Consequently, not to dedicate these sensors their own subchapter is not a downgrade of their importance for total tool functionality but simple a matter of the scope of this work.

5 Data Types Overview

This work is done on history data. Primarily, special events covering research memory data – often called high-speed data – collected by CoPilot® have been analyzed together with by CoPilot® downhole processed FSD. In addition, surface data have been used to gain supplementary information about drilling operations while high-speed data intervals had been recorded. Besides these data sets also run/well documentations and reports have been studied to figure out known problems and pursued targets. This chapter provides a short overview of the different data types used.

5.1 Research Memory/High-Speed Data

This data type represents the primary information source for downhole conditions. RMD is raw sensor data at high sample rates – usually 100 or 200 [Hz] but also 40 [Hz] are possible. It is collected in a post-event mode. That means, first data is sensed and temporary stored in a circular buffer and subsequently only written to memory by call. Data storage is induced from surface and not automatically nor permanently recorded by the tool itself. This is achieved by rising the drillstring RPM above a preset RPM threshold for an in advance defined period of time. Both thresholds are adaptable to specific drilling parameters. As data storage is externally triggered, an individual high-speed data set is named trigger.

The length of a high-speed trigger depends on the defined sample rate for storage. For example, a trigger with twelve sensor channels and a sample frequency of 100 [Hz] is 435 seconds long and one recorded at 200 [Hz] with the same number of channels is covering only a 215 seconds lasting interval.

Besides the sample rate also the number of sensor channels to store per trigger can be varied. Optional there are twelve channels available: x and y magnetometers; x, y, z, and tangential acceleration; x and y bending moment; WOB; TOB; annular and internal hydraulic pressure. Annular and internal temperature are not available as high-speed data. According to the intention of the application of CoPilot®, from just a single data channel up to the whole number of twelve channels can be selected for on-board storage during the pre-run tool calibration. A reduced number of channels per trigger enlarges the length of the trigger.

Triggers that have captured especially rare events, even if initially not intended to do so, can become highly beneficial for research and development later on. In such cases only a limited number of recorded data channels would impair analyses. For this reason and due to corresponding experiences made during the course of this work, it must be recommend to permanently store the whole set of data channels.

A further option regarding high-speed data unfortunately does not ease high-speed data handling. The file format of a trigger's high-speed data channels can either be defined as a binary format (.dat) or as ASCII (.asc) format. Only ASCII format offers the possibility of a quick data check as only that kind of files are readable by every text editor (e.g. WordPad or TextPad). Larger data/trigger quantities therefore are more comfortable to handle in ASCII format. What is more, whenever a program uses high-speed data for input, appropriate routines for both formats need to be implemented.

```
 1  5.102190e+003
 2  6.238981e+003
 3  5.960863e+003
 4  7.699320e+003
 5  8.128149e+003
 6  5.100332e+003
 7  5.201557e+003
 8  6.813756e+003
 9  6.372891e+003
10  6.268122e+003
11  7.337030e+003
12  6.967064e+003
```

Figure 27 – A few lines of a channel data file of a high-speed trigger (ASCII format; first column is just the line count of the text editor and not part of the data file itself).

In neither of the formats does the data have timestamps – a timestamp is the number of seconds since 12:00 AM January 1st, 1900. Furthermore, individual channel data files do not have a header that lists information like sample rate, data channel or physical unit (Figure 27). A trigger regarded on its own is a hardly useable set of files. To "decode" them an additional file, the research memory data file (extension: .RMD; ASCII format), and basic knowledge about CoPilot® is necessary. Which file contains which channel's data can be concluded from the file name: a data file is named with the mnemonic of the respective data channel. The physical units of data listed in these files are always in accordance with S.I. (see Table 1) – as throughout all CoPilot® data. Sample rate and start time of the trigger are stored in the RMD-file where also some additional trigger information can be found (Figure 28).

To correlate data coming from a variety of sources it is essential to ensure an accurate sample time assignment or in this respect better to call reassignment. When considering the first and the last date line of an individual data channel in a RMD-file it emerges that the time interval between these two dates is five seconds shorter than the in the header given sample time. When taking into consideration all other timestamps in between, it turns out that timestamps are only stored every five seconds. Hence, an single timestamp is representing a data interval five seconds in length. As a five seconds data block is time stamped after it has been recorded, the timestamp belongs to the last five seconds of data sampled and not to the future five data seconds. Therefore, the first high-speed data value had actually been measured five seconds before the date listed first in the RMD-file.

All RMD-files used during this work have been comprehensible and consistent. Each file has contained equally spaced timestamps. Irregularities of any kind in header nor data could not have been observed. In general, the package high-speed trigger data and RMD-file has appeared of high quality. Nevertheless, in regard to an improved

time consistency screening and a reduction of potential time error sources at later high-speed data processing, it must be recommended to add an additional file to the high-speed trigger data while on-board data storage, which contains the timestamps of every single data value, i.e. not every 5 seconds but every 1/sample frequency seconds the date is saved. This might be done in excess to the RMD-file or instead of it as e.g. its header information could also be read out from the corresponding RCD-file (research configuration data). The mentioned benefits should offset the additionally used memory space.

```
Co-Pilot RMD Header File
Reading from FLASH MEMORY DUMP FILE 'Cop_Run3.MEM'

RPM Max Trigger = 150.000
Check Time = 60
Trigger Time = 20
SampleTime = 215
Sample Rate = 200Hz
Channels From RCD = 12 (Actual Count = 12)


 Channel   Filename     Description
   16    Cop_Run3.C16    <Lateral (x-axis) Magnetometer>
   15    Cop_Run3.C15    <Lateral (y-axis) Magnetometer>
   14    Cop_Run3.C14    <Lateral (x-axis) Accelerometer>
   13    Cop_Run3.C13    <Lateral (y-axis) Accelerometer>
   12    Cop_Run3.C12    <Lateral (z-axis) Accelerometer>
   11    Cop_Run3.C11    <Tangential Accelerometer>
   10    Cop_Run3.C10    <Lateral (x-axis) Bending Moment>
    9    Cop_Run3.C09    <Weight>
    8    Cop_Run3.C08    <External Hydraulic Pressure>
    7    Cop_Run3.C07    <Lateral (y-axis) Bending Moment>
    6    Cop_Run3.C06    <Torque>
    5    Cop_Run3.C05    <Internal Hydraulic Pressure>

Record      1
Channel     Read       Write      (   Timestamp) Time/Date Expanded
   16     4233416           0     (  1145198097) Sun Apr 16 14:34:57 2006
   16     4281416        4000     (  1145198102) Sun Apr 16 14:35:02 2006
   16     4329416        8000     (  1145198107) Sun Apr 16 14:35:07 2006
   16     4377416       12000     (  1145198112) Sun Apr 16 14:35:12 2006
   16     4425416       16000     (  1145198117) Sun Apr 16 14:35:17 2006
   16     4473416       20000     (  1145198122) Sun Apr 16 14:35:22 2006
   16     4521416       24000     (  1145198127) Sun Apr 16 14:35:27 2006
   16     4569416       28000     (  1145198132) Sun Apr 16 14:35:32 2006
   16     4617416       32000     (  1145198137) Sun Apr 16 14:35:37 2006
   16     4665416       36000     (  1145198142) Sun Apr 16 14:35:42 2006
   16     4713416       40000     (  1145198147) Sun Apr 16 14:35:47 2006
   16     4761416       44000     (  1145198152) Sun Apr 16 14:35:52 2006
   16     4809416       48000     (  1145198157) Sun Apr 16 14:35:57 2006
```

Figure 28 – RMD-file header plus a few date lines of the first trigger.

5.2 Processed/Five Second Data

In contrast to high-speed data, which cover events only very limited in time, five second data provide a complete tool run downhole condition documentation. As the name indicates, FSD is sampled every 5 seconds.

FSD-files are large ASCII formatted data files. A FSD-file has one header line which labels the listed 60 columns. The number of rows depends on the period of time the

tool was operated. Usually, FSD-files have several tens of thousands of rows. Each row and hence each FSD-value of a row is tagged with time twice and in addition serially numbered. FSD-values therefore are easily to pick as either just the timestamp, date (down to seconds), or the unique sequence number is needed besides the respective column number.

Three columns are for mapping. Another ten columns list the diagnostics which are also evaluated with a sample frequency of 0.2 [Hz] and thus forming a part of FSD. The remaining 47 columns are filled up with static values calculated from raw data of the different channels. Most frequently average, maximum, and minimum values of a data channel or RPM per frame (five seconds) are stored but also root mean square (RMS) and root mean cube (RMC) values are sometimes determined.

These figures are based on 1000 Hertz raw data. That is the reason, why in most cases for example a maximum value picked at high-speed data (trigger with sample frequency of 200 [Hz] or lower) does not correlate with the maximum value given by FSD for the same time frame/interval. Unfortunately, a double-check regarding a correct time correlation of high-speed data with FSD is therefore impeded. Again, the importance of a highly accurate data sample time tagging, as the only concrete correlation scale, must be emphasized in this respect.

FSD occasionally shows time gaps between two consecutive data rows which are significantly longer than five seconds. These can be explained with normal drilling practices or CoPilot®'s operation principle. Whenever a stand of drill pipes is drilled off and another is added, mud circulation stops for a few minutes while connection is made. Downhole power supply of BHA tools is provided by a downhole generator actuated by a mud driven turbine. No circulation therefore causes a shut down of CoPilot®'s power supply and lastly data sensing and storage. This is the reason for relatively regularly occurring gaps of a couple of minutes in the data. However, pumps off, for whatever reason, always generates large gaps in FSD. A comparison with surface data can help to figure out circulation related FSD gaps.

CoPilot® itself produces time gaps with lengths of integer multiples of five seconds and in the range of some tens of seconds whenever a trigger is taken. Chronological such gaps are located exactly after a trigger interval. These gaps originate from the high-speed data transfer from the circular buffer to on-board memory as while this time span FSD cannot simultaneously be recorded.

These types of gaps come along with usual drilling and tool operations and are normal. Peculiar are gaps that are six or even only four seconds in length (Figure 30). Such intervals are quite frequent and an explanation for them could not be found during this work. Furthermore, a certain occurrence pattern have not been observed as well.

A flow rate related reason can most likely be excluded as such tiny variations (±1 second) of the standard five second interval are probably not pump induced. A problem at CoPilot®'s real-time clock, perhaps a roundoff error, appears as more reasonable. A clue for that assumption is the sometimes pure correlation of timestamps stored in the RMD-file with those of the FSD-file. It is relatively common that a trigger's start and/or stop timestamp(s) (from RMD-file) cannot be

found again at FSD, see Figure 29 and Figure 30. This is quite astonishing as both time data are generated by the same clock. Such discrepancies become critical when both data sets should be correlated. Small FSD sample interval variation should be subject to further analyses.

```
    5     3646078      166000     (  1124619057) Sun Aug 21 10:10:57 2005
    5     3670078      168000     (  1124619062) Sun Aug 21 10:11:02 2005
    5     3694078      170000     (  1124619067) Sun Aug 21 10:11:07 2005
    5     3718078      172000     (  1124619072) Sun Aug 21 10:11:12 2005

Record       2
Channel      Read       Write      (  Timestamp) Time/Date Expanded
   16     4961866      174000     (  1124679571) Mon Aug 22 02:59:31 2005
   16     4985866      176000     (  1124679576) Mon Aug 22 02:59:36 2005
   16     5009866      178000     (  1124679581) Mon Aug 22 02:59:41 2005
   16     5033866      180000     (  1124679586) Mon Aug 22 02:59:46 2005
   16     5057866      182000     (  1124679591) Mon Aug 22 02:59:51 2005
   16     5081866      184000     (  1124679596) Mon Aug 22 02:59:56 2005
   16     5105866      186000     (  1124679601) Mon Aug 22 03:00:01 2005
   16     5129866      188000     (  1124679606) Mon Aug 22 03:00:06 2005
   16     5153866      190000     (  1124679611) Mon Aug 22 03:00:11 2005
   16     5177866      192000     (  1124679616) Mon Aug 22 03:00:16 2005
   16     5201866      194000     (  1124679621) Mon Aug 22 03:00:21 2005
   16     5225866      196000     (  1124679626) Mon Aug 22 03:00:26 2005
   16     5249866      198000     (  1124679631) Mon Aug 22 03:00:31 2005
   16     5273866      200000     (  1124679636) Mon Aug 22 03:00:36 2005
   16     5297866      202000     (  1124679641) Mon Aug 22 03:00:41 2005
```

Figure 29 – RMD-file: start time (red circle) of trigger 2 of a CoPilot® run.

```
1124679545,13327,0,1,1,1,0,[illegible]0,-1.0000,Mon Aug 22 02:59:05 2005
1124679550,13328,0,1,1,1,0,[illegible]1.0000,-1.0000,Mon Aug 22 02:59:10 2005
1124679555,13329,0,1,1,0,0,[illegible].0000,-1.0000,Mon Aug 22 02:59:15 2005
1124679560,13330,1,1,1,0,0,[illegible]0,-1.0000,Mon Aug 22 02:59:20 2005
1124679565,13331,0,1,1,1,0,[illegible]0,-1.0000,Mon Aug 22 02:59:25 2005
1124679570,13332,0,1,0,0,0,[illegible].0000,-1.0000,Mon Aug 22 02:59:30 2005
1124679575,13333,0,1,0,0,0,[illegible].0000,-1.0000,Mon Aug 22 02:59:35 2005
1124679580,13334,1,1,0,0,0,[illegible]-1.0000,-1.0000,Mon Aug 22 02:59:40 2005
1124679585,13335,1,1,0,1,0,[illegible]00,-1.0000,Mon Aug 22 02:59:45 2005
1124679590,13336,1,1,0,1,0,[illegible]00,-1.0000,Mon Aug 22 02:59:50 2005
1124679595,13337,1,1,0,1,0,[illegible]-1.0000,-1.0000,Mon Aug 22 02:59:55 2005
1124679600,13338,0,1,0,1,0,[illegible]1.0000,-1.0000,Mon Aug 22 03:00:00 2005
1124679605,13339,1,1,0,1,0,[illegible]1.0000,-1.0000,Mon Aug 22 03:00:05 2005
1124679610,13340,0,1,0,1,[illegible]000,-1.0000,Mon Aug 22 03:00:10 2005
1124679616,13341,0,1,0,1,[illegible]000,-1.0000,Mon Aug 22 03:00:16 2005
1124679621,13342,1,1,0,1,[illegible]-1.0000,-1.0000,Mon Aug 22 03:00:21 2005
1124679626,13343,0,1,0,1,[illegible]-1.0000,-1.0000,Mon Aug 22 03:00:26 2005
1124679631,13344,1,1,0,0,[illegible]-1.0000,-1.0000,Mon Aug 22 03:00:31 2005
1124679636,13345,1,1,0,0,[illegible]0000,-1.0000,Mon Aug 22 03:00:36 2005
1124679641,13346,1,1,0,0,[illegible]0000,-1.0000,Mon Aug 22 03:00:41 2005
```

Figure 30 – A cutout of the first and last data columns of the FSD-file corresponding to Figure 29. Red: closed to trigger start time timestamp (first column) and date; blue: time gap of six seconds.

For this work a large number of CoPilot® runs and an even larger number of triggers had been scanned. Such a vast quantity of data cannot be handled manually anymore. For this purpose a MATLAB® routine has been written that quickly checks all available data (high-speed, FSD, surface) for consistency.

At data with high sample rates (≥100 [Hz]) a shift by up to a couple of data points is not seen as detrimental for the results of this work nevertheless any offset is not desirable. Time shifts of larger fractions of a second become critical and therefore must be detected and either corrected or in worst case the whole data sets must be ruled out.

The routine itself is not further discussed here but an example report of such a consistency check is given below:

```
------------------------------------------------------------------
DATA CHECK REPORT--------------------------------------------------
------------------------------------------------------------------
HIGH SPEED RAW SENSOR DATA:
    Trigger (specified by user): 6
    Sample rate: 200 Hz
    Trigger length: 215 sec.
    Available sensor channels:
        1.   DWOB
        2.   DTOB
        3.   MAGX
        4.   MAGY
        5.   ACLX
        6.   ACLY
        7.   ACLZ
        8.   ACLT
        9.   DBX
        10.   DBY
        11.   INP
        12.   ANP

PROCESSED DATA (GENERAL):
    Total number of triggers (RMD-file): 13
    Frame Sample Rate (FSR, specified by user): 5 sec.
    Processed data is NOT time consistent in the FSD-file!
        99.42483418% of the processed data are equally spaced by FSR.
        Time spans of two consecutive frames vary from 4 to 19218
        seconds.
PROCESSED DATA while TRIGGER 6:
    The frame sample rate/processed data are equally spaced while
    trigger 6.
    RMD- and FSD-file start times do NOT correlate at trigger 6!
        The closest by value of the FSD-file is taken!
            RMD trigger start timestamp: 1145202193
            Taken FSD trigger start timestamp: 1145202192 (Seq.:
            20271)
            Difference: -1 sec.
    RMD- and FSD-file stop times do NOT correlate at trigger 6!
        The closest by value of the FSD-file is taken!
            RMD trigger stop timestamp: 1145202403
            Taken FSD trigger stop timestamp: 1145202402 (Seq.:
            20313)
            Difference: -1 sec.

SURFACE DATA (GENERAL):
    Surface data is NOT consistent in time!
        Most frequent sample rate (assumed surface data sample rate,
        SSR): 10 sec.
        56.91800878% of the surface data are equally spaced by SSR.
        Time spans of two consecutive surveys vary from 0 to 376
        seconds.
SURFACE DATA while TRIGGER 6:
    The surface data is NOT consistent in time while trigger 6!
    There are time gaps of:
        4 sec. between t = -1 to t = 3 sec.
        1 sec. between t = 23 to t = 24 sec.
        9 sec. between t = 24 to t = 33 sec.
```

```
        1 sec. between t = 53 to t = 54 sec.
        9 sec. between t = 54 to t = 63 sec.
        1 sec. between t = 83 to t = 84 sec.
        9 sec. between t = 84 to t = 93 sec.
        6 sec. between t = 113 to t = 119 sec.
        4 sec. between t = 119 to t = 123 sec.
        6 sec. between t = 143 to t = 149 sec.
        4 sec. between t = 149 to t = 153 sec.
        1 sec. between t = 173 to t = 174 sec.
        9 sec. between t = 174 to t = 183 sec.
        6 sec. between t = 213 to t = 219 sec.
-----------------------------------------------------------------
-----------------------------------------------------------------
```

5.3 Surface Data

As the data check report above has already indicated, surface data is of varying quality. Surface data is not sampled by CoPilot® but usually by a third party at the well site. In general, it is not used for downhole analyses but for verification of downhole records. For example, if low high-speed downhole WOB readings have been recorded, first of all it must be checked if the bit is actually on bottom (bit depth to measured depth (MD)) and additionally what the surface WOB data are looking like. Furthermore, surface data usually describe performed drilling operations in more detail than relative short and generally composed drilling reports do.

Data quality is a big issue at surface records. Data sets of wells located all over the world have been used for this work. Hence, rig data came from a number of rigs of a variety of companies with a similar diversity of data sampling standards. Unfortunately, surface data quality and especially its sample rate have been of very low standard across the board. In some cases one might get the impression that data recording were manually triggered as sample intervals change that much. A surface sample rate of 10 seconds, if kept almost constant, represents already best-in-class sample rate. Rates of 20, 30, or 60 seconds are more common.

Some sampled surface parameters have been such obviously wrong (e.g. frozen or unrealistic values, or simply no rig exists which could have produced such data) that they could be ruled out immediately. What is more, at some data sets imperial and S.I. systems of units are mixed up. Not sticking to either system of units can easily become an error source later on. Even such exotic units like ampere have been used at a surface torque data record (actually it is the unit for strength of electrical current). A straightforward unit conversion in this respect is not possible anymore.

Due to all these limitations surface data is afflicted with, only a selected number of surface parameters have been employed in this work – all converted to S.I. units where necessary:

- MD, [m],
- bit depth, [m],
- block position, [m],

- RPM, [rpm],
- torque, [kNm],
- WOB, [N],
- total pump output, [l/min],
- standpipe pressure, [kPa],
- sate & time.

Date and time is perhaps the best example for what problems not standardized units and formats may create. As data handling and correlation is most often done by computers nowadays, a consistent format is essential. The possibilities to arrange day, month, year, hours, minutes, seconds, and sometimes even calendar day together with their formats are various. Unfortunately, the oil industry is making use of almost all of them. For this reason, it was necessary to write a special routine intended just to read and format dates and time as nearly the complete data handling during this work has been performed with computers. Standardization would save a lot of money in this respect by eliminating possible error sources and unproductive labor inputs.

Regarding CoPilot® service, it should be taken into consideration to permanently sense surface data at a high rate. The description of the whole dynamic system would be considerably eased. This would be most beneficial and recommended for runs where it is indented to take high-speed triggers for research. If this could be done by utilizing a rig's original sensor fleet or if additional transducers would be necessary, needs to be settled. In this respect, also a high frequency ROP measurement should be included to directly relate downhole observed dynamic phenomena to ROP.

6 Tangential Acceleration – Tangential Y-Axis Accelerometers Misalignment

6.1 General Description of Current Vibration Sensing

CoPilot® is provided with two identical triaxial accelerometer modules to sense lateral, axial, and torsional vibrations. The accelerometer modules are mounted on opposing sides equidistant from the centerline of the electronic sub. The electronic sub is, beside top sub and sleeve, one of the three main parts of CoPilot®. As the name indicates, the electronic sub is that part that carries all electronic boards as well as the total quantity of transducers.

Figure 31 – Triaxial accelerometer module.[21]

A photo of an accelerometer module is shown in Figure 31 and mounted, as 3D-graphics, in Figure 32. The sensing directions are symbolized by arrows on the sensor case. Comparison of these two figures reveals that CoPilot® does not retain the same sensing directions as initially marked on the case body by the accelerometer manufacturer.

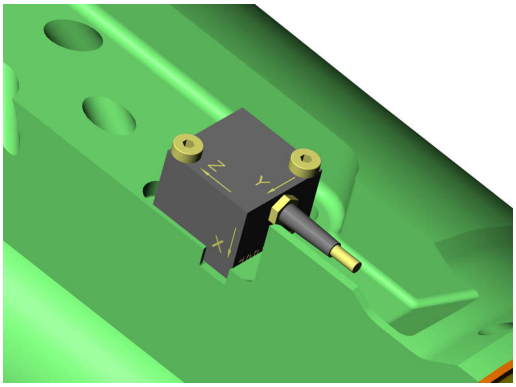

Figure 32 – Mounted triaxial accelerometer module (Z is pointing to the top of the sub and thus in up-hole direction).[38]

The accelerometer modules are symmetrically positioned and exactly aligned with respect to their cases throughout the range of all tool sizes.[39], [40], [41], [42], [43], [44], [45] A 3D-graphics of sensor placement together with the coordinate system of each accelerometer is shown in Figure 33. The depicted coordinate systems are only valid for acceleration sensing. The global coordinate system of CoPilot® (standard positive clockwise x/y/z coordinate system) is the bending coordinate system which is 45° misaligned to the accelerometer coordinate system. This misalignment is corrected during the calibration of the tool by a software based coordinate transfer.[8]

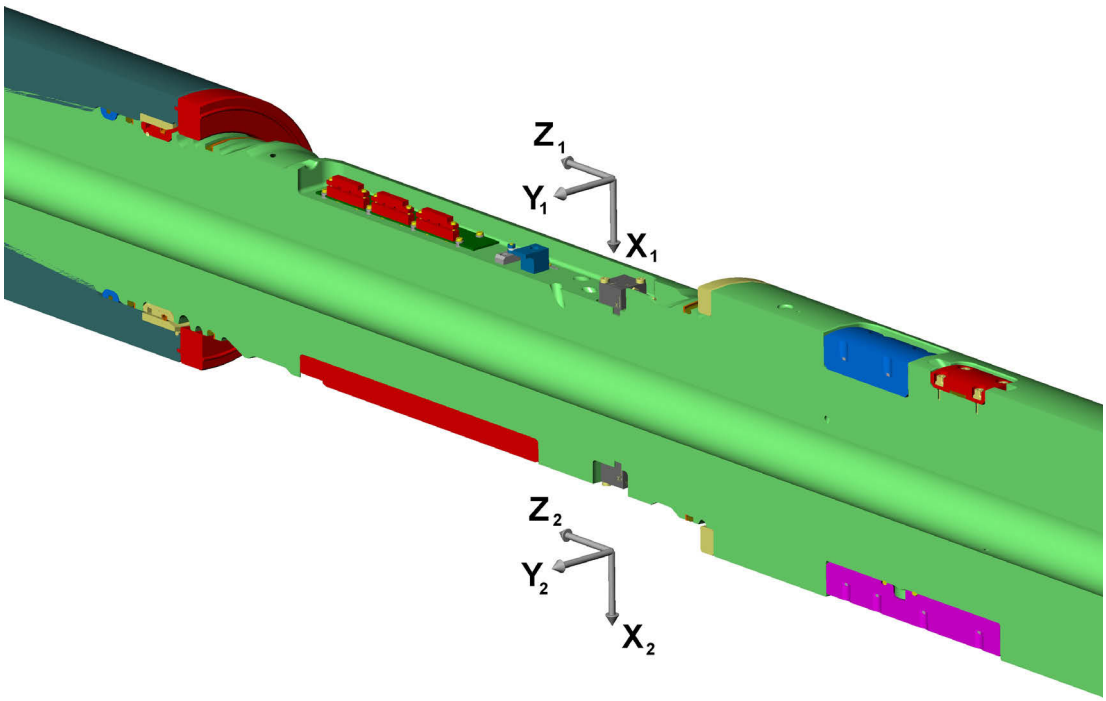

Figure 33 – Triaxial accelerometer placement and accelerometer coordinate system which is not identical with CoPilot's global coordinate system (top of the sub is left).[38]

Additionally, Figure 33 discloses that each direction, x, y, and z, is covered twice. The sensing directions of the triaxial accelerometers are oriented pairwise parallel. Furthermore, positive or respectively negative readings are generated by both sensors

when CoPilot® is accelerated in one direction. Thus, one accelerometer pair is responsible for sensing acceleration in a single direction (x, y, or z), resulting in two readings per direction.

Paired sensor placement is necessary since no possibility exists to place an accelerometer exactly at the center aligned with the tool axis. Along the tool's axis there is the inner bore for mudflow down to the bit. Only one single triaxial accelerometer located in some distance to the rotary axis would also see accelerations caused by RPM changes. A distinct detection of axial accelerations would not be possible. To place a second sensor exactly at the opposite side cures this problem as now rotary induced accelerations cancel out during processing the twofold axial acceleration data. What is more, the ability to measure tangential acceleration implies an accelerometer to be placed a certain radial distance away of the rotary axis anyway. Consequently, all mentioned requirements and limitations are fulfilled with a pairwise off-centered sensor placement.

At elastic or rotating objects – a drillstring is both – acceleration is dependent on its point of survey. To know where acceleration is measured is especially important and significant at tangential acceleration sensing. The paired design of the triaxial accelerometers and thus their different survey points make further data processing necessary. Tangential acceleration as well as axial accelerations are results of adequate combinations of the individual axial accelerometer channels. For the entire tool representative acceleration values are only available after these combinations.

To bring the six individual acceleration readings to one common point for axial and lateral accelerations as well as to get a reference radius for tangential acceleration, reference points need to be defined. A self-evident reference point for axial accelerations at rotating bodies as well as already predefined during sensors placement is a point on the axis of rotation. Its axial position is determined by the intersection point of an imaginary connection line between the sensing points of the two transducers with the rotary axis.

For acceleration in x-, y-, and z-direction this processing is straight forward. The paired sensing directions are parallel. Two pairs are always orthogonal to each other and thus already forming an orthogonal system. Additionally, the sensing point of one accelerometer has the identical radial distance to the reference point as its counterpart on the other side. These conditions enable the simple processing step of just averaging the sensor outputs of a pair and thus receiving the resulting acceleration at the reference point in that direction. See the equation below where x-acceleration has been taken as example:

$$a_x = \frac{X_1 + X_2}{2} \qquad \textbf{(E 6.1)}$$

Tangential acceleration is determined in a similar manner. Its vector is orthogonal on the radial vector pointing from the axis of rotation to the tangential acceleration survey point (radius). To determine tangential acceleration with the two triaxial accelerometer modules the following equation is applied (the subtraction is actually done in hardware):

$$a_{\text{tangential}} = \frac{Y_1 - Y_2}{2} \qquad \textbf{(E 6.2)}$$

Tangential acceleration's reference point/radius is appointed as the sensing radius after this processing step. The nomenclature of the equation above is consistent with Figure 33. Y_1 and Y_2 are the single y-axis accelerometer outputs. The subtraction defines the direction of positive respectively negative tangential acceleration. Positive acceleration is seen while increasing RPM and a negative one in cases with falling RPM.

Beside the three axial accelerations (x, y and z) and tangential acceleration also lateral acceleration is determined. Lateral acceleration is the vector sum of the x and y acceleration.[15] Its determination differs from the accelerations mentioned above as it is not calculated via the outputs of a pair of individual accelerometers but is already based on resultant accelerations in x- and y-direction.

$$a_{lateral} = \sqrt{a_x{}^2 + a_y{}^2} \qquad \textbf{(E 6.3)}$$

6.2 Tangential Acceleration Data

Tangential acceleration is seen as a key parameter for stick-slip severity classification. Therefore, a closer look was taken on the data's reasonableness and its applicability as a classification parameter before an implementation in the design of a new stick-slip diagnostics algorithm. Tests with the actual tool to verify tangential acceleration data were excluded at the beginning as they are accounted as too extensive and costly for a first review. Anyway, tests are still considered as an option where analyses and correlations cannot prove the appropriateness of sensor outputs.

The tangential acceleration check appears as straight forward as CoPilot® has the ability to determine its instantaneous RPM and hence provides a second source of tangential acceleration data. RPM measurements are based on magnetometer readings and thus RPM is independent of accelerometer outputs. Therefore, two self-contained sources of tangential acceleration are provided by CoPilot®. This is an important condition as it enables disclosure of sensor related malfunctions or calibration errors via comparison of both data.

Each tangential acceleration source has its individual sensing radius. To get comparable tangential accelerations a reference point or radius to which both accelerations correspond has to be defined. This is, as already mentioned above, due to the radial dependence of tangential acceleration. A radius half of the tool's nominal size is set as reference radius. For example, all tangential acceleration readings either received from accelerometers or via magnetometers measured by a 6¾" (0.17145 [m]) CoPilot® are converted to and thus refer to a radius of 0.085725 [m].

The used unit for acceleration is changed from [g], CoPilot®'s standard unit of acceleration, to [m/s²]. Although the discussion belongs to a rotating system, all parameters are handled with units of lateral motion for the purpose of better visualization.

Tangential acceleration, derived from magnetometer readings, is simply calculated by converting the magnetometer based instantaneous RPM values to meters per second and subsequently differentiating them. A general dimensionless example of how velocity and acceleration correlate to each other is shown in Figure 34.

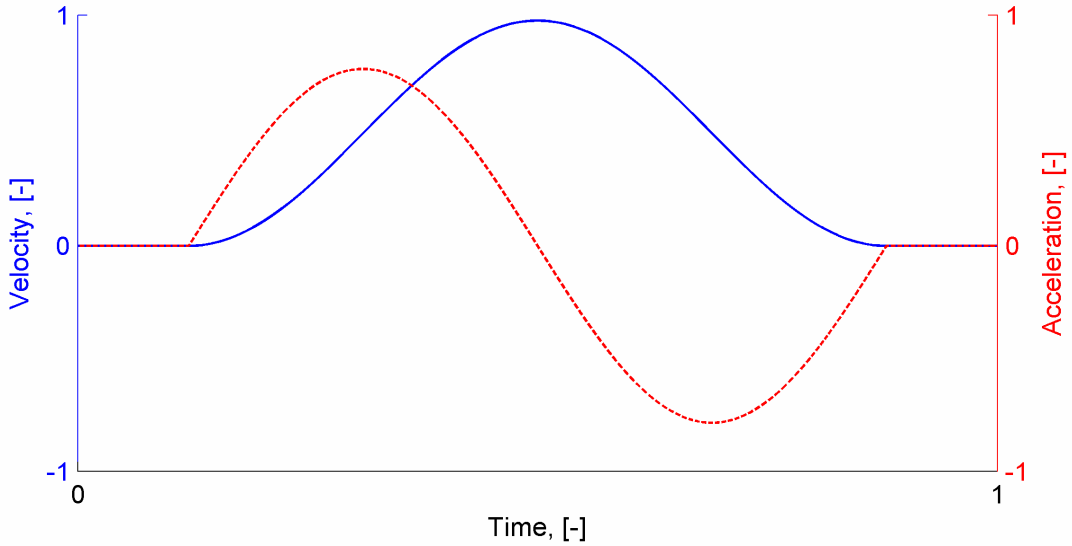

Figure 34 – Dimensionless velocity-acceleration-relation – a velocity peak example.

Regarding Figure 34 it can be stated that acceleration is zero when velocity is constant. Acceleration becomes positive while velocity is increasing and respectively negative during a fall in velocity. While keeping that in mind, Figure 35 and Figure 36 should be inspected.

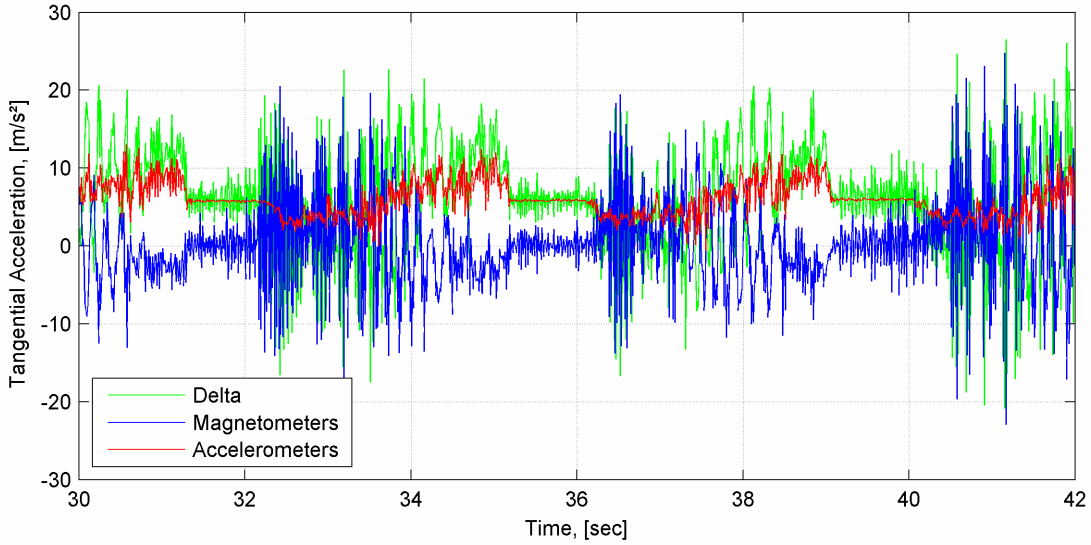

Figure 35 – Tangential accelerations measured by the accelerometers (red) and derived form magnetometers outputs (blue). Shown is a 12 seconds cutout of a 435 seconds long trigger sampled at 100 [Hz]. Delta (green) is the difference of the accelerometers to magnetometers data.

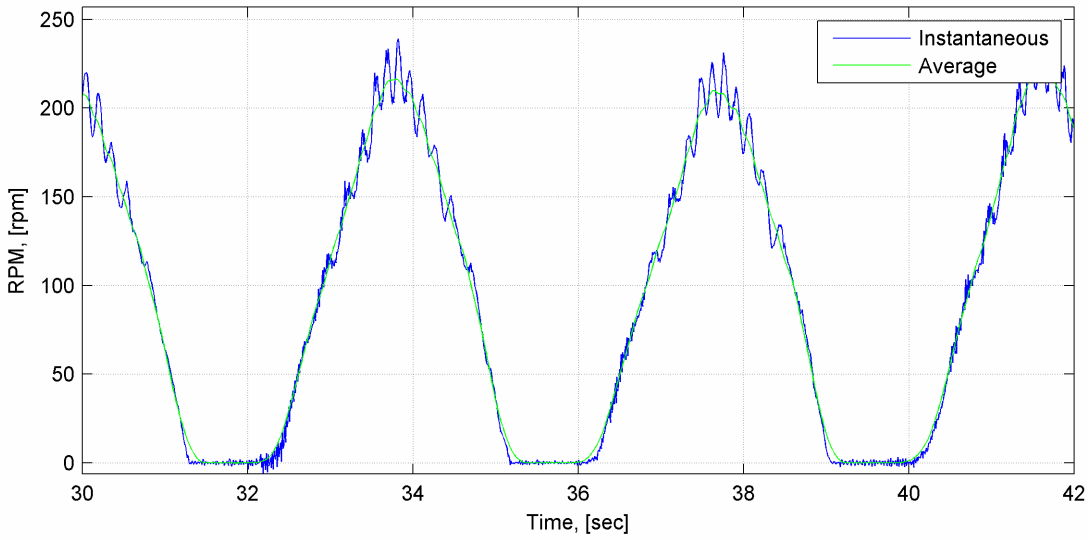

Figure 36 – Instantaneous RPM (blue) of the section shown in Figure 35. Average RPM (green) is the by a moving average (0.4 [sec] times 100 [Hz] elements) filtered instantaneous RPM. The average RPM is shifted backwards by half of the average filter length (0.2 [sec]) to compensate the resultant time lag due to the used average filter type.

The actually measured tangential accelerations as depicted in Figure 35 differ quite a lot from the ideal case (Figure 34). The roughly similar trend (fluctuations around zero) of the tangential acceleration from magnetometers (TAM) is a result of its calculation. There, a possible constant fraction has been removed to achieve comparable results with the accelerometer readings. However, the data exhibit a quite erratic behavior. The most likely reason is its origin in instantaneous RPM and consequently a carryover of noise and other adverse effects which had altered the instantaneous RPM. Anyway, TAM is close to zero at zero RPM and significantly higher or lower while RPM peaks or troughs which in round terms matches the expected trend.

A similar behavior can be observed at the tangential acceleration received from accelerometers (TAA) as well. However, two things are remarkable at TAA: first, its fluctuation range is considerable smaller than the one of TAM and, second, TAA falls almost never blow zero (only once (at 37.5 [sec]) during the 12 seconds cutout of Figure 35).

None of these points is just a temporarily limited event accidentally caught by the cutout section. TAA shows this behavior while the whole 435 seconds long trigger. The second point can even be emphasized more when RPM is calculated via integration of TAA. The result is a raise of almost 64 revolutions per minute just while the 12 seconds cutout and an increase of about 2346 [rpm] during the entire trigger. Neither such long lasting positive acceleration nor those extremely high RPM values are realistic. Whereat, not to forget that these numbers are relative numbers. The absolute values could (theoretically) even be larger.

The first trial to get an appropriate match of both data sets is a moving average filter. Therefore, TAM is now derived from the average RPM and TAA is also filtered by the same moving average filter (0.4 seconds time interval). The disadvantage of the used filter type is, that it results in a time shift depending on the filter length (i.e. how

many elements are used for filtering). However, this type of average filter is applied as such a type is currently implemented in CoPilot® for averaging RPM and it delivers quite good results. The filter design parameters are exactly known and therefore the resultant time lag can be and is compensated. Finally, both curves have been shifted to time axis by eliminating constant fractions. The processed characteristics are depicted in Figure 37.

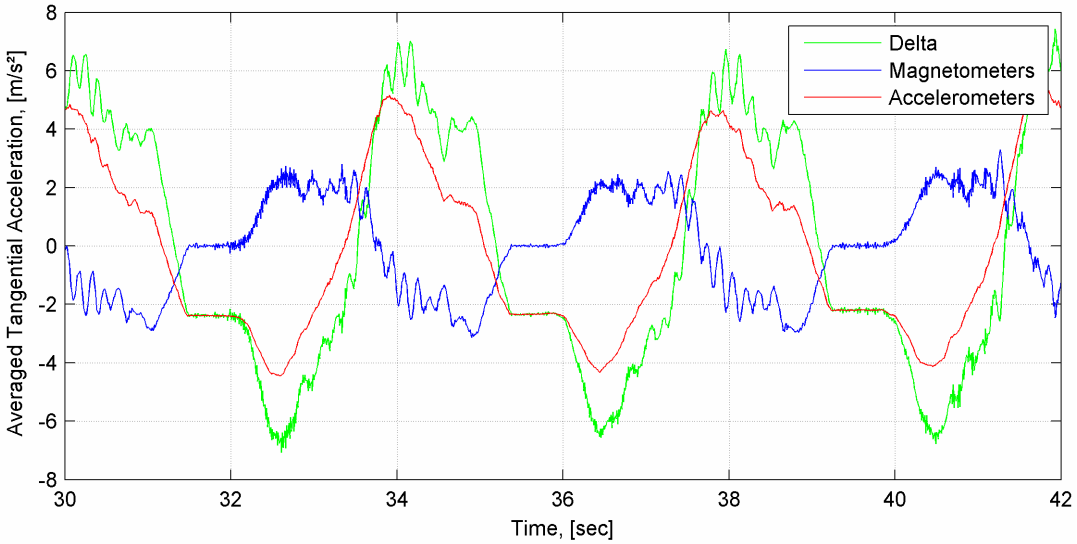

Figure 37 – Averaged tangential acceleration data.

Regarding TAM, while comparing Figure 37 with Figure 35, obvious improvements in interpretability of the data have been achieved. Also with respect to Figure 36, TAM appears now reasonable and by that it is validating the application of TAM as a reference for TAA. In the following, the worked out TAM is used as reference for TAA.

The appearance of TAA has changed significantly after filtering. In contrast to before the performed averaging, TAA shows now higher amplitudes than TAM. The most probable reason is an instantaneous RPM which is afflicted with noise and its consequent influence on TAM. Exaggerated minima and maxima are therefore the result. TAA did not lose that much amplitude which should be an indicator for a more accurate measurement.

Furthermore, between both tangential accelerations a phase shift of about 180 degrees can be observed. Sections with nearly constant accelerations can be found at both curves at around 32, 36, and 40 seconds. The correlation of these constant sections leads to the conclusion that the phase shift is not a result of a time difference between both data. More likely is an algebraic sign permutation somewhere either in software or hardware of CoPilot®. For this reason, TAA is inverted and the result is plotted in Figure 38.

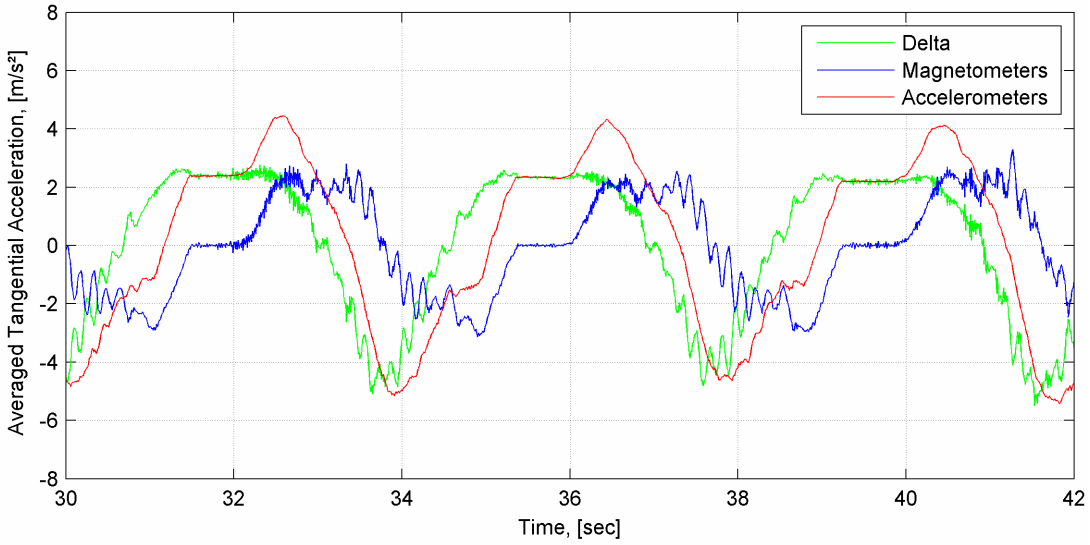

Figure 38 – Averaged tangential accelerations with inverted accelerometer data.

The TAA inversion reduces the difference between both data sets (delta) but still the result is by far not an acceptable match. Remarkable at Figure 38 are the characteristics of the delta. When considering Figure 36, the trend of delta appears as the mirrored course of the RPM. The inversion is just an effect of the delta determination as TAM is taken as reference and delta represents the difference of TAA in relation to it. The other way round, the mirror effect would vanish. This surprising correlation might indicate a RPM influence at TAA.

Up to now, the data processing of TAA is delivering unsatisfactory tangential acceleration characteristics. Obvious and easy to cure effects on TAA data cannot be identified anymore. Other influencing factors need to be discovered.

Also the possibility of a nonrecurring transducer defect has been investigated. But as the same behavior could also be observed at acceleration data from several other wells, where different (in size and tool/serial number) CoPilot® tools had been run, a single corrupt sensor can be excluded.

X-, y-, and z-accelerations appear reasonable. Hence, a general accelerometer problem seems to be unlikely. To identify the reason of TAA's unexpected behavior, further investigations are focused on how tangential acceleration is actually measured in CoPilot®.

6.3 Detailed Investigation of Tangential Acceleration Sensing

The triaxial accelerometer modules are small cubes with bundled wires exiting the case at one side. The dimensions of such a module are shown in Figure 39.

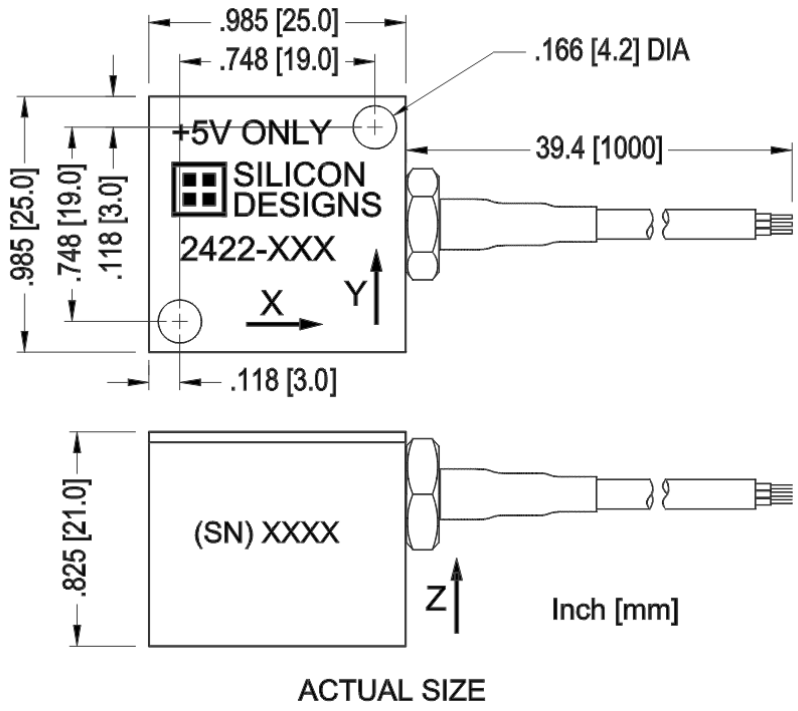

Figure 39 – Triaxial accelerometer case dimensions (labeled sensing directions do not correlate with CoPilot®'s).[38]

The currently in CoPilot® implemented sensing directions together with their corresponding sensing points are depicted in Figure 40.

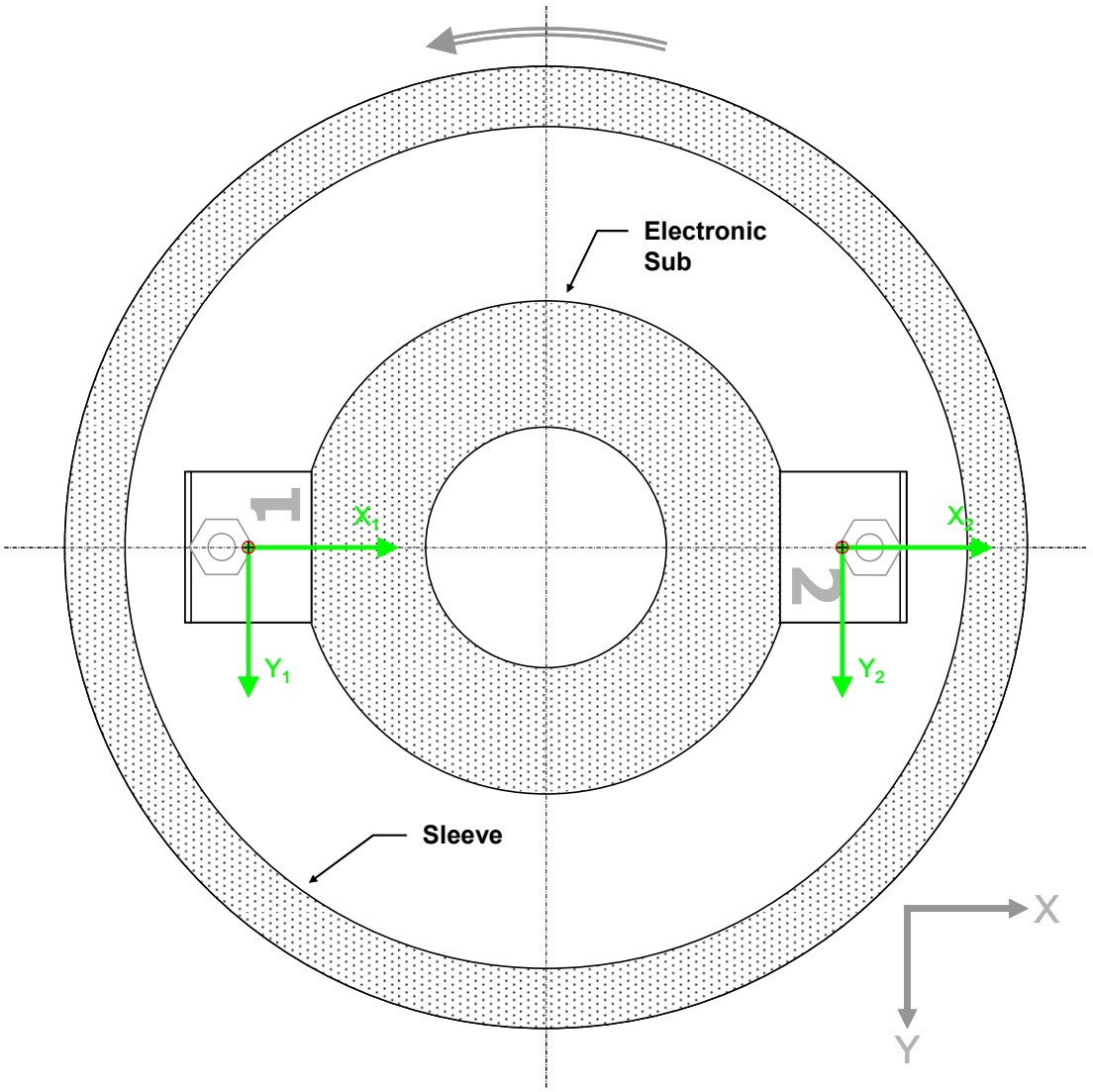

Figure 40 – Cross-section of CoPilot® right below the accelerometers location. Shown are the two triaxial accelerometer modules (1 and 2) mounted on the electronic sub and covered by the sleeve. The acceleration sensing point is marked by a black cross surrounded by a red circle. Sensing directions are symbolized by green arrows. The view is in up-hole direction (positive z-direction). Sensing in z-direction is implemented in CoPilot® for the same point (i.e. in the yz-plane also centered with respect to the sensor case). Depicted is the accelerometer coordinate system (the coordinate system rotates together with the tool!). The drawing is not to scale and simplified wherever possible.

When assuming the in CoPilot® implemented sensing points and directions as correct, excluding any sensor failures, and presuming software to work properly, no error can be detected. Consequently, acceleration data (axial and tangential) with expected reasonable behavior should be eventually received. That in reality this is not to full extent the case as has already been discussed above.

The accelerometer case is small but compared to the sub size – especially at smaller CoPilot® sizes – it qualifies. Up to now, no closer look has been taken at the actual internal design of a triaxial accelerometer module. The case centered sensing position is currently only a conclusion based on technical drawings of CoPilot® ([39], [40], [41], [42], [43], [44], [45]), the tangential acceleration radii specified at the technical data sheets ([30], [31], [32], [33]), and the outer dimensions of the

accelerometer case. Especially, the tangential acceleration radii mentioned in CoPilot®'s specifications refer to a case-centered sensing position.

If the conclusion or the data it is based on is wrong and an off-centered sensing point would actually be the case, then this has a significant impact on transducer measurements. Such a misalignment could definitely be a reason for the still existing differences between TAA and TAM. A potentially not centered sensing point would have multiple positioning possibilities within the case.

Therefore, the following assumption is made: the real sensing points are not located where shown in Figure 40 and implemented in CoPilot®. To verify this assumption, the internal design of the accelerometer modules needs to be known. For this reason, the latest transducer datasheets ([46], [47]) have been obtained from the accelerometer module manufacturer. In the following paragraphs the internal module design will be discussed.

6.3.1 Triaxial Accelerometer's Internal Design

The triaxial accelerometer module is actually not one single transducer but consists of three individual accelerometers – one per axis. A module combines three orthogonally mounted analog single-axis accelerometers – all of identical type. Such single-axis accelerometer elements are shown in Figure 41 and combined as an open frame triaxial sensing module in Figure 42.

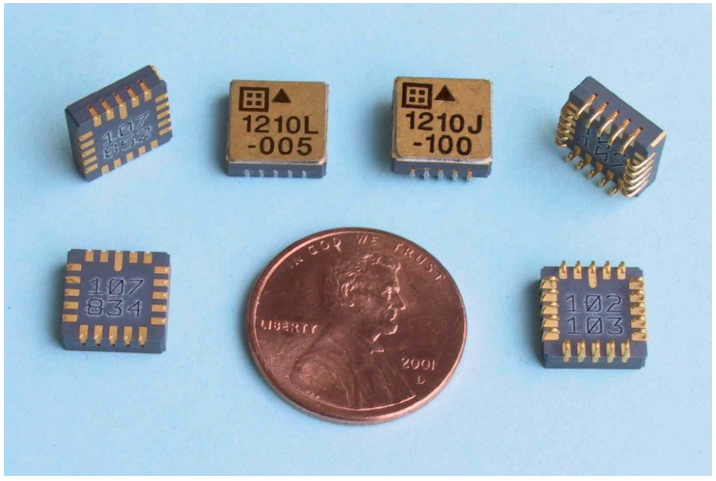

Figure 41 – Analog single-axis accelerometer packages (two different package types are shown).[21]

CoPilot®'s actual triaxial accelerometers are not of that open frame type like the one shown in Figure 42. In fact, it is housed in an epoxy sealed, anodized aluminum case. However, Figure 42 offers a good impression of how the sealed type does internally look like.

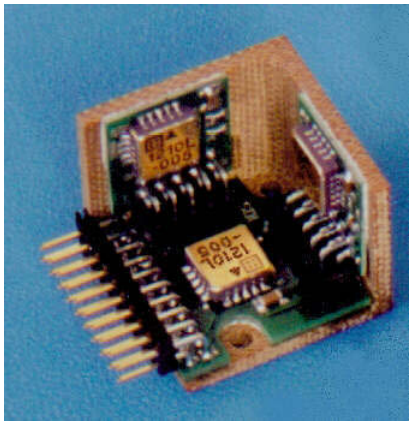

Figure 42 – Three-axes, open frame accelerometer assembly. The picture does not show an opened module of the same type as incorporated in CoPilot® but one with similar internal locations of the single-axis accelerometers.[21]

The exact location of the single-axis accelerometers in the aluminum case is shown in Figure 43. The coordinate system drawn in black next to the case body is the one used by the sensor manufacture. The blue coordinate system is the one defined for the "upper" accelerometer in CoPilot® ("upper" with regard to Figure 33, accelerometer axes subscript 1). For the second, the "lower" accelerometer, the positive x- and y-axes directions would flip.

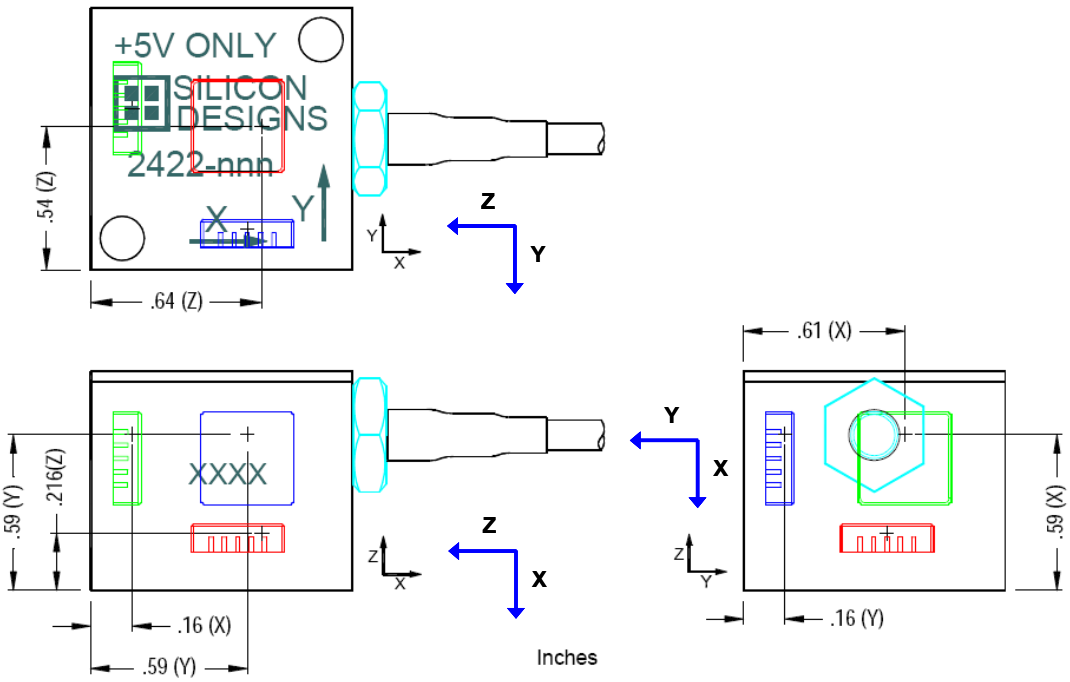

Figure 43 – Sensor locations in the aluminum case (CoPilot®: red: x-direction, blue: y-direction, green: z-direction). Points of surveys are marked by black crosses. Units: [in]. (Modified after [38])

Figure 43 verifies the above made assumption. The sensing point is, in contrast to CoPilot®'s current implementation, not located at the center of the case. Moreover, there is not only one, for all directions identical, sensing point but there are three.

Each direction has its own sensing point as each direction has its own accelerometer. None of the sensing points ever lies in the middle between two edges of the case.

6.4 Misalignment Effects

Regarding the axial acceleration surveys, no significant influence of the sensing point misalignment is expected, because:

- **Sensing directions** are still **orthogonal** to each other.
- Individual **axial components** of both triaxial accelerometers are still **parallel** to each other.
- The averaged axial accelerations have **no radial offset** due to identical sensor orientation on the electronic sub (wires downwards, case cover pointing radial outwards).
- The three different **sensing** point **radii** are **ineffectual** as they cancel at averaging the two individual axial readings.
- The **location discrepancies** between the different sensing points along the tool axis can be neglected due to their **marginal** sizes.

That the misalignment does not significantly influence the axial acceleration measurements is also confirmed by actual survey data as they show reasonable characteristics. However, as no detailed axial acceleration data investigation with respect to data correctness has been carried out, only mounting related errors can be excluded at this point. To check for and exclude other errors, a more detailed analysis would be necessary.

The negligible impact on the sensed axial accelerations can be explained by only minor lateral and axial shifts of the sensing points. Concerning tangential acceleration, the misalignment problem is more severe as there are also angular changes involved as depicted in Figure 44.

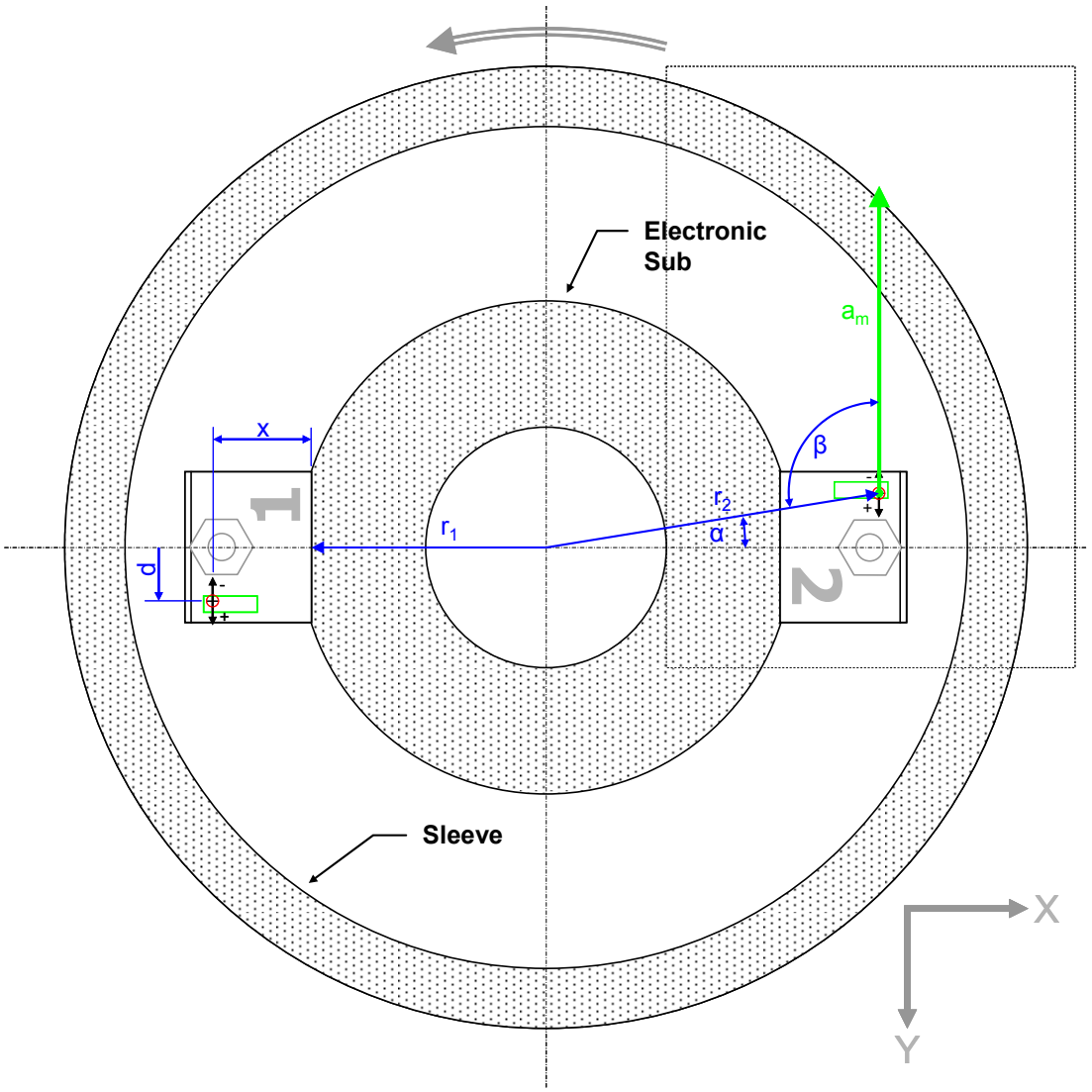

Figure 44 – Actual current y-direction sensing location and measured acceleration a_m. The y-axis accelerometer pair is drawn as green rectangles (acceleration sensing element's center of mass marked by a black cross surrounded by a red circle and with additional two arrows pointing in positive respectively negative sensing direction (at Figure 43 the same element is marked in blue!)). X- and z-axis sensing elements are not shown. The y-axis accelerometer misalignment is represented by the angle α. Dimensions (blue) are depicted only once but identical and valid for both modules (1 and 2). The dashed rectangle marks the cutout as shown in Figure 45 and Figure 48. The drawing is not to scale and simplified wherever possible.

Figure 44 discloses that the individual y-axis accelerometers actually do not measure the true tangential acceleration as their sensing direction is not orthogonal ($\beta = 90° + \alpha$) to the radius (r_2). As a result, the following two factors gain influence on the sensor outputs and thus need to be considered:

- The accelerometers see only a reduced tangential acceleration as their sensing directions are not pointing exactly to the direction of true tangential acceleration. The reduction is a constant, α (and thus tool size) dependent factor which steadily alters sensor readings.

- The second factor is a RPM dependent factor – the centrifugal acceleration. The radial misalignment causes a fractional recording of centrifugal acceleration. This

is also a more or less permanently present factor as it appears whenever the tool is rotated. Centrifugal acceleration only disappears at zero RPM but tangential acceleration does as well. That the tool size (radius) has no impact will be shown later on.

Every factor (error) will now be discussed in more detail in the following sections.

6.5 Software Based Tangential Acceleration Errors Correction

6.5.1 Centrifugal Acceleration Error

The centrifugal acceleration error, E_c, is discussed first for the reason that the measured acceleration, a_m, has initially to be correct with respect to this error before a correction of the angular misalignment error, E_a, is possible.

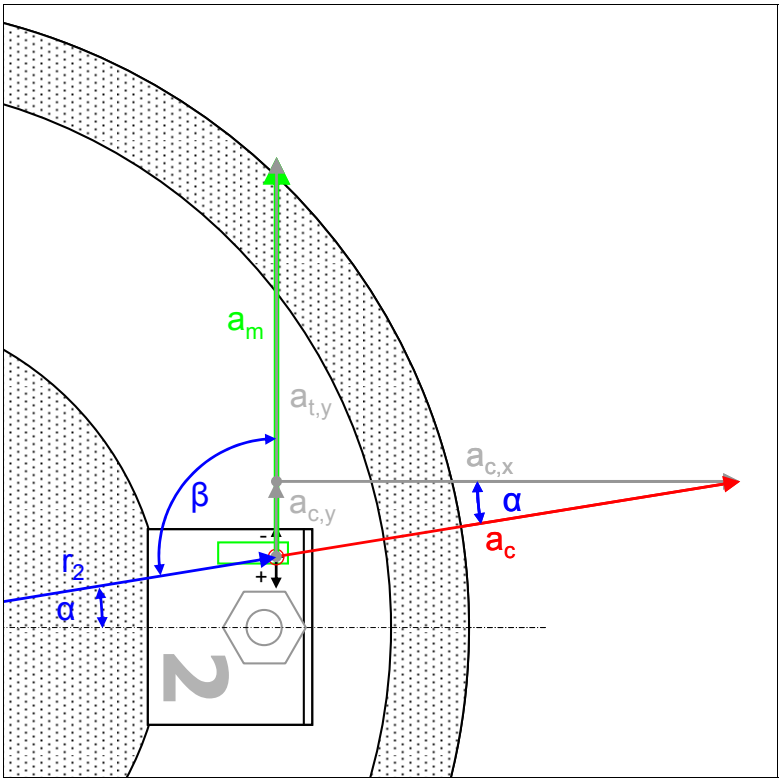

Figure 45 – Centrifugal acceleration error E_c (identical with $a_{c,y}$).

A snapshot of the centrifugal acceleration influence on sensor readings is shown in Figure 45. The general equation of centrifugal acceleration, a_c, is:

$$a_c = \frac{v^2}{r} \qquad \textbf{(E 6.4)}$$

Concerning CoPilot®'s dimensions, the error magnitude depends solely on the instantaneous RPM (equivalent to velocity, v). Variations in tool size and thus in radius, r, show absolutely no effect on the error's magnitude. In Figure 46 the error trends for all four sub sizes are plotted whereat it becomes obvious that their trends are identical as the curves coincide.

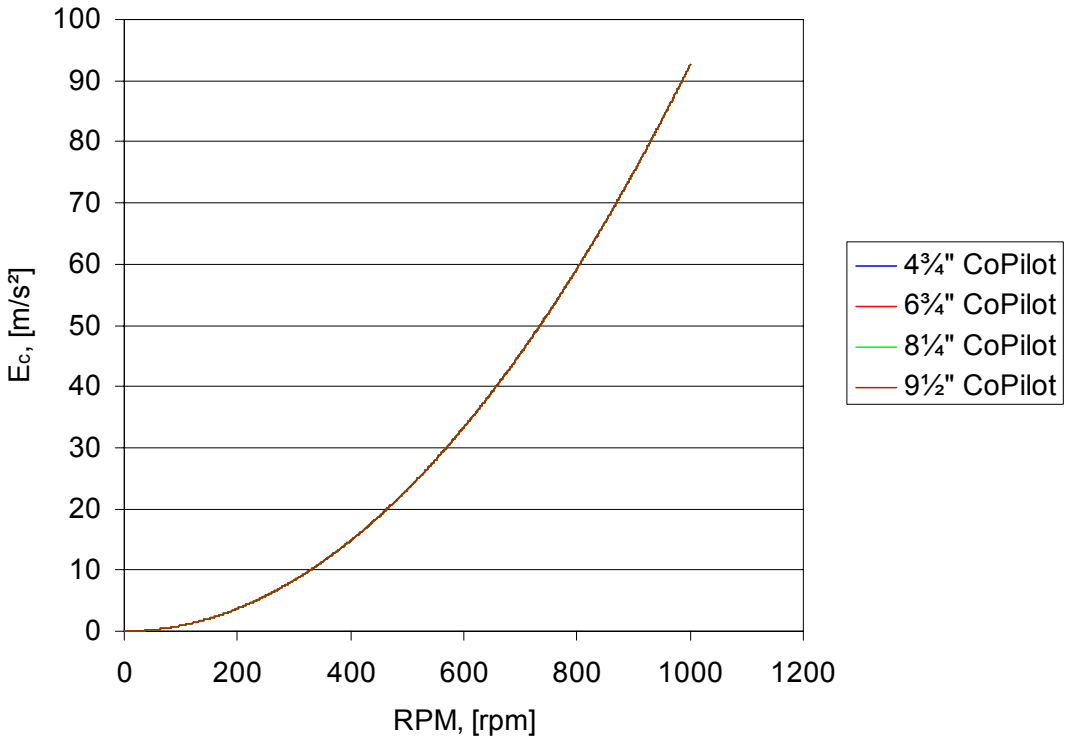

Figure 46 – Centrifugal acceleration error, E_c, trends of all CoPilot® sizes for a 0 to 1000 [rpm] range.

The reason for the error correspondence is, that α is a function of r_2 (see Figure 44). The radius r_2 is the vector sum of the tool size depend radius r_1 and the size independent values x and d. X is the distance from the sensor case bottom to the y-acceleration sense element's center of mass and a sensor specific property. As such, x has a for all tool sizes constant value of 14.99 [mm]. The displacement, d, actually the reason of both errors, is also a sensor specific property and thus constant for all tool sizes as well. Its value is 8.45 [mm]. Consequently, whenever r_2 is changed also α is indirectly modified in a manner that finally the error size is not influenced.

The instantaneous centrifugal acceleration error can be calculated with the following equation:

$$E_c = a_{c,y} = \frac{\left(RPM \cdot \frac{1}{60} \cdot 2 \cdot \pi \cdot r_2 \right)^2}{r_2} \cdot \sin\alpha \qquad \textbf{(E 6.5)}$$

The results of the equation above are plotted for a 0 to 1000 [rpm] range in Figure 46. The y-axis accelerometer misalignment angle can be computed by:

$$\alpha = \tan^{-1}\left(\frac{d}{x + r_1} \right) \qquad \textbf{(E 6.6)}$$

All used size specific parameters are listed in Table 4:

Tool Size	r_1	r_2	α
[in]	[mm]	[mm]	[°]
4¾	25.33	41.20	11.830
6¾	46.32	61.89	7.843
8¼	58.40	73.87	6.565
9½	64.28	79.72	6.081

Table 4 – Y-axis accelerometer sensing points coordinates.

The E_c fraction of the total accelerometer misalignment error is the dominant error fraction as can be clearly identified when comparing Figure 38 with Figure 47. The corrected TAA as shown in Figure 47 is calculated by:

$$a_{t,y} = a_m - E_c \qquad \textbf{(E 6.7)}$$

Whereat, E_c is equivalent with $a_{c,y}$ and a_m represents the raw measured tangential acceleration data of TAA. All already discussed processing steps (averaging, inversion, and removal of constant fraction) are subsequently performed after the error correction.

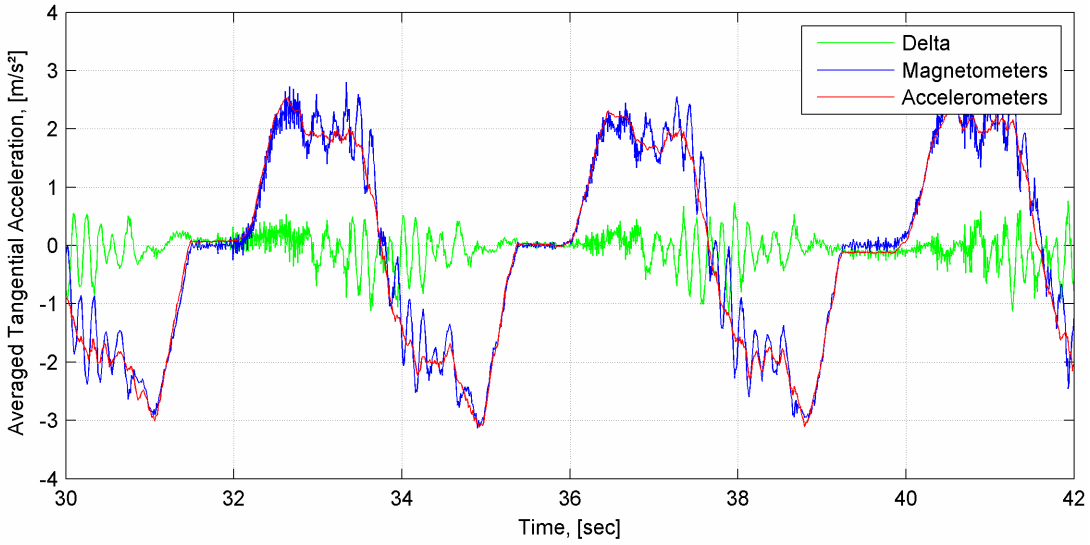

Figure 47 – TAA after centrifugal acceleration error correction.

The centrifugal acceleration error is tremendous but its correction has been quite successful at the used example data set. However, in general the correction is critical. In order to cure TAA form E_c the correction algorithm makes use of the instantaneous RPM data. Hence, the corrective measure is fully dependent on instantaneous RPM (see Equation 6.5) and unfortunately also on its data quality.

TAM is derived from the instantaneous RPM and is not adequate useable prior averaging (to get rid of noise). Instantaneous RPM on its own seems not to be totally impeccable – especially without any filtering. At the here performed TAA correction, TAA gets the full influence of the raw, unfiltered, instantaneous RPM. However, not to use the instantaneous RPM would lead to a worse match of both curves. At this point, it can not definitely be excluded that the here achieved good correlation is just a result of the influence of the instantaneous RPM, which is affecting both TAM and TAA.

6.5.2 Angular Misalignment Error

In Figure 48 the effect of the angular misalignment error, E_a, is shown. The true tangential acceleration is labeled as a_t and the actual sensor output is named a_m (measured acceleration). The angular misalignment error represents the reduced detection of tangential acceleration. CoPilot® is simply not able to measure the total true tangential acceleration as its y-axis transducers are not pointing exactly in the direction of actual tangential acceleration. Consequently, the sense elements see only the component $a_{t,y}$ of a_t. E_a, in percent, can be calculated with the following equation:

$$E_a = (1 - cos\,\alpha) \cdot 100 \qquad \textbf{(E 6.8)}$$

When looking at the equation above it is obvious that E_a is a function of the tool size as α is tool size dependent. Generally, it can be stated that the error is getting smaller

with increasing tool diameter and vice versa due to the fact that d is constant for all CoPilot® sizes.

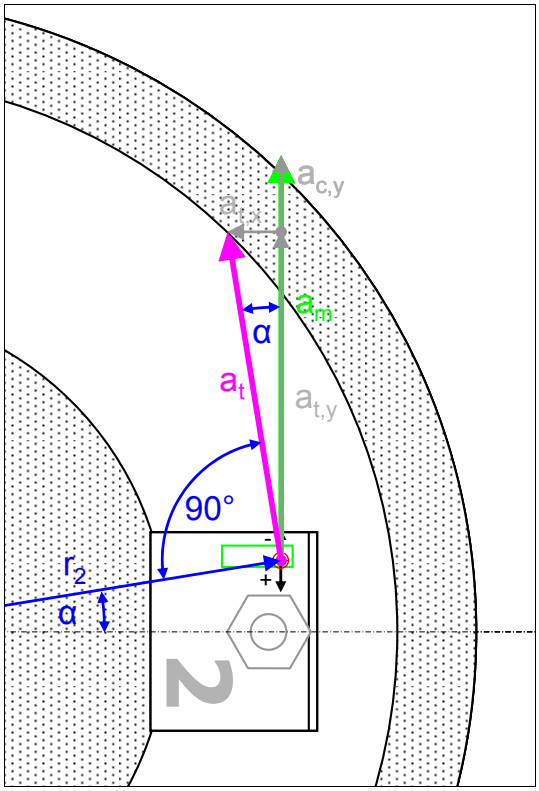

Figure 48 – Angular misalignment error. a_t is the true tangential acceleration. a_m is the measured acceleration. $a_{c,y}$ is the y-component of the centrifugal acceleration.

A list of the magnitudes of the tangential acceleration misalignment error for the four tool sizes is given by Table 5:

Tool Size	α	E_a	C_a
[in]	[°]	[%]	[-]
4¾	11.830	2.12	1.021702
6¾	7.843	0.94	1.009443
8¼	6.565	0.66	1.006600
9½	6.081	0.56	1.005659

Table 5 – Angular misalignment error, E_a, and angular misalignment correction factor, C_a.

Eventually, the true tangential acceleration can be calculated via:

$$a_t = a_{t,y} \cdot \frac{100}{100 - E_a} \qquad \textbf{(E 6.9)}$$

Or with:

$$a_t = a_{t,y} \cdot C_a \qquad \textbf{(E 6.10)}$$

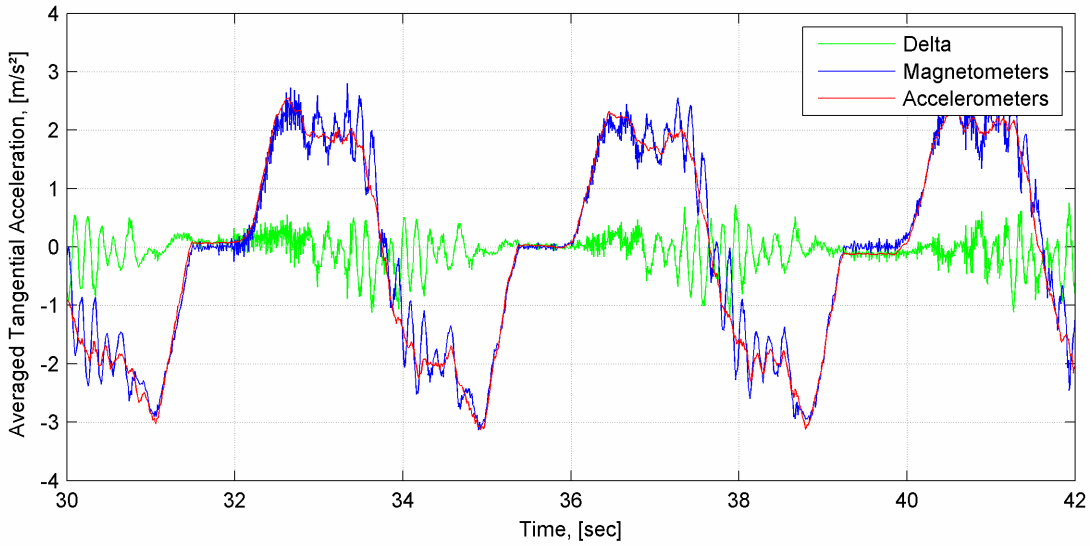

Figure 49 – Averaged TAM and averaged and corrected (with respect to E_c and E_a) TAA.

The changes due to the second correction are marginal and at the graphs almost undetectable (compare Figure 47 with Figure 49). Sometimes it is not necessary, applicable, or worth it to correct such relative small errors, especially in this respect when regarding the larger tool sizes (the example data was collected by a 9½" CoPilot®). However, concerning this error it is straight forward and with very little computational effort possible to correct the tangential acceleration readings. Thus, it is recommended to execute this correction as well as it eliminates one known inaccuracy.

6.5.3 Software Based Error Correction Summary

In total, the following software based correction steps were performed to get the fairly good match of tangential acceleration data from both sources:

1. Correction of the accelerometer's detection surplus due to **centrifugal acceleration** sensing.
2. Correction of the accelerometer's under-detection due to **angular** sensor **misalignment**.
3. Proper averaging/**filtering** of both data sets, TAM and TAA.
4. **Inversion** of the accelerometer data.
5. Removal of **constant fractions** at TAM and TAA.

The used averaging time interval of 0.4 seconds as well as the filter method of the moving average is the same as currently implemented in CoPilot® to average RPM. The length of the averaging time interval turned out as most suitable for both, TAM as well as TAA. Tests with other filter lengths led to better matches only in a few cases. It is not exactly known why identical filter lengths deliver best results at both

data sets as the data is resulting from different sensor types. A thinkable reason could be the link between TAA and TAM during the centrifugal error correction. Furthermore, why exactly with a 0.4 seconds filter length such a match is achieved can not be answered.

6.6 Possible Corrective Measures

Below, a selection of possible corrective measures to cure the misalignment problem is presented:

1. **Software based correction** as discussed in the paragraphs above:

   Pros:
   - None of the existing tools has to be physically modified.
   - No future sub design changes.
   - Only possibility to correct history data.
   - "In-house" modifications only.
   - Probably the cheapest solution.

   Cons:
   - Correction is mainly based on problematic instantaneous RPM measurement.
   - Loss of the option to double-check the RPM values via the tangential acceleration outputs and vice versa.
   - Correction is tool size variant.
   - In the future, the necessity to process tangential acceleration data sensed by accelerometers would be questionable due to the cross correlation with the other, anyway present, tangential acceleration source.

2. Utilization of the same triaxial accelerometer modules but mounted on the electronic sub in a **shifted position,** which ensures tangential alignment of the sense direction of the individual y-axis accelerometers.

   Pros:
   - No software changes necessary.
   - Same triaxial accelerometers can be used.
   - TAA surveys are independent of instantaneous RPM.
   - TAA can be verified via TAM and vice versa.
   - "In-house" modifications only.

   Cons:
   - Electronic sub body needs to be modified (existing and future ones).
   - Space between electronic sub and sleeve might be too little for a full correction (full extent sensor shift).
   - Quite extensive corrective measure as already a number of tools exist.

3. Application of a **modified triaxial accelerometer module** with an exactly centered y-axis acceleration sensing point in a case with outer dimensions identical with those of the current module. This is a thinkable option as Figure 42 and Figure 43 indicate that the aluminum case of the triaxial accelerometer module is not too tightly packed. The internal design should offer enough space to relocate the y-axis sensing element right at the center. Potential necessary lateral or/and axial shifts of x- and z-axis sense elements (with respect to CoPilot®'s axes labels!) are not critical and thus additionally offering a higher degree of flexibility for internal y-axis accelerometer relocation.

   Pros:
   - No changes at the electronic sub.
   - No changes in software necessary.
   - Modification applicable to all existing tools as only two screwed on sensor modules need to be replaced (still the same internal transducers, outer dimensions, wires, and power consumption).
   - TAA surveys are independent of instantaneous RPM.
   - TAA can be verified via TAM and vice versa.

   Cons:
   - The internal design modifications are potential but not assured.
   - Costs are unknown.
   - Modifications need to be done by the accelerometer manufacturer.

6.7 Conclusions

Tangential acceleration is a highly useful parameter to classify the dynamic behavior/conditions of the tool/BHA/drillstring.

The presence of the accelerometer misalignment has been proved true. Its effects on tangential acceleration sensing have been discussed. In the future, if desired to use tangential acceleration data, corrective actions need to be taken. A software based correction, as developed here, is a good means to correct history data. As a permanent solution, a software based correction is questionable.

The only diagnostics that is affected by tangential acceleration is torsional vibration.[8] Torsional vibration diagnostic information is currently not used for real-time optimization.

By naming the corrected tangential acceleration as true tangential acceleration does not necessarily mean that the for y-axis misalignment corrected tangential acceleration readings are the real, true, by the tool experienced, tangential acceleration values. It stats nothing more than the sensor readings are corrected for these specific, constructional induced errors. The presence of further undetected survey errors can not be excluded at this point – especially as both tangential accelerations are liked via the correction algorithm. To achieve absolute certainty

concerning the correctness of the readings, additional verifications would be necessary.

One last point to mention: filtering has been performed only at a very basic level (just averaging). Further improvements in data match maybe will achieved with a better, more sophisticated, source specific filter design.

6.8 Recommendations

To correct already existing tangential acceleration data, the here discussed software based correction algorithm appears as expedient and hence can be applied.

In the future, physical changes will be necessary. When disregarding the costs (as they are not known up to now), the above mentioned corrective measure of modified accelerometer modules (point 3) is the solution to favor.

The tangential acceleration radii mentioned in the technical data sheets of CoPilot® ([30], [31], [32], [33]) could not be confirmed. Their source and accuracy should be proven.

7 Downhole Rotary Speed

Downhole, RPM is detected by sensors which observe earth's magnetic field variations resulting from sense position changes due to string rotation. The entire RPM survey is based on readings of two magnetometers which measure the magnetic field intensity in x and y direction. The operation principle, limitations, and drawbacks of magnetometers have been already discussed in a previous chapter. This chapter covers the magnetometer data processing and RPM data generation of CoPilot® as well as a results analysis.

7.1 Pipe Rotation Speed Determination

As already mentioned above, the calculation of the downhole RPM is based on readings of two orthogonally mounted magnetometers. The raw sensor data passes the data acquisition step (compensation, decimation, etc.) first. Then the processed sensor data is normalized with respect to the vector sum of the x and y magnetometer readings, *MagX* and *MagY*:

$$\overline{MagX(i)} = \frac{MagX(i)}{\sqrt{MagX(i)^2 + MagY(i)^2}} \quad \textbf{(E 7.1)}^{[15]}$$

$$\overline{MagY(i)} = \frac{MagY(i)}{\sqrt{MagX(i)^2 + MagY(i)^2}} \quad \textbf{(E 7.2)}^{[15]}$$

In the next step, the in-phase, *r(t)*, and quadrature components, *q(t)*, are computed:

$$r(t) = \overline{MagX(i-1)} \cdot \overline{MagY(i)} - \overline{MagX(i)} \cdot \overline{MagY(i-1)} \quad \textbf{(E 7.3)}^{[15]}$$

$$q(t) = \overline{MagX(i-1)} \cdot \overline{MagX(i)} + \overline{MagY(i-1)} \cdot \overline{MagY(i)} \quad \textbf{(E 7.4)}^{[15]}$$

The third step is the calculation of the instantaneous RPM ([rad/s]) by taking the arc tangent of the in-phase to quadrature component ratio and scaling the whole term with the sample frequency, *SF*:

$$rps(t) = SF \cdot \tan^{-1} \frac{r(t)}{q(t)} \quad \textbf{(E 7.5)}^{[15]}$$

Finally, the number of samples with values less than the backward rotation threshold (-0.2 radians per second) is captured and the average RPM is calculated by averaging the instantaneous rotary speed using a moving boxcar over a 400 milliseconds long data interval. The resulting output values of the pipe rotation speed determination

stage are the instantaneous RPM, the averaged RPM as well as the backward rotation counter.

7.2 Magnetometer Readings and RPM Simulator

As the current stick-slip diagnostics algorithm is solely based on downhole RPM data, a closer look on gathering the RPM needs to be taken. To evaluate the RPM calculation method, measured magnetometer data and their resulting RPM values are of limited use. Noise, formation properties, a mud motor, or the drilling fluid are some of the factors which can influence RPM measurements. Thus, clean magnetometer data can hardly be obtained from real surveys. Beside this lack, controllable RPM trends are also desirable for analyzing the RPM detection ability of CoPilot®.

A simulator has been designed to serve these needs, see Figure 50. It is able to generate synthetic magnetometer data deduced from a freely definable input RPM trend. That followed, the generated magnetometer data is run through the RPM algorithm where eventually again a RPM trend is calculated. At the end, a comparison of the input RPM trend with the received output trend can disclose contingent limitations of CoPilot®'s RPM detection algorithm.

To widen the use of the simulator, it is extended with the ability to simulate a close to real magnetometer behavior. Like every sensor, magnetometers are not perfect in their way of operation. They add a certain degree of distortion to the "image" they take of reality. Constructional and design related errors can be determined quite well by tests. Hence, sensor manufacturer usually specify know sensor errors. For that type of magnetometer incorporated in CoPilot® given errors are used to alter the behavior of the imaginary magnetometers of the simulator from ideal to a close to real sensing behavior.

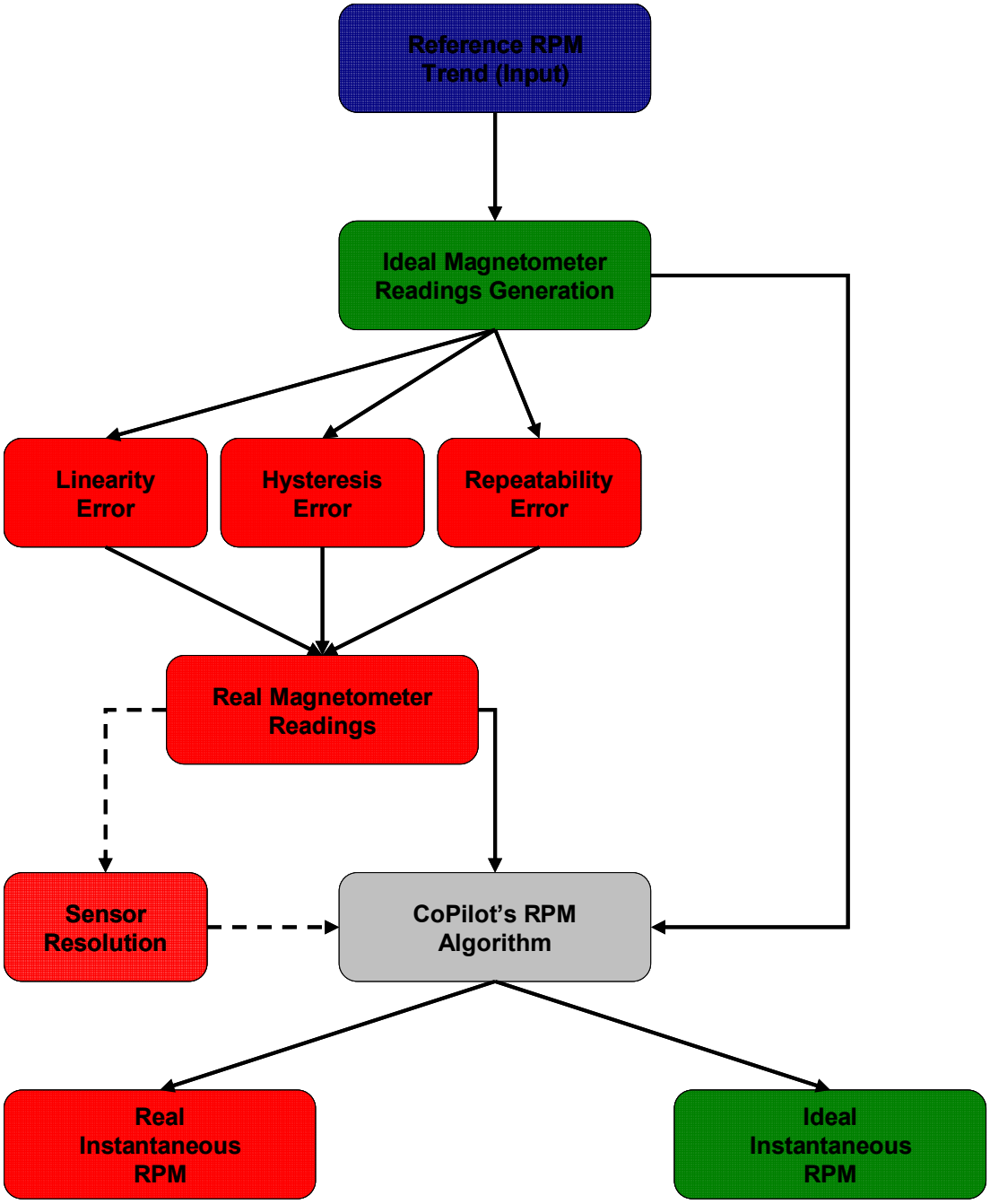

Figure 50 – Block diagram of the magnetometer readings and RPM simulator.

The design of the programmed magnetometer readings/RPM simulator will be discussed in the following paragraphs. The corresponding code is added at the end of this work (see Appendix and attached CD).

7.2.1 Input RPM Trend

The definition of the input RPM trend is the first step. Whether a trend is manually defined with individual time/RPM pairs, a predefined one is used, or a RPM trend is generated with a certain wave form (sinusoidal, triangular, nearly rectangular) – all

these options are offered by the simulator – is up to the simulator user. Also any thinkable combination is possible. However, a very important condition is an identical sample rate through out all RPM trend fragments. To ensure that, RPM input trends with too low sample rates have to be interpolated and others with too high rates need to be down sampled with respect to the finally desired sample frequency.

Correctly defined input RPM is specified by two 1-by-n matrices with an identical number of elements. One is the time matrix filled with, according to sample frequency spaced, time values. The other is the corresponding RPM matrix.

The working principle of the simulator is demonstrated at the example input RPM sequences depicted in Figure 51. That sequence is composed of a manually specified section (from 0 to 70 [sec]) and two sine-functions with different amplitudes but identical frequencies (from 70 to 95 [sec] and 95 till 120 [sec]). Whereat, the high amplitude sinusoidal RPM interval reaches negative RPM levels and hence simulates backward rotation as well.

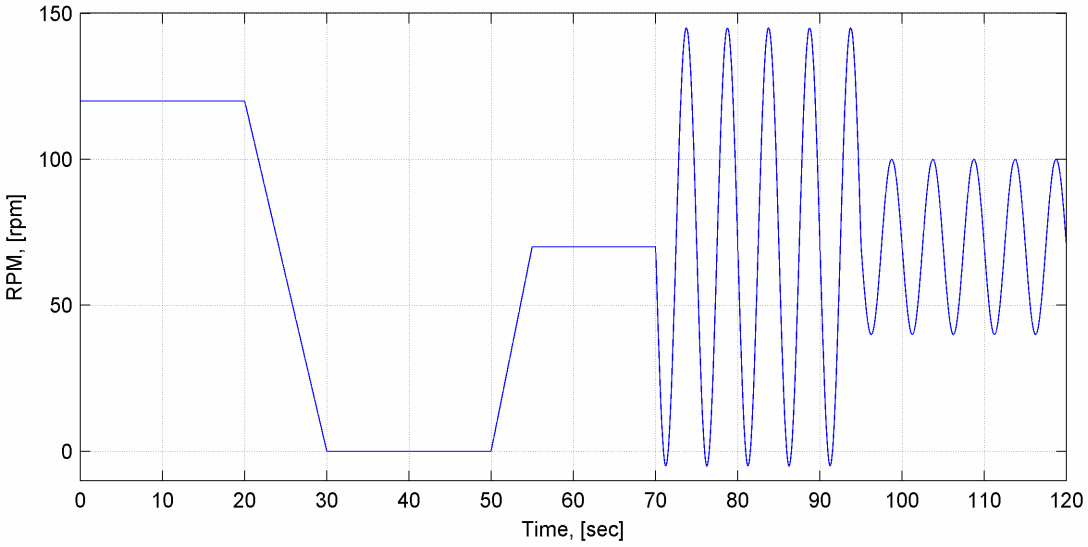

Figure 51 – Input RPM example sequence. Sample frequency: 100 [Hz].

7.2.2 Ideal Magnetometer Readings Generation

Taking the entered RPM trend as mold, ideal x- and y-magnetometer readings are computed. The term “ideal” is used for data that is absolutely free of errors in respect of sensory and environmental (measurand) concerns. The generation is performed in three steps:

First, pipe rotation angle increments are calculated with respect to two consecutive instantaneous RPM samples. Increments become positive in case of forward rotation and negative while the imaginary sub is rotating backwards. Their magnitude depends on the instantaneous RPM and is getting larger with higher rotational speeds and vice versa.

The maximum RPM value at the input RPM trend is restricted by the used sample frequency or, the other way round, a certain (absolute) maximum input RPM requires a minimum sample rate. A too low sample frequency in conjunction with high rotational speeds can lead to pipe rotation angle increments larger than 180°. Increments larger than 180° would result in magnetometer reading phase jumps. This unrealistic behavior must be avoided either by increasing the sample frequency or by a redesign of the input RPM trend.

All calculated pipe rotation angle increments are cumulatively summed up in the next step. By doing that, the corresponding directions to which the imaginary x- and y-magnetometers are pointing are received for each time value in the defined time matrix. For example, if the x-magnetometer is at time t_0 at position $\alpha_0 = 0°$ and at t_{1000} at $\alpha_{1000} = 5940°$ then the pipe has turned 16.5 times between t_0 and t_{1000}.

The last step is the magnetometer readings calculation from the cumulative pipe rotation angle data together with a scaling according to a definable, maximum, lateral, earth's magnetic field intensity. The calculation is straight forward: x-direction data is the cosine of the cumulative pipe rotation angle (with an optional start time direction factor) scaled by the defined maximum magnetic field. Y-magnetometer readings are calculated in the same way with the only difference of using sine instead of cosine.

Figure 52 shows the output of first step in processing the input RPM sequence – the generated ideal magnetometer readings. At lower frequencies/revolutions the phase lag of 90° (π/2) is relatively good identifiable in the figure.

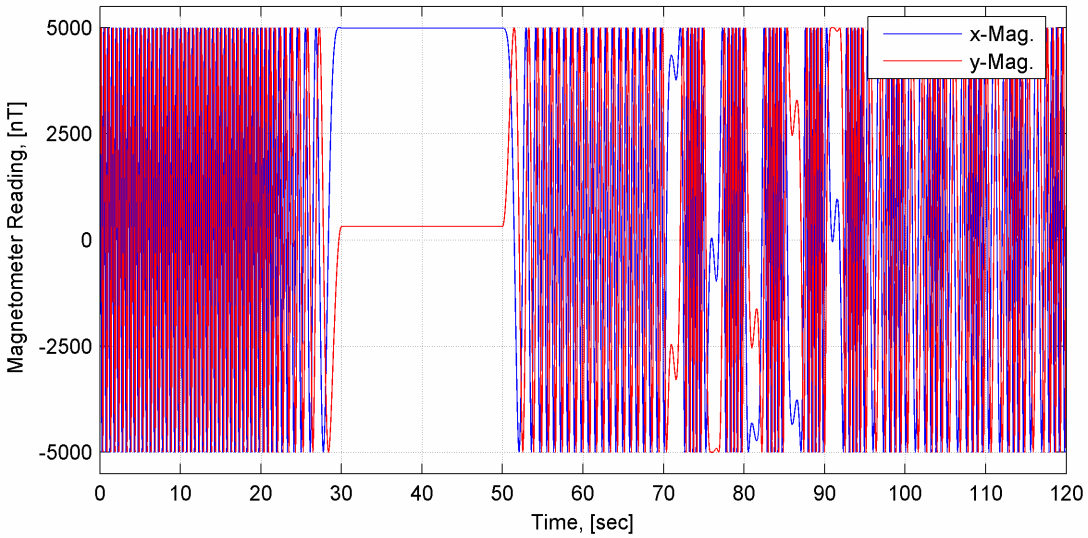

Figure 52 – Synthetic ideal magnetometer readings based on the RPM trend of Figure 51. Sample frequency: 100 [Hz]. Maximum lateral earth's magnetic field intensity: 5000 [nT].

In reality, the measured lateral earth's magnetic field intensity depends on azimuth and inclination of the well at the current sensor position as well as the orientation of the tool in the wellbore. Usually, a tool is not centered in the borehole nor fully aligned with its axis. Thus, depending on tool's global orientation the maximum lateral earth's magnetic field strength can reach values between 0 and 60000 [nT][8],

[19], whereat the upper limit represents already the maximum earth's magnetic field strength seen at the terrestrial poles.

7.2.3 Ideal Instantaneous RPM Calculation

The paragraphs above describe the simulation of CoPilot®'s rotational states. After delimitating the external conditions and how CoPilot® recognizes them, it is of interest what output is received when processing the simulated ideal magnetometer data with the in chapter 7.1 described algorithm.

The resulting "measured" RPM is plotted in Figure 53 together with the delta to the above defined input RPM sequence. The delta appears at the graph as equal to zero. Actually, its order of magnitude is below 10^{-11}. Only at zero RPM delta is exactly zero. Generally, a minor RPM dependence of delta can be observed. To actually assign that very little error to the RPM determination algorithm is not possible as its size is in a range where it can hardly be differentiated from a computational rounding error. Thus, the RPM determination algorithm can be regarded as highly accurate and perfectly working at such ideal conditions.

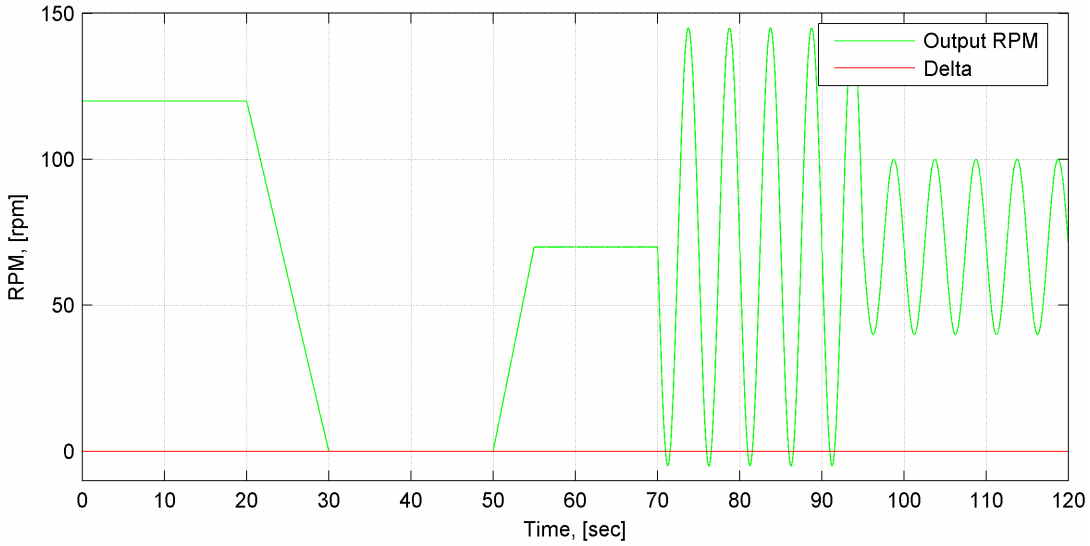

Figure 53 – Instantaneous RPM as CoPilot® would detect it with ideal magnetometer data of Figure 52. Delta is the difference to the defined input RPM sequence (Figure 51).

7.2.4 Real Magnetometer Readings Simulation

As – unfortunately – reality is rarely ideal, an approach is made to train magnetometer readings a kind of real behavior. Unpredictable external influences which can cause reading deflections like magnetic hot spots, casing, moving conductive mud etc. would need a detailed cause and effect analysis to be simulated. As such interferences are not permanently presented as well as changing in

magnitude and thus being very case specific phenomena, they are not covered by the here discussed simulation approach.

Here, the focus is put on steady, sensor induced shortcomings. As the data processing part (RPM determination algorithm) has already been checked and rated as without any deficiencies, a closer look is taken on the data source (magnetometers) as a possible true-to-measured-divergence origin.

A sensor is a device that's output(s) change(s) with respect to a variation of its specific measurand in a known and repeatable manner. As it is hardly possible to achieve a perfectly fixed ratio between measurand and reading variations, especially through out wide sensing ranges, some, usually well known, errors must be accepted.

In this context, the strategy is to alter the generated ideal magnetometer readings by such known errors. In the following sections, errors, specified by the magnetometer manufacturer, are analyzed and their implementation in the simulator is discussed.

7.2.4.1 Linearity Error

The characteristic curve of a magnetoresistive sensor (magnetometer) is s-shaped and (ideally) passes through the origin with an almost linear behavior at small applied fields (Figure 54). Earth's magnetic field intensity is quite low (30 - 60 [μT][19]) compared to the sensing field range of the in CoPilot® incorporated magnetometers. Therefore, surveys always lie in that almost linear region of the characteristic curve.

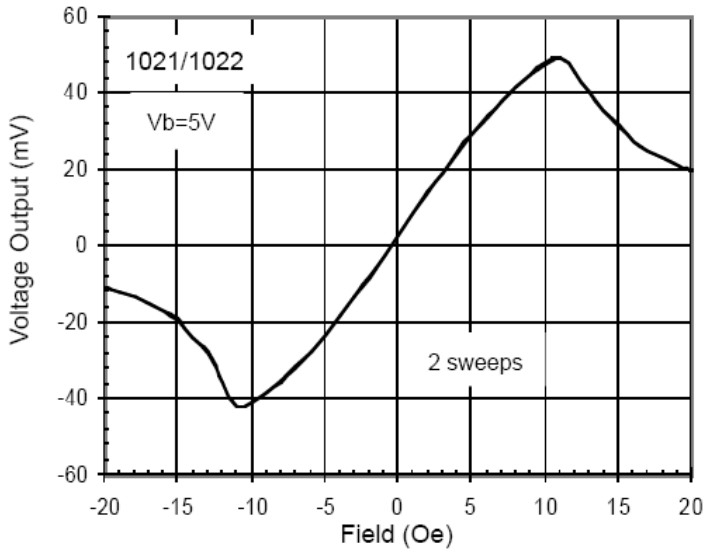

Figure 54 – Characteristic curve of CoPilot®'s magnetometers (sensor output versus magnetic field; 1 [Oe] ≡ 100 [μT]).[20]

The characteristic curve is compared to a straight line to determine linearity. The straight line is defined for a certain range (see Figure 55, black line between H_1V_1 and H_4V_4; actually ±100 [μT]) and a specific fit to the characteristic curve. For this case, it passes trough the start- and the endpoint of the defined range as well as the

origin. All three points are elements of both the characteristic curve and the straight line. Consequently, the linearity error is zero at these points.

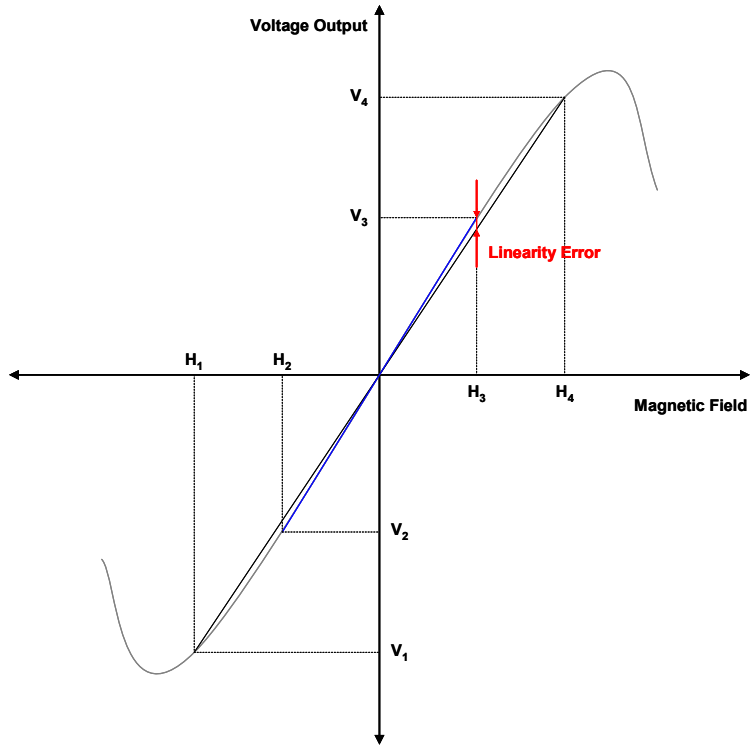

Figure 55 – Linearity error and how it is implemented in real magnetometer behavior simulation (blue line). The depicted characteristic curve (gray) is an example and doesn't represent to the actual magnetometer characteristic.

For the sake of simplicity, due to lack of further more accurate error specifications, and as a result of the characteristic curve shape (s-shaped) the maximum error (0.05 [% FS]) for the range +/-100 [µT] is assumed at 60 [µT] (maximum Earth's magnetic field). At field intensities smaller than 60 [µT], the error is linearly reduced till zero at zero magnetic field intensity. For "positive" fields the error is added, leading to a higher sensor reading, and for "negative" fields it is subtracted, resulting in reduced readings respectively. Actually, the here calculated linearity error does not alter the linearity of the characteristic curve of the initially used ideal sensor model (infinite straight line with positive slope) as the result is again a straight line but it shifts the slope towards a greater value.

7.2.4.2 Hysteresis Error

Some types of sensors show a sensing behavior as they would have a kind of memory. Depending on what they sampled in the past their current readings are influenced. Such a history influenced sensing characteristic is called hysteresis. Magnetometers are a type of sensor that is prone to hysteresis.

Hysteresis is not fully developed until at least one complete (rotation) cycle has been performed. For example, the input quantity has once to go up from minimum to

maximum magnitude and fall back to the minimum again before a full hysteresis effect has emerged.

The characteristic curve of the very first measurements from zero to maximum/minimum is different to all later developing readings. Furthermore, the curve from maximum to minimum is not the same as the one from minimum to maximum due to that kind of memory effect – hysteresis. This effect is not only limited to magnetoresistive sensors. However, at MR sensors the main source of hysteresis is a partially sensor magnetization.

The hysteresis error is a measure of the maximum difference between the upper and lower segment of the characteristic curve, see Figure 56. Usually the position of the specified error is exactly in between the maximum and minimum sensor input.

The hysteresis curve's shape varies according to the size of the minimum/maximum applied magnetic field within defined limits. In positive and negative y-direction (sensor output) the hysteresis curve approximates two horizontal (to x-axis parallel) asymptotes. That means, an infinite strong applied magnetic field (input) does not create infinite high output values. This maximum range of the curve is only reached when the magnetometer is fully magnetized.

The exact shape of CoPilot®'s magnetometer's hysteresis curve is not further specified by the sensor manufacturer. The range of magnetic field intensities, the error was determined for, is quite large compared to the one of earth's magnetic field. The regions close to the asymptotes will never be reached – by far not. The shape of the hysteresis curve for small fields is more "lens-shaped" instead of a "double-s-shaped" form.

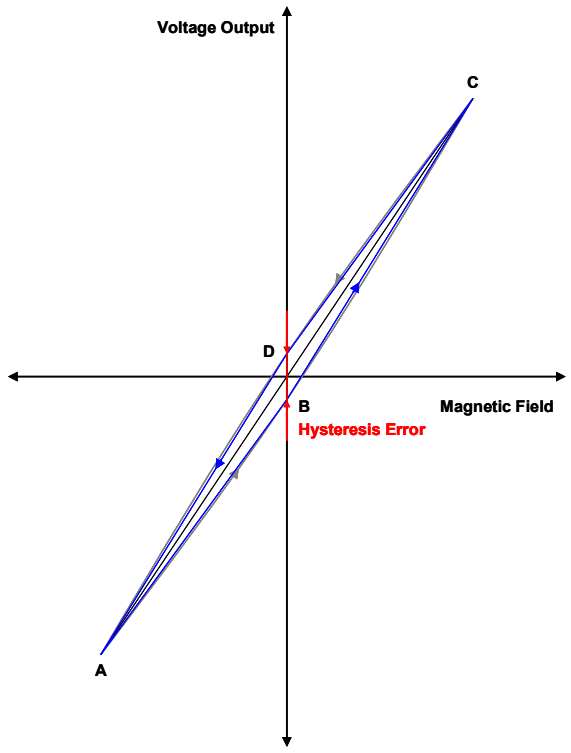

Figure 56 – Hysteresis curve example for a magnetic field of low intensity (gray) and its approximation with a parallelogram (ABCD; blue) in the simulator.

For the sake of simplicity, due to lack of an accurate specified hysteresis curve for the range ±60 [μT], and as a result of the characteristic curve's shape at small applied fields, the hysteresis curve is approximated by a parallelogram (Figure 56). The corner points of the parallelogram, given in [μT], are:

$$A = \begin{pmatrix} -60 \\ -60 \end{pmatrix},$$

$$B = \begin{pmatrix} 0 \\ -\dfrac{Hysteresis\ Error}{2} \end{pmatrix},$$

$$C = \begin{pmatrix} 60 \\ 60 \end{pmatrix},$$

$$D = \begin{pmatrix} 0 \\ \dfrac{Hysteresis\ Error}{2} \end{pmatrix}.$$

At the minimum (A) and the maximum (C) the error is zero. At the points B and D (zero field intensity) the hysteresis error reaches its maximum. For field intensities between minimum/maximum and zero the corresponding error is calculated by linear interpolation either on the segment ABC, for increasing field intensities, or on the segment CDA, while decreasing intensities. The initial assumed ideal characteristic curve is a straight line passing trough points A and C as well as the origin (black line in Figure 56). To get away from the ideal case towards a more realistic one, the hysteresis errors (positive and negative in sign) are added to the ideal characteristic curve.

The hysteresis error calculation comprises, besides the approximation of the curve by a parallelogram, potential little inaccuracies around the points A and C (maximum and minimum magnetic field intensity). These result form discrete field measurements (sample frequency dependent spacing of measurements). If maximum or minimum (A or C) is not exactly hit by a sample but shortly before or after then a correct allocation to the right segment (upper or lower) of the hysteresis curve is not possible.

7.2.4.3 Repeatability Error

The repeatability error covers all other sensor errors that do not belong either to linearity or hysteresis (if no other error type is explicitly specified). The repeatability error is a random error. As such, its influence is quite significant throughout the whole magnetic field range because its magnitude is not a function of the applied field and its relative size is identical with the hysteresis error (0.08 [% FS]). Thus, every sample can be affected by the entire repeatability error.

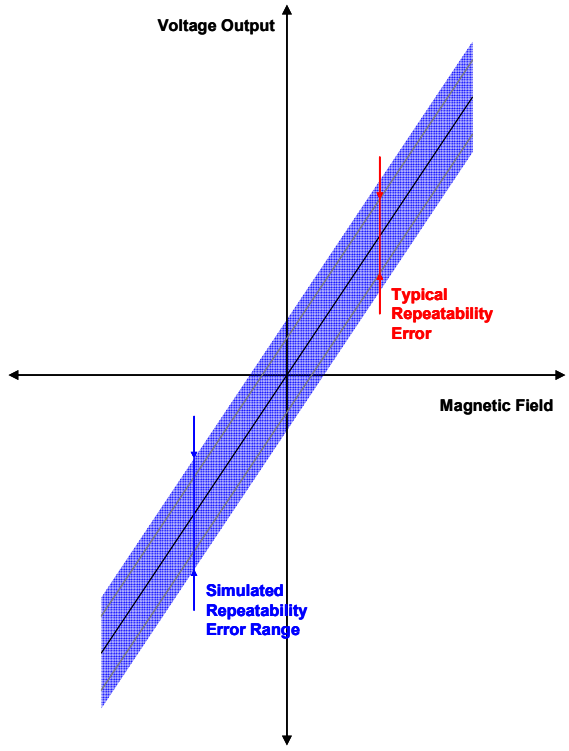

Figure 57 – Repeatability error outline and simulated error range (blue).

At the magnetometer specifications it is given as typical error. Maximum and minimum errors are not specified. A real sensor's repeatability error will vary around this typical value. To respect that, a range of ±50 [%] the typical error size is assumed out of which the simulated error magnitude is randomly picked and added to or subtracted from the ideal straight line characteristic curve.

7.2.4.4 Sensor Resolution

Sensors do also have a certain resolution. Resolution is optional included in the simulator. Correlations with real magnetometer readings turned out that the simulated resolution influence is too severe. Simulated readings jump almost only between the total error's range maximum and minimum. For this reason, the resolution simulation option is actually not activated. A possible reason why such a significant sensor resolution influence is not seen at real readings is the decimation process of the raw data where the readings are down sampled from 1000 [Hz] to 200, 100 and 40 [Hz].

7.2.4.5 Sensor Errors General

Recapitulatory, it can be stated that the linearity error increasingly deflects the ideal characteristic curve (straight line) the closer the applied magnetic field approaches its extremes, while on the other hand the hysteresis error is gaining its highest significance around zero field intensity. The repeatability error is a random error and

as such it is present throughout the whole magnetic field range with identical probability and magnitude distribution.

All errors are specified as typical errors. At the simulator it is not regarded that the linearity and hysteresis error's relative size can vary around that value and thus has not necessarily to match the actually given typical size. This limitation is accepted as two out of three errors are implemented in the simulator as self-contained models which would not work properly with varying relative error magnitudes. Whereas, at the repeatability error, which it is just a random error, an error range is assumed (±50 [%]) to get away from that specified, single, constant error magnitude as in reality there is a certain variance as well.

The output of each of the three error simulation steps is an error matrix with identical size like the two generated ideal magnetometer readings matrices. Finally, the real magnetometer readings are obtained by adding the error matrices to both ideal magnetometer readings matrices – for x- and y-direction respectively. This straight forward last simulation step for real data is enabled due to a RPM element/magnetometer reading related error matrices filling during the error simulation.

7.2.4.6 Simulation Versus Measurement

To simulate real magnetometer readings a couple of assumptions have been made. Some non trivial effects have been not included in the simulator (constant fractions, magnetic hot spots, conductive mud, etc.). Furthermore, at actual measurements CoPilot®'s decimation process probably compensates some of the mentioned errors as well as certain not simulated effects to an unknown extend. These facts together with a general simulation reasonability check ask for verification of the simulator results with measured data.

Three different wells in three different geographical regions (earth's magnetic field intensity is not everywhere the same throughout the globe) are selected for verification. Not two measured data sets were sampled by the same tool (different serial numbers). Additionally, only data intervals with zero tool rotational speed are chosen to ease results comparison.

Example well names and countries they are located in are:

- Well A: Canada
- Well B: Indonesia
- Well C: Germany

It must be mentioned, that the measured magnetometer data is dimensionless as CoPilot® does not scale it to a physical unit, whereas the simulated one is given in Tesla. The maximum lateral earth's magnetic field intensity, stated for each example well, is the absolute value of the oscillation limits. This means that while the tool is rotating, the magnetometer readings oscillate between the defined positive and negative maximum lateral earth's magnetic field intensity. By considering that, one

may get a good impression about the dimensions of the total signal variations compared to the in the following shown enlarged cutouts of almost pure noise.

To detect micro motions of the string and so to avoid a comparison of movement with noise, the correlation between the readings in x and y-direction is checked as well. Basically the x-readings are a cosine and the y-readings a sine signal which would show the in Figure 58 depicted ideal relation.

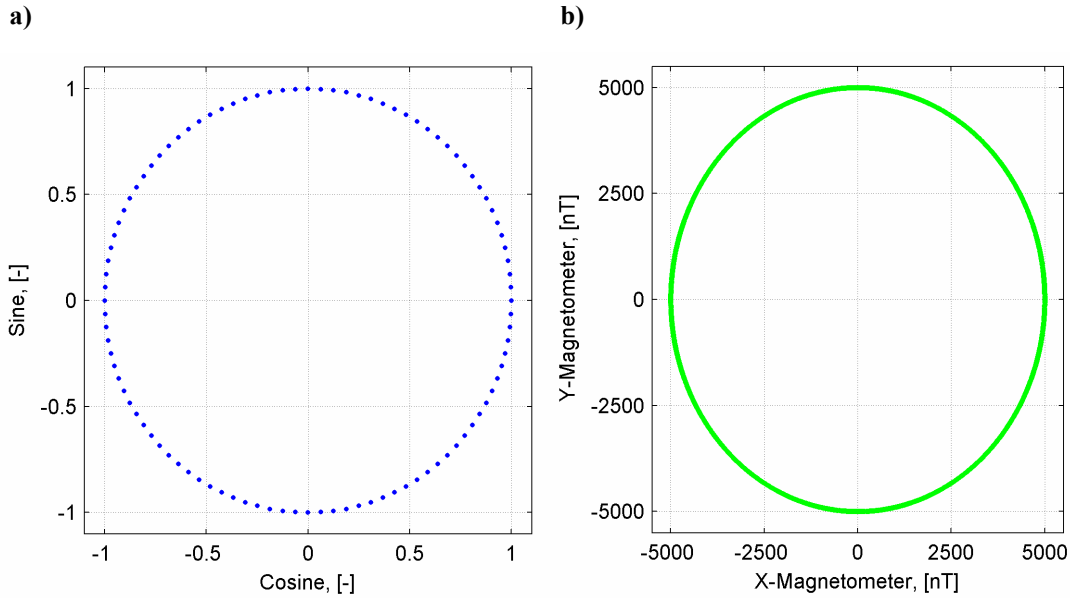

Figure 58 – Example of cosine-sine-relation (a), 100 points) and the x- and y-magnetometer relation of simulated ideal sensing behavior (b), all data points of input RPM sequence (Figure 51)). Actually, both relations deliver perfect circles and appear only at the plots a little distorted.

So, if the measured magnetometer data will show some kind of similar, circular-shaped relation (even when it appears o-shaped in the graph), it is an indication of properly working magnetometers. While, if the short data cutout of an initially appearing zero RPM period seems to be obviously a segment of its corresponding circle, it indicates that the tool was actually rotating or slightly swinging back and forth. In cases where such a relation cannot be clearly observed both channels (x- and y-magnetometer) should deliver just noise.

7.2.4.6.1 Well A

The data was captured by a 6 ¾ “ CoPilot® incorporated above the PDM in a motor BHA. A tri-cone-bit was used and the drilling fluid was oil-based. Figure 59 shows a one second cutout of by one of CoPilot®’s magnetometers measured earth’s magnetic field intensity.

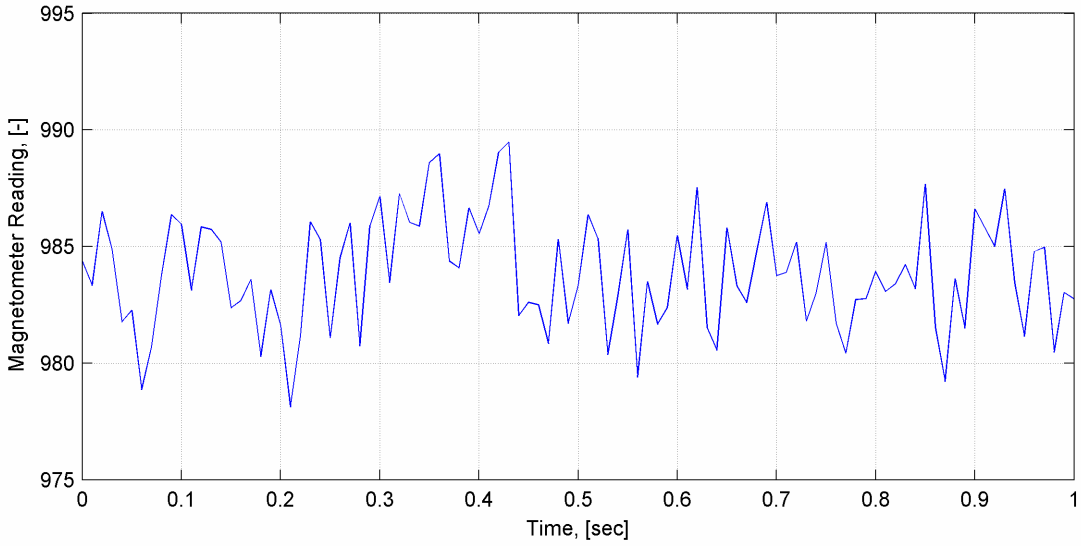

Figure 59 – Well A: During a non-rotating period by one of CoPilot®'s magnetometers sampled data. Sample frequency: 100 [Hz]. Maximum lateral earth's magnetic field intensity: ~2100 [-].

Actually, a measured magnetic data sequence captured while a period of absolutely no string rotation (surface RPM of zero) is most appropriate for comparison with the simulation results. Furthermore, the pumps should not work as they introduce some vibrations as well. The first condition is fulfilled for the shown example. The second one is never met as pumps off would also imply a switching off of CoPilot®'s power source.

A drawback of Well A is the motor in the BHA. The in Figure 59 shown data is sampled while drilling in sliding mode. Whenever the pumps are working also the motor is turning. A motor generates a certain amount of reactive torque especially when the bit is on bottom. Additionally, it is a source of high energetic lateral vibrations. The reactive torque depends on the bit formation interaction as well as on WOB. For this case, WOB is quite calm and almost constant at 25.0 [t] during the cutout.

What is more important is torque and tangential acceleration as their fluctuations would indicate BHA rotation. Therefore, both must not be too shaky to accept a data segment for simulation verification. The corresponding near-bit torque and tangential acceleration of the cutout are shown in Figure 60.

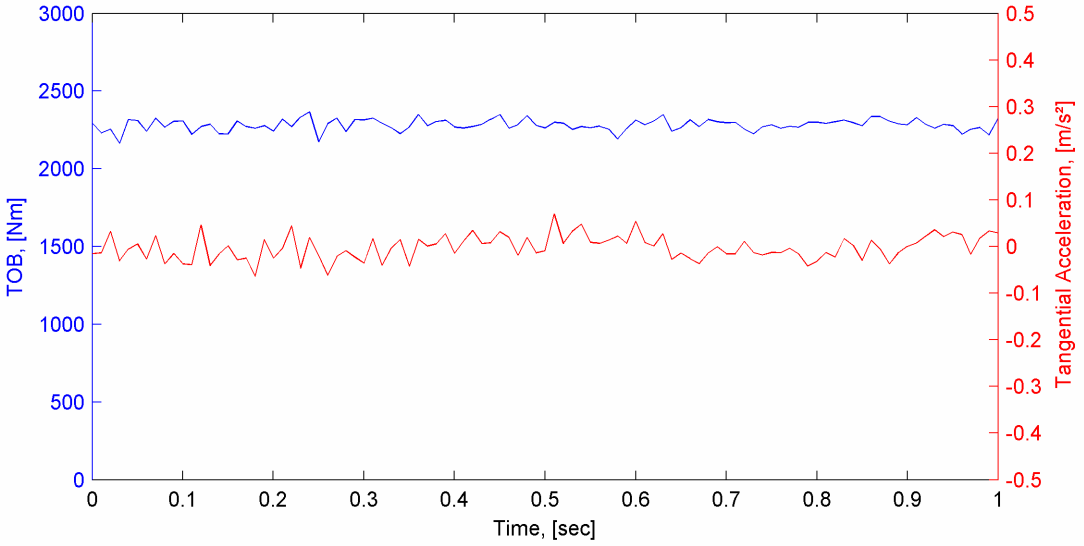

Figure 60 – Well A: Torque on bit and (corrected) tangential acceleration for the same time interval as shown in Figure 59.

Torque is more or less constant and thus indicating a torsional stationary BHA. Tangential acceleration should be considered with care as the actual measured acceleration has constant as well as RPM dependent offsets (mentioned already in a previous chapter). The shown tangential acceleration is corrected for these offsets. As a result, RPM, a function of magnetometer data, is influencing tangential acceleration and consequently also its noise is transferred to the tangential acceleration data. Therefore, little fluctuations like the ones seen in Figure 60 will always be present.

However, the depicted tangential acceleration confirms the chosen measured magnetometer data cutout as suitable due to the lack of off-trend peaks or troughs. Consequently, both parameters qualify the selected measured magnetometer readings as a valid and proper criterion.

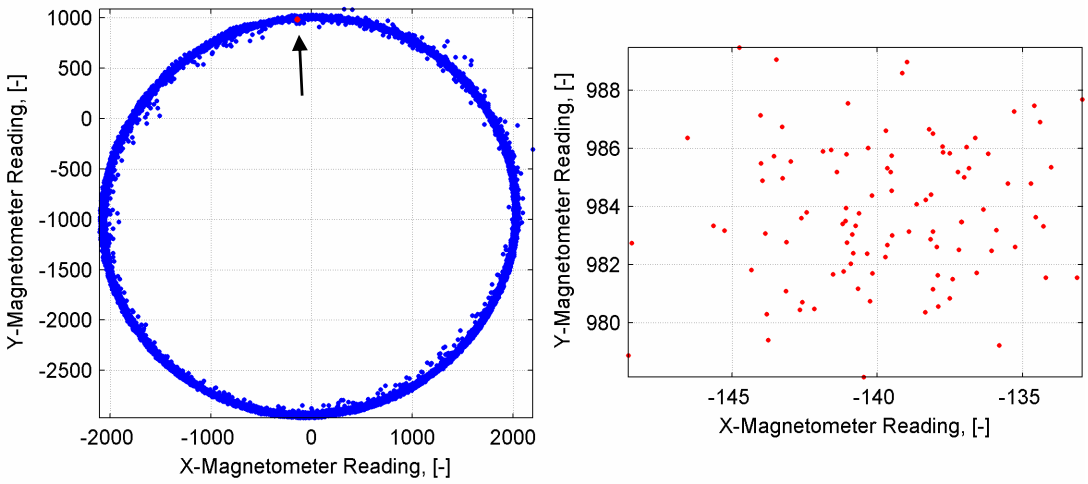

Figure 61 – Well A: Relation of both measured magnetometer signals of the whole trigger (left) and a blow-up of the discussed cutout (right). Axes are of equal scale.

Referring to Figure 61, it does not clearly indicate any particular motion. The variance of the y-magnetometer signal is almost identical with the one of x-direction. In case of motion with respect to the current "circle position", the range of the y-signal would be significantly smaller.

The result of the simulator for an ideal and a simulated real magnetometer signal are shown in Figure 62. No "fine-tuning" of the simulator was performed. The plotted results are generated just by adding all above mentioned sensor errors to the ideal sensor characteristic curve. However, such a good match is surprising. Fluctuation ranges as well as signal characteristics are almost identical. Of course, a sample to sample comparison shows almost no correlation between both data sets but also would not make any sense. Such a comparison is meaningless as it would compare random noise to random noise.

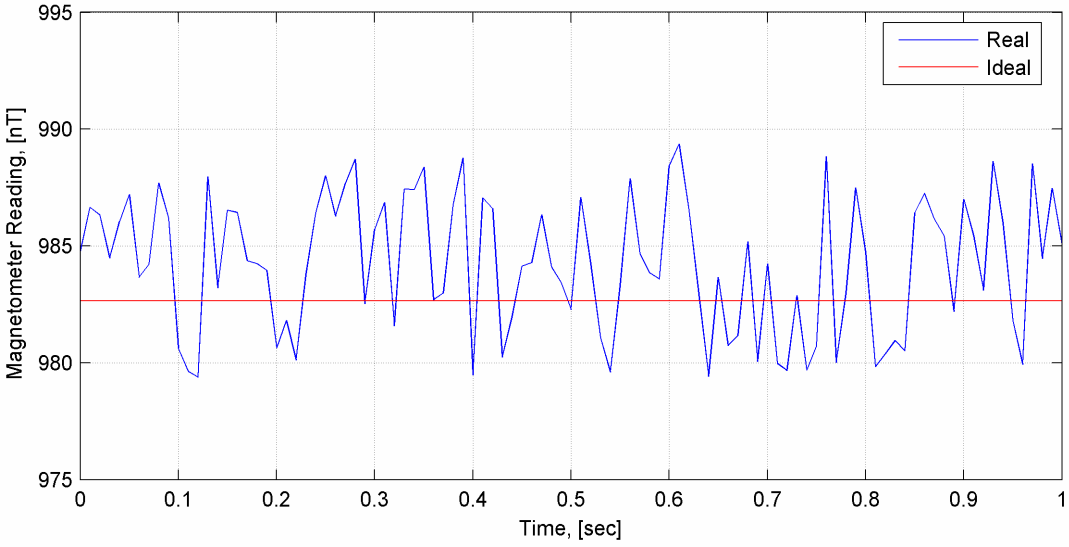

Figure 62 – Well A: Simulated magnetometer readings with ideal and real sensing behavior. Sample frequency: 100 [Hz]. Maximum lateral earth's magnetic field intensity: 2100 [nT].

7.2.4.6.2 Well B

The BHA of Well B is a rotary steerable BHA. Below the 6 ¾ " CoPilot® there are the following components: reamer, MWD, PDM, steering unit, and a PDC bit. The mud type is OBM. While the taken cutout the string is not rotating. Thus, the incorporated reamer should not have any effect on the data. The bit is on bottom and solely driven by the PDM.

Torque shows little oscillations (Figure 63) with about the same frequency as WOB is swinging around 9.5 [t] (±200 [kg]). The corrected tangential acceleration is more or less frozen at a low positive level. As it is staying at this level for about the first quarter of the high speed trigger, until the string starts to rotate, an offset in the accelerometer data is very likely. That the sensors work at all, demonstrate the last three quarters of the trigger.

No obvious correlation between TOB oscillations and tangential acceleration changes validate the assumption that also the BHA of Well B is stationary. Furthermore, Figure 64 confirms that conclusion by not indicating any significant relation of measured x- and y-magnetometer data during the cutout.

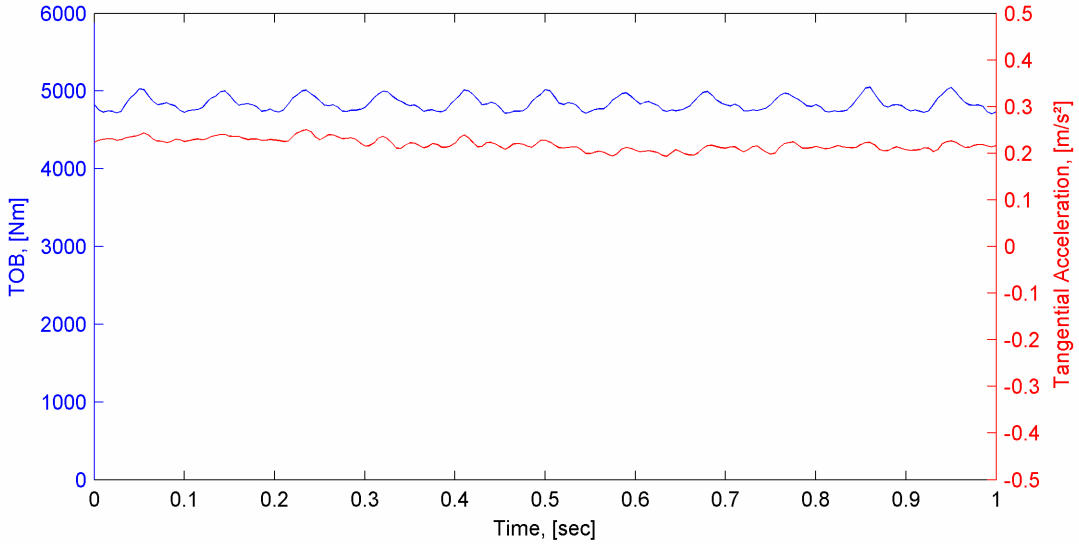

Figure 63 – Well B: Torque on bit and (corrected) tangential acceleration.

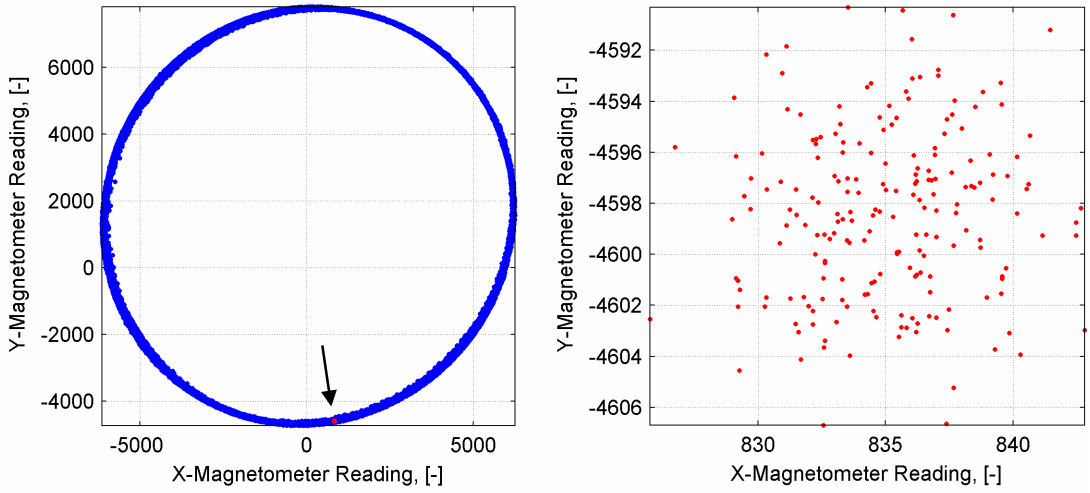

Figure 64 – Well B: Relation of both measured magnetometer signals of the whole trigger (left) and a blow-up of the discussed cutout (right). Axes are of equal scale.

The measured magnetometer data is plotted in Figure 65. Figure 66 shows the simulation results.

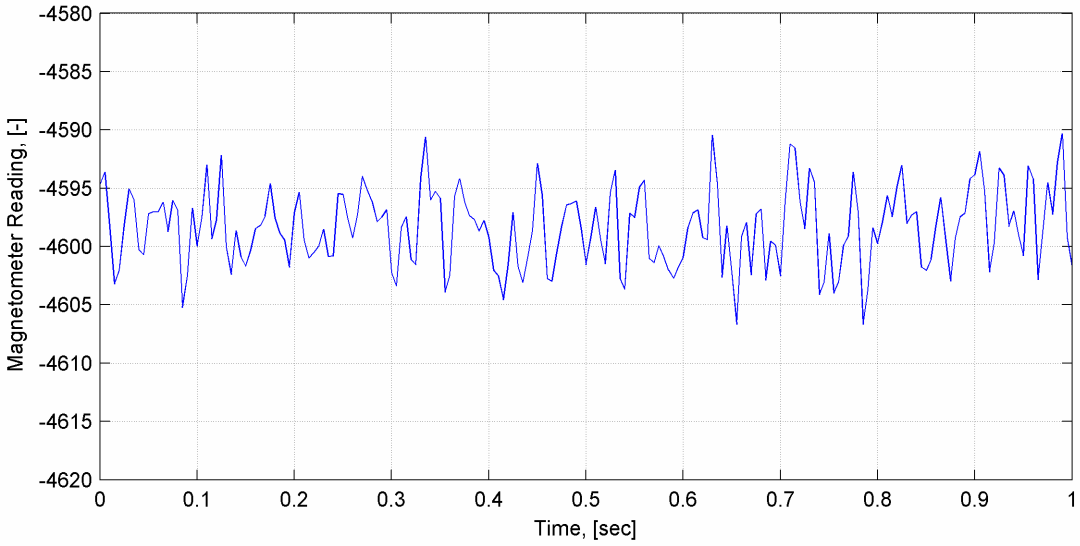

Figure 65 – Well B: Measured magnetometer data. Sample frequency: 200 [Hz]. Maximum lateral earth's magnetic field intensity: ~6200 [-].

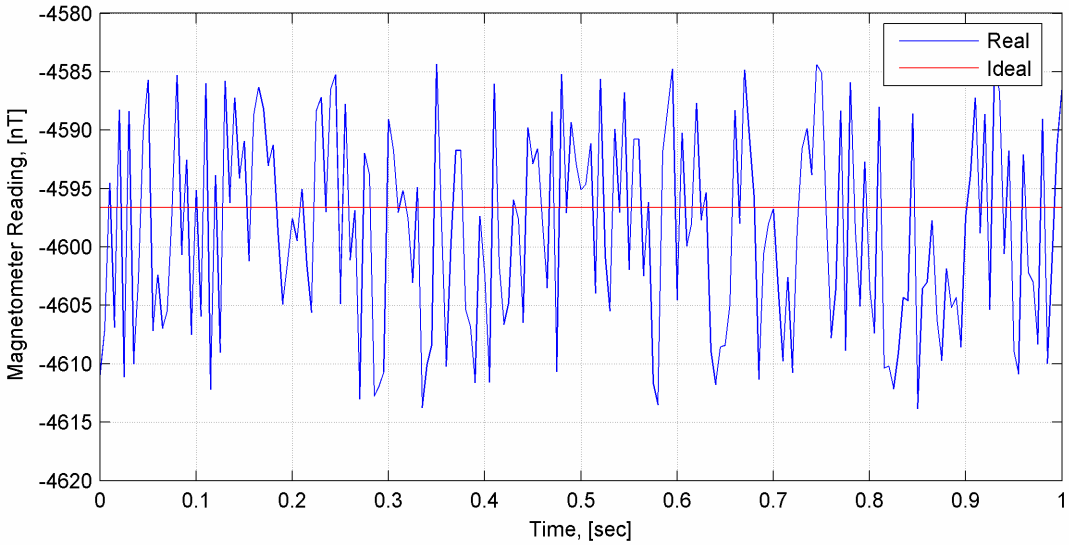

Figure 66 – Well B: Simulated magnetometer readings with ideal and real sensing behavior. Sample frequency: 200 [Hz]. Maximum lateral earth's magnetic field intensity: 6200 [nT].

The correlation of measured and simulated readings at Well B is not as good as at Well A. The simulated signal oscillation range (noise) is about twice the size of the measured on. Of course, that obvious discrepancy could easily be removed by just using the repeatability error like specified and not letting it getting 50 percent larger in both direction, positive and negative (absolute plus 100%). But as a consequence, Well B would not be comparable to Well A anymore solely because of that changed simulation parameter. Data of Well A and B was not sampled by the same tool. Therefore, it is also possible that the repeatability error of tool B is closer to the specified typical one.

As it is the aim to verify the simulator, parameter changes are not allowed and thus not executed.

When disregarding the signal's amplitude range, the general characteristics appear still quite similar.

7.2.4.6.3 Well C

At reference Well C a 4 ¾" CoPilot® sampled the data. The tool was just separated from the impregnated bit by a mud motor. Drilling fluid was a NaCOOH/KCOOH water-based mud (WBM). WOB is slightly shaking around 1.1 [t].

Although the tool run at Well C was a test of that new tool size, the data basically appear reasonable and Well C is selected as a reference well as well. Only one limiting factor belongs to that well – the tangential acceleration. At the section plotted in Figure 67 it seems to be almost perfectly constant but at a negative level. Considering the whole high speed trigger, a proper sensed tangential acceleration appears questionable.

Actually, the shift to a negative level was introduced during tangential acceleration correction where also a constant fraction had been removed. As the original measured tangential acceleration is nearly zero in the first half of the trigger whereas in the second half it only reaches occasionally positive values, the elimination of the constant fraction (subtraction of mean value) results in a shift towards negative values (after performed signal inversion). As the reason why tangential acceleration almost never touches zero in the second trigger half is not known and as such a behavior is regarded as abnormal, tangential acceleration is not considered at this well due to serious doubts in the accuracy of the measurement.

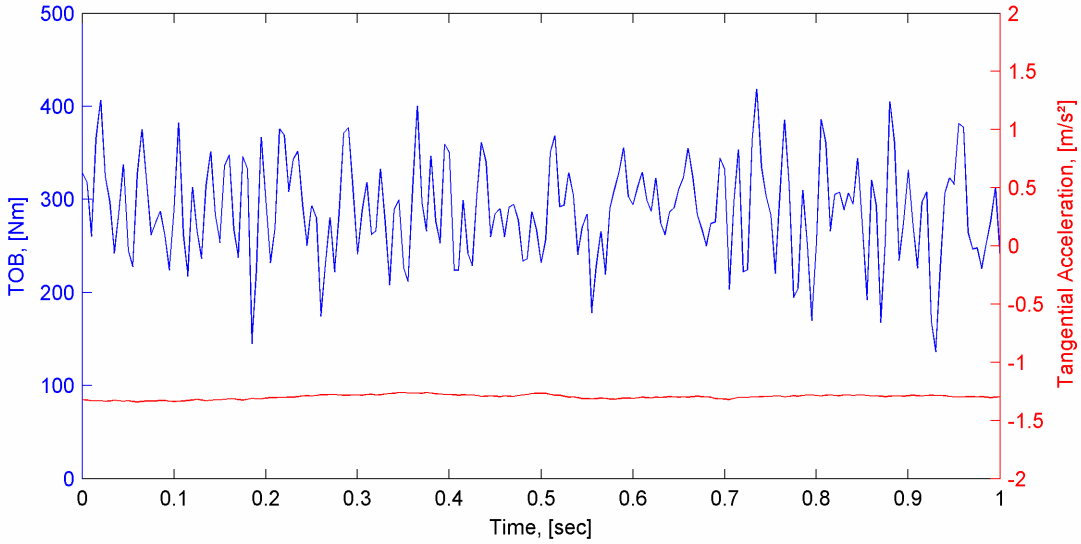

Figure 67 – Well C: TOB and (corrected) tangential acceleration.

TOB looks quite spiky in Figure 67 but by relative means it is more or less constant, additionally when taking into consideration that the torque sensing error is up to 500 [Nm]. Solely based on information gained from Figure 67, the cutout of Well C data could be considered as a valid reference with potential zero BHA motion.

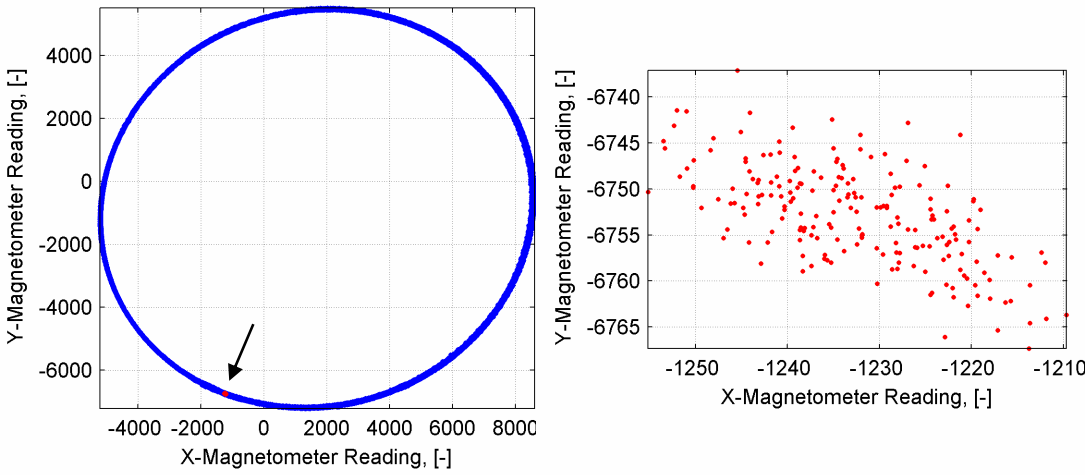

Figure 68 – Well C: Relation of both measured magnetometer signals of the whole trigger (left) and a blow-up of the discussed cutout (right). Axes are of equal scale.

Whereas, some potential drillstring motion can definitely not be excluded anymore when Figure 68 is regarded. Considering the "circle-position" of the magnified measured data segment even emphasizes more the anyway obvious presents of a rotary motion trend at the cutout samples. The measured RPM and its oscillation range are not considerably different to the ones of the other example wells. However, this last example should not be rated too high for verification as some micro motions of the BHA were most portably present while sampling the data.

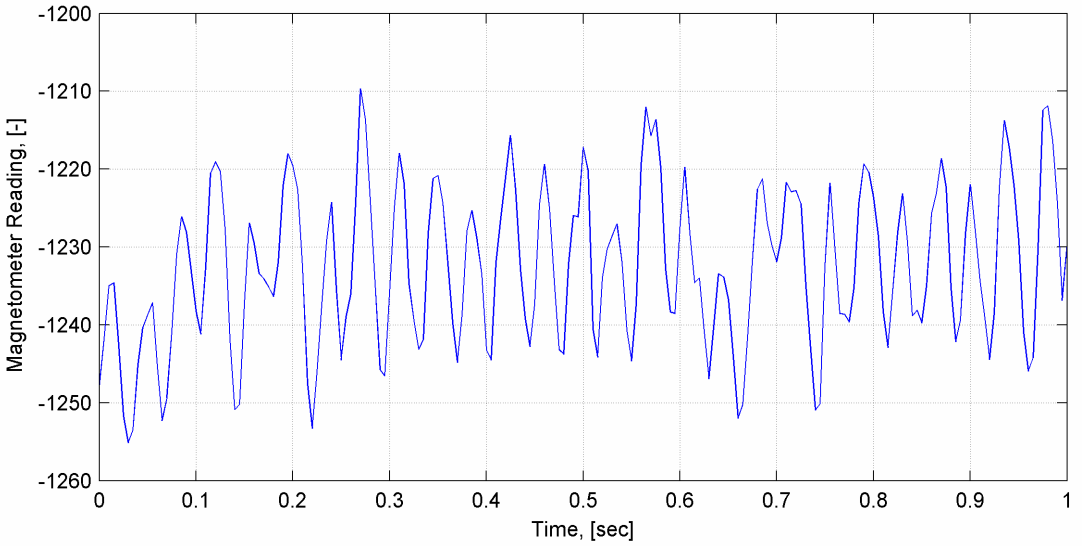

Figure 69 – Well C: Measured magnetometer data. Sample frequency: 200 [Hz]. Maximum lateral earth's magnetic field intensity: ~6600 [-].

Figure 69 shows the measured and Figure 70 the simulated readings. At this example both data ranges are close together and thus probably indicating a better repeatability error correlation. However, this is contrary to example Well B and thus addressing that better match to the possible pipe rotation would also be a viable interpretation. Additionally, to mention is the higher peak density at the simulated data whereas the

measured data appears smoother. Anyway, the simulation results are not that far away from the measured ones, what is quite astonishing for that not perfect reference well.

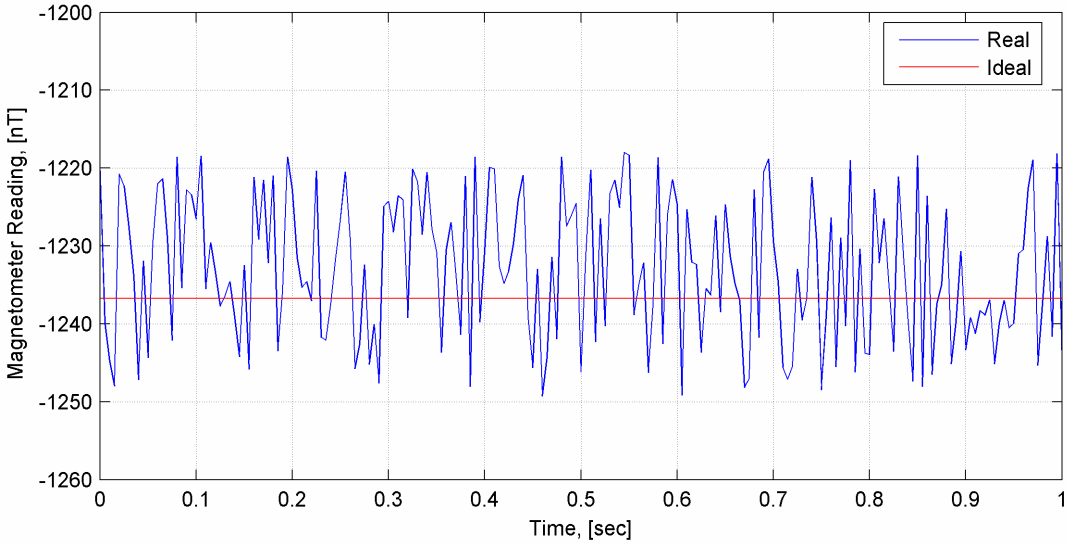

Figure 70 – Well C: Simulated magnetometer readings with ideal and real sensing behavior. Sample frequency: 200 [Hz]. Maximum lateral earth's magnetic field intensity: 6600 [nT].

7.2.4.6.4 Conclusions and Recommendations

Basically, the simulated readings match the measured data quite well. 200 [Hz] simulated data compared to the 100 [Hz] data sticks out a little bit as it is obvious more spiky. A reason for that is seen in CoPilot®'s raw data decimation process. 200 [Hz] simulated readings are just twice as many as 100 [Hz] simulated readings with identical properties. This is not the case at measured data of CoPilot®.

Regarding100 [Hz] data simulation, it is more similar to measured samples than 200 [Hz]. Hence, for magnetometer readings simulation it is recommended to use a sample frequency of 100 [Hz].

Furthermore, other observed deviations of the simulated readings from the measured ones could also result from in the simulator not included external influences on the magnetometers. For example, quite frequently a significant constant fraction at the measured data can be seen. Sometimes, that fraction is that high that no zero-crossing of the signal is achieved anymore. In terms of linearity error as well as hysteresis error, the operating region on the characteristic curve of the sensor is shifted considerably and thus causing completely different error magnitudes. Such an influence of a constant fraction is not covered by the simulator.

Probably an even better match could be achieved by simulating 1000 [Hz] raw sensor data and subsequently processing it with the same algorithms as used in CoPilot® to generate 40, 100 or 200 [Hz] data. This approach was not only thought about but also tried to be implemented in the simulator. The problems that arose so far were all addressed to limited computational power. A change from 100 to 1000 [Hz] is

leading to skyrocketing computation times and thus making the simulator impracticable for the desired purpose. Anyway, 100 [Hz] simulation results appear quite good and absolutely reasonable and based on that the simulator can be used for further general analysis.

7.2.5 Real Instantaneous RPM Calculation

By making use of the built simulator, the effect of a real imperfect sensor on CoPilot®'s RPM detection algorithm is investigated. Again, the in Figure 51 shown RPM sequence is taken for analysis.

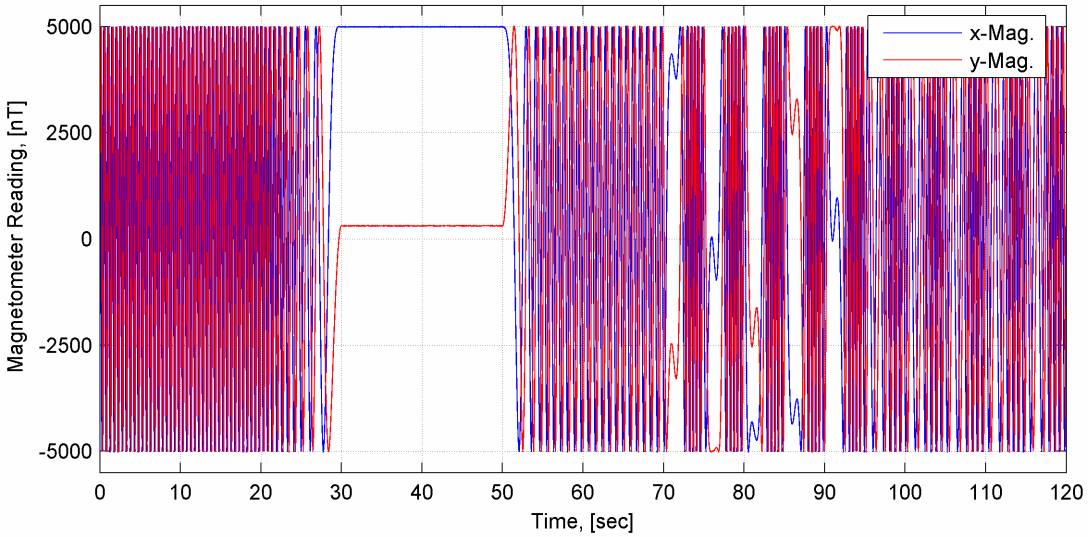

Figure 71 – Noise (sensor errors) afflicted, synthetic magnetometer readings of the RPM trend of Figure 51. Sample frequency: 100 [Hz]. Maximum lateral earth's magnetic field intensity: 5000 [nT].

The in Figure 71 shown simulated real sensor readings are plotted hardly distinguishable from the ideal ones of Figure 52. However, the signals are no more perfectly smooth but afflicted with noise (sensor errors) as similar signal blow-ups like Figure 62, Figure 66 and Figure 70 demonstrate. What happens when with an absolutely known RPM trend close to real magnetometer readings are simulated, and finally the RPM trend is recaptured after running the simulated readings through CoPilot®'s RPM detection algorithm, is shown in Figure 72.

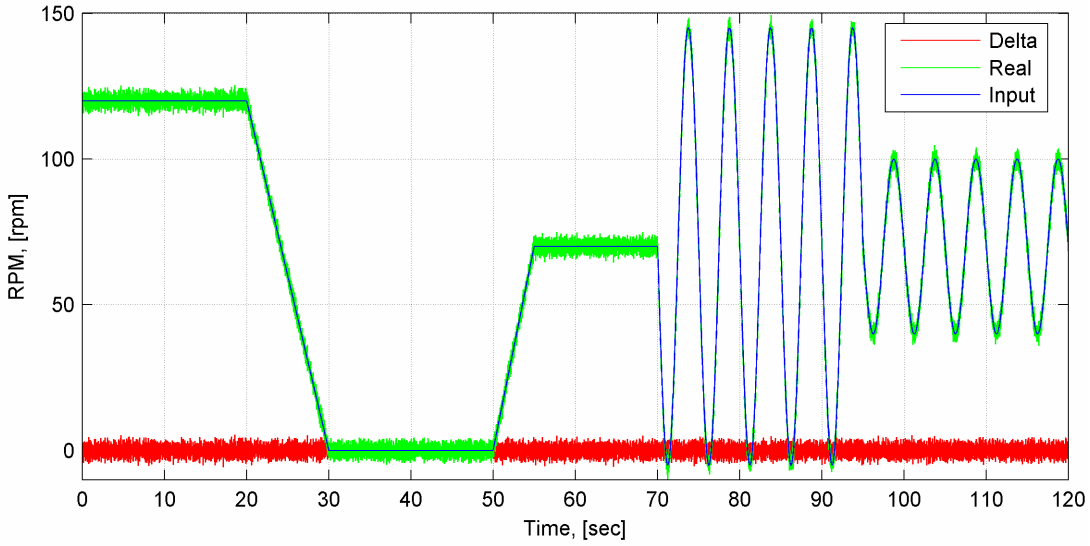

Figure 72 – Pipe rotational speed based on simulated sensor data which imitates real sensing behavior. Sample frequency: 100 [Hz].

As the RPM detection algorithm has been proven to work properly, it must be concluded that every noise related signal variation is misleadingly translated to RPM values and therewith senor noise is carried over to RPM. Anyway, CoPilot®'s RPM detection ability, solely rated, is outstanding good when disregarding adverse external influences.

Due to the simulator design, the absolute error (delta) throughout the whole test sequence has about the same range of magnitude. For low revolutions per minute the error magnitude has already been proven above. A priori, the error range at higher rotational speeds should be taken just as a very rough estimate because possible RPM induced noise (errors) has not been investigated here nor implemented in the simulator.

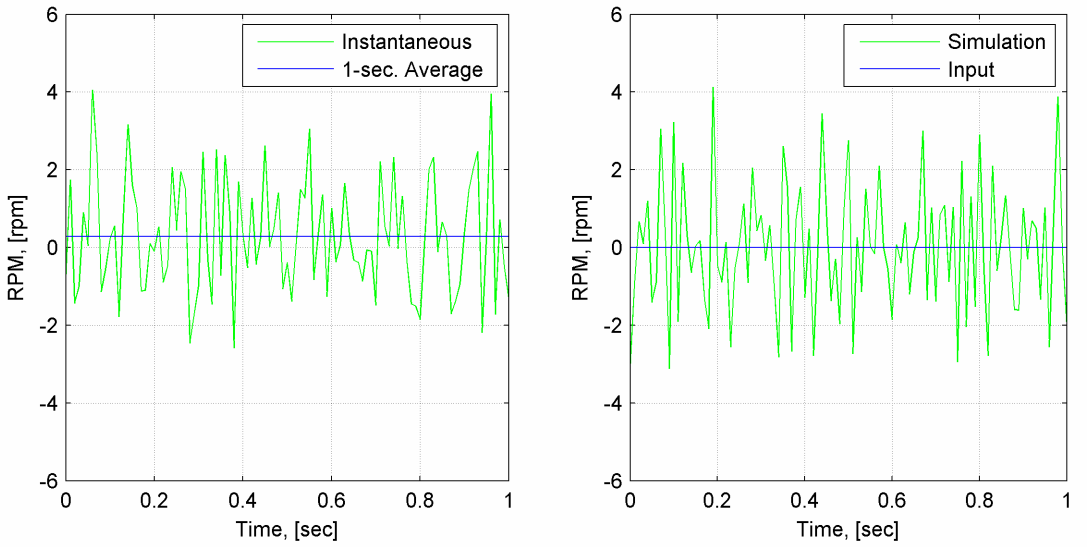

Figure 73 – Comparison of measured RPM (left, sample frequency: 100 [Hz], maximum lateral earth's magnetic field intensity: ~2100 [-]) to simulated RPM (right, sample frequency: 100 [Hz], maximum lateral earth's magnetic field intensity: 2100 [nT]). The right signal is and should not be a copy of the left one but should and does have similar characteristics.

What is more, the with sensor errors simulated RPM matches measured data quite well (see Figure 73).

The effects on CoPilot®'s stick-slip diagnostic results will be analyzed in a chapter later on.

7.3 Conclusions

Under perfect conditions with assumed ideal sensor characteristics, CoPilot® would be able to gauge its rotary speed absolutely free of errors.

The RPM calculation method itself is exactly performing to expectations – highly accurate.

When considering non-ideal conditions, the limited accuracy of the magnetometers is carried over through to the RPM calculation, resulting in some noise in the RPM data.

In general, the by sensor errors induced noise levels do alter the results at a moderate scale. When disregarding other detrimental influences on magnetometers, the measured instantaneous RPM should be a fair estimate of the actual tool rotational speed.

To sum up, the **magnetometers** are the **limiting factor**. Improvements on their accuracy would directly affect RPM data quality.

8 Current Stick-Slip Diagnostics Algorithm*

The currently implemented stick-slip diagnostics algorithm is basically a statistical analysis of the RPM trend and a subsequent results classification with respect to predefined thresholds.

The stick-slip classification is based on two indicators:

- Severity
- Direction

Both indicators will be discussed in more detail in the following sections.

8.1 Severity

Severity determination makes use of an entropy statistic, Q, with the following equation:

$$Q = \frac{\sqrt{\left|\left(\overline{x^3} - \bar{x}\cdot\overline{x^2}\right)^2 + 4\cdot\left(\overline{x^2} - \bar{x}\cdot\bar{x}\right)\cdot\left(\overline{x^2}\cdot\overline{x^2} - \bar{x}\cdot\overline{x^3}\right)\right|}}{\left|\bar{x}\right|\cdot\left(\overline{x^2} - \bar{x}\cdot\bar{x}\right)} \qquad \textbf{(E 8.1)}^{[15]}$$

The average statistics, $\bar{x}$, $\overline{x^2}$, and $\overline{x^3}$, are calculated as follows whereat N is the number of elements of the input data set (modified after [15]):

1st Order Statistic: $$\bar{x} = \frac{1}{N}\sum x \qquad \textbf{(E 8.2)}$$

2nd Order Statistic: $$\overline{x^2} = \frac{1}{N}\sum x^2 \qquad \textbf{(E 8.3)}$$

3rd Order Statistic: $$\overline{x^3} = \frac{1}{N}\sum x^3 \qquad \textbf{(E 8.4)}$$

* While this work has been done a CoPilot® firmware upgrade, which also affected the stick-slip diagnostics algorithm, were performed. Therefore, the actual currently employed stick-slip diagnostics algorithm differs from the in this chapter presented one. However, all stick-slip diagnostic data used during this work were still generated by the algorithm which is named "current" throughout this work.

The entropy computation is always based on four frames and thus covering not only the current frame (five seconds long) under investigation but additionally also the last three (history) frames. For this reason, the moments of rotational speed over 20 seconds in total influence the entropy result. Furthermore, prior the entropy is calculated a check for very low RPM variance is made. If the dimensionless check parameter is below a defined limit then Q is set equal to zero. The check condition is the following:

$$\frac{\overline{x^2}}{\bar{x}\cdot\bar{x}} - 1.0 \quad < \quad 0.0002 \qquad \textbf{(E 8.5)}^{[15]}$$

Finally, the received entropy is normalized that a full-scale deflection in rotary speed is equal to 1.0.

$$Q_n = \frac{Q}{\sqrt{2}} \qquad \textbf{(E 8.6)}^{[15]}$$

8.2 Direction

Events of backward rotation are captured by a backward rotation counter. The counter quantifies the fractions of backward rotation over a certain period of time. The limit for backward rotation is currently set at -0.2 radians per second. If the ratio of collected backward rotation counts to the total number of data elements exceeds 0.1, the looked at RPM data set is assessed as stick-slip of highest level (diagnostic word state 7) – full stick-slip with backward rotation.

8.3 Diagnostics

Stick-slip events are categorized by a total number of eight levels (Table 6). Primarily, the entropy is compared against a predefined set of seven thresholds. A classification of stick-slip severity levels/diagnostic word states between 0 and 6 is indicating that the entropy is equal to or greater than the corresponding threshold. Level 7 is in this respect an exception as it makes use of the direction parameter as well. Therefore, either highest entropy values or 10 percent of the data is exceeding the backward rotation threshold leads to a level 7 diagnostics.

				Thresholds			Thresholds		Thresholds							
Word State	**Decimal**	**0**		**1**		**2**	**3**		**4**		**5**		**6**		**7**
	Binary	000		001		010	011		100		101		110		111
Stick-Slip Severity		***Low***	**0.2**	***Normal***	**0.4**	***Normal***	**0.6**	***Oscillation***	**0.8**	***Oscillation***	**1.0**	***Stick-Slip***	**1.2**	***Stick-Slip***	**8.0**	***Backward***

Table 6 – Diagnostics thresholds (modified after [15]).

8.4 Algorithm Analysis

8.4.1 The Ideal Case

To be able to solely investigate the diagnostics algorithm's function, all adverse influences due to imperfect input parameters need to be eliminated. For this reason, the RPM data is not taken from measurements but synthetically generated with exactly defined trends. Such examples where all input parameters are manageable are called "ideal" in this context.

a) Normal:

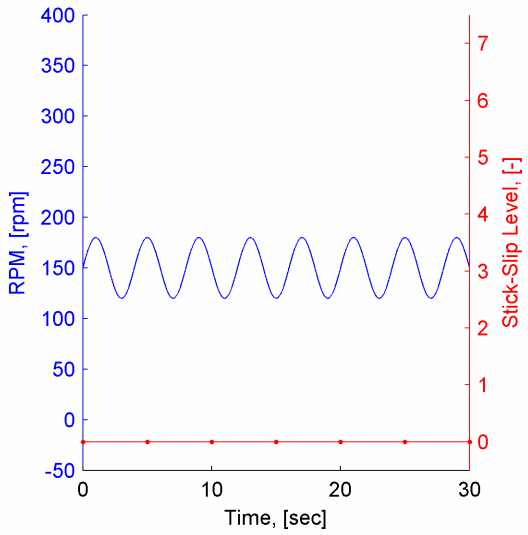

b) Oscillation:

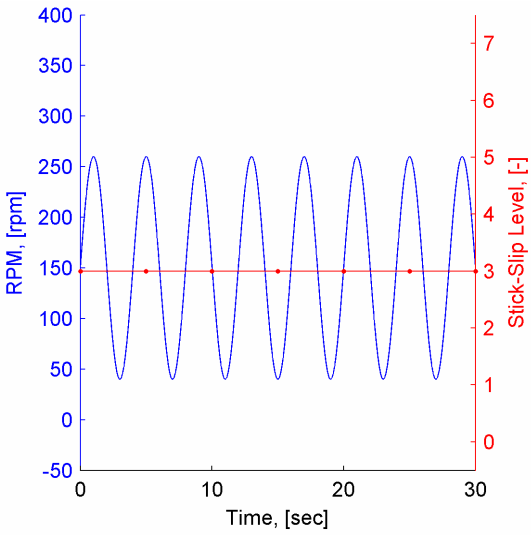

c) Stick-Slip:

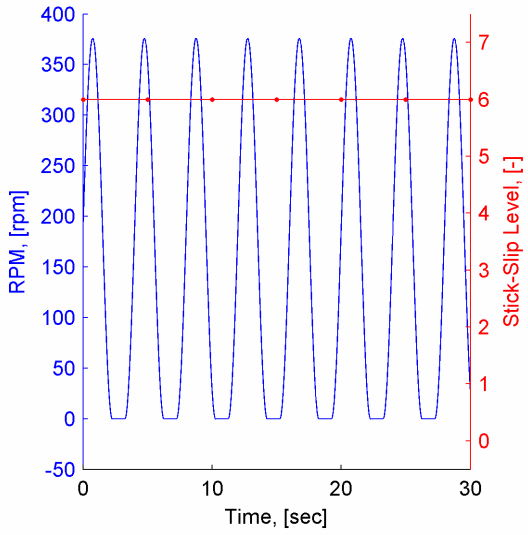

d) Backward Rotation:

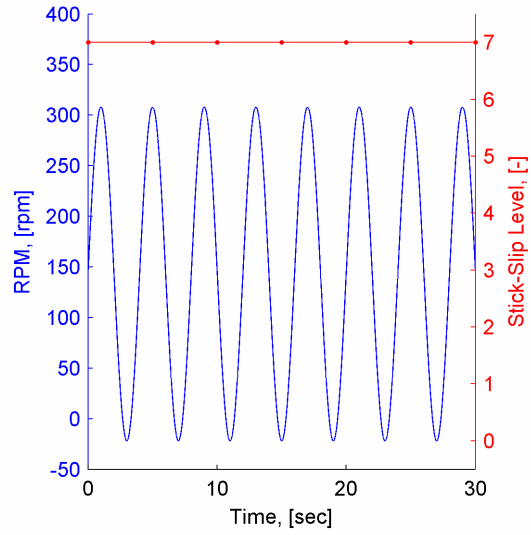

Figure 74 – Synthetic diagnostics examples of the current stick-slip algorithm with varying ideal RPM ranges. The average downhole RPM (= surface RPM) is 150 [rpm] and identical throughout all examples as well as the oscillation period length of 4 seconds. Each of the stick-slip levels (red dots) belongs to the 20 [sec] of RPM data before the marker. Sample frequency: 200 [Hz].

In this chapter all presented graphs are generated with a sample frequency of 200 [Hz]. Actually, CoPilot® uses only a sample rate of 40 [Hz] for RPM calculation and thus stick-slip diagnostics. For these ideal cases, a higher sample frequency does not harm the general trends nor alter single parameters significantly but results in a better resolution.

Figure 74 shows four stick-slip diagnostics examples. All RPM trends are without any similarities between each other (BHA, drillstring length, etc.) besides an identical average RPM and the same oscillation period length.

As the input parameter – the drillstring revolutions – of the stick-slip diagnostics algorithm is defined, the diagnostic behavior can be observed. Such varying RPM oscillation ranges should result in accordingly different stick-slip levels which actually is the case as Figure 74 confirms. Thus, the in Figure 74 analyzed RPM trends indicate a proper diagnostic capability of the algorithm.

Just a short objection on average RPM data: all four stick-slip examples have the same average RPM (150 [rpm]). It is distressingly what a bulk of information can be lost by pushing averaging too far.

Figure 74 covers only RPM oscillation range variations. Real drillstrings see not only periodical (and of course erratic as well) RPM changes but also the frequency of the changes is not constant over time (e.g. increasing drillstring length with ongoing drilling progress). Thus, the influence of the RPM oscillation frequency is investigated next.

8.4.1.1 RPM Oscillation Frequency Influence

The following parameters are used for RPM trend generation to examine the current stick-slip algorithm's susceptibility to RPM oscillation frequency variations:

Minimum RPM:	40	[rpm]
Maximum RPM:	260	[rpm]
Average RPM:	150	[rpm]
Oscillation frequency:	0.05 – 50	[Hz]
Sample frequency:	200	[Hz]

The synthetically generated ideal RPM data is a sinus-wave with varying frequency. Basically, the parameters are the same (except of the varying RPM oscillation frequency) as the ones used for case b) in Figure 74.

While keeping the RPM oscillation amplitude constant and just varying the oscillation frequency, the current stick-slip algorithm rates the stick-slip severity like shown in Figure 75.

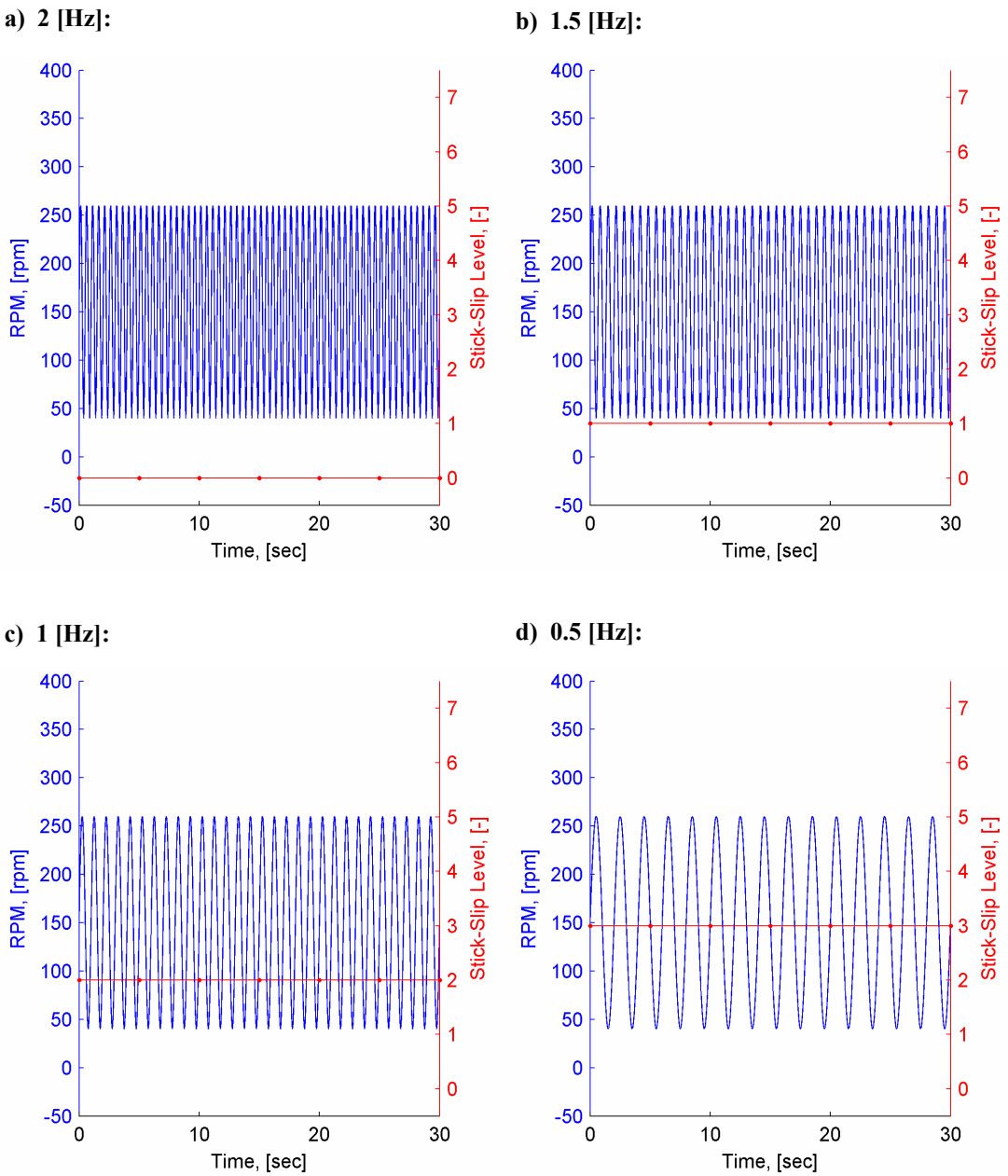

Figure 75 – Synthetic diagnostics examples of the current stick-slip algorithm with varying ideal RPM oscillation frequencies. Sample frequency: 200 [Hz].

From Figure 75 it must be concluded that the current stick-slip algorithm is RPM oscillation frequency sensitive. Four different RPM oscillation frequencies lead to four different stick-slip levels. Moreover, how the algorithm reacts on frequency changes is alarming as the severity level increases with falling oscillation frequency.

Actually, higher frequencies cause higher stresses and strains in the BHA as it has to accelerate and decelerate more often in the same period of time while still touching unchanged maximum and minimum RPM levels. Therefore, an influence of RPM oscillation frequency on the stick-slip diagnostics is desirable in general but the current one is unfortunately contrary. If there is a frequency influence at the diagnostics algorithm, it should lead to higher severity levels at higher oscillation frequencies.

To get an idea about the RPM oscillation frequency influence, Figure 76 is calculated. It shows the (averaged) normalized entropy, basis of stick-slip levels 0 till 6, versus the RPM oscillation period length. The RPM function is the same as specified for Figure 75. The data is plotted for oscillation frequencies from 50 – 0.05 [Hz]. Frequencies higher than 5 [Hz] (below period length 0.2 [sec]) are plotted more for a general algorithm analysis purposes than due to in reality expected, by bit and/or drillstring friction excited, RPM oscillation frequencies. The upper limit is simply set by 0.05 [Hz] as it is the lowest frequency where a whole oscillation period can be trapped by the 20 seconds interval which the algorithm uses for diagnostics. For longer period lengths/lower frequencies the algorithm does not see anymore at least one complete oscillation period and thus misinterpretation would be the result anyway.

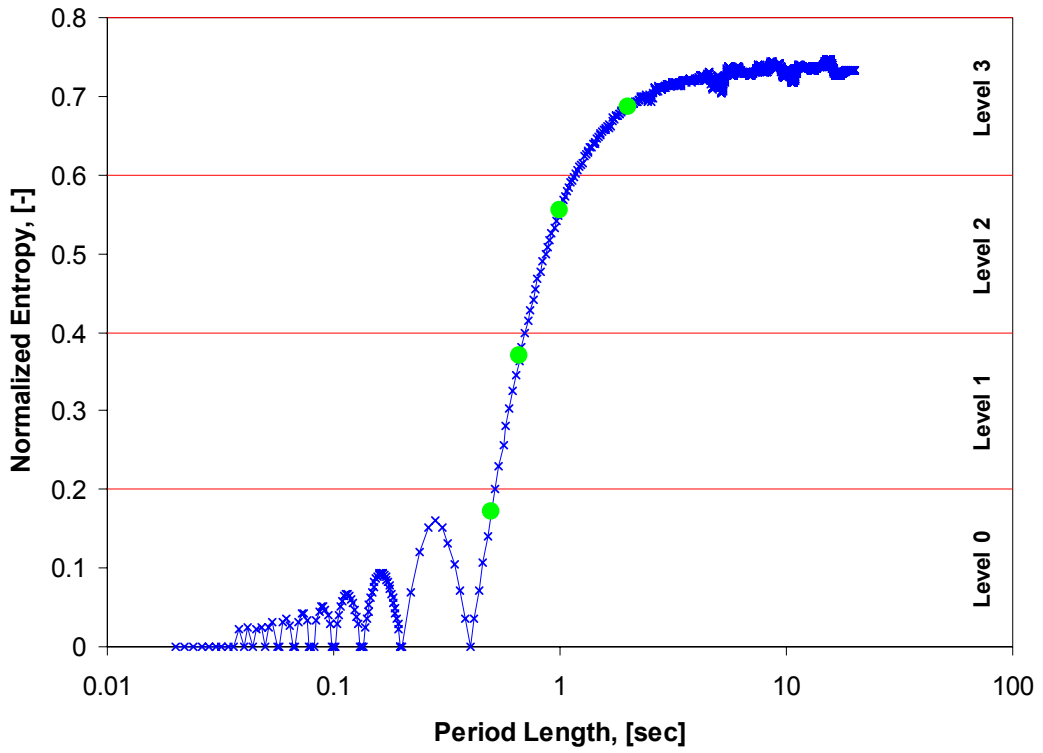

Figure 76 – Normalized entropy (averaged) for varying ideal RPM oscillation frequencies (50 – 0.05 [Hz]). The green dots symbolize the averaged entropy values of the examples of Figure 75. Sample frequency (for entropy calculation): 200 [Hz]. Graph data density: 0.02 – 0.2 [sec]: 500 [Hz], 0.2 – 20 [sec]: 50 [Hz].

The entropy characteristic of Figure 76 seems to approach an asymptote at about 0.74 [-] at very low oscillation frequencies. Below a period length of around 3 seconds (0.333 [Hz]) the entropy falls quite rapidly and eventually reaches zero at a period length of 0.4 seconds (2.5 [Hz]). From this point until the lower interval limit, the entropy trend is a succession of peaks and roots till finally staying at zero. Actually, the entropy does not necessarily to reach exactly zero but, as mentioned above, will be set to zero for very low signal variance as well.

The most critical region in respect to stick-slip analysis can be addressed to the interval between the last root till the entropy is getting quite close to its asymptote (at

Figure 76: between 0.4 and 3 seconds). This region of moderate frequencies can absolutely contain the RPM oscillation frequency of a drillstring. For such an event, a tiny oscillation frequency change could result in a causeless severity level jump. An increase in RPM oscillation frequency is able to turn down the resulting stick-slip level till zero and vice versa. In reality you do not know the oscillation frequency nor are instantaneous downhole RPM data in real-time available at the surface where it could be read out. Thus, the stick-slip severity level can solely be delusive.

When assuming the algorithm was originally designed for lower frequency regions, thus consequently for the highest possible severity level, then stick-slip underestimation can occur. Short large in diameter and thus torsional stiffer drillstrings with relatively high stick-slip oscillation frequencies would therefore cause lower diagnosed stick-slip severity levels. Whereas, for a long slender drillstring with lower oscillation frequencies the algorithm tends to diagnose rather high levels.

Regarding Figure 76 it must be stated, that the shape of the curve appears very similar to a filter frequency response. A clue that reinforces this impression is the root at 0.4 seconds of period length which is exactly the length of the moving boxcar filter used to average the RPM before being evaluated by the current stick-slip algorithm. It needs to be taken into consideration that this stick-slip determination problem might be primarily an effect of the moving boxcar filter which is a processing step before entropy is calculated. Therefore, Figure 76 is generated again (see Figure 77) but at the current stick-slip algorithm the moving boxcar filter is disabled to allow entropy calculations to be based on instantaneous RPM.

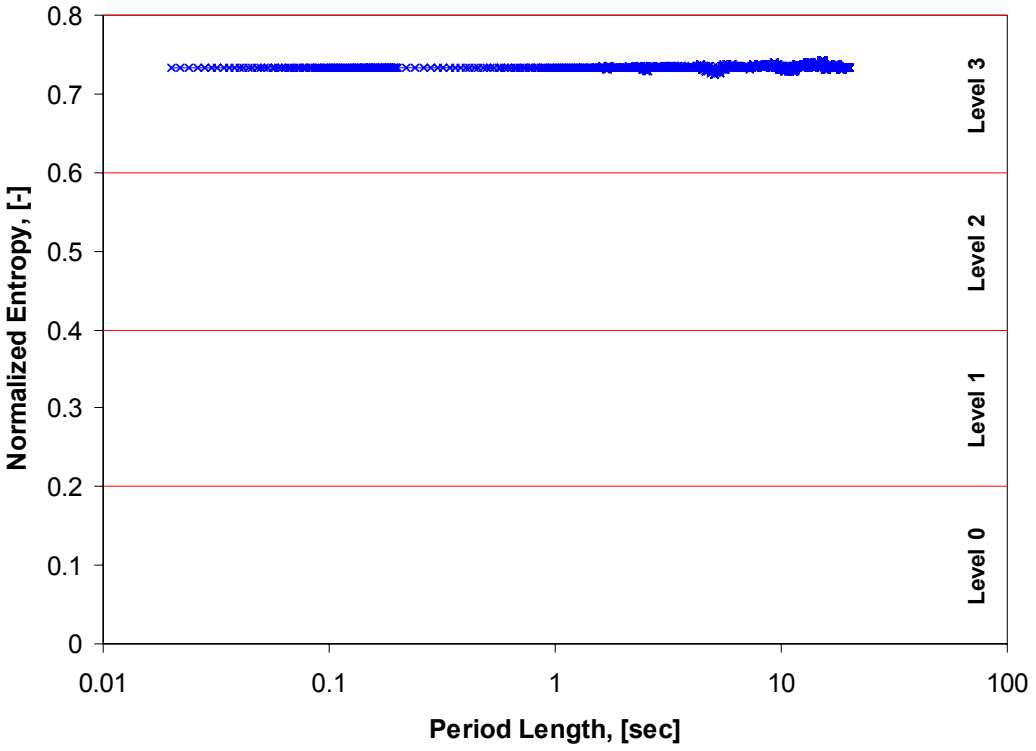

Figure 77 – Normalized entropy (averaged) for varying ideal RPM oscillation frequencies (50 – 0.05 [Hz]). The entropy is determined from instantaneous RPM data which is in contrast to Figure 76 and

the current stick-slip algorithm where entropy is based on averaged RPM. Sample frequency (for entropy calculation): 200 [Hz]. Graph data density: 0.02 – 0.2 [sec]: 500 [Hz], 0.2 – 20 [sec]: 50 [Hz].

The simulation results (Figure 77) go along with the suspicion. If entropy of instantaneous RPM is computed the RPM oscillation frequency influence fully disappears. For the here discussed example, the RPM oscillation frequency influence can be solely addressed to the in the current stick-slip algorithm implemented moving boxcar.

It must be taken into account that at this example ideal RPM data (totally absence of noise) is used which is already generated at the defined sample frequency. The effect of the raw, measured, instantaneous RPM is unknown. Mavericks and noise probably would adversely affect the results most of the time as the average filter's purpose is to eliminate or at least reduce such influences.

Furthermore, measured RPM data is filtered and decimated a certain number of times before it is actually passed on to the moving boxcar. Hence, it appears very likely that not only the moving boxcar filter influences entropy results but also the filters of the decimation process. This hypothesis cannot be further evaluated as full scale simulations (1000 [Hz] data plus processing and decimation steps) exceed available computational power/time.

This phenomenon again highlights the problem with imperfect input data and its source for follow-up problems. Why in this subchapter always averaged entropy values were taken will be explained in the section below.

8.4.1.2 FSR Influence – Fringe Effects

Another problem encountered while the simulation of the ideal examples is the influence of the frame sample rate or more precise that the RPM signal is split into rigid frames. RPM entropy will vary depending on whether a RPM frame/set starts at a trough, a peak, a zero-crossing, or anywhere else in between. This may result in different stick-slip levels for one and the same RPM trend just caused by different frame start values.

For example, two surveys which recorded identical RPM trends are analysis for stick-slip. At one survey frames are accidentally picked at RPM troughs and at the other the frames are always start at zero RPM by change. Finally, just this little difference is responsible for two different stick-slip levels for actually the same RPM trend. These fringe effects are also the reason why in Figure 76 and Figure 77 an averaged entropy is plotted as the instantaneous one of the overlapping 20 seconds RPM analysis intervals is not constant in contrast to the continuous RPM trend.

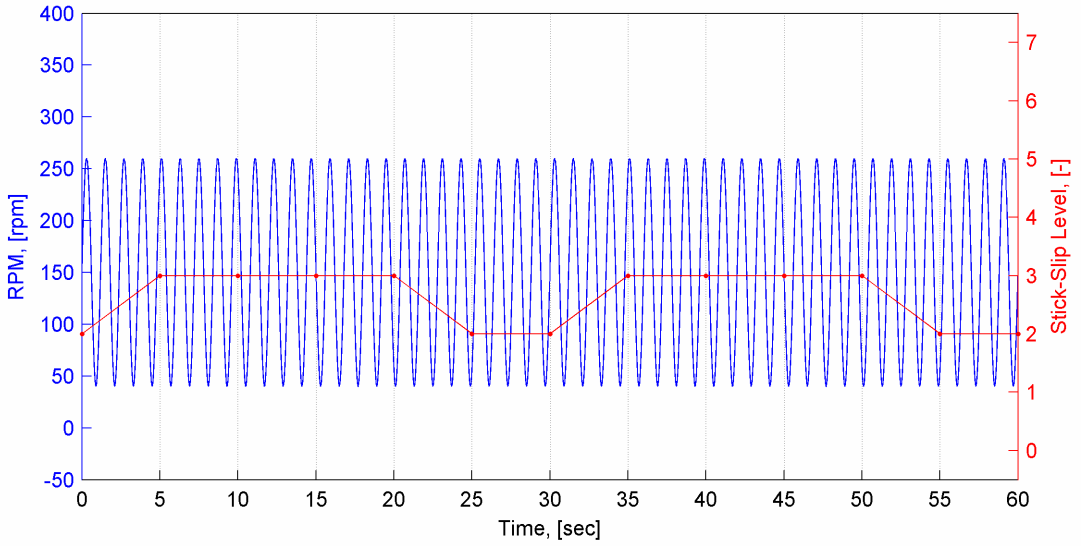

Figure 78 – High frequency example of frame sample rate influence. RPM oscillation frequency: 0.8333 [Hz].

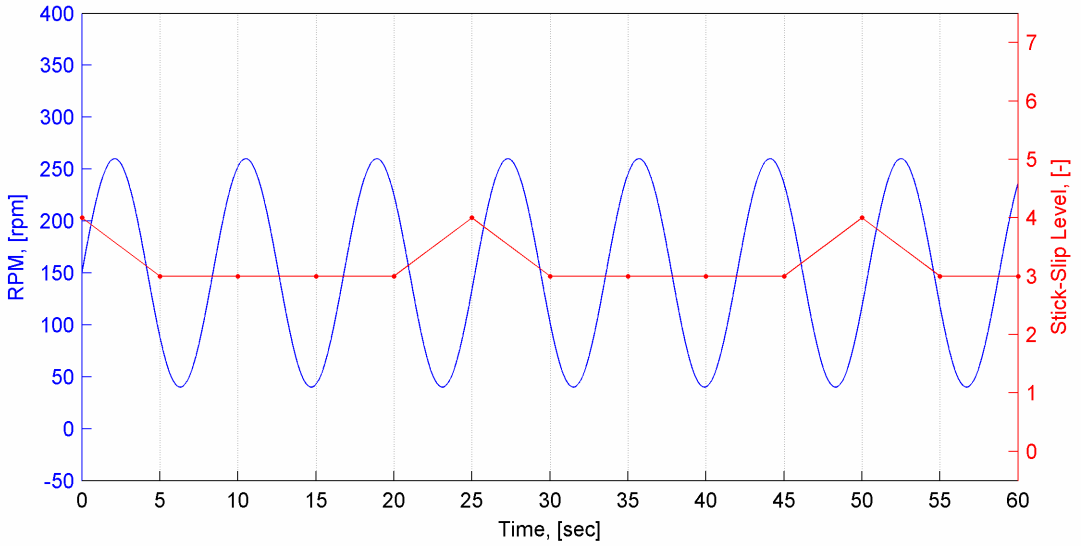

Figure 79 – Moderate frequency example of frame sample rate influence. RPM oscillation frequency: 0.12 [Hz].

This problem can even gain more significance when the ratio of the RPM oscillation frequency to the frame sample frequency is in that way adverse, that the RPM trend phase at the beginning of a frame is not identical with the one at the frame's end. Thus, permanently changing RPM values at the frame's start/end are the result. Such – quite frequent – cases result in entropy oscillations and could eventually cause changing stick-slip levels for a RPM trend with actually constant entropy.

In Figure 78 and Figure 79 two examples of that shortcoming with different RPM oscillation frequencies are depicted. When regarding the grid lines every five seconds the changing start and end RPM values per five seconds frame are easily discoverable and so substantiate the stated above. Entropy oscillation ranges can exceed a value of 0.1 [-]. Just imagine seeing only the stick-slip levels of those two

cases. Would someone actually expect such absolutely constant RPM oscillations present down there?

Stick-slip level deflections appear only in cases where the average entropy is getting close to level thresholds. In that regions frame sample rate induced entropy variations can result in an over- or underrated stick-slip severity. RPM oscillations with an integer number of oscillations per frame deliver always constant entropy values as of course start and stop RPM values do not change.

8.4.2 The Real Case

The chapter above dealt only with ideal conditions and all adverse influences from input parameters were excluded. In reality the algorithm has to function properly with real and hence not perfect input data. Real life application experiences demonstrated that diagnosed stick-slip levels are sometimes inappropriate. Two examples are shown in Figure 80 and Figure 81.

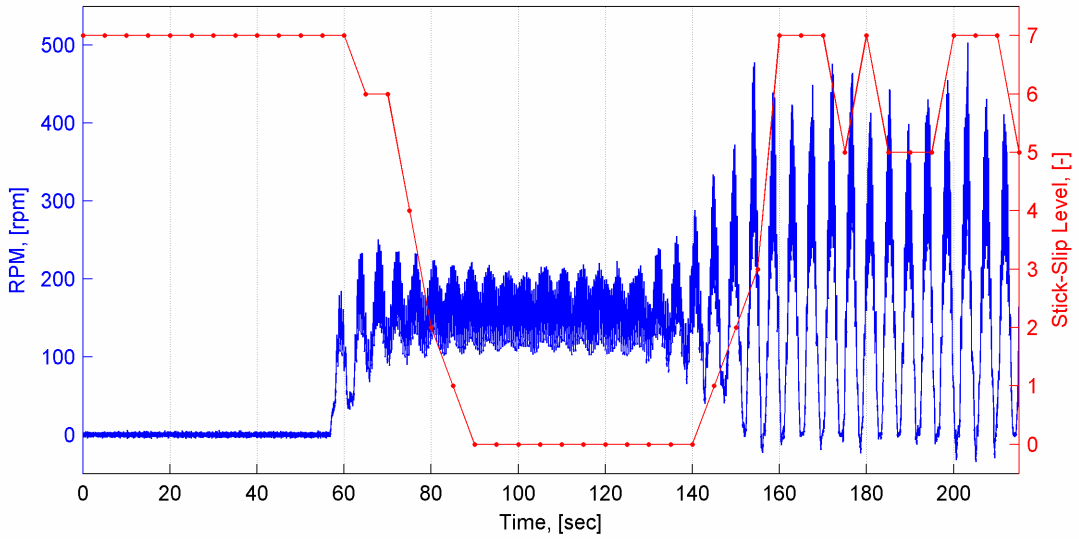

Figure 80 – Example 1 (Well B): Instantaneous RPM trend over a complete high speed trigger (sample frequency: 200 [Hz], 215 [sec] long) and resultant stick-slip levels.

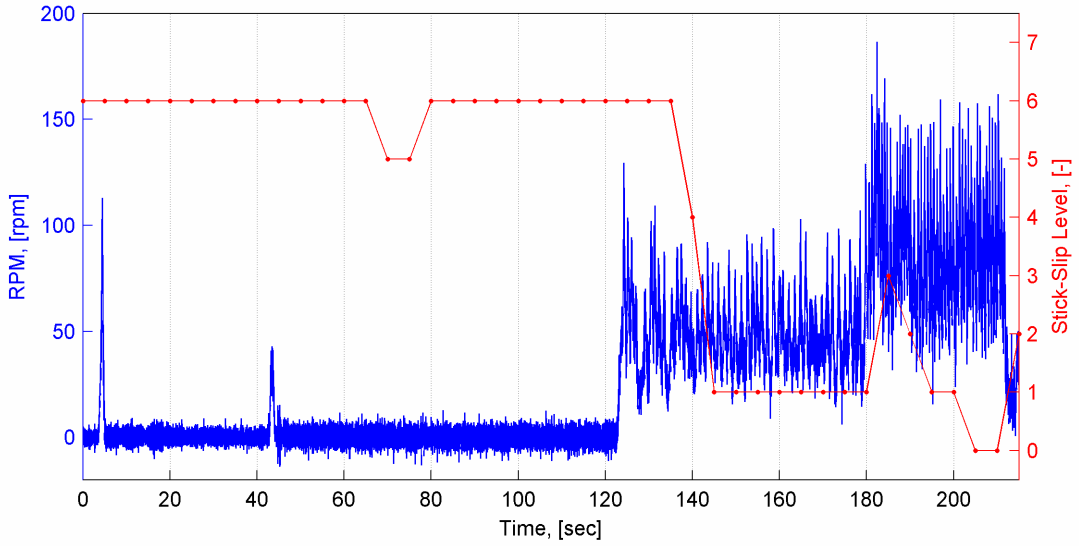

Figure 81 – Example 2 (Well C): Instantaneous RPM trend over a complete high speed trigger (sample frequency: 200 [Hz], 215 [sec] long) and resultant stick-slip levels.

What both examples disclose are very high diagnosed stick-slip levels while rotational speed trends that do not indicate any stick-slip occurrence nor should bear any danger for the BHA. It can be observed that whenever the average RPM elevates from zero, stick-slip levels start to better reflect the stick-slip severity of the RPM characteristics.

As the stick-slip diagnostics algorithm is based on severity (entropy) and direction, these two parameters are examined to figure out the reason for that inappropriate behavior. Both are unfortunately not stored in CoPilot®'s on-board memory. Thus, ex post they need to be computed again. Such a second parameter calculation performed by a computer and not by CoPilot® itself and in addition as the code is executed by a different program/computer language can be a source of inaccuracies. To roughly prove the appropriateness of the computer results Figure 82 and Figure 83 are generated.

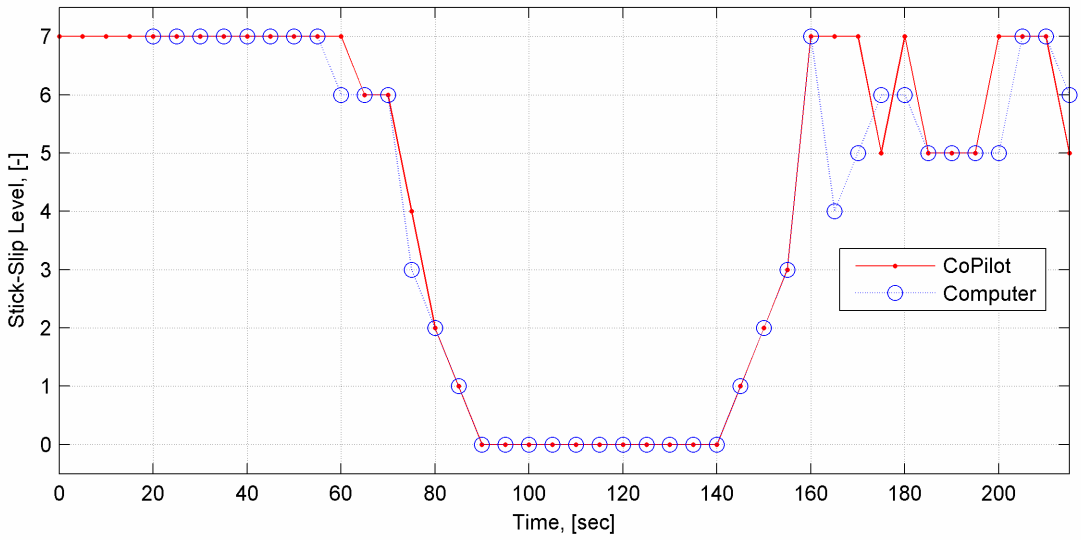

Figure 82 – Example 1: Stick-slip diagnostics from CoPilot® memory versus the diagnostic analysis executed by a computer. Sample frequency of the diagnosed data: 40 [Hz].

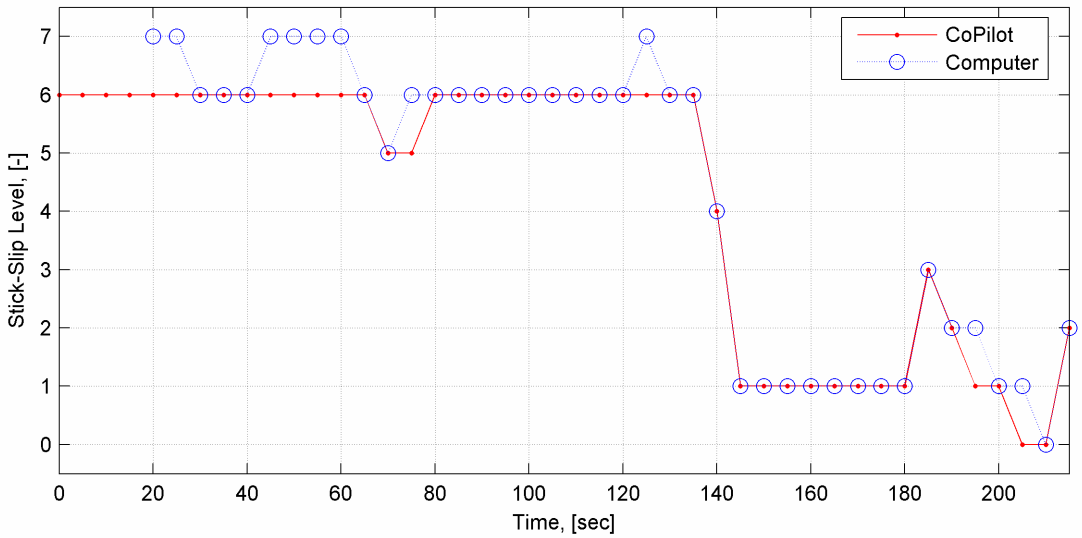

Figure 83 – Example 2: Stick-slip diagnostics from CoPilot® memory versus the diagnostic analysis executed by a computer. Sample frequency of the diagnosed data: 40 [Hz].

Both figures confirm the above mentioned concerns by representing just a general match of the results of both sources and disclose some shortcomings of the computer diagnostics. But in principle their trends correspond and by that legitimating the conclusion of a reasonable translation and execution of the algorithm's code.

A possible reason for that deviations is the decimation process from 200 [Hz] down to 40 [Hz] data as there were four out of five samples discarded. Thus, the by CoPilot® kept values are not necessarily the same like the ones kept by the computer. The computational accuracies do probably differ as well. Furthermore, some predefined functions (filter, arc tangent, pi, etc.) are used at the computer implementation that do not necessarily deliver with CoPilot® identical results. Last but not least, as the actual diagnostic codes that were executed in these two tools while they were sampling and diagnosing the data was not available, some discrepancies due to that could also not be excluded a priori.

For the reason that the general stick-slip classification trends are quite similar anyway, even most of the time identical, the assumption is made that this should be also true for the severity (entropy) as well as the direction parameter. Based on that, it is tried in the following to ascertain the reason of that severe stick-slip overvaluation while low RPM levels.

8.4.2.1 Severity and Direction

At the beginning, severity and direction are looked at, see Figure 84 and Figure 85.

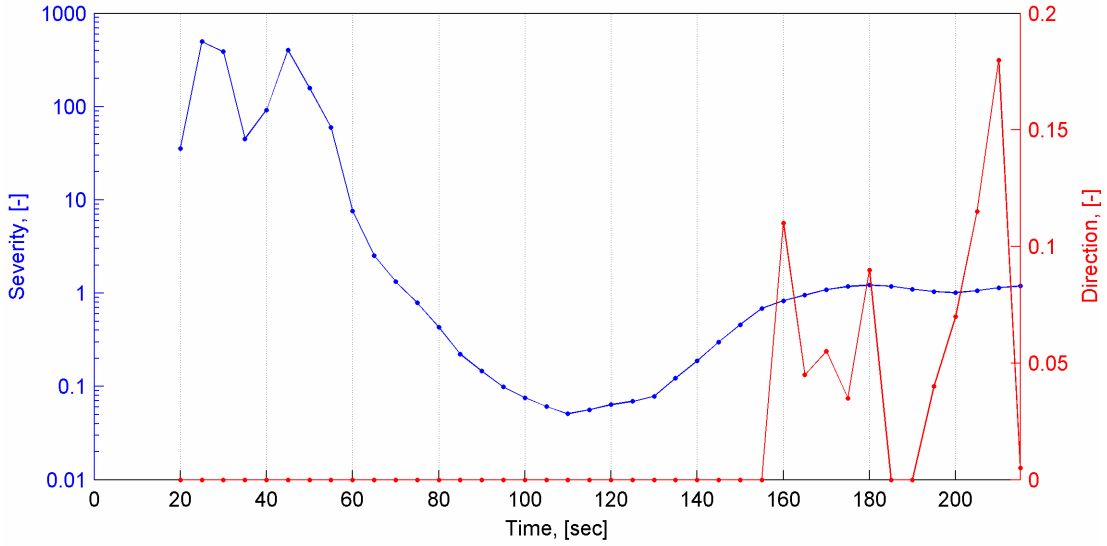

Figure 84 – Example 1: With computer ex post calculated severity and direction parameters based on from 200 [Hz] decimated down to 40 [Hz] RPM data. As the complete high speed trigger is shown, the first severity value (as well as direction) appears at 20 seconds because a 20 seconds interval is necessary for determination of one value.

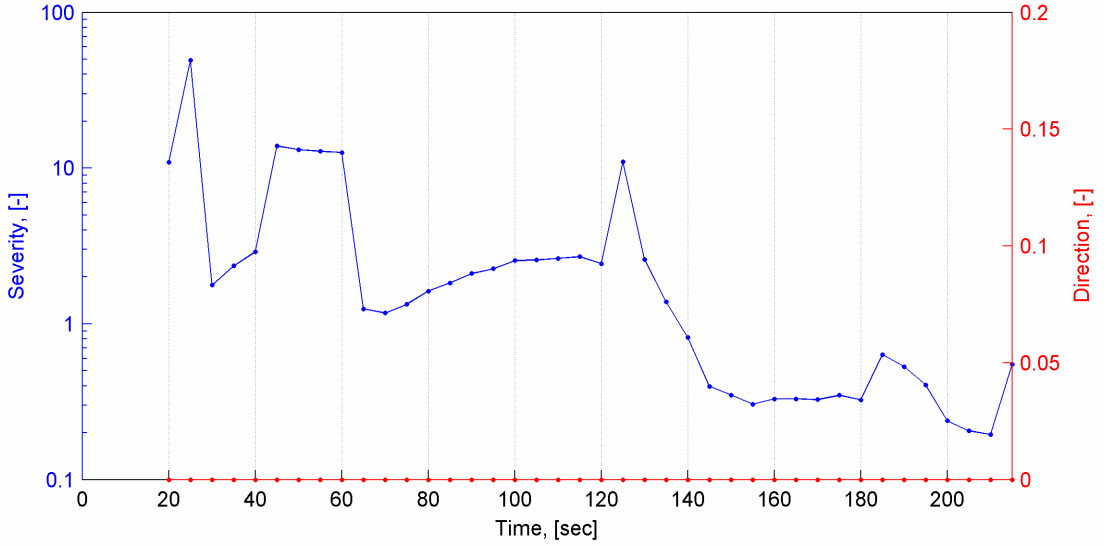

Figure 85 – Example 2: With computer ex post calculated severity and direction parameters based on from 200 [Hz] decimated down to 40 [Hz] RPM data. As the complete high speed trigger is shown, the first severity value (as well as direction) appears at 20 seconds because a 20 seconds interval is necessary for determination of one value.

It seems that high frequent, low level RPM oscillations, which might be just noise, let boom severity whereas direction shows no direct correlation to misinterpretation even while the level 7 plateau at the beginning of Example 1. Direction is hardly triggered as the backward rotation threshold is almost never exceeded. At this point, the direction parameter can be excluded as a primary cause for that type of stick-slip misinterpretation. However, a general expulsion of misleadingly interpreted stick-slip due to direction values cannot be endorsed here.

Severity (entropy) appears significantly more affected by RPM characteristics. Therefore, the following subchapters will focus on severity.

8.4.2.2 RPM Oscillation Amplitude to Average RPM Ratio

To get granular on severity and thus on entropy, the RPM influence is investigated. First, it is hypothesized that severity (entropy) is identical for identical RPM oscillation amplitude to average RPM ratios no matter what absolute values are achieved. To support that hypothesis, four example RPM trends are generated (ideal; neglecting noise and errors), see Figure 86, and followed by the calculation of their severity (Figure 87).

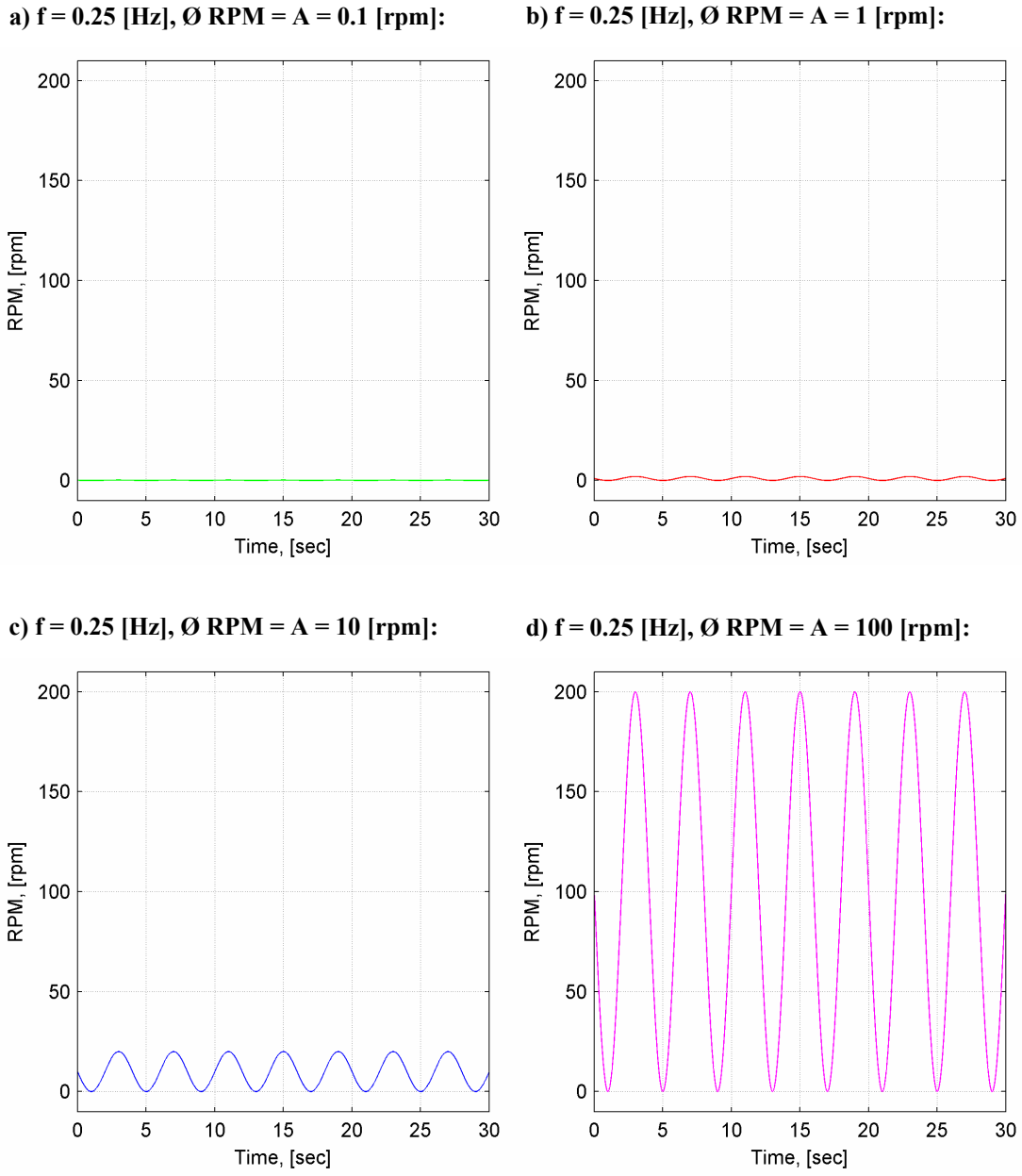

Figure 86 – Four different RPM oscillations with identical oscillations amplitude, A, to average RPM, Ø RPM, ratios as well as oscillation frequencies, f. Plotted data density: 200 [Hz].

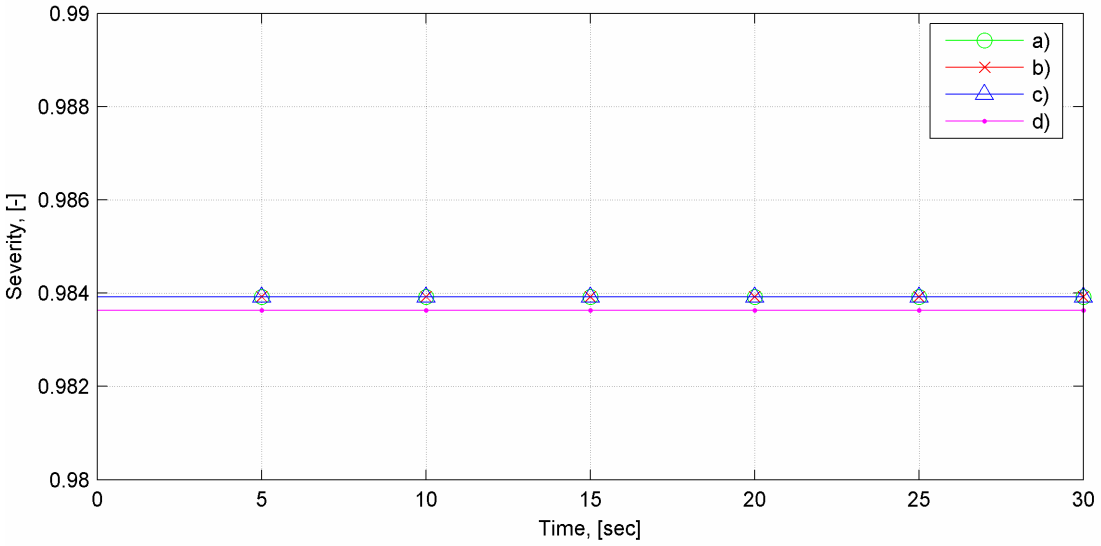

Figure 87 – Severity values (averaged entropy) of the four RPM examples of Figure 86.

When regarding the last two figures, the hypothesis made cannot be rejected. Changes in RPM oscillation range – even of a factor ten – result in almost identical severity outputs and at the end in the same (high) stick-slip level. It is obvious that the stresses, a BHA would be exposed to, vary considerably from example a) to d). Nevertheless, stick-slip levels do not reflect that. Therefore, low amplitude, low RPM level oscillations can easily cause too high stick-slip levels while uncritical dynamic drillstring conditions.

The fact that actually severity of example d) is slightly lower than the severity of the other three examples can be attributed to the 40 [Hz] data sample rate used for analysis as it resolves oscillation tips no more that accurate.

Hence, when considering stick-slip misinterpretation examples 1 and 2 (Figure 80, Figure 81), a low to moderate frequent, low amplitude RPM oscillation component (like example a)) underlying the depicted RPM characteristics might be a thinkable reason for that wrong stick-slip detection. However, if that behavior is really undesirable needs further discussion as the average rotary speed varies from well/run/section/BHA/application to well/run/section/BHA/application. General dynamic conditions stay the same but of different scale. Therefore, curing that effect might result in losing the core ability of the algorithm – to detect stick-slip – at all.

8.4.2.3 Low Average RPM Effect

Another point that should be considered is the reaction of entropy (severity) on input data at which almost half of the number of samples is negative – what easily can happen at very low average RPM with normal till high noise levels. The parameter that is expected to be most relevant is average RPM. Whereat average RPM is equivalent with the first order statistic of the entropy formula.

The examination is conducted in the following sequence: first, a 40 [Hz] noise afflicted RPM signal is simulated (by the above already discussed simulator). Initially, with an average RPM of zero. Then the average RPM level is increased step by step and simultaneously the severity development is tracked. The simulated RPM signal at its start and stop position is shown in Figure 88.

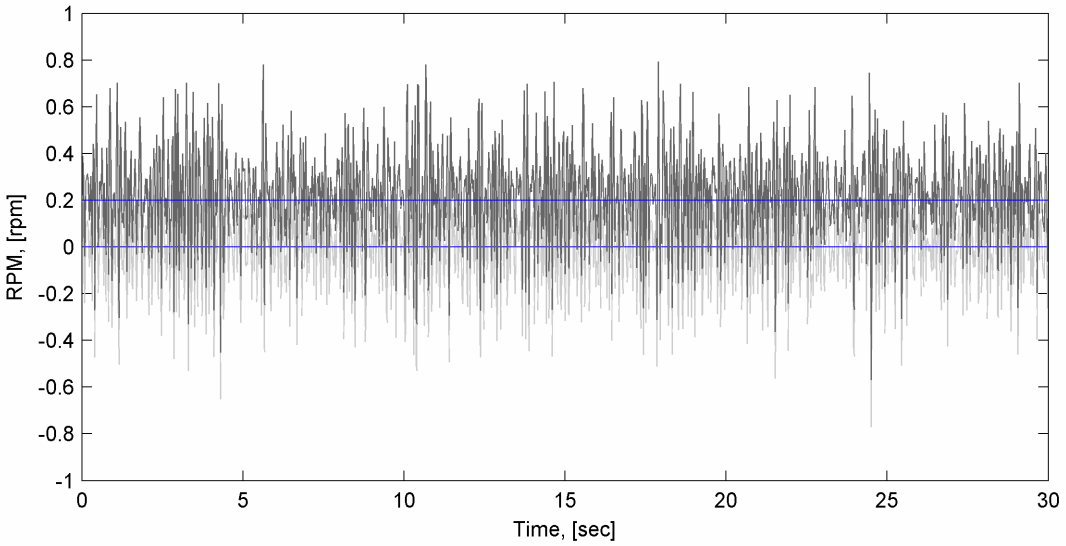

Figure 88 – Simulated, noise afflicted, 40 [Hz] RPM signal that is gradually by 0.001 [rpm] increments shifted from an average RPM level of 0 [rpm] (lower blue line) to a level of 0.2 [rpm] (upper blue line).

Figure 89 shows the received severity as a function of average RPM. Severity of the simulated RPM signal fluctuates slightly due to its "close to real" properties and effects already discussed above. To get one representative severity value, severity is averaged over the whole simulated RPM signal. These averaged data is plotted in Figure 89.

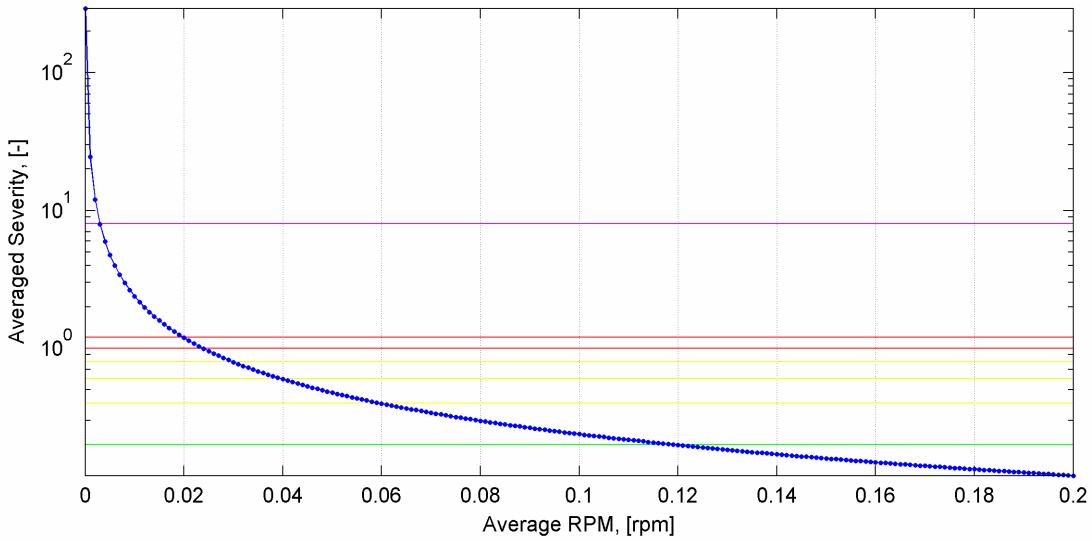

Figure 89 – Averaged severity versus average RPM levels of the in Figure 88 depicted RPM sequence for the there mentioned average RPM range (characteristic curve for only that particular RPM trend). The colored horizontal lines symbolize the lower thresholds of the stick-slip diagnostics according to their color coding.

When considering Figure 89, a question that might come to mind concerns the existence and significance of such small average RPM levels at measured data. Additionally, even the set upper average RPM limit of 0.2 [rpm] appears marginal small and thus maybe unimportant at real life applications. In fact, this is not true. Averaging kicks out quite a portion of noise and thus discloses the existence of such very low average RPM levels at measured data no matter if related to heavy noise or real motion.

For example, the simulated RPM signal in Figure 88 is pretty similar to the first 55 seconds of the measured RPM trend in Figure 80 (Example 1). The average RPM of that, by CoPilot® measured, data is 5.1E-05 [rpm]. Now, when assuming that not only both RPM trends (of course regarded at identical 40 [Hz] sample rates) are similar but also their severity functions, then Figure 89 can be used to estimate severity at Example 1 with respect to average RPM. A rough magnitude check with the corresponding severity section in Figure 84 confirms a sufficient correlation of the simulated severity function (Figure 89) with the measured severity characteristics of Example 1 as well.

Measured average RPM is that low that it is located very left, close to the first data (severity) value, in Figure 89. The accordant average severity is of a magnitude that the stick-slip diagnostics algorithm returns level 7. Even considerable severity fluctuations would not immediately result in a lower stick slip level. Consequently, after a comparison of Figure 80, Figure 84, and Figure 89 it must be concluded, that the low average RPM effect appears as the main cause of CoPilot®'s stick-slip misinterpretations at low to zero rotary speeds.

To sum up, the influence of low average RPM levels on diagnostic results seems to be, besides the prior discussed effects, an always present deflection at such low RPM levels. This last oddity can be explained due to the inverse proportionality of the first order statistic (average RPM) in Equation 8.1 (entropy/severity). The equation is undefined in case of zero average RPM. Noise (a random signal fluctuation) is almost insignificant for 1^{st} order statistics. Hence, at zero rotational speed also a close to zero average RPM is calculated. While on the other hand, noise is disproportionately influencing 2^{nd} and 3^{rd} order statistics. As long as this noise influence relation is distorted, wrong severity values are the result.

Finally, not to forget the above mentioned second example. Also a stick-slip level deflection to 6 is not unlikely as indicated by a considerable number of severity data points located between the upper and lower threshold of level 6. However, Figure 89 is only able to reflect a general trend of the severity function and must not be used for detailed analysis of other data sets than the here discussed ones as the curve is RPM trend specific. Actually, the 40 [Hz] RPM trend while the interval 55 – 120 seconds of Example 2 shows an about six-times higher fluctuation range. Additionally, its average RPM level is 8.1E-02 [rpm] and so three orders of magnitude larger compared to Example 1.

8.5 Recapitulation and Conclusions

With the assumption of **perfect magnetometers** and a RPM trend that is limited in its oscillation parameters, the current **stick-slip algorithm** is **performing** quite **well** and returns a rough first impression of CoPilot®'s RPM trend downhole. However, it must be critically mentioned to draw any conclusions upon tool threats from a statistical interpretation of velocity data (RPM). Stresses and strains result from forces. Force is a function of acceleration, thus change in velocity over time. Consequently, for a threat related stick-slip classification the current algorithm seems to be inadequate.

Even with assumed perfect conditions, the algorithm is **susceptible** to **RPM oscillating frequency** changes. Diagnosed stick-slip levels are oscillation frequency dependent. Contrary to stress development, stick-slip levels decrease with increasing RPM oscillation frequencies and vice versa. This effect could be related to the moving boxcar filter implemented in the current stick-slip algorithm.

The stick-slip algorithm does not continuously analyze RPM data. The **chopped RPM data stream** (frames) is the reason for **stick-slip level oscillations** while interpreting RPM data with actual constant properties. This effect appears only around stick-slip level thresholds and is in its size and occurrence of secondary importance.

The algorithm assesses only relative RPM changes. As long as **average RPM** to **RPM oscillation range** keep their **ratio**, severity and thus stick-slip level classification will stay at one and the same level. This property is contradicting tool threat concerns.

The most significant error of the current stick-slip diagnostics algorithm is the entropy formula's tremendous susceptibility to noise at very low average RPM levels. Whenever the drillstring is getting close to a standstill, **noise** is differently gaining influence at the statistics the entropy is based on. The result is an increase in the diagnosed stick-slip severity level with decreasing average RPM. Finally, at a stationary BHA the wrongly interpreted noise causes **highest stick-slip levels** to be indicated.

To train the entropy formula characteristics, which correlate with actual stick-slip threads as well as allow critical dynamic drillstring condition identification and classification, is by far not an easy and straight forward task when considering the susceptibility of the entropy formula to not ideal (in quality and characteristics) input data. Taking remedial actions on all found deficits would primarily cure the effects but let not necessarily disappear their sources.

What is more important is that the diagnostics unambiguousness and adequateness seem not to be ensured by that algorithm. In conclusion, all these concerns lead to the development of a new approach for stick-slip classification, which will be discussed in the following chapter.

9 Design of a New Stick-Slip Diagnostics Algorithm

Stick-slip is a pipe rotational speed phenomenon. As such, RPM is the first choice when stick-slip should be detected. Other parameters like TOB, WOB, tangential and axial accelerations can indicate stick-slip events as well but their unambiguousness in doing so is limited.

Stick-slip occurrence and the resultant threat for CoPilot® and the adjacent MWD and LWD tools in the BHA is not directly linked. Low frequent, low maximum RPM stick-slip would definitely stress such tools less than a high frequent, high maximum RPM stick-slip period.

The bit must be considered in a different way as backward rotation can easily lead to cutter losses (PDC-bits). Furthermore, extraordinary high rotational speeds, reached while slip phases, could cause bit bounce which also chops bit life significantly. Both axial vibrations and backward rotation are therefore minor harmful to "intelligent" BHA components due to their relative low magnitude but the bit is considerably more sensitive to them. Consequently, backward rotation and bit bounce indication is very important for a trouble-free drilling progress.

The new stick-slip algorithm design is split up into two different parts to unlink the sole stick-slip detection from stress evaluation:

- Drilling Performance While Stick-Slip (DPWSS)
- Tool Life (TLL)

DPWSS is the dynamic phenomenon diagnostics. The detection covers the range from little RPM oscillations till severe stick-slip. Furthermore, this part should rate whether stick-slip is adverse for ROP and thus remedial action would be necessary or ROP does not suffer from stick-slip and therefore drilling parameters need not necessarily to be changed. Backward rotation detection is also a duty of that part. Bit bounce is already covered by a diagnostics algorithm on its own and for this reason not covered by this nor the other part.

The TLL section of the new algorithm rates torsional oscillations as "lethal", dangerous, critical or normal. Based on the sensed conditions the remaining tool life is predicted. The working principle is comparable to a performance-based maintenance interval scheduling of a modern car. By respecting the working conditions of the past (since last maintenance), maintenance intervals are shortened or extended.

A detailed discussion is given in the following subchapters as well as a development version of the new algorithm as MATLAB® script is added at the end of this volume (see Appendix and attached CD). The code is designed only for development and demonstrative purposes and must not be used for real tool implementation.

9.1 Drilling Performance While Stick-Slip

9.1.1 Stick-Slip Detection

Currently the downhole RPM trend is described by a single parameter (severity level) that not only indicates stick-slip occurrence but also should represent stick-slip resultant threats for the BHA. As already mentioned above, that parameter is primarily based on a statistical approach which should solely fulfill both tasks – unfortunately with limited accuracy.

For stick-slip indication a new approach (Stick-Lag Method) has been developed as well as a very simple and straight forward analysis (MM-approach) is discussed in the following two subchapters. The only task of both approaches is to signal whether stick-slip has developed and how severe it is or just to return that every thing is running within normal uncritical limits. These methods are not designed for any BHA threat correlations!

9.1.1.1 Stick-Lag Method

Of course, a new stick-slip identification method should vanquish known shortcomings either regarding data quality or stick-slip detection problems as well as avoiding an introduction of new errors. The following list summarizes some points the new method needs to respect:

- Not sticking to (single) RPM samples but identification should be based on a larger scale.
- RPM data noise and mavericks must be restricted in their influence on the interpretation result.
- Focus on stick-slip events (currently only 3 out of 8 levels actually indicate some kind of stick-slip).
- Gathering of time of stick-slip events to enable correlations with other data channels.
- Easy to communicate and conceivable description of stick-slip states (for example, with just an entropy value of 1.1 [-] (stick-slip level 5) it is not easy to imagine the actual downhole RPM trend).
- RPM independent identification functionality (different average RPM levels should not alter results).

9.1.1.1.1 RPM Data Preparation

The Stick-Lag Method characterizes each RPM oscillation (of appropriate frequency) first by up to four specific parameters (see Figure 90):

- Stick-Lag, SL, unit: [sec]
- Top-Lag, TL, unit: [sec]
- Bottom-Lag, BL, unit: [sec]
- Oscillation Range, OR, unit: [rpm]

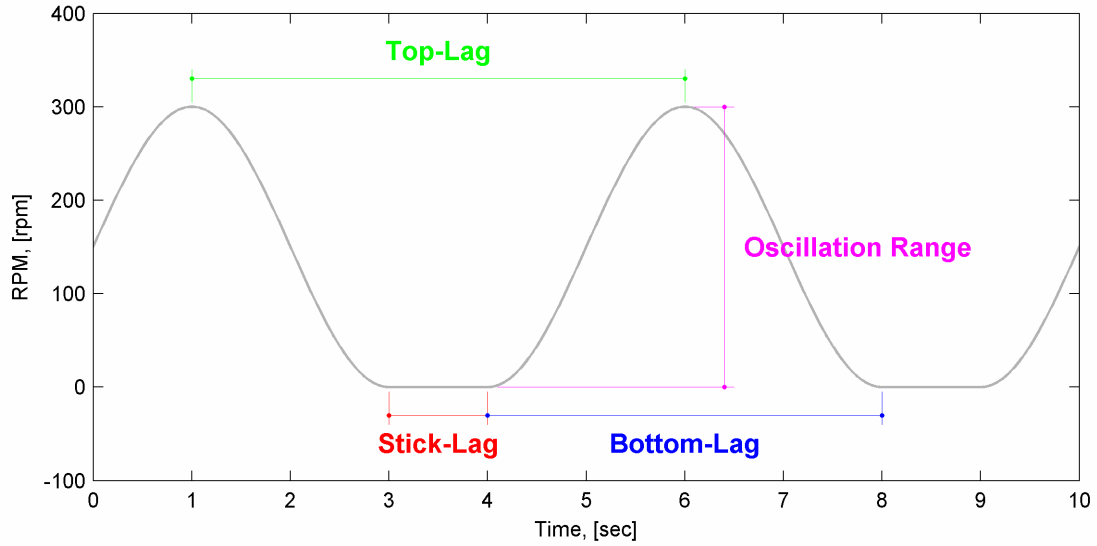

Figure 90 – Parameter declaration of the Stick-Lag Method.

TL is the time between two consecutive RPM peaks and is equivalent to the oscillation's period length. SLs, times of zero rotation, exist only while stick-slip whereat a possible period of backward rotation would be an element of SL as well. For harmonic oscillations with stick-slip, BL is equal to TL deduct by SL. Without stick-slip, BL is equal to TL and thus also of the size of a period length. OR is the range between a troughs RPM minimum and the maximum RPM of the consecutive peak.

Basically, data preparation is a split-up of the RPM data into traceable timeframes (SLs and TLs) or better to say a spilt-up into single oscillations as TL is a function of RPM oscillation frequency. Compared with the current stick-slip algorithm these frames are not fixed in their length (5 seconds respectively 20 seconds at stick-slip diagnostics). As time intervals are considered, sample frequency impairs their resolution/accuracy. Generally, a higher sample frequency results in more precisely picked lags.

Every single RPM sample is assigned twice, once to a class (specific TL) but also to a subclass (SL or BL). For this reason, every RPM sample belongs to a TL but also either to a SL or BL respectively.

Single (stick-slip) oscillation picking and time labeling are key factors of the method. These data preparation steps are not only for the Stick-Lag Method of crucial importance but also whenever other parameters than RPM are consulted to interpret a certain RPM characteristic. Correlations with other data channels are only possible via time. Currently, RPM is statistically analyzed with the drawback of losing the ability to precisely assign time to a certain event of interest. This limitation is now eliminated by this new analytical approach.

Beyond this method however tracking of SL and TL is necessary to classify backward rotation and, what is more important, it would not be possible to determine the reason of stick-slip (bit or drillstring friction) without the knowledge of these time intervals. As a result, even when the new method is rejected as a substitute for the current algorithm, at least SL and TL tracking should be implemented as a viable analysis feature.

As the stick-slick detection ability of the new method is based on the specific lags, an accurate, reliable, and stable algorithm would be necessary to pick them. This is the most critical point of that new approach as there could easily be introduced a new error source. The importance of this point cannot be overemphasized!

The code, added at the end of this work, uses a very simple but unfortunately also only moderate accurate working lag-picking algorithm. Hence, some special conditions are in the code which would not be necessary at a better lag-picking algorithm. However, it is suitable enough to serve first testing and developing needs. Its working principle is outlined in the following.

First, the RPM signal is split up into peaks and troughs by comparing each sample to an average RPM function and accordingly assigning it to a peak or trough related data segment. Using an average RPM function (5-second-average or heavily filtered RPM) is critical, as it locally can significantly be deflected (e.g. while long stick periods) which can disable proper peak-trough-separation. To improve that, CoPilot® should have to know the RPM it should instantaneously rotate (e.g. surface RPM) and not trying to estimate it with average RPM approaches.

Furthermore, an unambiguous peak/trough classification of the most recent peak/trough segment is not possible until crossing a certain threshold (here, the average RPM function is used as such) as the future RPM trend is unpredictable and peak/trough classification impossible. Consequently, RPM data from the last fully developed peak/trough till the most recent RPM sample cannot be used.

After RPM peak/trough determination, their maximum respectively minimum is identified to find lag limits. This is performed on a moderately averaged RPM signal as otherwise high frequent components, noise, or mavericks could lead to wrongly picked tips. As tip time is the parameter of interest, accurate tip time detection is more important than the actual maximum/minimum instantaneous RPM values itself.

Every maximum position (time) is already a lower respectively upper limit of two consecutive TLs. At stick-slip absence, every minimum position is also a lower respectively upper limit of two consecutive BLs at the same time. If stick-slip is present, the minimum location is used to delimit the SL around it. A stick event is assumed whenever the averaged RPM minimum of a trough is below 0.5 [rpm] (“equal to zero limit”). In such a case, the instantaneous RPM segment of that particular trough interval is searched from both sides (beginning and end) for the first values below the “equal to zero limit”. The found corresponding time values define the lower and upper SL limit (are shifted a little bit if showing negative RPM values).

SLs need to be picked at the instantaneous RPM because averaging could reduce lag considerably. Filtering (averaging) alleviates extremes in the signals. Thus, by peaks

surrounded, relatively short, flat regions like a stick phase will be reduced or even completely filtered out. This effect needs to be considered only in at SL picking as TLs are picked between two inflexion points of the RPM trend. The position of inflexion points is not that much affected by filtering. BLs are located between an upper and a lower limit of two consecutive SLs.

As the length of a SL influences the subsequent RPM maximum of the slip phase, RPM oscillation range is the difference between a trough's minimum and its subsequent peak's maximum picked on the moderate averaged RPM.

A lag picking example of the development version is shown in Figure 91. Additionally, the problem with the most recent peak or trough differentiation can be observed as the averaged RPM (black) has not yet crossed the average RPM function (magenta) and therefore no TL can be assigned.

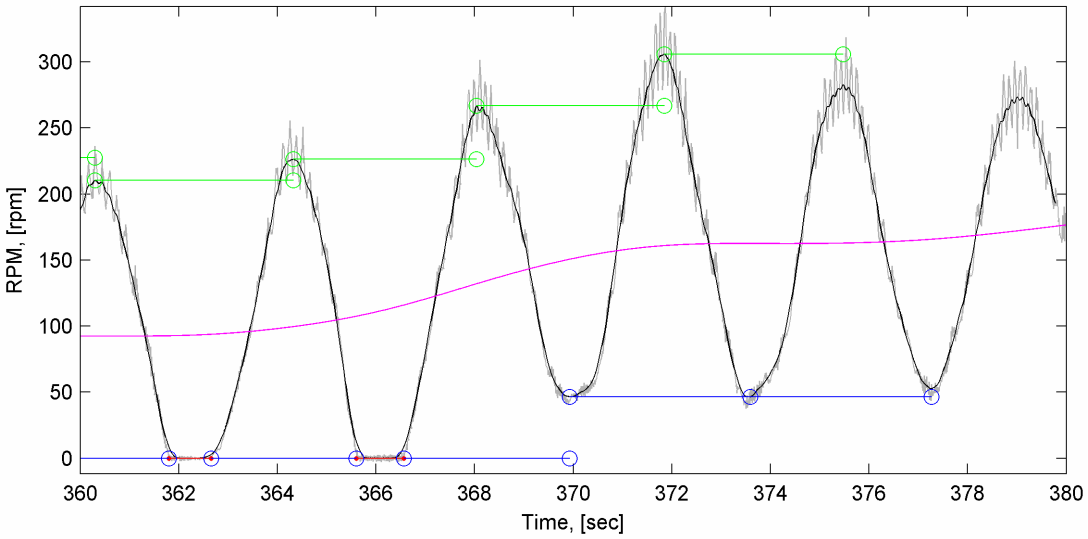

Figure 91 – Automated lag picking example of Stick-Lag Method. Red: SL, blue: BL, green: TL, magenta: average RPM function, gray: instantaneous RPM, black: averaged RPM. Sample frequency: 100 [Hz].

9.1.1.1.2 Stick-Slip Diagnostics

The output of the data preparation section needs to be evaluated. This is done in the stick-slip diagnostics section.

RPM trends from roughly constant until severe oscillations have to be categorized. To stay consistent with all other diagnostics of CoPilot®, again a classification with levels from 0 to 7 is used. The Stick-Lag Method does not necessarily stick to a level-type classification but also other types of diagnostics output would be possible. On the other hand, keeping the same output style eases the comparison of the old to the new stick-slip diagnostics algorithm.

Diagnostics is composed of two different ratings. One covers RPM trends from a constant characteristic till oscillations of which the minima just touch the zero RPM

line (not jet a developed SL). This rating is responsible for output levels from 0 to 2. The other rating, that covers the majority of levels (from 3 to 7), refers to cases where actual stick-slip is detected. In summary, when regarding the total level spectrum then one part relates to just "normal" oscillations and the other to stick-slip oscillations.

For each rating a characteristic parameter, LP (level parameter), is calculated which enables a subsequent level classification. Both level parameters are dimensionless. At normal oscillations the following formulae are decisive:

$$LP_{0-2} = \frac{OR}{2 \cdot \overline{RPM}} \qquad \textbf{(E 9.1)}^{[29]}$$

$$\overline{RPM} = \frac{MAXRPM + MINRPM}{2} \qquad \textbf{(E 9.2)}$$

MAXRPM and *MINRPM* are the upper respectively lower RPM limit of *OR*.

If at the RPM trend a SL has been detected the formula below is applied:

$$LP_{3-7} = \frac{SL}{TL} \qquad \textbf{(E 9.3)}$$

LP_{3-7} is the time fraction while CoPilot® is not rotating forward (sticks). RPM data of the SL are also elements of TL.

After the level parameter has been calculated it is compared to specific thresholds to assign it to a certain stick-slip level. The thresholds are listed in Table 7.

Stick-Slip Level	LP_{0-2}		LP_{3-7}		Oscillation Type
0	0	0.4	0		Normal
1	0.4	0.7	0		
2	0.7	1	0		
3	> 1		0	0.125	Stick-Slip
4	> 1		0.125	0.250	
5	> 1		0.250	0.375	
6	> 1		0.375	0.500	
7	> 1		> 0.500		

Table 7 – Stick-Lag Method's diagnostics level thresholds.

When such a level now is sent up to the surface it is very easy to get a rough impression of the downhole PRM trend. For example, a stick-slip level 1 would mean that the BHA at the location of CoPilot® is swinging ± 40 to 70 % around the average RPM (E 9.2) which usually is identical with the surface RPM. A diagnosed level of 5 on the other hand would indicate that CoPilot® stands still 25 to 37.5 % of

the time (or is rotating backwards). Thus, these levels are more concrete than the current ones. A stick-slip diagnostics example is shown in Figure 92 and Figure 93.

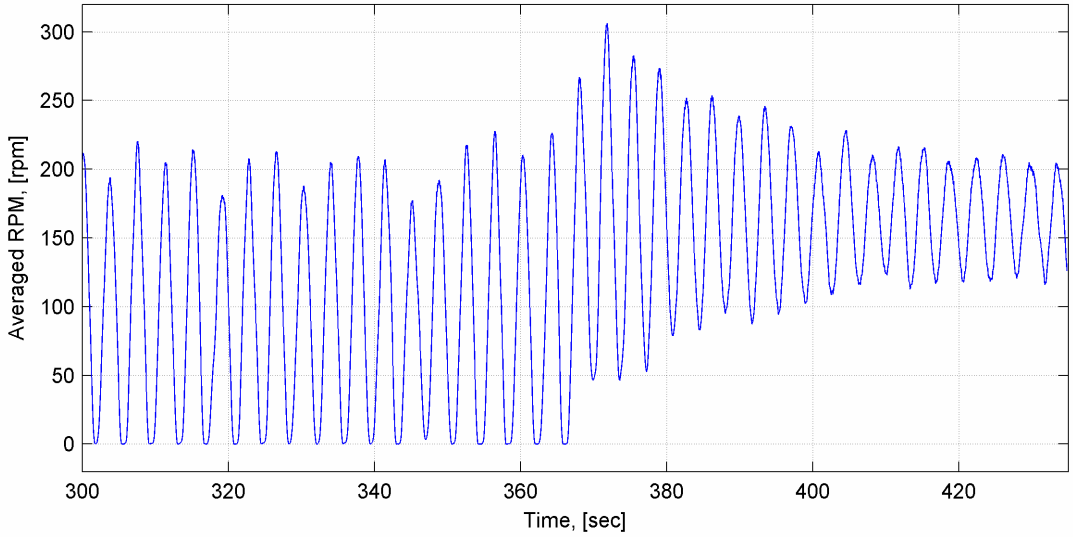

Figure 92 – Averaged RPM trend. Sample frequency: 100 [Hz].

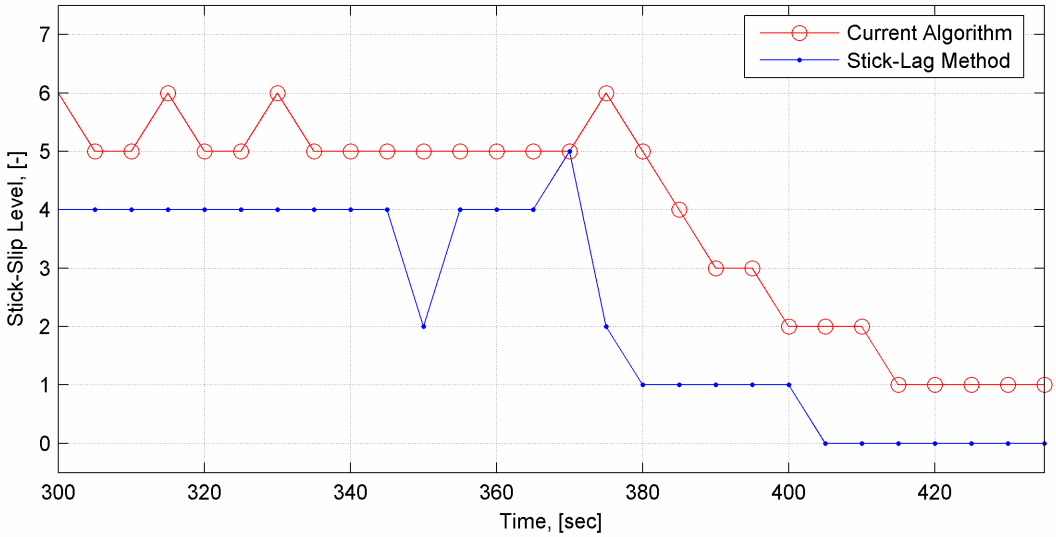

Figure 93 – CoPilot®'s current stick-slip diagnostics (red) versus the Stick-Lag Method (blue) results of the in Figure 92 depicted RPM trend.

Remarkable is the RPM trough at about 347 seconds in Figure 92 which demonstrates that every single oscillation is analyses. At that trough, the BHA does not stop to rotate which is immediately indicated by the Stick-Lag Method by a diagnostic level of 2. In general, stick-slip levels of the new method appear a little bit lower than the ones of the current algorithm. However, an old to new level comparison is improper as they are totally differently determined. Anyway, their diagnostic trends are quite similar.

To achieve a better comparability of both algorithms the output sample rate, OSR, of the Stick-Lag Method is also set to 5 seconds. Actually, this contradicts the fundamental structure of the Stick-Lag Method with its flexible analysis intervals.

The effect is, that for example one single low frequent RPM oscillation, longer than 5 seconds, could be responsible for two or even more 5 seconds spaced stick-slip level updates. While on the other hand, high frequent RPM oscillations (more than one oscillation per 5 seconds) need to be averaged if not only a fraction of the 5 seconds data stream (the last oscillation) should be solely responsible for the classification of the whole frame.

The optimum OSR of the Stick-Lag Method is a flexible one. Only in the case when a new event (stick-slip oscillation) is analyzed its corresponding stick-slip level is returned. However, for nearly constant, event free RPM sequences diagnostics need to be determined also after a certain time period to receive regularly stick-slip level updates even when the level has not changed. Otherwise, long periods of no sent and received stick-slip levels could misleadingly lead to the conclusion that CoPilot® is not working properly.

9.1.1.2 MM-Approach

The MM-approach is a straight forward stick-slip occurrence indicator and is another alternative to the current algorithm or the Stick-Lag Method. It implies neither a diagnostics section nor complex data preparation.

When sticking to a 5 seconds OSR, it appears appropriate enough to receive every 5 seconds minimum RPM (M) and maximum RPM (M) to get a fair impression of the RPM conditions the BHA was exposed to while the last interval. Minimum and maximum RPM traps are already employed in CoPilot®'s signal processing software thus making this method very easy to implement.

Regarding near future telemetry systems, beyond old-school mud-pulse-telemetry, transfer rates will go up. The more the bottle-neck of downhole to surface communication is removed the less will be the need for highly sophisticated downhole data analysis algorithms. Today when for example only ever 30 seconds a maximum and minimum RPM value is received at surface it is fine. In the near future maybe both values can be transmitted every second. Eventually, one day every sample could be sent bringing instantaneous near-bit RPM up to the surface.

This is a method which moderately accurate works at the moment but it is definitely one that will not expire with time and will gain more and more applicability in the future.

9.1.2 Drilling Performance

Does stick-slip really adversely affect drilling performance all the time or is a ROP reduction just an occasional effect?

When regarding a long enough period of time the average drillstring RPM is identical for every point along the string (not valid for the section below a mud motor). At the end of the day each BHA component and especially the bit were rotated by an identical number of times.

A little thought experiment with the following assumptions:

- An ideal drillstring-drilling-rig combination ensures downhole WOB to be kept at its set value all the time.
- A perfect bit is used, which delivers a linearly increase in ROP with increasing RPM and furthermore has no tendency to bounce nor gets susceptible to any damage at any RPM level.
- All other negative effects (e.g. like cutting transport problems) are excluded as well.

With these assumptions stick-slip would actually have no effect on ROP. ROP losses while stick phases are fully balanced by ROP peaks during slip phases. Thus, at the end of the day the same distance has been drilled no matter if with or without stick-slip. Unfortunately, the more a real drilling process differs from that assumed ideal case the more the drilling performance will suffer from stick-slip events.

From just a drilling performance perspective (disregarding any stick-slip related threats for BHA components and resultant unplanned tripping actions) near-bit ROP would be the optimal drilling performance classification parameter while stick-slip. Near-bit ROP data would enable to rate stick-slip whether it is harmful to fast drilling or not. Thus, wrongly triggered expensive and/or time consuming remedial actions like WOB reduction, drilling fluid property changes, or even BHA design adjustments due to stick-slip effect overestimations could be avoided.

CoPilot® is equipped with a number of different sensors. It is imaginable that one or a combination of some sensors is indicating ROP and thus would enable an immediate and tool closed implementation of near-bit ROP in the stick-slip classification. In the following, data channels which might be able to indicate near-bit ROP are discussed in that respect and it is mentioned why they are actually not applicable for near-bit ROP detection.

9.1.2.1 Axial Acceleration

CoPilot® senses acceleration in axial direction. Theoretically, integration of that signal should deliver axial velocity (ROP). When considering the following points it becomes obvious that the axial acceleration cannot indicate near-bit ROP at normal drilling conditions with the currently used accelerometer type:

- The distance drilled per hour is usually in the range of 10 to 60 [m]. For example, assuming a very high ROP of 60 [m/h] and a data sample rate of 100 [Hz] then an average MD increment between two samples would be 1.667E-04 [m]. In other words, the drillstring would move in axial direction downwards a sixth of a millimeter between two survey points. This is a very,

very short distance which moreover would be sensed indirectly via acceleration. Thus, when even assuming an extreme case of axial acceleration where the ROP of 60 [m/h] falls to 0 [m/h] within one second then an axial acceleration of just -1.667E-02 [m/s²] (1.7E-03 [g]) would be seen. The resulting acceleration due to that severe change in drilling performance is marginal compared the sensor's accuracy. The accelerometer's input range is ±50 [g] (FS). Sensed accelerations are afflicted with errors of 0.5 – 2 % FS – in other words up to ±1 [g] and thus about 600 times larger than the acceleration of the discussed example. But not only sensor accuracy is limiting a near-bit ROP detection via axial acceleration but also noise (from bit, pumps, heave, etc.) which is larger in magnitude than such small accelerations due to drilling progress. Additionally, usual ROP changes are smaller or even almost insignificant from one to the other sample at such high sample rates.

- The second important point is that there must be some axial acceleration acting to be able to determine instantaneous axial velocity at all. This is only the case whenever ROP (axial velocity) is changing. A constant ROP results in zero axial acceleration and consequently in zero measured axial velocity. Therefore, ROP measurements would start to drift depending on how smooth the gain in depth is.

In summary, axial acceleration is inapplicable for near-bit ROP estimations. First, due to the pure accelerometer accuracy for that application and second because of the integration step that disregards periods of constant ROP.

9.1.2.2 Weight on Bit

At first glance another possible ROP indicator seems to be WOB. Every decrease of WOB seen by CoPilot® is indicating fast drilling progress (as long as the drillstring is not pulled). The faster WOB falls the higher the ROP is, would be therefore a valid conclusion. However, modern drilling rigs do automatically keep a predefined WOB value. For example, when assuming a shallow vertical well it can happen (at ideal conditions) that every reduction in WOB downhole is immediately compensated by the rig at the surface. In this case downhole WOB will appear almost constant and thus ROP indication would be impossible.

Another concern pops up when considering a well with a long horizontal section where the drillstring is under compression most of the time. The amount a WOB reduction is immediately compensated by a not surface induced down-slid of the drillstring would never be known due to the lack of fixed downhole reference points. The effects of such a compensation do not necessarily be recognizable at the surface. Uncontrolled axial movements dilute the ROP detection as it cannot be measured whether the sensed WOB loss is related in its full extent to ROP or just only a fraction has actually been sensed while a part had been immediately compensated by an axial drillstring movement. Hence, for what the rig is responsible for in the paragraph above could be accomplished by a long drillstring as well.

Beside these problems, the conversion from force variations to depth changes would be not a trivial task and as such a possible major source of inaccuracy.

9.1.2.3 Torque on Bit

A properly working drill bit causes a characteristic reactive torque. The lower TOB the less formation is destroyed and vice versa is therefore a valid conclusion.

The problem with this statement or even TOB observations at all is that they are too general to actually infer ROP changes in detail. Regarding different bit types (roller-cone, PDC, impregnated, natural diamond, coring, drag), each develops its individual TOP characteristics. Furthermore, the formation they have to drill is quite often heterogeneous and as such it is permanently demanding different torques to be destroyed.

Another point to mention is BHA design. Whenever an additional torque generating BHA component (e.g. reamer) is placed in the BHA below CoPilot®, any drawn conclusions from TOB to get ROP become wrong because of a measured but not depth increasing torque.

Recapitulatory, TOB is too case/condition/situation specific to allow a general ROP indication. In addition, like at the WOB discussion above, the conversion of TOB changes to meters drilled per time would not be straight forward.

9.1.2.4 Pressure

Almost every piece of rock that has been destroyed by the bit (cutting) is carried to surface by mud. The more cuttings floating in the mud the more its density is shifted towards the rock density. Slow drilling propagation produces only a few cuttings whereas high ROPs generate heaps of floating rock fragments. A higher fluid density results therefore in a higher downhole pressure and links by that ROP to pressure changes. CoPilot® is equipped with an annular pressure sensor and hence can detect annular pressure variations.

Initially, annular pressure appears also as a suitable ROP indicator but by just considering the following two points pressure has to be refused as a ROP indicator as well:

- The annular cross-sectional area is not the same at every BHA run. Even during a single run the annular cross-sectional area can change significantly due to variations in borehole quality (e.g. wash-outs, swelling formations, etc.). The annular cross-sectional area influences the annular volume. Assuming a reference cuttings volume that is transported from bit to surface by mud then the resultant length of the liquid column (cuttings and mud) in the annulus is a function of annular volume. Consequently, the resultant downhole annular pressure seen by CoPilot® depends on annular cross-

section. Unfortunately, the annular-cross-sectional area is influenced by many, sometimes unknown, parameters (bit size, drillstring dimensions, wellbore caliber, temporary cutting beds, etc.) which ultimately affect the hydraulic pressure as well. CoPilot®'s sensed annular pressure therefore cannot be exclusively related to ROP and thus not allowing to draw exact conclusions from hydraulic pressure changes on ROP.

- Downhole pressure is only influenced by true vertical depth (TVD) and not by MD. At a horizontal section (constant TVD) the reference cuttings volume has to be transported first through the whole horizontal section before it causes pressure changes. Thus, leading to a lack in accuracy with respect to time but also to the ROP value itself as along a horizontal section the mud can easily pick up cutting beds, possibly with different properties, and therefore causing "wrong" pressure changes (regarding ROP indication).

A conversion from pressure variations to MD changes would here even be more challenging.

9.1.2.5 Temperature

Whenever rock is destroyed also heat is generated. Bit off-bottom and circulating results in almost equal bore and annular temperatures. Bit on-bottom and rotating primarily rises the annular temperature. Consequently, a comparison of internal and annular temperature separates drilling from pure circulating hours. To reason ROP from that relation would imply the knowledge of the amount of heat generated by a certain bit type in a particular formation when drilling at a specified ROP. Also the cooling properties (specific heat capacity, heat transfer coefficient, etc.) of the mud have to be considered, as the heat that the mud can carry is necessary to know. Thus, many unknowns must be gathered somehow and there first of all the bit formation interaction and not to forget the instantaneous formation drilled. All these concerns award that temperature approach only a theoretical status as an adequate ROP indicator.

9.1.2.6 Recapitulation and Conclusions

Currently CoPilot® is not able to measure ROP. However, it has got incorporated some sensors which in sum offer some hints to moderately reason drilling performance.

ROP would be a necessary parameter to be able to implement drilling performance to the stick-slip algorithm. Such an implementation would allow the next step from just stick-slip indication ("stick-slip is present") towards a cause and effect feedback provided by CoPilot® ("stick-slip is present and responsible for x [m/h] ROP reduction" or "stick-slip is present but has no effect on ROP").

9.1.3 Backward Rotation

Stick-slip related backward rotation can be attributed to two reasons/types:

- **Type I:** While the stick period energy is stored in the drillstring as it is twisted up. During the slip phase the energy is released again when the string is rotating faster than actually driven. If enough energy had been initially stored, the string does not only recover to its zero-twisted position while the slip phase but even goes beyond that (break-out direction). In such a case it stores energy again. Eventually, this surplus of revolutions (energy) compared to the rest of the string is compensated by backward rotation. Characteristic for that type of backward rotation is a negative TOB peak seen by CoPilot®.
- **Type II:** If CoPilot® is located above a mud motor, a sudden reactive torque increase of the PDM can cause CoPilot® and the whole BHA to be turned backwards until the drillstring balances that additional torque demand. This type can be characterized by a positive TOB peak and occurs quite frequently in sliding drilling mode as while high string RPMs (rotary mode) the reactive torque needs to be higher to stop the string and turn it backwards.

As the developed new stick-slip diagnostics algorithm is based on the above presented Stick-Lag Method, it is also possible to implement not only backward rotation indication but also backward rotation type identification. Backward rotation determination and its classification are additional separate features of the new algorithm and does not influence the stick-slip level magnitude.

As the TOB trend while and around a backward rotation period is characteristic for its type, a TOB investigation delivers the corresponding backward rotation type.

At the beginning, it is necessary to specify which events are counted as backward rotation. The current stick-slip diagnostics algorithm regards every RPM sample with a value below -0.2 [rad/s] as such. As backward rotational speed is seen as less appropriate for backward rotation delimitation due to their basically low values as well as to ensure not misleadingly picking a single, RPM threshold exceeding backward rotation maverick the new backward rotation threshold is set at -2 [°]. Meaning only cases where CoPilot® was turned backwards at least by 2 degrees are regarded as a real backward rotation event. This does respect backward motion related threats more than RPM related damages which would prefer a speed based separation. The latter are in this case not that critical as only low backward rotational speeds are achieved. For example, for a PDC bit a few degrees of backward rotation at high WOB loads could already result in a serious damage whereas the velocity of the backward turn is of minor effect.

9.1.3.1 Backward Rotation Type I

A backward rotation event is classified as Type I if 50 [%] of the measured TOB values during backward rotation (backward-rotation-lag) are smaller than zero. As

unfortunately TOB sensing is not absolutely free of errors, a limit which is taken as equivalent to zero is introduced to accurately delimit Type I backward rotation events. Such a limit is solely at this type necessary as only there the determination is based on a comparison of a measured value to an absolute one (TOB of 0 [Nm] for the ideal case). The limit is tool size specific and equal to the by the manufacturer specified total sensing error of TOB, see Table 8.

Tool Size	Total Error TOB
[in]	[Nm]
4¾	500
6¾	750
8¼	1000
9½	1000

Table 8 – Backward Rotation Type I torque limits (equivalent to CoPilot®'s total TOB sensing error).[30], [31], [32], [33]

How a RPM and TOB trend of a stick-slip event with Type I backward rotation can look like is shown in Figure 94. CoPilot®'s position in the BHA while it sampled that data was above the mud motor, which was equipped with a tri-cone bit. The diagnosed stick-slip levels of the current algorithm as well as the ones of the new algorithm are depicted together with the backward rotation type interpretation result in Figure 95.

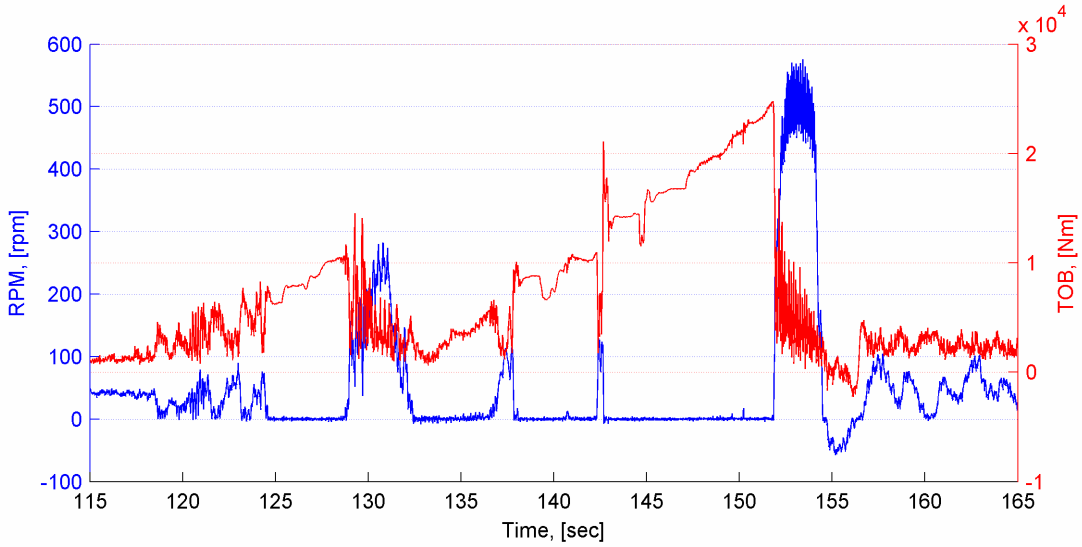

Figure 94 – Stick-slip with Backward Rotation Type I (at 155 [sec]). Sample frequency: 100 [Hz].

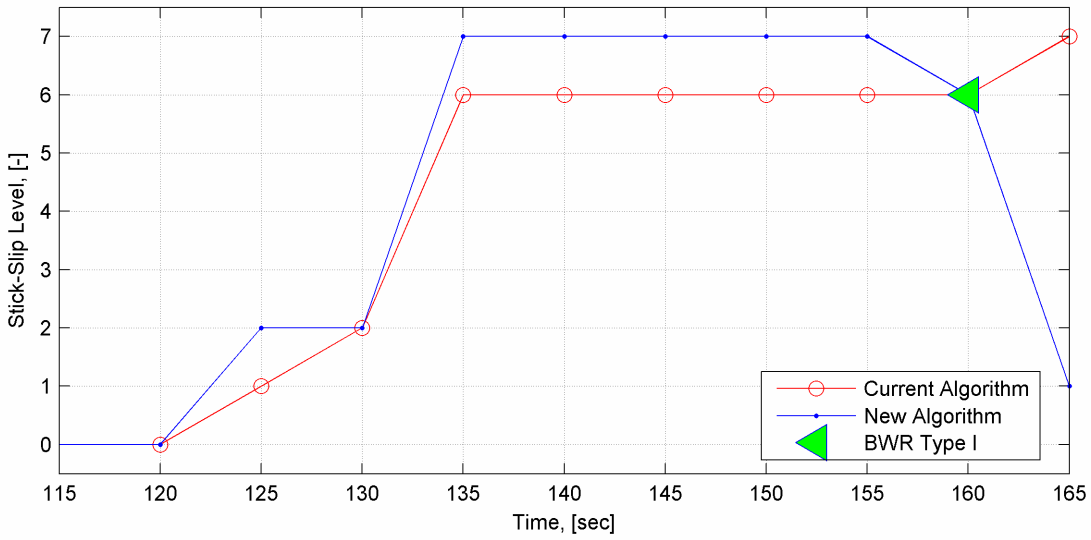

Figure 95 – Stick-slip diagnostic levels of the current algorithm (red) and the new one (blue) with its backward rotation (BWR) type indication feature. Based on the data of Figure 94.

9.1.3.2 Backward Rotation Type II

Backward Rotation Type II is only diagnosed if a mud motor is in the BHA and CoPilot® is located above the motor. The classification is based on a comparison of average TOB of the backward rotation period (Interval 1) to average TOB of an interval of identical length located exactly before Interval 1 (Interval 2). If average TOB of Interval 1 is larger than average TOB of both intervals (Interval 1 & 2) and average TOB of Interval 2 is smaller than the average TOB of both intervals then the backward rotation event is classified as Type II. An example of stick-slip with Type II backward rotation is depicted in Figure 96.

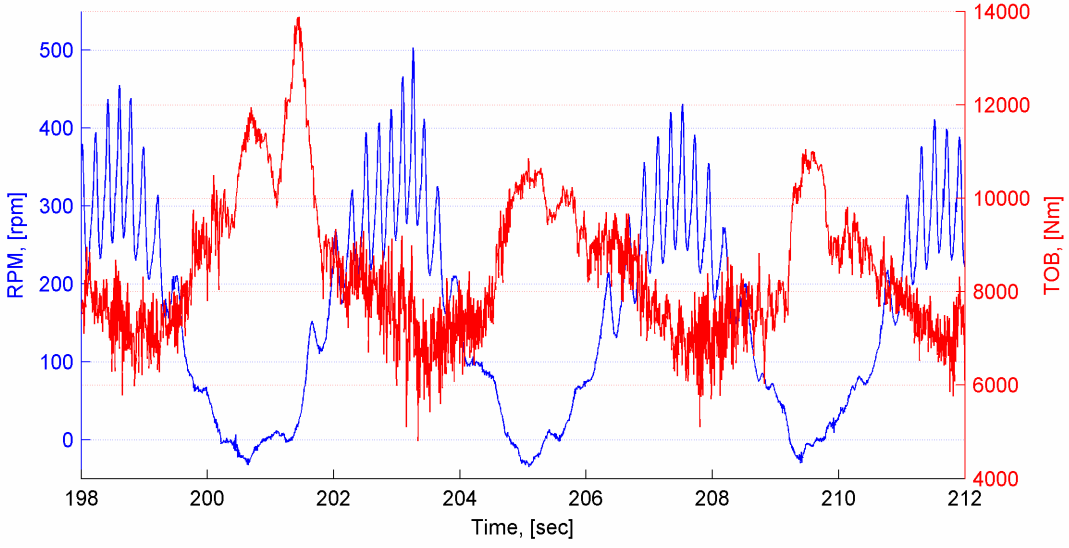

Figure 96 – Stick-slip with Backward Rotation Type II (at 200.5, 205 and 209.5 [sec]). Sample frequency: 200 [Hz].

Figure 96 shows that the torque minimum of a stick-slip oscillation with Type II backward rotation is located before the SL/backward-rotation-lag. This indicates that the whole potential energy which has been stored during drillstring twisting is already dissipated into kinetic energy and a new storage cycle starts before RPM has yet reached zero.

The characteristic TOB jump caused by a mud motor is most obvious at the third TOB peak (209.5 [sec]) in Figure 96. Such a sudden TOB increase cannot be caused by surface rotation as the torsional weak drill pipe section dampens surface induced torque jumps. While on the other hand PDMs can be responsible for such TOB jumps as they can almost immediately develop high reactive torques. Momentarily they are balanced by inertia of the heavy BHA collars but eventually result in a RPM reduction and finally in backward rotation.

In general, any increase in TOB with simultaneous negative pipe rotational speeds imply an active torque source (PDM) below CoPilot®. For this reason, it is not possible to get Type II backward rotation without a mud motor below CoPilot®. In case of absence of a PDM, a TOB increase at a positive level can never happen while CoPilot® and consequently the bit at the same time is rotating backwards.

The by the current and new algorithm diagnosed levels of the RPM trend of Figure 96 together with the backward rotation classification of the new method is shown in Figure 97.

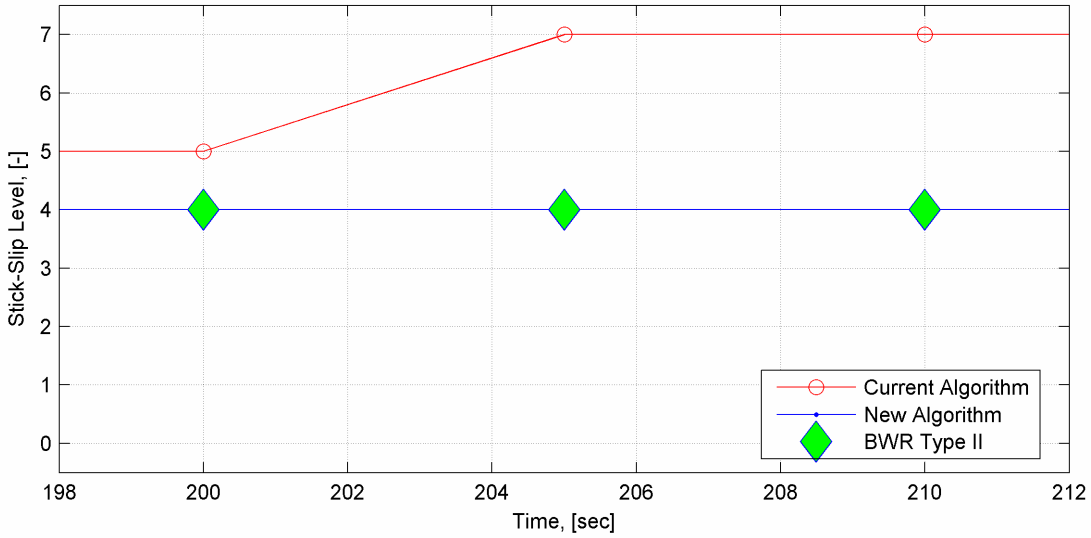

Figure 97 – Stick-slip diagnostics levels of the current algorithm (red) and the new one (blue) with its backward rotation (BWR) type indication feature. Based on the data of Figure 96.

9.1.4 Stick-Slip Causation

To determine whether stick-slip has developed due to bit-rock-interaction (bit friction) or due to high friction along the drillstring (drillstring friction), the TOB trend is investigated again. A prerequisite for TOB data interpretation is the

knowledge of torque sources by which CoPilot® can be affected and where they result from. CoPilot® detects only torque which is caused by resistances against rotation located somewhere below it. Any energy loss occurring above CoPilot® cannot be seen by it.

Another point to stress in this respect is that if stick-slip occurs, one of these frictions must be the reason for the developed stick-slip. Only bit friction can be measured by CoPilot® while drillstring friction cannot. Hence, a significant TOB peak while the TL indicates bit friction (actually it is the total friction below CoPilot®) as major stick-slip causation. On the other hand at the absence of such a torque peak drillstring friction (in a very broad sense as any restriction against rotation above CoPilot® like a reamer for example is summed up as drillstring friction) is the dominant stick-slip source.

None of these reasons, especially bit friction, will ever be solely responsible for stick-slip under real drilling conditions. Only the magnitude of their fractional contribution to stick-slip development is changing from case to case. For example, would already drillstring friction causes stick-slip even before the bit is on bottom (100 [%] drillstring friction causation), drilling would be impossible as the energy transfer down to the BHA is even not high enough to smoothly rotate the sole drillstring. Whenever in the subsequent text one or the other stick-slip causation is stated then it is refered to the major contributor that causes stick-slip but it does not expel other causations to be proportionately involved as well.

The position of CoPilot® in the BHA might dilute the causation classification's reasonableness. The closer CoPilot® is positioned to the bit the sharper or more reasonable the classification is. The reason is that quite a number of collars, stabilizers, or in extreme a reamer between bit and CoPilot® can be responsible for a significant portion of torque which is not only the result of just bit-rock-interaction. Therefore, the larger the distance between bit and CoPilot® is the larger is the fraction of drillstring friction which is counted as bit friction. For this reason, a position of CoPilot® as close as possible to the bit is advantageous. A PDM between bit and CoPilot® is not that critical as its reactive torque is a function of bit-rock-interaction.

The appearing moments of inertia are usually insignificant compared to the bit related torque. The amplitudes of by stick-slip caused tangential acceleration oscillations are normally too little (hardly exceed 0.5 [m/s²]) to cause relevant moments.

9.1.4.1 Implementation in the New Stick-Slip Algorithm

As already mentioned above, only bit friction alters CoPilot®'s TOB readings. Thus, the classification routine tries to find TOB trends characteristic for bit friction. If it cannot detect a characteristic sequence, drillstring friction is returned as the major causation of the backward rotation at the stick-slip event under investigation.

To automate the causation analysis, first of all a threshold needs to be defined to separate insignificant TOB oscillations from bit friction indicating trends. The threshold is set to 10 [%] change in TOB and its comparative value, CF (causation factor), is defined by the following equation:

$$CF = \frac{MAXTOB - MINTOB}{MAXTOB + MINTOB} \cdot 100 \quad > 10\,[\%] \qquad \textbf{(E 9.4)}$$

A relative criterion is chosen because a threshold specified by an absolute value appears as inappropriate as bit torque depends on bit diameter, bit type, WOB, formation properties, and many other parameters and thus it would result in too situation specific absolute values.

The next step is to pick TOB maximum, MAXTOB, and minimum, MINTOB, at the TL interval under investigation. Both values are determined at moderately averaged TOB data to reduce the risk of picking mavericks and also to improve the stick-slip causation classification reliability.

Another condition is set to further elevate the causation classification result's quality: while a single stick-slip event and thus in the time interval of a TL, the TOB minimum is always located before the TOB maximum. Therefore, this order is also taken as a condition for the relative position of the picked TOB minimum with respect to the maximum.

The last condition which must be fulfilled to allow bit friction to be diagnosed as major stick-slip causation is the difference between MAXTOB and MINTOB. It has to be greater than the torque values defined in Table 8 with regard to the corresponding tool size. This condition is intended to reduce noise influence and is nearly always fulfilled.

The elementary precondition: the stick-slip causation classification routine checks at the very beginning whether stick-slip has been diagnosed at all and, only in case, it screens all above mentioned conditions. If every condition is passed, the result is a classification as bit friction. If even one condition stops the algorithm, the output is drillstring friction. In case of stick-slip absence also no stick-slip reason can be and is determined. An example with instantaneous RPM and the resultant stick-slip diagnostics plus causation are given below (Figure 98, Figure 99).

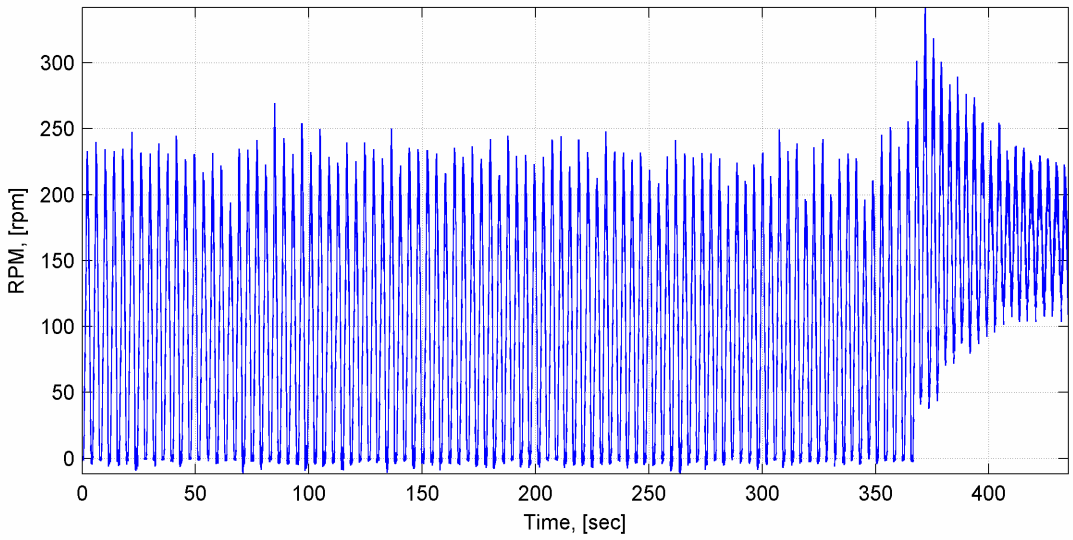

Figure 98 – Instantaneous RPM. The 9 ½" CoPilot® was a component of a rotary steerable BHA (w/o PDM). Shown is a stick-slip dying out example. Sequence length: 435 [sec]. Sample frequency: 100 [Hz].

The RPM trend of Figure 98 seems to show periods of backward rotation but as it is unfiltered instantaneous data almost all negative RPM values are noise on one hand (not detectable at the scale of the figure) or do not pass the threshold of -2 [°] effective backward rotation on the other hand.

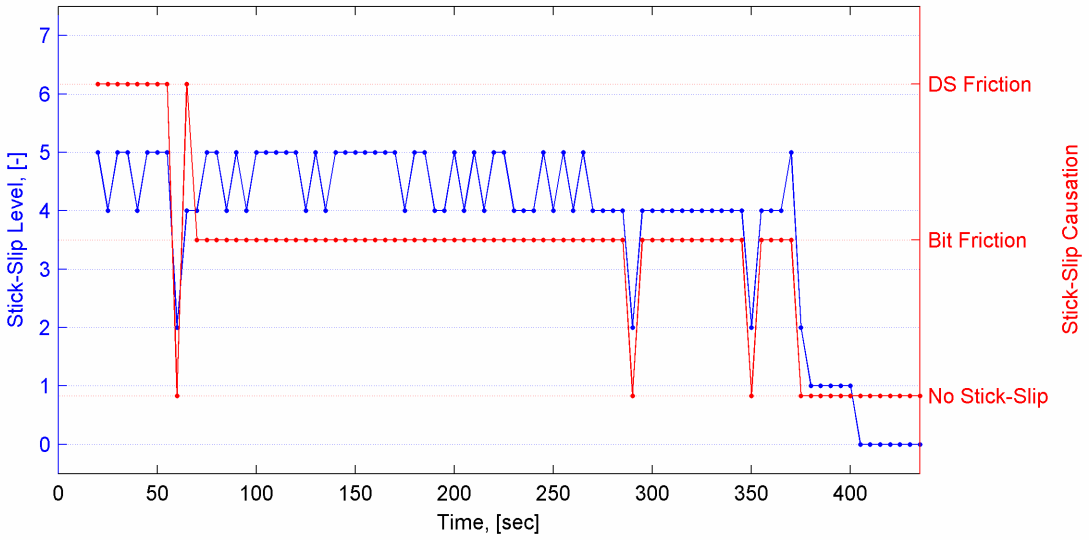

Figure 99 – Stick-slip diagnostic levels (new algorithm) and stick-slip causation of the RPM trend in Figure 98. The first 20 seconds are not plotted due to the calculation which is based on a 20 seconds data interval.

Figure 99 shows something very unlikely. The jump from a relative long period of drillstring (DS) friction as stick-slip causation to an almost permanent bit friction causation level cannot be just straight forward related to an actual drilling situation. It is hardly possible that a significant drillstring friction will vanish that abrupt and permanent (except e.g. due to an application of friction reducing mud additives (lubricants)). Of course a significant rise of WOB would also cause stick-slip causation to swing towards bit friction but would definitely alter the RPM/stick-slip

trend as the total acting friction (bit plus string) would increase. A RPM/stick-slip behavior change cannot be observed. Consequently, it is necessary to take a closer look on the actual TOB data set to figure out the reason for that strange behavior, see Figure 100.

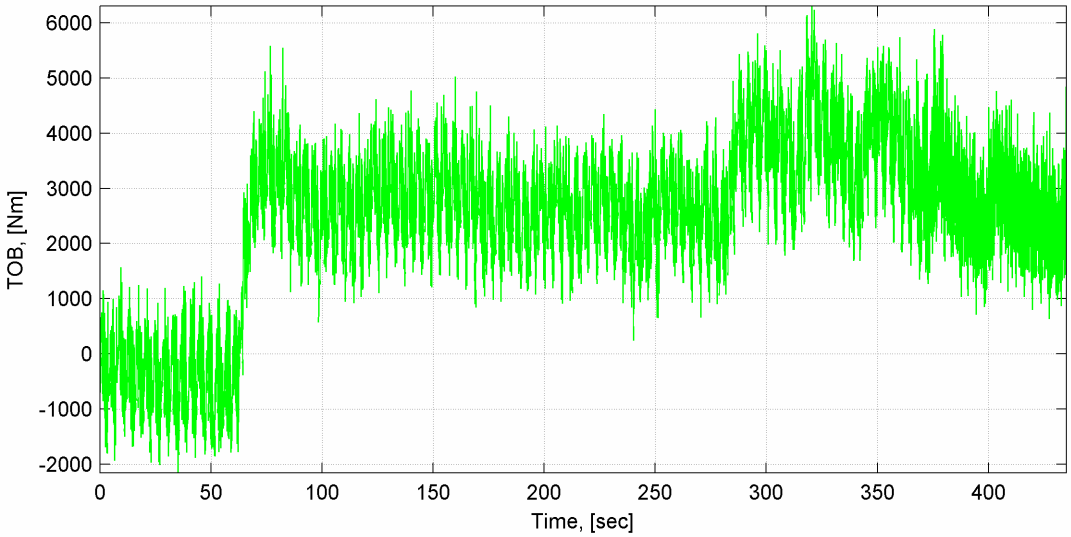

Figure 100 – TOB data of the in Figure 98 and Figure 99 discussed example. Sample frequency: 100 [Hz].

Referring to Figure 100, the TOB trend shows a significant step at about 70 seconds. When comparing Figure 98 to Figure 100 this significant step cannot be found in the RPM data nor can any influence be detected. Undoubtedly, such a large step must result in certain RPM changes (for example compare the oscillation's magnitude in the interval 150 – 200 seconds at TOB with the resultant one of RPM in Figure 98).

Due to the lack of any effect at RPM it must be assumed that TOB got stuck at that low primarily negative level. Furthermore, at about 70 seconds the sensors or whatever the reason was recovered again. Consequently, the stick-slip causation classification results a basically correctly diagnosed but unfortunately meaningless at the beginning as the data is afflicted with a severe offset. This problem points out the necessity of a globally linked (throughout CoPilot®) data plausibility check with a corrupt data indication before data analyses will be performed.

In total, the stick-slip causation detection routine of the development version is already working quite well. Stick-slip causation does not change frequently and without reason. While periods of no SL also no stick-slip causation is correctly indicated. Of course, the set thresholds and limits are a first but however suitable trail. Analyses of an increasing number of stick-slip triggers should offer some range for fine tuning of the currently used thresholds and limits. Finally, this should result in more stable diagnostics even at tricky data.

9.2 PDM as Rotational Dynamic Regime Boundary

A PDM in a BHA generates a second rotational dynamic regime in the drillstring. Components located below a PDM are exposed to other rotational conditions than the rest of the string. The PDM represent the boundary between these two rotational dynamic regimes.

Above a PDM rotary speed and torque is solely provided by the rig at the surface. All components below a PDM see not only the surface RPM but also in addition the PDM RPM. This is a very important point when regarding stick-slip and where it is detected. Furthermore, a PDM is a second, a downhole torque source which is active whenever mud is circulated. Components below a PDM can be rotated without rotating the whole drillstring.

The current stick-slip algorithm does not take into account a PDM as a possible BHA component. Consequently, CoPilot® only observes the conditions of that rotational dynamic regime to which it is exposed to and the other is totally unconsidered. The bit is usually the only component mounted below a PDM. Only special types of mud motors provide power transmission from top to bottom end and thus enable LWD tools to be run below it. Additionally, a too long distance between bit and adjustable kick off (AKO) is not favorable in terms of directional drilling.

At the moment it is necessary to decide whether CoPilot® should observe the upper or lower rotational dynamic section by selecting its corresponding relative position to the PDM. Thus it is only possible to focus either on the bit (CoPilot® below PDM, same regime as the bit) or on MWD and LWD tools located in the BHA above the PDM (CoPilot® above PDM, same regime as MWD and LWDs).

When just regarding stick-slip relevant parameters it is possible to take a look on the other side of the boundary (PDM) by making use of other available data channels of CoPilot®. This enables to “keep an eye” on both rotational dynamic regimes and the detection of their corresponding stick-slip levels.

9.2.1 How CoPilot® is Able to Monitor Both Rotational Dynamic Regimes

Data channels that distinctively show stick-slip occurrence at a specific rotational dynamic section are first of all the RPM, followed by torque, and last but not least tangential acceleration. All three parameters are either directly captured by CoPilot® as a PDM does not decisively influence their values no matter whether measured above or below the PDM or they can be calculated by using additional data channels.

When considering stick-slip, the most important parameter is RPM (of a particular section). As CoPilot® is not only able to measure its own rotary speed but also to

compute PDM rotor revolutions, it "knows" the RPM of the drillstring elements on the other side of the mud motor. With this "knowledge" stick-slip can already be detected beyond a PDM.

A point that must be mentioned in this respect is the accuracy of CoPilot®'s PDM RPM measurement. The motor RPM algorithm makes use of the rotor stator eccentricity at a PDM and its resulting vibration signal. Eccentricity is not a malfunction of the motor but a fundamental element of its working principle. PDM caused vibrations are detected by CoPilot®'s accelerometers but also recorded together with the strain data (both only lateral). By providing CoPilot® with the configuration of the motor, e.g. the number of rotor lobes, it is able to pick out the motor excitation related frequency from the acceleration or bending frequency spectrum and to convert it to mud motor RPM.

None of the involved sensors behaves ideally. Furthermore, masses of non motor related vibrations at a variety of frequencies and intensities are simultaneously measured. The distance between motor and CoPilot® can change significantly from BHA to BHA design. Eventually, the used data is filtered several times. Thus, when considering all these potential sources of inaccuracy, CoPilot®'s motor RPM data gathering needs to be reconsidered if it is applicable for stick-slip detection on the other side of a PDM. For example, it can be vital for bit life of a PDC bit whether the bit is rotated forward with 2 [rpm] or already backwards at the same speed.

In this respect, accuracy is crucial and in consensus with steadily improving service quality a direct PDM RPM measurement should be taken into account. Upcoming mud motor types are equipped with a power transmission line. Motor design should easily allow to incorporate a sensor which measures the relative velocity between the stationary and rotating part of the motor.

Motor RPM sampling rate must be chosen in correspondence with CoPilot®'s high speed data rates to ensure equal resolution and accuracy for both dynamic sections. In addition, the sensor signal needs to be accessible for tools located either below or above the PDM. These are relative minor engineering steps but would allow a full and accurate BHA stick-slip monitoring beside other optimization advantages resulting from a precisely measured mud motor RPM.

The second parameter heavily influenced by stick-slip is torque. Torque is defined as positive when it drives the drillstring to rotate in clockwise direction (forward). PDMs transfer positive torque unchanged from their bottom to top end (while pumps on). In contrast, negative torque is uncoupled from transmission as it is acting in the same direction like the PDM's reactive torque. In theory there is an upper limit for this uncoupling effect. For example, if the stator would be rotated faster backwards than the PDM's rotor is turning forward, it will change from motor mode to pump mode and start to transfer negative torque as well. This is a condition usually not expected to be reached in oilwell drilling.

As mentioned above, the new algorithm uses torque to classify backward rotation and stick-slip causation types. As in one case also negative torque is a criteria (Backward Rotation Type I) and negative torque will never result from somewhere

below the PDM nor would be able to pass it in any direction, CoPilot® should be preferentially added to the BHA above a motor.

Furthermore, the only possible backward rotation type below a PDM (Type I) is easily detectable via accurate instantaneous RPM measurements of both CoPilot® and PDM and needs no torque data for classification. Concerning stick-slip causation, it appears slightly advantageous to locate CoPilot® as close as possible to the bit – consequently below the motor – as determination influencing drillstring friction is reduced to a minimum. However, the last point should not be rated too high.

Tangential acceleration, the last named parameter above, can be received from accurate high speed RPM data. It is not necessary to sense tangential acceleration individually if the RPM data is of high quality. Thus, a PDM is not a problem for tangential acceleration surveys of neither side but stresses the need for highly accurate motor RPM data.

9.2.2 CoPilot®'s Position Relative to a PDM

Mud motors generate and simultaneously separate rotational dynamic regimes. Not every dynamic effect is able to pass a motor unchanged or even to pass it at all. Therefore, a mud motor uncouples the dynamic sections to some extend. Due to its design, a mud motor is acting as somehow a vibration damper in axial and torsional direction. At the same time it is also a major source for lateral vibrations due to its rotor stator eccentricity and the excitation caused by an rotated AKO sub with an angle larger than zero.

CoPilot®'s BHA position is virtually unlimited as long as power supply is possible. The majority of LWD tools and especially MWD tools are best positioned close to the bit. The intention to use CoPilot® together with that of other MWD/LWD tools usually makes it necessary to rank their order in the BHA according to their priority to achieve a desired BHA performance.

From a stick-slip point of view, CoPilot® should not be mounted below a PDM for the reasons discussed earlier in this text. A too high uphole position should also be avoided because drillstring friction is increasingly influencing TOB readings. Additionally, WOB is getting lower and lower as a closer position to the neutral point is occupied. What is more, vibrations are increasingly dampened and bending moments are less linked to bit action to name same other effects. Consequently, the ideal BHA position for CoPilot® in the here discussed respect would be exactly above a PDM. If no motor is used, CoPilot® becomes another competitor for the closest position to the bit.

9.2.3 Implementation in the New Stick-Slip Algorithm

The effect of a PDM in the BHA on stick-slip detection is implemented straight forward in the new stick-slip algorithm. First, the presence of a PDM and CoPilot®'s relative position to it is specified. This is a step which is currently not performed during programming CoPilot® for a run. Thus, it would represent a little change in the field operation procedures.

By specifying CoPilot®'s relative position, the algorithm is triggered to analyze both dynamic sections. RPM and torque data of each section is processed individually by the new algorithm. The same algorithm is simply applied twice – once for each dynamic section. As stick-slip causation is not related to any dynamic section it is only once globally determined.

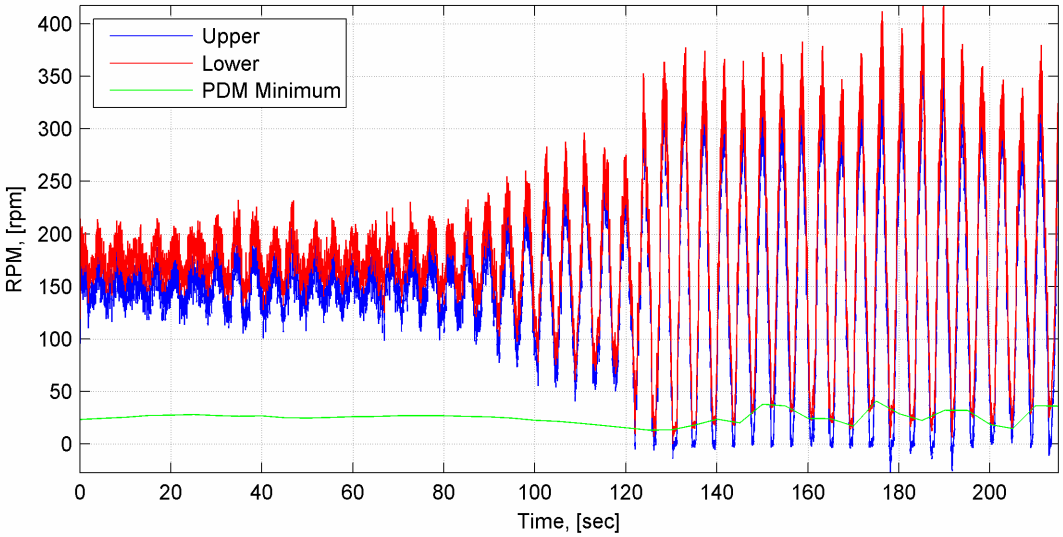

Figure 101 – Instantaneous RPM example of a BHA with two rotational dynamic regimes. CoPilot® is located in the upper section (above PDM). Lower section's data is calculated via FSD PDM minimum RPM. Sample frequency: 200 [Hz].

Figure 101 shows an example where two rotational dynamic regimes had been present at a motor BHA. CoPilot® collected data from the upper section, where it was located, whereas the RPM values of the lower section are calculated. As currently no high speed motor RPM data is stored and a full implementation of the complex motor RPM detection algorithm appeared as unnecessary for the here discussed development version, high speed motor RPM data is simply generated via linear interpolation of the minimum motor RPM FSD which is available from on-board memory. In this respect, minima are taken as the focus lies on low RPM values.

The diagnostic results of the new algorithm of both dynamic sections together with levels resulting from the current algorithm are depicted in Figure 102. The example indicates that already a very low speed PDM is able to eliminate the danger of bit backward rotation.

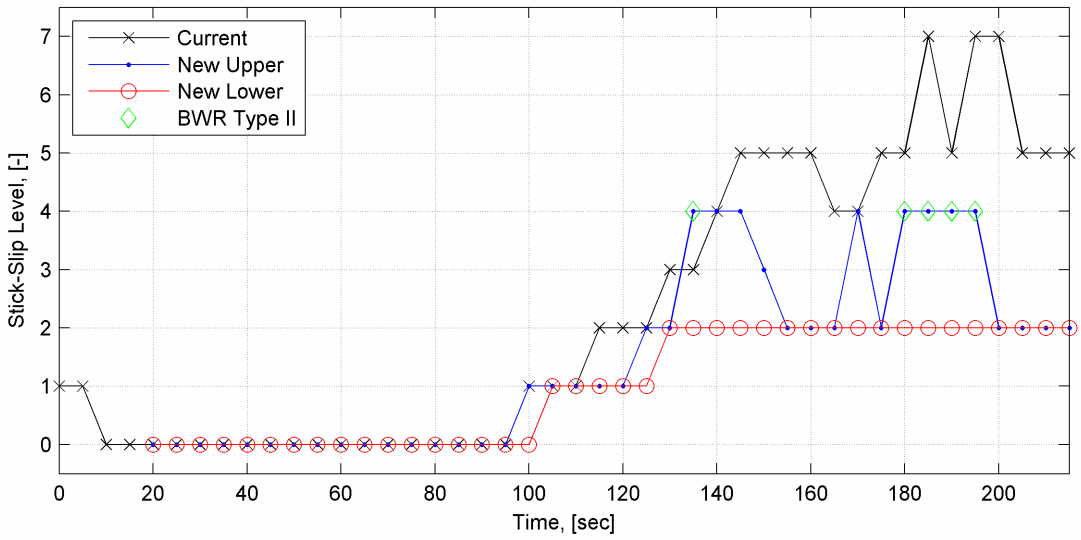

Figure 102 – Stick-slip diagnostics of RPM data shown in Figure 101.

9.3 Tool Life

Failures of entire MWD or LWD tools or even just a sudden loss of a single functionality of such tools might become very costly but – in most cases even more detrimental – it is always an obvious downgrade in service quality no matter if the string has to be pulled or not. On the other hand, short scheduled tool maintenance intervals can prevent some failures but cause also undesirable and unfortunately often unnecessary expenditures. Thus, two different policies can be figured out which service companies can alternatively pursue: either the risk is taken to get punished for tool failures but money is saved at maintenance or money is preemptively spent for planned tool maintenance and therewith the risk of expensive tool failures is reduced. Either way includes a high degree of uncertainty making the decision for one or the other policy to not a trivial task. This is the dilemma every service company faces.

The car industry has a similar problem. They cannot control under what conditions their products (cars) are used but should provide and guarantee an as long as possible mean time between failures. Also in this case short maintenance intervals are costly and time consuming and therefore the car industry's costumers are not willing to accept them. For this reason, maintenance intervals became an important argument when selling cars during the last decade.

With the advent of electronic systems controlling more and more functions of a modern car also sensors of any kind found their way into cars. An increasing number of sensors together with systems able to process sensor signals elevated car maintenance to the next level. Usage scenario predictions and resultant maintenance interval estimations are no longer that important as a sensor equipped car continuously monitors and stores its working/use conditions and according to these data it variably defines maintenances times on its own. Such vehicle use dependent maintenance systems were the solution for the reliability-maintenance-cost-dilemma

of the car industry. CoPilot® is suitable to become the centerpiece of a system able to handle this problem in the drilling industry.

CoPilot® is equipped with all necessary sensors to monitor working conditions right there downhole at the BHA. Especially the for electronic board's reliability important parameters temperature and triaxial vibrations are measured. Loads, torque, bending moments, and pressures are also recorded, enabling mechanical integrity and fatigue observations.

Highly equipped logging BHAs can achieve considerable lengths. CoPilot® is a single spot sensing tool. A total monitoring of such a BHA makes pre-run dynamic drillstring analyses necessary. Dynamic drillstring analyses can disclose dynamic hot spots and thus allowing appropriate positioning of CoPilot® to observe the most critical section. In extreme, there is also the possibility to us more than one CoPilot® tool.

In general, stress monitoring with respect to a single dynamic dysfunction appears as less useful as tools are exposed to the total stress regime. A split-up especially with regard to the effects on tool life is critical. Whereas, relating failures to certain operating conditions is very important to uncover weak points and thence be able to improve the tool's reliability. However, this text covers stick-slip and in this respect stick-slip related stress and strain is discussed in the following to rate the actual danger of stick-slip.

9.3.1 Stick-Slip Related Stresses

Basically, stick-slip are severe rotary speed oscillations. Thus, potential harmful stresses result from both velocity changes and high velocity peaks. As a consequence, tangential and centrifugal acceleration are the parameters to look at to figure out stress maxima.

9.3.1.1 Tangential Acceleration

During the stick period the drillstring is twisted up and energy is stored (potential energy). At the point the potential energy exceeds the restriction against rotation, it is suddenly released causing the drillstring to tremendously speed up. Such rapid velocity changes may lead to high tangential accelerations. Two stick-slip examples, recorded by CoPilot®, together with the resulting measured tangential accelerations are shown in the next two figures.

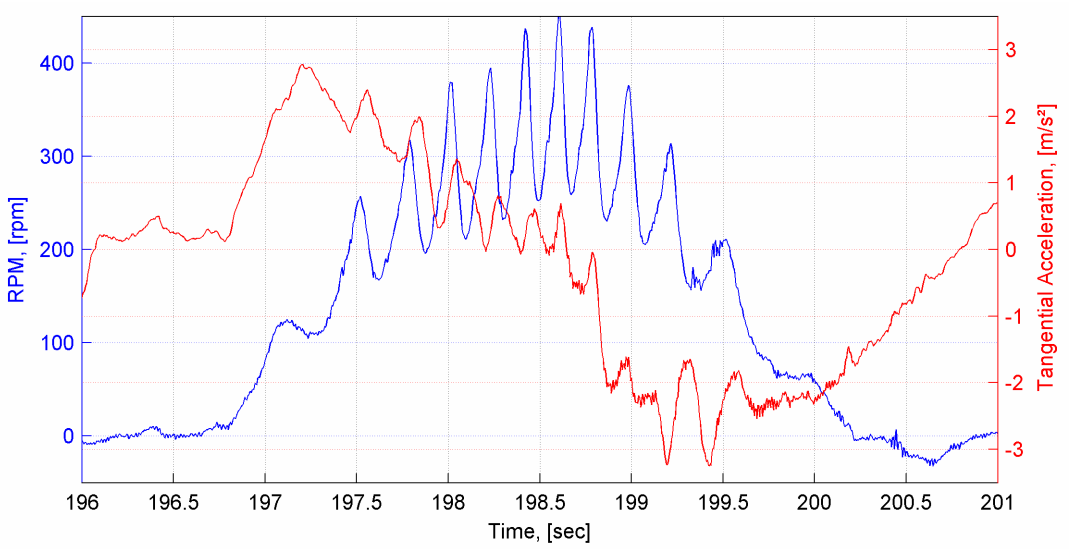

Figure 103 – Example 1: max. instantaneous RPM: 455 [rpm], max. tang. acceleration: 2.8 [m/s²], min. tang. accel.: -3.2 [m/s²], sample frequency: 200 [Hz]. Tangential acceleration was sensed by accelerometers and is corrected and slightly averaged.

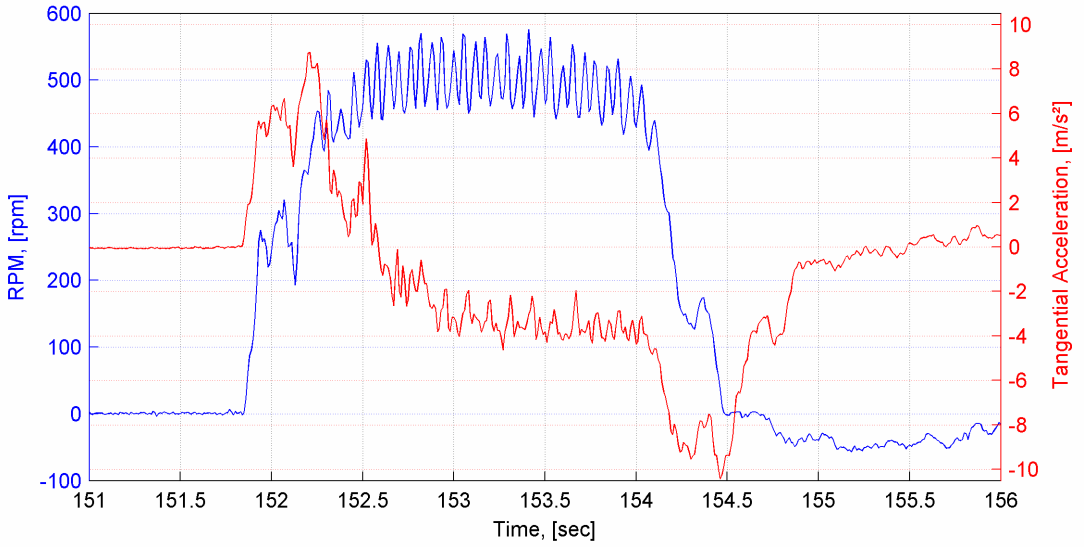

Figure 104 – Example 2: max. instantaneous RPM: 576 [rpm], max. tang. acceleration: 8.7 [m/s²], min. tang. accel.: -10.4 [m/s²], sample frequency: 100 [Hz]. Tangential acceleration was sensed by accelerometers and is corrected and slightly averaged.

Example 1 (Figure 103) is a moderate stick-slip RPM peak whereas Example 2 (Figure 104) shows a very severe stick-slip event. When just considering the RPM data, both RPM peaks would infer high tangential accelerations. Actually, this initial false estimation needs to be reassessed after the measured tangential acceleration data has been investigated.

The acceleration values of Example 2 only slightly exceed 1 [g] while those of Example 1 even only reach in extreme one third of gravity. Bearing in mind that Example 2 is a case of severe stick-slip, tangential acceleration in general rarely exceeds 5 [m/s²]. This is nearly equivalent to half of the gravitational acceleration. These very low acceleration maxima and their corresponding stresses should not be dangerous for any tool.

Cyclic stress reversals are more critical than stresses permanently acting in a single direction. Stick-slip causes cyclic stress reversals but the reached tangential acceleration related stresses are that little that tangential acceleration can be regarded as harmless under "normal" stick-slip conditions. RPM changes appear abrupt and sharp at the plotted RPM data but objectively assessed they are quite moderate. To substantiate this point the following two figures show simulated RPM peaks with their corresponding tangential acceleration trends.

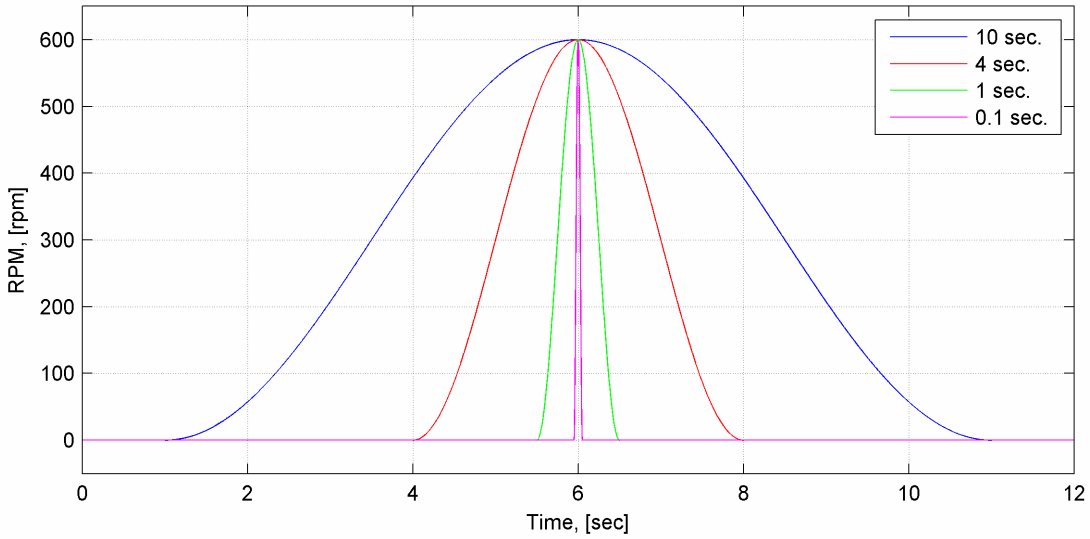

Figure 105 – Four RPM peak examples with period lengths of 10, 4, 1 and 0.1 seconds.

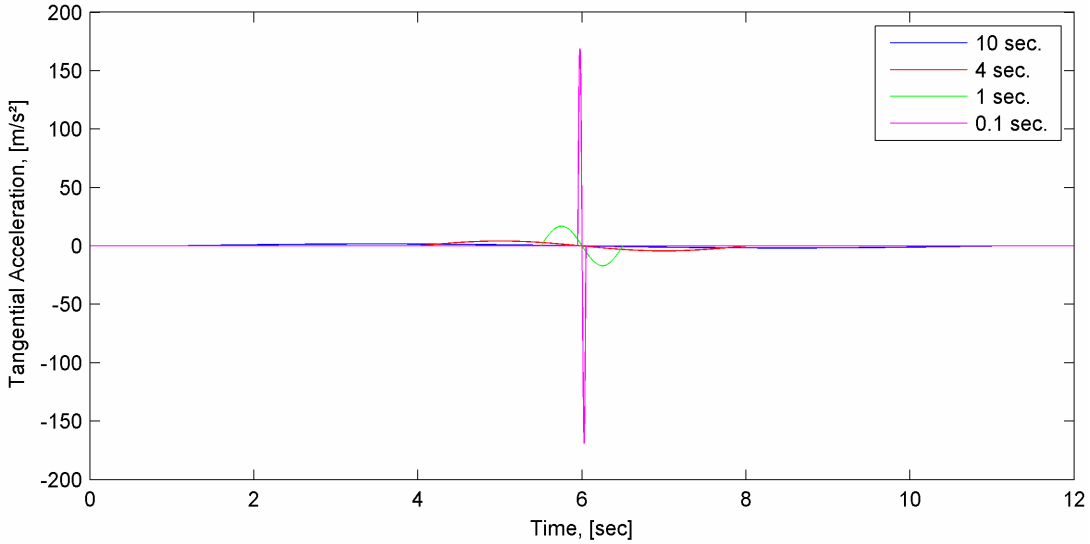

Figure 106 – Tangential acceleration trends of the RPM peak examples shown in Figure 105. Maxima: ±1.7 [m/s²] (10 sec.), ±4.2 [m/s²] (4 sec.), ±16.9 [m/s²] (1 sec.), ±168.9 [m/s²] (0.1 sec.).

Figure 105 shows four sinusoidal RPM peaks with different period lengths. A sinus like peak shape is taken to approximate stick-slip RPM peaks because such a shape fits quite well in reality observed RPM peaks. Their resulting tangential acceleration trends are shown in Figure 106. Tangential acceleration is proportional to RPM and inversely proportional to period length. Consequently, either extremely high RPM

peaks per unit period length or very short period lengths per unit RPM maximum cause tangential acceleration to reach dangerous levels.

The shown examples with period lengths of 10 and 0.1 seconds represent more or less exceptions. A period length of 10 seconds is already quite long for stick-slip. Such a length would indicate a very long, slender, and thus torsional weak drillstring. Whereas, the 0.1 seconds period length constitutes the other and even less likely extreme. A drillstring that would produce such sharp stick-slip RPM peaks has to be enormous stiff under torsional loads.

The red and the green curve symbolize more realistic stick-slip scenarios. Most stick-slip problems are located in the range of 1 to 4 seconds period lengths. This is not a stick-slip property but more related to standardized tool sizes and preferred diameters for similar hole depths. Even in the very heavy stick-slip case of 1 second period lengths, tangential acceleration does not rise above 2 [g].

Usual drilling practices and parameters together with material properties prevent tangential acceleration from reaching dangerous levels. A priori, tangential acceleration cannot be branded as totally uninfluential to tool life of any tool under any drilling condition. However, many cases demonstrated that its magnitude normally stays far below critical values.

9.3.1.2 Centrifugal Acceleration

Whenever the whole drillstring or just the section below the PDM is rotated, centrifugal forces are acting on every element located off-center the axis of rotation. In contrast to tangential acceleration, the centrifugal acceleration to velocity (RPM) relation is of second order. This means, doubling the velocity results in a four times higher centrifugal acceleration, see equation E 9.5.

$$a_c = \frac{v^2}{r} \qquad \textbf{(E 9.5)}$$

This quadratic relation lets centrifugal acceleration appear as more critical for tool life than tangential acceleration with its linear relation. Thus in the following it is examined what realistic magnitudes of centrifugal acceleration are. With regard to CoPilot®'s four tool sizes it is figured out if dangerous levels can be reached while normal drilling operations.

Referring to Figure 107, the development of centrifugal acceleration with increasing RPM is determined. The dotted line marks the upper sensing limit (50 [g]) of the accelerometer type incorporated in CoPilot®. CoPilot®'s x-direction accelerometer pair senses centrifugal acceleration as it is pointing in radial direction. Correctly speaking, one element measures a positive and the other a negative acceleration due to their identical coordinate system.

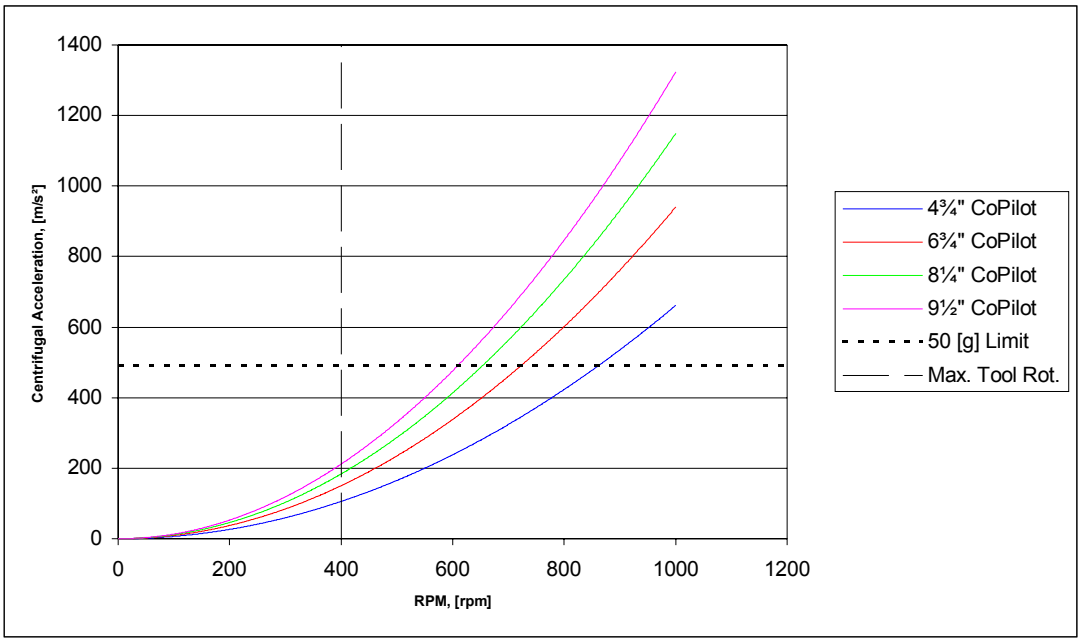

Figure 107 – Centrifugal acceleration versus RPM. Calculated for the nominal tool radius.

There are two problems that Figure 107 discloses: first, CoPilot® is designed for a relative low maximum tool rotational speed of only 400 [rpm][30], [31], [32], [33], [34], [35], [36], [37]. It has already been shown that stick-slip events can easily generate RPM peaks that considerably exceed this limit (see Figure 103 and Figure 104 for example). Every limit overstepping represents an out of specifications operation.

Second, in extreme cases (e.g. CoPilot® has been positioned below a high speed PDM and stick-slip is skyrocketing RPM maxima) even the maximum sensing range limit of the accelerometers might be exceeded with the consequence of unknown and perhaps adverse effects.

The exact RPM values where 50 [g] of centrifugal acceleration are achieved are listed in Table 9. These values are calculated for a radius equal to the nominal tool radius.

Tool Size	Centrifugal Acceleration at 400 [rpm]		RPM with 50 [g] Centrifugal Acceleration
[in]	*[m/s²]*	*[g]*	*[rpm]*
4¾	105.8	10.8	861
6¾	150.4	15.3	722
8¼	183.8	18.7	653
9½	211.7	21.6	609

Table 9 – Centrifugal acceleration limits of CoPilot® as marked in Figure 107.

When regarding CoPilot®'s maximum rotation limit as equivalent to its maximum allowable centrifugal acceleration, then centrifugal acceleration must be considered

as critical for tool life. Centrifugal acceleration is not a cyclic reversing stress but an up and down swelling one – especially while stick-slip. Therefore, the additional negative effect of cyclic stress reversals is not given. Generally, centrifugal acceleration has to be classified as more adverse for tool life than tangential acceleration because of its significant larger achievable magnitudes.

9.3.1.3 Resulting Effective Acceleration

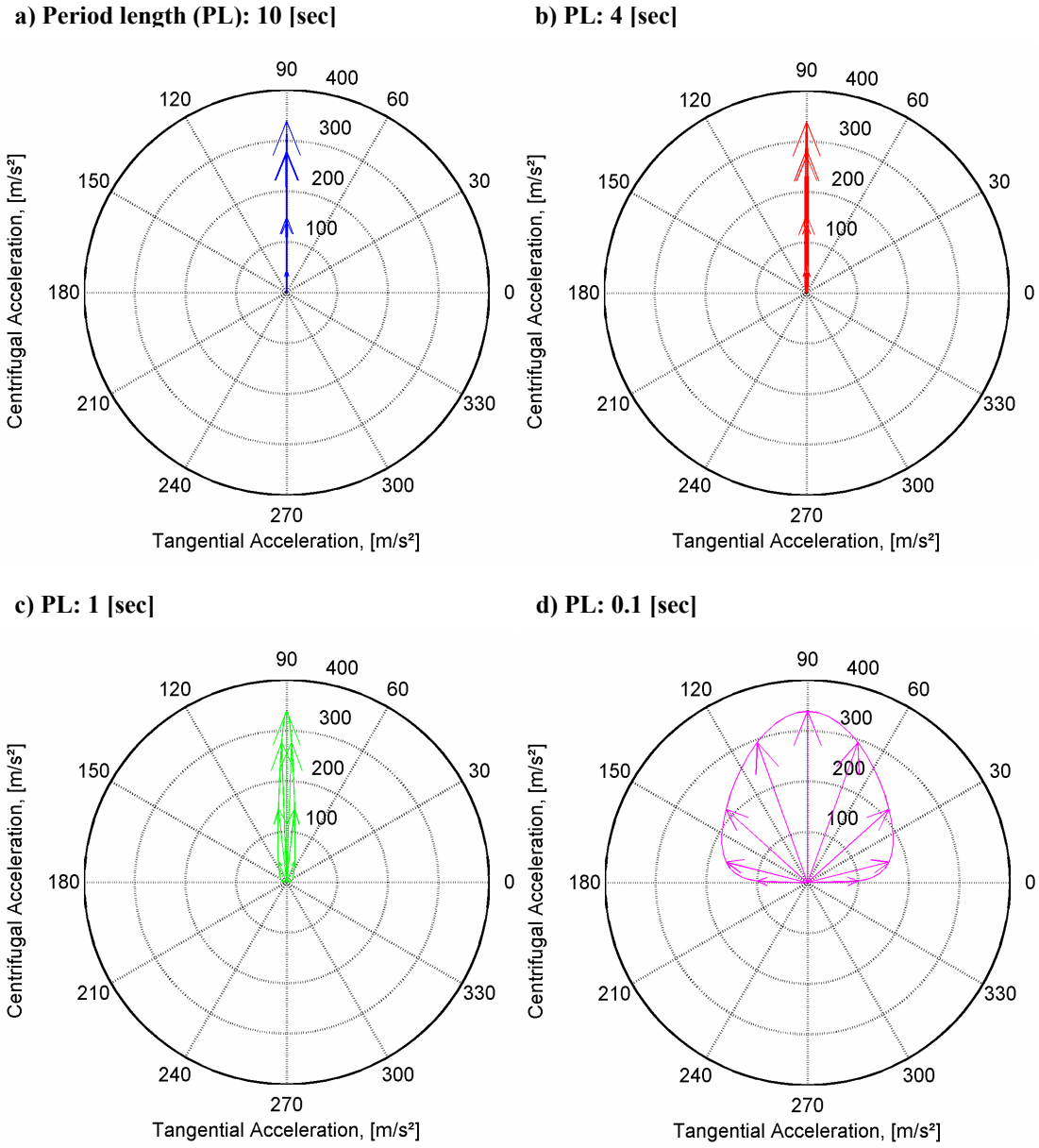

Figure 108 – Resulting effective acceleration for an element at the surface of a 6 ¾" collar experiencing the velocity changes shown in Figure 105.

The effective acceleration an element observes while rotating with varying speeds is a combination (vector sum) of tangential and centrifugal acceleration. Only if RPM is kept at a constant level, tangential acceleration vanishes and the resulting effective

acceleration is equal to the centrifugal acceleration. Thus, centrifugal acceleration can solely act whereas tangential acceleration always appears in conjunction with centrifugal acceleration.

Figure 108 shows the effective acceleration for an element located at the surface of a 6 ¾" collar experiencing the velocity changes shown in Figure 105. As the maximum RPM is identical at all four examples also the maximum centrifugal acceleration is constant. Figure 108 gives a good impression of the evolution of magnitude and direction of effective acceleration while a stick-slip event. Whereat, the shape of the area the effective acceleration vector outlines varies with changing RPM peaks. Thus, even relatively flat and wide shapes are possible. However, highest effective acceleration values are only achieved with large RPM maxima and consequently high centrifugal accelerations.

9.3.2 Tool Lifetime Count Down

CoPilot® senses all relevant data for a detailed working conditions observation. Post-run, these stored data can be used to manually investigate might occurred failures. Indisputably, failures must be avoided. Therefore, a detected critical condition should immediately trigger some alarm. CoPilot® is already doing that with its transmitted diagnostic levels. Not always is it possible to sufficiently adjust drilling parameters to drill calm and smooth all the time. A permanent and history dependent tool life monitoring would be necessary to get indication how long the BHA is able to perform under specific conditions with respect to its in the past experienced stresses.

With CoPilot® two factors of the failure process are known: the reason, which is the by the tool seen stress (start point), and the result (end point) as damage at the tool. Every failure which had happened assists to outline working parameters the tool cannot withstand. On the other hand, harsh but successful runs approach the most adverse conditions which the tool is able to survive and by that delimiting the operation limits from the other side.

Unfortunately, a very large number of failure and successful run data are necessary to actually infer operation limits for an acceptable range of operation conditions. Data gathering from normal tool applications can be quite time consuming in this respect or very incomplete if a tool is new and thus has not yet been used that much. It is never satisfactory to know just a few extremes a tool can survive or where it is already harmed or overstrained. That is why it is important to get realistic stress, temperature, and pressure figures that the tool is capable to withstand. If an exactly outlined stress-tool-life function is known, CoPilot® is able to monitor and predict its tool life automatically and on its own.

A stress-tool-life function will not be achieved straight forward as it is a multi parameter function (temperature, pressure, vibrations, tool size, WOB, bending moments, etc.). Usually, the weakest points are the electronic boards. Due to well known material properties, calculated designs, and finite element simulations metal collars are usually less prone to failures. However, in cases of a permanent collar failure it is often quite easy to choose a more massive design next time or simply

change to a better suitable material. Electronic elements are small in size and sometimes difficult to protect against vibrations and temperature but have to perform accurate under rough downhole conditions. For these reasons it is intelligible that electronic elements are more susceptible to failures than solid metal parts.

Tool life prediction becomes absurd with low manufacturing quality. Highest manufacturing and quality control standards for every component are crucial. By all means it must be ensured that every tool is of identical quality. High manufacturing tolerances could lead to considerable variations in tool life and thus disable reliable tool life prediction. Therefore, it would not justify the effort to develop such a system.

For the discussion here a high and constant tool quality is presupposed. Therefore, ways to receive a stress-tool-life function need to be found. Two options are available which both should be taken into consideration when developing a stress-tool-life function:

- detailed field data analyses,
- (destructive) laboratory tests.

Detailed field data analyses have the advantages of real drilling conditions and already available data. However, there are also some problems involved with this approach: enormous data quantities need to be analyzed as not only failure events are relevant but also clean runs. Most of the data is not centrally stored in a data base and reasonably linked. There are no standard for research data gathering resulting in different sample rates and a varying number of stored channels. Surface data is usually of poor quality and quantity. Drilling operations and decisions sparsely documented. The result is, that the workload related to this approach is unpredictable and thus the costs are as well.

Laboratory tests and in this context also destructive tests represent the other option. It is possible to simulate and fully adjust expected and desired conditions. The amount of data to handle is drastically reduced. The most significant disadvantage of laboratory tests is the destruction of tools or at least the destruction of critical components and this not only once but several times. This fact could be a considerable cost factor.

Strictly speaking, all influencing parameters have to be varied and investigated during laboratory tests. As mentioned above, the electronic parts are of special interest. Electronic components are most susceptible to temperature variations and vibrations. Other possible detrimental parameters are either sealed off, low in magnitude, or simply less critical for electronics. Therefore, tests can be limited to variations in temperature and vibration levels.

Furthermore, not full-scale tests with entire tools are necessary as test runs with the electronic boards mounted on a test carrier should be sufficient. This would also enable an easy check whether tool size is a parameter to consider. Also before a number of full range temperature test sequences is run, the actual influence of temperature should be estimated by a low and high temperature test. Possibly, only the effect of vibrations needs to be extensively investigated at several endurance tests with different vibration severities. Furthermore, shock tests should be carried out. In

summary, it seems to be unnecessary to perform vibration tests for every tool size and the full temperature range which significantly reduces the total number of tests.

Any design modifications or constructional improvements of a tool can influence its stress-tool-life function. Such changes would make a new function evaluation necessary. In this respect, only laboratory tests are possible as field data will only be available later on.

9.3.3 Tool Life Prediction Example

Due to the present lack of laboratory test data and a this work's workload exceeding deduction of a real stress-tool-life function from field data nor any knowledge if different stress events are straight forward summable, a simplified example is set up to demonstrate the basic ideas behind the potential tool life feature of the new algorithm.

The following assumptions are made:

- temperature effects are neglected,
- the absolute value of effective acceleration is taken and its direction is neglected,
- stress events and the effect on tool life are assumed to be summable,
- a stress-tool-life function is assumed with respect to Woehler's curve,
- a minimum tool life for normal operation conditions is assumed.

Disregarding all simplifications, the development of a stress-tool-life function is necessary anyway, as it is an essential part of the tool life prediction. Woehler's cycle stress versus cycles to failure curve's characteristic appears as quite reasonable for an expected stress-tool-life function of electronic components. Originally, Woehler's curve refers to material fatigue.

In this context it must be stated that this assumption is not based on any data but solely on the speculations of the author. Therefore, the here shown and used stress-tool-life functions must not be used for any actual tool life prediction nor any application exceeding the demonstrative purpose of the in this respect presented example! A changing stress-tool-life function will significantly influence the results of the tool life prediction.

Stick-slip related stresses show a moderate rate of change. In general, shocks are not typical for stick-slip. The shock survival limit of CoPilot® (45 [g] with a pulse duration of 0.025 [sec][30], [31], [32], [33], [34], [35], [36], [37]) is set as the immediate tool failure point of the assumed stress-tool-life function (zero percent tool life). This is the only known condition the tool is actually specified for.

The lower limit, no influence of stress magnitude on tool life (asymptote), is a conclusion. The maximum rotational speed is identical for all CoPilot® sizes and represents an acceleration level the tool has to withstand by specification. For this reason, effective accelerations up to a magnitude equal to the centrifugal acceleration at maximum rotational speed (400 [rpm]) is assumed as uninfluential to tool life (see

Table 9 for corresponding values). The characteristics of the stress-tool-life function between these two points is manually fitted in, imitating the trend of Woehler's curve. The artificially generated stress-tool-life functions of all four tool sizes are shown in Figure 109.

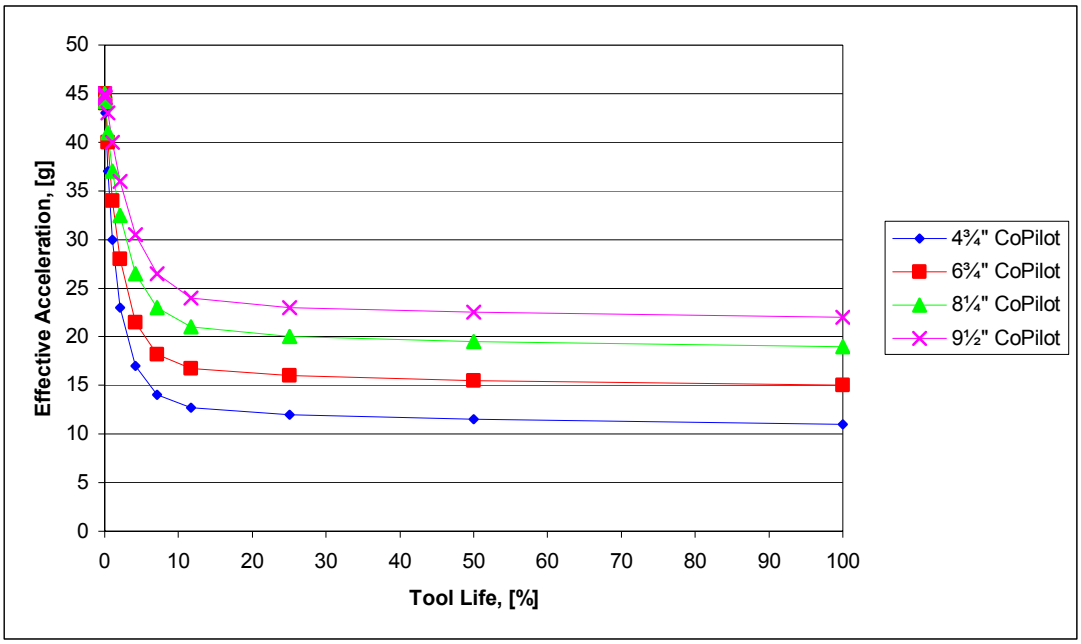

Figure 109 – Assumed stress-tool-life function of all CoPilot® sizes. These functions must not be used for actual tool life predictions.

Figure 109 is not a semi-log plot like Woehler's curve. The depicted functions would also appear s-shaped, if the abscissa is logarithmically scaled. It is not done in this respect as also at zero tool life an acceleration value needs to be defined and plotted which would not be possible on a logarithmic scale.

When comparing Figure 109 with Figure 107 it stands out that the from Figure 107 expected higher stress resistance of smaller tools cannot be found again in Figure 109. In fact, the exact opposite is observed. The reason for that strange behavior is addressed to the identical maximum rotational speeds of all four tool sizes. Figure 107 indicates higher possible RPM levels for smaller tool sizes before the same stress level is reached. The specified maximum rotational speed does not reflect that. If just safety concerns or downsizing compromises or whatever the reason might was to use a uniform maximum RPM level, experiences showed that smaller tools are actually more likely to fail in general. Therefore, even if Figure 109 seems to appear contrary to Figure 107, it is actually based on reasonable assumptions.

High speed data of a complete CoPilot® run is not available. A single high speed trigger is taken instead and treated as a full run data set. The size of the tool that recorded the data in Figure 110 is 6 ¾".

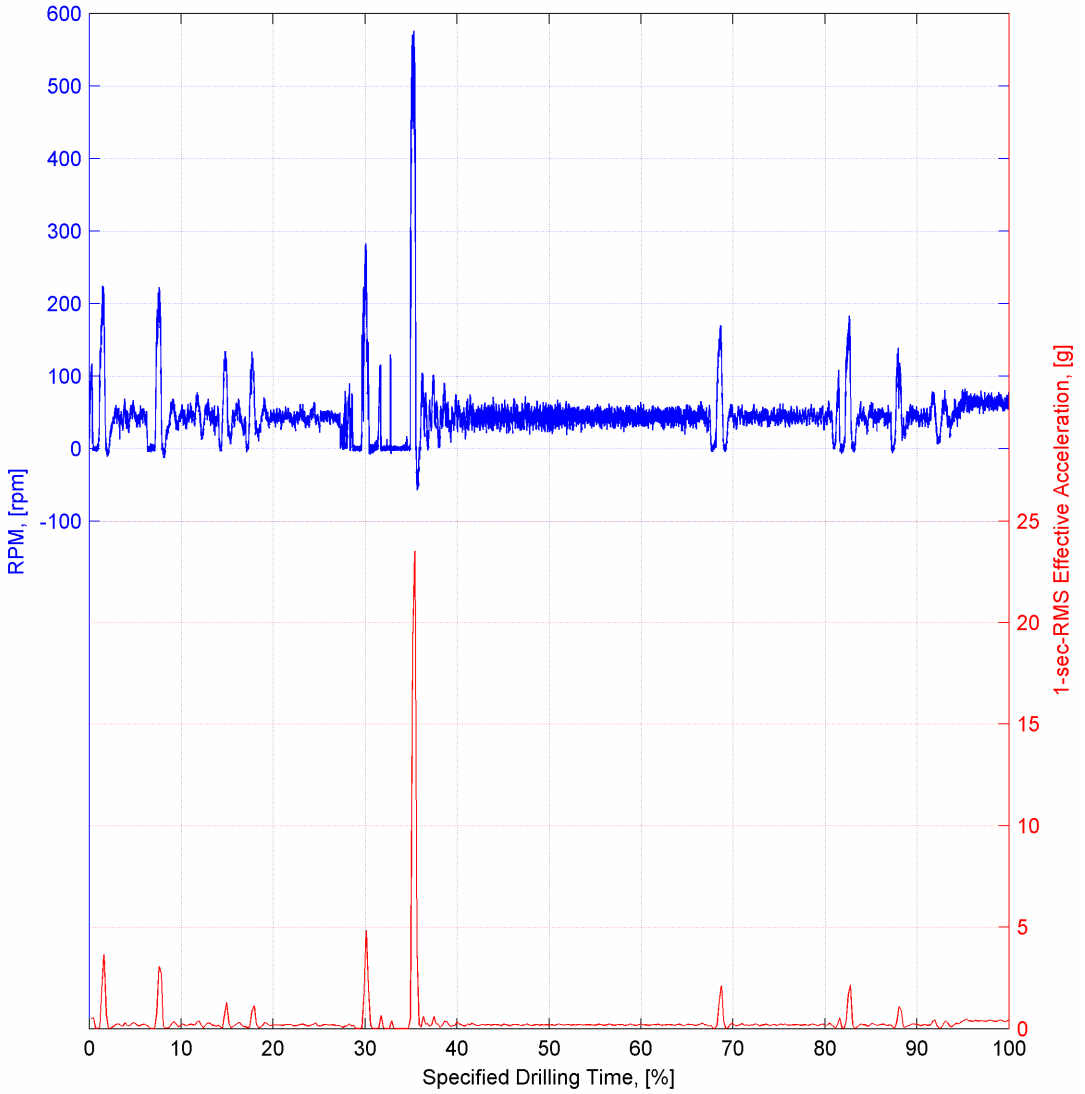

Figure 110 – Example RPM (sample frequency: 100 [Hz]) and effective acceleration (averaged over a 1 second interval).

In Figure 110 the RPM and effective acceleration trends are depicted which are taken as a whole run sequence for the example. The nonlinear RPM to effective acceleration relation becomes quite obvious when comparing e.g. RPM and effective acceleration peaks at 30 and 35 [%] specified drilling time.

The effective acceleration is averaged over a 1 second interval. This is necessary as noise and mavericks which cause higher values would reduce tool life prediction for no reason. Whereas, noise and mavericks leading to lower values would not balance in average the overestimation as tool life cannot be extended anymore once it is reduced. Averaging solves that problem.

To predict tool life each 1-sec-RMS effective acceleration value needs to be evaluated according to its effect for tool life. For the discussed example, Figure 110 is providing the cause and Figure 109 enables effect evaluation. The gained results after assessing and summing up all values is shown in Figure 111.

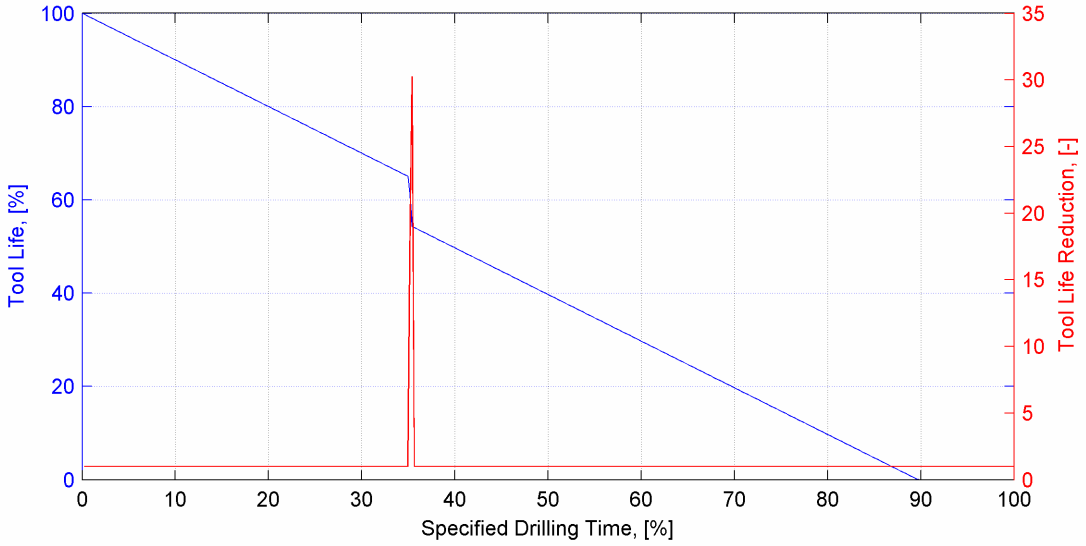

Figure 111 – Tool life prediction.

Referring to Figure 111, only one acceleration peak is severe enough to harm tool life. The others are too little to adversely affect the tool with respect to the assumed stress-tool-life function.

Tool life reduction offers a scale for getting more vivid figures. In this case, the tip of the tool life reduction peak exceeds slightly 30. Under normal conditions, one minute of drilling time would also reduce tool life by one minute. At operation conditions like in the example, a one minute drilling time would cost 30 minutes of tool life.

In other words, when assuming 7 days of specified drilling time for a new (maintained) tool and operating that tool at conditions with a tool life reduction factor of 30, then it would cause very likely a POOH after only 5.6 hours due to a failure of the tool. To replace a BHA components every 5.6 hours when it is indented to run 168 hours is never an acceptable option. In such cases the failure reason, for example severe stick-slip, must be found and eliminated. The full range of CoPilot®'s diagnostics provides helpful information in that respect.

Knowing tool life offers a number of advantages:

- Lower maintenance costs as tools are only serviced when their remaining tool life would not allow a safe rerun.
- Reduction in shipping expenditures.
- Reduces the risk when reusing an already run tool by exactly knowing its previous working conditions.
- The order of a knew tool can immediately be triggered when observing critical operation conditions before the tool actually fails. This is especially important at remote locations or if no back-up tool is available at the well site.
- The current BHA condition can be evaluated before drilling a tricky section.
- Reduction of unplanned POOHs.
- Reduction of nonproductive time.
- Improved short-term planning.

This example expounds the advantages of tool life monitoring. The monitoring method discussed in this subchapter is fictitious. The at the beginning made assumption must be kept in mind. For example, if stress events are not summable, tool life prediction would become much more complex. Furthermore, other stress-tool-life functions than the assumed ones would have a major impact on the results. A slow dying behavior of the tool has been assumed but it cannot be excluded that tools might fail immediately after surpassing a certain stress limit and are almost unaffected by conditions below that limit. Therefore, the first step must be a detailed tool failure behavior analysis.

Without knowledge about how tools fail under certain conditions, a tool life prediction stays fictitious. Lab tests and field data analyses are essential to extracted real figures. Based on such results, a method to predict/monitor tool life, like the one discussed in the paragraphs above, can be developed. Eventually, not to forget the potential for immediate tool reliability improvements due to early failure detection while laboratory tests. Long-term thinking, tests and analyses expenditures should be offset by profits from competitive advantages resulting from extended tool lives and accurate tool life prediction.

10 Conclusions

A drillstring may experience dynamic conditions which are detrimental to its component's reliability or even in severe cases it can result in the immediate destructive of certain tools. A fast and reliable detection of drilling dynamic dysfunctions and a detailed monitoring of the effects of set remedial actions can usually avert expensive failures. Baker Hughes INTEQ developed a service (CoPilot®) intended to monitor dynamic and static conditions of a BHA in real-time. Applications of services like CoPilot® will gain more and more power with the increasing number of multi-branched, multilateral, long reach wells drilled by BHAs fully equipped with latest directional control and formation evaluation tools in the near future.

The downhole environment, sensors are exposed to, is harsh and thus not beneficial to precise measurements. However, the high-speed data sampled by CoPilot® appeared most of the time reasonable. A detailed downhole data quality analysis has not been performed due to the lack of reliable reference values which are only given at laboratory tests. Possible irregularities at the high-speed data sample rate could also not be figured out as the data is stored without sample time. Inconsistencies in time stamping between data stored in RMD- and FSD-files were discovered. Their reason is most likely related to CoPilot®'s real-time clock. A comprehensive investigation on this problem has not been done. Surface data is generally of varying quality and therefore normally only providing rough limits for downhole data checks.

Currently, CoPilot® is construction-conditioned not able to correctly sense tangential acceleration. The y-axis accelerometer pair is not pointing in the direction of tangential acceleration. As a result, just a fraction of the actual tangential acceleration is measured together with a significant portion of centrifugal acceleration. A software-based correction is possible but due to a concatenation with other data channels and therewith error sources it is not recommended.

The CoPilot® sub's rotation is measured with respect to earth's magnetic field. Sensors can only see changes in field intensity due to their rotation as long as they are not orthogonally aligned with a streamline of the field. Oilwell drilling is a 3D task. Hence, at every subsurface point (but of course at the surface as well) there exist two directions where CoPilot® is not able to detect its own rotational speed if it is pointing in either. Transducers do have certain sensing errors and magnetic sensors are susceptible to other magnetic hotspots as well. For these reasons, CoPilot® is permanently delivering downhole RPM data but if orientated close to or fully aligned with a streamline of the magnetic field it is of pure accuracy. The algorithm used to calculate downhole RPM from biaxial magnetometer readings is perfectly working. Potential inaccuracies could be all addressed to low input data quality.

The characteristic of the current stick-slip diagnostics algorithm has been investigated. Observed diagnostics malfunctions could be simulated and finally related to the entropy formula the algorithm is primarily based on. A few minor diagnostics variations due to data handling could be figured out as well. The most

severe misinterpretation of the stick-slip diagnostics algorithm – highest stick-slip levels at actual zero string rotation – could be addressed to an excessive RPM data noise sensitivity of the entropy equation at very low till zero average drillstring rotational speeds. Therefore, the diagnosed stick-slip levels of the current algorithm cannot be fully trusted without regarding additional data. The discovered shortcomings of the current algorithm led to the development of an alternative stick-slip diagnostics algorithm.

The newly developed stick-slip diagnostics algorithm is no longer based on a statistical analysis of the RPM data but is time-based and single stick-slip event focused. To pick every single stick-slip oscillation and assign it with time enables correlations with other data channels and therefore a better stick-slip problem resolution. As a result, stick-slip causation detection and backward rotation type analyses could be implemented in the new algorithm as additional features. Furthermore, the new algorithm is taking into consideration the presence of a PDM in the BHA. The trend of the received new diagnostic levels is basically similar to the old one when it was correctly working. The new algorithm provides a better communicable and imaginable description of stick-slip states and a surplus of indicators for improved remedial action selection.

Tool life is a topic that could only be theoretically discussed in this work. The limited time and the lack of concrete stress-failure figures of the tool allowed no actual analysis. However, if such figures can be made available, CoPilot® is able to monitor all relevant parameters and with an adequate routine a prediction of an imminent failure appears possible. In this respect the main problem is not related to downhole monitoring issues anymore but to not existing knowledge of effects of downhole conditions.

In general, analyzed downhole data offered no indication for high tangential accelerations due to stick-slip. More critical is RPM which can reach extremely high values while slip periods. CoPilot®'s maximum rotational speed limit is easily exceeded at stick-slip. High RPM peaks might be responsible for the development of dynamic dysfunctions which are related to high RPM levels. Whirl, for example, would cause not only large centrifugal forces but also severe lateral vibrations. Low frequent, low maximum RPM stick-slip appears as little detrimental to tool reliability due to the moderate magnitude of resulting forces. Backward rotation is primarily a problem of PDC bits but can be fully eliminated by adding a PDM to the BHA.

Stick-slip, if not of extreme severity, is not seen as a major detrimental factor to tool reliability nor drilling performance.

Historical dynamic downhole data is an invaluable competitive edge. Product reliability improvements, while-drilling services optimizations, BHA design revaluations, or additional factors for advanced bit selection are just a few advantages analyses of such data could yield. The company's in-house downhole data management practice does not currently reflect that high value of these data. Today, downhole data is loosely spread all over the globe, poorly documented, hardly linked to related information and in general its access is difficult.

11 Recommendations

As long as the current stick-slip algorithm is used for real-time stick-slip diagnostics, additional data (surface RPM, downhole torque, WOB, etc.) should be used for results verification. In the near future, the algorithm should be replaced by one less sensitive to sensor noise. This also offers the opportunity to implement additional features and the consideration of a possible PDM in the BHA.

A complete and accurate implementation of the effects of a PDM in stick-slip diagnostics requires highly accurate PDM RPM data. For this reason but also for an improved mud motor monitoring, it is recommended to equip future PDM models with a RPM sensor. This should be possible with relative little engineering effort as the latest type of mud motors are already provided with a power transmission line.

The during this work developed new stick-slip diagnostics algorithm makes use of a routine that picks single stick-slip events at the RPM data. The used routine is a simple and only moderately tested development version. As the correct stick-slip event identification is essential to the new algorithm, a lot of additional work must be done to totally design, fully develop, and excessively test the stick-slip event picking routine. In this respect it should be though about a version that is able to detect the instantaneous stick-slip oscillation frequency to better separate stick-slip related RPM oscillations from other superimposing RPM oscillations and noise.

Beside a sole dynamic assessment of stick-slip also one with respect to drilling performance should be performed. For this purpose (but by far not just limited to this) downhole ROP measurements are necessary and should be developed. That this is not an easy task has also been shortly mentioned in this work. However, downhole ROP data would be highly beneficial to a number of analyses and should therefore offset the effort for developing such a system.

Analyses and diagnostics are first of all influences by their input data quality. Whenever data analyses are automated, also automated input data plausibility checks should be implemented because the final outputs do not necessarily reflect corrupt input data.

The accelerometer placement with respect to tangential acceleration must be reviewed. A permanent software-based data correction is not recommended. Design modification either at the electronic sub or at the triaxial accelerometer case and the internal sense element placement are to favor.

Regarding the high RPM maxima reached while stick-slip oscillations, CoPilot® should not be positioned below a PDM in the BHA. Below a PDM CoPilot® would earlier exceed its specified maximum rotational speed limit.

The inconsistencies of RMD-file timestamps to FSD-file timestamps need further investigations. Furthermore, it must be recommended to add to every stored trigger a file containing the sample times of every single stored high-speed value to ease

correlations and allow sample rate quality checks. As an alternative, the high speed data could be stored in a matrix which substitutes the individual channel files. Currently, it only can be taken for granted that all the data is equally spaced according to the specified sample frequency.

Efforts should be made to improve surface data quality and ensure a minimum number of collected data channels. High surface data quality is of special importance whenever CoPilot® data is used for research and development.

Tool life reliability can only be monitored and assess in real-time when the conditions the tool is able to withstand and the corresponding times are known. Destructive endurance tests should be performed to receive figures for tool life prediction. CoPilot® should be tested for different single and multiaxial vibration levels at different temperatures but also the shock resistance capability should be evaluated. Full scale tests are expensive. Tests of electronic boards and sensors should be sufficient.

Data management of CoPilot®'s downhole records must considerably be improved to fully capitalize its advantages. A first step could be the standardized and permanent documentation of the intentions that caused to take a particular high-speed trigger. For example, the CoPilot® field engineer just has to tick at a standardized report form the trigger reason (e.g. a stick-slip event, a tool failed, sudden parameter change, etc.), writes down the trigger number and date and time of storage and if necessary adds a few comments. Later on, all relevant data of a job (high-speed triggers, FSD, surface data, reports, documentations, logs, failure analyses, etc.) is uploaded to a data base and linked with respect to country, time, depth, BHA, trigger reason, failures, and so on. Eventually, this would allow a companywide, fast, and easy access to the entire available information without wasting numerous man hours for a manual data organizing and screening odyssey whenever a project would like to make use of that data. At the end, it should be possible to search the data base for e.g. certain recorded dynamic phenomena, wells drilled in specific geographic regions, certain run depths, occurred failures, and other aspects. The better the data is prepared, the higher the benefits will be.

12 References

[1] LEINE R.I., VAN CAMPEN D.H., KEULTJES W.J.G.: “Stick-slip Whirl Interaction in Drillstring Dynamics”, Journal of Vibration and Acoustics, April 2002, Vol. 124, p. 209 - 220

[2] Baker Hughes INTEQ: “Navi-Drill® Motor Handbook”, 10th Edtition, Rev C, Baker Hughes Incorporated, January 2006

[3] *www.key-to-steel.com*, (04.08.2007)

[4] HEISIG G., ROBNETT E.W.: “CoPilot – Drilling Performance Service – Focus on Drilling Dynamics”, Presentation Slides, Baker Hughes INTEQ, 1999

[5] ROBNETT E.W., HOOD J.A., HEISIG G., MACPHERSON J.D.: “Analysis of the Stick-Slip Phenomenon Using Downhole Drillstring Rotation Data”, SPE/IADC 52821, SPE/IADC Drilling Conference, Amsterdam, Holland, 9-11 March 1999

[6] RICHARD T., DETOURNAY E., FEAR M., MILLER B., CLAYTON R., MATTHEWS O.: “Influence of bit-rock interaction on stick-slip vibrations of PDC bits”, SPE 77616, SPE Annual Technical Conference and Exhibition, San Antonio, Texas, 29. September – 2. October 2002

[7] ROBNETT Edward W.: “CoPilot Operations Manual – Section 1 – Service Overview”, CoP-20-70-0000-02-01, Rev. A, Baker Hughes INTEQ, January 2005

[8] ROBNETT Edward W.: “CoPilot Operations Manual – Section 2 – Detailed Description of Service”, CoP-20-70-0000-02-01, Rev. A, Baker Hughes INTEQ, January 2005

[9] ROBNETT Edward W.: “CoPilot Operations Manual – Section 4 – Operating Procedures”, CoP-20-70-0000-04-01, Rev. A, Baker Hughes INTEQ, January 2005

[10] ROBNETT Edward W.: “CoPilot Operations Manual – Section 5 – Troubleshooting”, CoP-20-70-0000-05-01, Rev. A, Baker Hughes INTEQ, January 2005

[11] ROBNETT Edward W.: “CoPilot Operations Manual – Section 6 – Specifications”, CoP-20-70-0000-06-01, Rev. A, Baker Hughes INTEQ, January 2005

[12] ROBNETT Edward W.: “CoPilot Operations Manual – Section 10 – Appendices”, CoP-20-70-0000-10-01, Rev. A, Baker Hughes INTEQ, January 2005

[13] HEISIG Gerald: “CoPilot® - Real-Time Drilling Optimization – Enhanced Drilling Performance And Risk Management”, Presentation Slides, Baker Hughes INTEQ, 25.08.2006

[14] HEISIG G., SANCHO J., MACPHERSON J.D.: “Downhole Diagnosis of Drilling Dynamics Data Provides New Level Drilling Process”, SPE 49206, 1998 SPE Annual Technical Conference and Exhibition, New Orleans, Louisiana, 27-30 September 1998

[15] MACPHERSON John, HANTZKO Hendrik: “Software Design Specification – CoPilot DSP Internal Design”, Version 3.0, Dwg. No. 77591FD200, Rev. A, Baker Hughes INTEQ, 31.10.2002

[16] BAUMGARTNER Franz: “Magnetoresistiver – Sensor”, NTB Sensordatenbank/Labor Elektrische Messsysteme, Fachhochschule Buchs, *www.ntb.ch/Pubs/sensordemo/*, (31.07.2007)

[17] *www.ssec.honeywell.com/magnetic/datasheets.html*, "Magnetic Sensor Overview", (27.02.2007)

[18] *www.wikipedia.org*

[19] *leifi.physik.uni-muenchen.de*, (06.03.2007)

[20] *www.magneticsensors.com,* (04.01.2007)

[21] *www.silicondesigns.com*, (16.03.2007)

[22] *www.baumersensopress.com*, (01.08.2007)

[23] *www.maschinendiagnose.de*, (01.08.2007)

[24] *www.straingage.com*, (01.08.2007)

[25] *physchem.kfunigraz.ac.at*, (01.08.2007)

[26] CAMMINADI Marco: "Grundlagen zum Messen mit Dehnungsmeßstreifen (DMS)", Fachhochschule Gelsenkirchen, Fachbereich Physikalische Technik, *www.blh.de*, (01.08.2007)

[27] ENGLUND David R.: "The dual element method of strain gauge temperature compensation", Abstract, NASA, Lewis Research Center, Cleveland, OH, 1987, Bibliographic Code: 1987STIA...8912276E, ,*adsabs.harvard.edu*, (02.08.2007)

[28] *www.vishay.com*, (02.08.2007)

[29] Baker Hughes INTEQ: VSS stick-slip calculation.

[30] Baker Hughes INTEQ: "Technical Data Sheet – 4 ¾" CoPilot", CoP-20-60-0475-00-B, Baker Hughes Incorporated, 2006.

[31] Baker Hughes INTEQ: "Technical Data Sheet – 6 ¾" CoPilot", CoP-20-60-0675-00-B, Baker Hughes Incorporated, 2006.

[32] Baker Hughes INTEQ: "Technical Data Sheet – 8 ¼" CoPilot", CoP-20-60-0825-00-B, Baker Hughes Incorporated, 2006.

[33] Baker Hughes INTEQ: "Technical Data Sheet – 9 ½" CoPilot", CoP-20-60-0950-00-B, Baker Hughes Incorporated, 2006.

[34] Baker Hughes INTEQ: "Technical Data Sheet – 4 ¾" OnTrak", OTK-20-60-0475-00-C, Baker Hughes Incorporated, 2006.

[35] Baker Hughes INTEQ: "Technical Data Sheet – 6 ¾" OnTrak", OTK-20-60-0675-00-C, Baker Hughes Incorporated, 2006.

[36] Baker Hughes INTEQ: "Technical Data Sheet – 8 ¼" OnTrak", OTK-20-60-0825-00-B, Baker Hughes Incorporated, 2006.

[37] Baker Hughes INTEQ: "Technical Data Sheet – 9 ½" OnTrak", OTK-20-60-0950-00-C, Baker Hughes Incorporated, 2006.

[38] HEISIG Gerald: "Misalignment in CoPilot", Presentation Slides, Baker Hughes INTEQ

[39] Baker Hughes INTEQ: "ELECTRONIC SUB 30KPSI FOR 4,75" COPILOT2 – MILLING SLOTS", Dwg. No. 10177028, Sheet 3 of 8, Rev. A1, Date of Release: 26.09.2006

[40] Baker Hughes INTEQ: “ELECTRONIC SUB 6.3/4” CO PILOT 2 30KPSI”, Dwg. No. 10182804, Sheet 5 of 9, Rev. A, 18.07.2006 (not released)

[41] Baker Hughes INTEQ: “ELECTRONIC SUB 6.3/4” CO PILOT 2 30KPSI”, Dwg. No. 10182804, Sheet 8 of 9, Rev. A, Date of Release: 31.07.2006

[42] Baker Hughes INTEQ: “ELECTRONIC SUB 8.1/4” COPILOT 2 MILLING”, Dwg. No. 10081635, Sheet 5 of 6, Rev. H (being modified, 09.07.2003) , Date of Initial Release: 25.10.2001

[43] Baker Hughes INTEQ: “ELECTRONIC SUB 8.1/4” COPILOT 2 MILLING”, Dwg. No. 10081635, Sheet 6 of 6, Rev. H (being modified, 09.07.2003) , Date of Initial Release: 25.10.2001

[44] Baker Hughes INTEQ: “ELECTRONIC SUB 9.1/2” CO PILOT 2 MILLING”, Dwg. No. 10092994, Sheet 5 of 6, Rev. C (10.07.2003) , Date of Initial Release: 09.04.2001

[45] Baker Hughes INTEQ: “ELECTRONIC SUB 9.1/2” CO PILOT 2 MILLING”, Dwg. No. 10092994, Sheet 6 of 6, Rev. C (10.07.2003) , Date of Initial Release: 09.04.2001

[46] Silicon Designs, Inc: “Model 2422 – Triaxial Analog Accelerometer Module”, Data-Sheet, Version June 2005, www.silicondesigns.com (16.03.2007)

[47] Silicon Designs, Inc: “Model 1210 – Analog Accelerometer”, Data-Sheet, Version June 2004, www.silicondesigns.com (09.01.2007)

[48] STAVLAND M., WOLTER H., EVANS J.G.: “Mitigating Application-Specific Challenges Through a Total System Approach”, IADC/SPE 99122, IADC/SPE Drilling Conference, Miami, Florida, U.S.A., 21-23 February 2006

[49] “INTERMAGNET – Technical Reference Manual”, Version 4.2 (2004), *www.intermagnet.org*, (04.12.2006)

[50] geomag.usgs.gov, (04.12.2006)

[51] Baker Hughes INTEQ: “D-RAW User’s Manual”, Baker Hughes INTEQ, 77223UM220 Rev. A, 27. May 1994

[52] BARTHA Alexander Robert: “Dry Friction Backward Whirl of Rotors”, Dissertation ETH No. 13817, Swiss Federal Institute of Technology, Zurich, 2000

[53] *www.dog.dnr.state.ak.us*, (05.01.2007)

[54] *www.grandpridec.com*, (05.01.2007)

[55] CHANDLER Brett R., JELLISON Michael J., PAYNE Mike L., SHEPARD Jeff S.: “Advanced and emerging drillstring technologies overcome operational challenges”, World Oil, October 2006, p. 23-34

[56] BOURGOYNE Jr. A.T., MILLHEIM K.K., CHENEVERT M.E., YOUNG Jr. F.S.: “Applied Drilling Engineering”, SPE Textbook Series, Vol.2, ISBN 1-55563-001-4

[57] PROHASKA Michael: “Drilling Engineering I”, lecture notes, Mining University Leoben, Austria, WS 2002/03

[58] AADNØY B.S., ANDERSON K.: “Design of oil wells using analytical friction models”, Journal of Petroleum Science and Engineering, Volume 32, p. 53-71, 2001

[59] Baumer sensopress: “Abschlussbericht: Projekt Copilot – Baker Hughes INTEQ”, Projekt Nr. 508871, 18.04.2002

[60] Baumer sensopress: “Machbarkeitsstudie und FEM Analyse – Projekt Copilot – Dehnungssensor Torque”, Projekt Nr. 508871, Baker Hughes INTEQ, 11.10.2002

[61] *sensing.honeywell.com*, (27.02.2007)

[62] TESSARI R.M., WARREN T.M.: “Drilling with Casing Reduces Cost and Risk”, SPE 101819, 2006 SPE Russian Oil and Gas Technical Conference and Exhibition, Moscow, 3-6 October 2006

[63] FEAR M.J., ABBASSIAN F., PARFITT S.H.L.: “The Destruction of PDC Bits by Severe Slip-Stick Vibration”, SPE/IADC 37639, 1997 SPE/IADC Drilling Conference, Amsterdam, The Netherlands, 4-6 March 1997

[64] HEISIG G., CAVALLARO G., JOGI P., HOOD J., FORSTNER I.: “Continuous Borehole Curvature Estimate While Drilling Based on Downhole Bending Moment Measurements”, SPE 90794, SPE Annual Technical Conference and Exhibition, Houston, Texas, U.S.A., 26-29 September 2004

[65] *www.bakerhughesdirect.com*, (19.01.2007)

[66] Baker Hughes INTEQ: “ELECTRONIC SUB ASSY 6.3/4” CO PILOT 2”, Dwg. No. 10087691, Sheet 1 & 2 of 2, Rev. X, 24.11.2006

[67] Baker Hughes INTEQ: “ASSY TRANSDUCER PRESS (HERCULES)”, Dwg. No. 10075534, Sheet 1 of 1, Rev. A, 18.06.2001

[68] HOLZMANN, MEYER, SCHUMPICH: “Technische Mechanik – Kinematik und Kinetik”, 6. Auflage, Stuttgart, 1986, ISBN 3-519-06521-5

[69] HAUPTMANN Peter: “Sensoren”, Wien, 1991, ISBN 3-446-16073-6

[70] TRÄNKLER Hans-Rolf (Hrsg.): “Sensortechnik”, Berlin, 1998, ISBN 3-540-58640-7

[71] “Sensoren und Signalverarbeitung”, hrsg. Von der Technologievermittlung der Technischen Universität Hamburg-Harburg, Hamburg, 1988

[72] HOFFMANN Josef: “MATLAB und SIMULINK in Signalverarbeitung und Kommunikationstechnik”, München, 1999, ISBN 3-8273-1454-2

[73] LERCH Reinhard: “Elektrische Messtechnik”, 3. Auflage, Berlin, 2006, ISBN 978-3-540-34055-3

[74] MEYER-BÄSE Uwe: “Schnelle digitale Signalverarbeitung – Algorithmen, Architekturen, Anwendungen”, Berlin, 2000, ISBN 3-540-67662-7

[75] KAMMEYER K.D., KROSCHEL K.: “Digitale Signalverarbeitung – Filterung und Spektralanalyse mit MATLAB-Übungen”, 4. Auflage, Stuttgart, 1998, ISBN 3-519-36122-1

[76] KREDLER Christian: “Materialien zu Stochastik 1 - Einführung in die Wahrscheinlichkeitsrechnung und Statistik”, Zentrum Mathematik, Lehrstuhl für Mathematische Statistik, Technische Universität München, WS 1997/98

13 Nomenclature

Abbreviation	Description	Unit
A	Amplitude	[case specific]
a_c	Centrifugal acceleration	[m/s²]
$a_{c,x}$	x-component of a_c	[m/s²]
$a_{c,y}$	y-component of a_c (identical with E_c)	[m/s²]
AKO	Adjustable kick off sub	[-]
$a_{lateral}$	Lateral acceleration (xy-direction)	[g]
a_m	Measured tangential acceleration (accelerometers)	[g]
AMR	Anisotropic magnetoresistance (effect)	[-]
APLS	Advanced porosity logging service (service mark)	[-]
ASCII	American standard code for information interchange	[-]
a_t	True tangential acceleration	[m/s²]
$a_{t,x}$	x-component of a_t	[m/s²]
$a_{t,y}$	y-component of a_t	[m/s²]
$a_{tangential}$	Tangential acceleration	[g]
a_x	Axial acceleration in direction x	[g]
a_y	Axial acceleration in direction y	[g]
a_z	Axial acceleration in direction z	[g]
B	Magnetic flux density	[T]
BHA	Bottom hole assembly	[-]
BL	Bottom lag	[sec]
BWR	Backward rotation	[-]
C	Torsional stiffness of the drillpipe	[Nm]
C_a	Angular misalignment correction factor	[-]
CD	Compact disk	[-]
CF	Causation factor	[%]

Abbreviation	Description	Unit
CTD	Coiled tubing drilling	[-]
CWD	Casing while drilling	[-]
d	Later displacement of the y-axis acceleration sensing point from accelerometer case center	[mm]
DC	Drill collar	[-]
DIA	Diameter	[mm], [in]
DP	Drillpipe	[-]
DPWSS	Drilling performance while stick-slip	[-]
DS	Drillstring	[-]
DSP	Digital signal processor	[-]
E_a	Angular misalignment error	[%]
E_c	Centrifugal acceleration error	[m/s²]
ECD	Equivalent circulating density	[kg/m³], [ppg]
f	RPM oscillation frequency	[Hz]
f_0	Measured stick-slip oscillation frequency	[Hz]
FS	Full scale	[-]
FSD	Five second data	[-]
FSR	Frame sample rate	[Hz]
H	Hook load	[N]
H	Magnetic field intensity	[Am]
HWDP	Heavy weight drillpipe	[-]
I	Moment of inertia of the BHA	[kg m^2]
ID	Inner diameter	[in], [mm]
LP	Level parameter	[-]
LWD	Logging while drilling	[-]
M	Mass of BHA	[kg]
MAXTOB	TOB maximum	[Nm]
MD	Measured depth	[m], [ft]
MINTOB	TOB minimum	[Nm]
MM	Maximum/minimum RPM	[-]
MR	Magnetoresistive	[-]

Abbreviation	Description	Unit
MWD	Measuring while drilling	[-]
N	Number of data values/elements	[-]
OBM	Oil-based mud	[-]
OD	Outer diameter	[in], [mm]
OR	RPM oscillation range	[rpm]
OSR	Output sample rate	[Hz]
PCD	Printed circuit board	[-]
PDC	Polycrystalline diamond compact bit	[-]
PDM	Positive displacement motor	[-]
POOH	Pulled out of hole	[-]
Q	Entropy	[-]
r	Radius	[mm]
R	Resistor, resistance	[Ω]
r_1	Radius from rotary axis to accelerometer case bottom	[mm]
r_2	Radius from rotary axis to y-axis acceleration sensing point	[mm]
RCD	Research configuration data	[-]
RCLS	Rotary closed loop system (AutoTrak®)	[-]
RIH	Run in hole	[-]
RMC	Root mean cube	[-]
RMD	Research memory data	[-]
RMS	Root mean square	[-]
ROP	Rate of penetration	[m/h], [ft/h]
RPM	Revolutions per minute	[rpm]
RTD	Resistive temperature device	[-]
S.I.	Le Système international d'unités (french), international system of units	[-]
S/G	Strain gauge	[-]
SG	Specific gravity	[-]
SL	Stick lag	[sec]
SN	Serial number	[-]

Abbreviation	Description	Unit
SNAP	Band-limited signal used in vibration diagnostics	[-]
SSR	Surface data sample rate	[Hz]
t	Time	[sec]
T	Torque on bit	[Nm]
TAA	Tangential acceleration sensed by accelerometers	[m/s²]
TAM	Tangential acceleration determined via magnetometers	[m/s²]
TL	Top lag	[sec]
TLL	Tool life	[-]
TOB	Torque on bit	[Nm]
TVD	True vertical depth	[m], [ft]
U	Voltage	[V]
v	Velocity	[m/s]
V	Voltage	[V]
W	Weight on bit	[N]
WBM	Water-based mud	[-]
WOB	Weight on bit	[N], [t]
x	Axis/direction	[-]
x	Distance between accelerometer module case bottom to y-axis acceleration sensing point	[mm]
$\bar{x}$	First order statistic (mean)	[-]
X_1	Output of x-axis sensing element of accelerometer 1	[g]
X_2	Output of x-axis sensing element of accelerometer 2	[g]
$\overline{x^2}$	Second order statistic	[-]
$\overline{x^3}$	Third order statistic	[-]
y	Axis/direction	[-]
Y_1	Output of y-axis sensing element of accelerometer 1	[g]
Y_2	Output of y-axis sensing element of accelerometer 2	[g]

Abbreviation	Description	Unit
z	Axis/direction	[-]
Z_1	Output of z-axis sensing element of accelerometer 1	[g]
Z_2	Output of z-axis sensing element of accelerometer 2	[g]
α	Misalignment angle	[°]
β	$\beta = \alpha + 90°$	[°]
ε	Relative strain	[-]
Φ	Bit angular position	[-]
Ω	Bit angular velocity	[rad/s]
Ω_o	Imposed and steady-state angular velocity	[rad/s]
3D	Three-dimensional	[-]

Appendix

The computer language, which was used throughout this thesis project, is MATLAB® by The MathWorks, Inc. (*www.mathworks.com*). All simulations, most of the data processing, the majority of generated figures, and last but not least the new stick-slip diagnostics algorithm were handled with MATLAB®.

The following program version and configuration was used:

Version: 7.0.1.24704 (R14) Service Pack 1

Toolboxes: Signal Processing
Communications

All written scripts and functions are stored on the to this volume attached CD.

To the following routines is explicitly referred in the text:

ACLTCorrection	Script. Software based accelerometer's tangential acceleration data correction (Chapter 6.5). This routine is also available and used as function (*correctACLT*).
MagsRPMSimulator	Script. The in Chapter 7.2 presented magnetometer readings and RPM simulator.
NewStickSlipDiagnostics	Script. The developed new stick-slip diagnostics algorithm (Chapter 9).

The rest of MATLAB® files attached are all functions and are called up at least once in either of the above listed scripts. The purpose of each routine is always briefly explained in its header.

Some of the routines will not work without access to CoPilot® memory data. There is no downhole data of any kind stored on the CD at all!